THE MICROMAGNETISM OF VIDEO RECORDING TRACKS WRITTEN ON CoNi METAL EVAPORATED TAPE (MET)

by George John Sinclair

submitted for the degree of Doctor of Philosophy at the Department of Physics and Astronomy, University Of Glasgow.

September 1990

ProQuest LLC.
789 East Eisenhower Parkway
P.O. Box 1346
Ann Arbor, MI 48106 – 1346

ACKNOWLEDGEMENTS

Much of the credit for the successful completion of this thesis must go to the many people who helped me during the course of the study. First of all I would like to thank my supervisor, Professor R. P. Ferrier, for excellent guidance throughout. Special mention is also due to Professor J. N. Chapman and also Dr S. M^{c}Vitie who both provided useful discussions and substantial practical assistance throughout the course of this work.

I am indebited to both my parents, and also my girlfriend Elaine, for their support and encouragement without which this thesis could not have been completed.

I would also like to thank the members of the technical staff who maintained the electron microscope facilities at Glasgow University.

Finally for providing financial assistance and equipment I would like to thank both the SERC and Thorn EMI.

DECLARATION

This thesis is a record of the work carried out by me in the Department of Physics and Astronomy at the University of Glasgow between October 1986 and September 1989. The work described herein is my own, apart from the manufacture of the films and some of the bulk magnetic data detailed in chapter 6. All films were provided by Thorn EMI Central Research Laboratories in Hayes. The bulk magnetic results were kindly obtained by Dr J. P. C. Bernards at Philips Research Laboratories in the Netherlands.

Some of the results in Chapter 7 were reported at the International Colloquium on Magnetic Films & Surfaces, ICMFS-12, a satellite meeting of the International Conference on Magnetism 1988.

This thesis has not previously been submitted for a higher degree.

INTRODUCTION

This thesis describes a CASE project between The Department of Physics and Astronomy of the University of Glasgow and Thorn EMI Central Research Laboratories (CRL). Thorn EMI were considering full scale production of the Metal Evaporated Tapes (MET) studied in this thesis, while at the same time assessing the commercial viability of such a project. Initially therefore the films were produced on a prototype fabrication rig which, given approval, would be scaled to meet the projected demand and also provide samples for study. Unfortunately a corporate decision taken at an early stage of the project shifted the emphasis of research at CRL and the MET project was dropped. As a consequence of this many of the requests made by Glasgow University for additional samples and further recording experiments could not be met. We mention these facts to account for any suggestion that the work contained herein might not appear to have been conducted in a logical and scientific manner, which could possibly have increased both the validity and scientific value of conclusions which were reached.

SUMMARY

The main objective of the work described in this thesis was to study the micromagnetic structure of 8mm video recording tracks. We attempted to quantify the written magnetisation patterns and correlate the results with the bulk magnetic characteristics of each of the different samples analysed. We studied the micromagnetics as a function of the physical and magnetic characteristics of the films and also the wavelength of the recorded signal.

The basic principles of ferromagnetism are outlined in chapter 1, and then in chapter 2 we describe the way in which the technology of magnetic recording harnesses these properties. Chapter 2 also provides details of the recording format used in video 8. This section concludes with the demands now placed on the physical and magnetic characteristics of the materials which these high storage density applications require.

The high resolution required to examine the written tracks necessitates the use of electron microscopy and chapter 3 describes the basic beam specimen interactions and illustrates the ways in which contrast can be produced which relates to the magnetisation within the sample.

Chapter 4 details the specific requirements of the Differential Phase Contrast (DPC) mode of Lorentz Electron Microscopy which have to be met if quantitative interpretation of the information is to be possible. This section also indicates the operational limits of this technique and the relevance of these on the results.

The next 3 chapters (5-7) contain the results which form the main body of this thesis. The fabrication

procedure of the films and the physical and compositional characterisation of the samples is detailed in chapter 5. Chapter 6 contains the results of the bulk magnetic characterisation of these MET films The quantitative micromagnetic results obtained from each film, at two recording densities, form the basis of chapter 7. We also detail small angle scattering experiments which were necessary to establish the validity of the quantitative results.

The final chapter, chapter 8, suggests ways in which we feel that much of the information which we obtained, about the micromagnetic structure of the recorded samples, could be improved now that the DPC system has recently been modified. We also comment on the relevance of new techniques now available and how these might add to our existing knowledge of the micromagnetic structure produced within ferromagnetic materials when subjected to localised magnetic fields.

CONTENTS

CHAPTER 5: MET Fabrication, Specimen Preparation and the Physical & Compositional Characterisation of the MET films

CHAPTER 6: The Bulk Magnetic Characterisation of the Metal Evaporated Films

CHAPTER 1 FERROMAGNETISM

1. INTRODUCTION

This section describes the basic origin of ferromagnetism and describes the various energy contributions which a magnetic material has as a result of this, and also the way in which these energy terms depend on the magnitude and orientation of the magnetisation.

1.1 BASIC FERROMAGNETISM

Ferromagnetism describes a state in which the individual magnetic moments of the constituent atoms are aligned parallel to one another, and this alignment extends over a considerable distance, often equivalent to several hundreds of lattice repeats in extent. This alignment is found even when these materials are not subjected to an applied magnetic field, in contrast to paramagnetism, and further this cooperative behaviour is exhibited even at elevated temperatures. The explanation for this type of behaviour lies within the framework of the 'Pauli Exclusion Principle'

The Pauli Principle addresses the indistinguishability of electrons and states that the wave-function describing a system of electrons must be anti-symmetric As the complete wave-function is comprised of a spatial part and a spin part, any attempt to alter the spin state of the system - ie to magnetise it, must also change the spatial state if this antisymmetry is to be preserved. Thus a redistribution of charge follows any alteration to the

magnetic state of the system and consequently, in addition to overcoming the dipolar magnetic force, the far greater Coulomb force must be overcome. This explains why these regions of aligned magnetic moments were found at temperatures where the thermal energy would be far in excess of the coupling strength attributable to dipolar interactions. Within the lattice structure of a typical ferromagnet, the energy required to overcome the magnetic force from dipolar interactions with neighbouring atoms is equivalent to the thermal energy at ~1K. The Curie temperature for ferromagnetic cobalt is approximately 1400K. The temperature at which the magnetic ordering disappears is known as the Curie temperature T_c; at this the orientation of each intrinsic moment is randomised through thermal agitation. At temperatures above T_c, a ferromagnetic material behaves as a paramagnet. When below the Curie point, the spontaneous magnetisation of such materials is distributed over small regions within which the local alignment of atomic moments is high. Although a high degree of alignment is present within these zones the net magnetisation of the whole sample is normally much less, due to the significant cancellation between zones of conflicting magnetisation alignment. These regions are known as 'magnetic domains' and their intersection as the 'domain wall'.

1.2 MAGNETIC DOMAIN FORMATION

Predicting the micromagnetic domain structure adopted by a ferromagnetic material can only be attempted if the form of each contributory interaction is known and its

behaviour well understood. This information alone however is insufficient and knowledge of the previous magnetic history of the sample is also needed. In a ferromagnetic material the most stable domain structure is obtained by minimising the total potential energy of the system. The total potential energy can be treated as the sum of three terms, the exchange energy, the magnetocrystalline anisotropy energy and the magnetostatic energy. The origin and form of each of these will now be discussed.

1.3 EXCHANGE ENERGY

The exchange energy is the energy associated with the relative orientation of the spin vectors of neighbouring particles. The energy (U) attributable to exchange for two atoms i and j, is given by

$$U = -2J\ \underline{S}_i.\underline{S}_j$$

where J is the exchange integral. The magnitude of the exchange integral is generally determined by the volume of space that the two wave-functions, describing the particles with spin vectors $\underline{S}_i$ and $\underline{S}_j$, have in common. The form of this overlap integral is shown schematically in figure 1.1. To favour parallel alignment of spins, and support the ferromagnetic state, the particles must have a positive exchange integral J, and hence an interatomic separation somewhere in the range between p and q, as illustrated in figure 1.1. Atoms possessing a permanent magnetic moment but which have an atomic separation outwith this range do not exhibit ferromagnetism, however

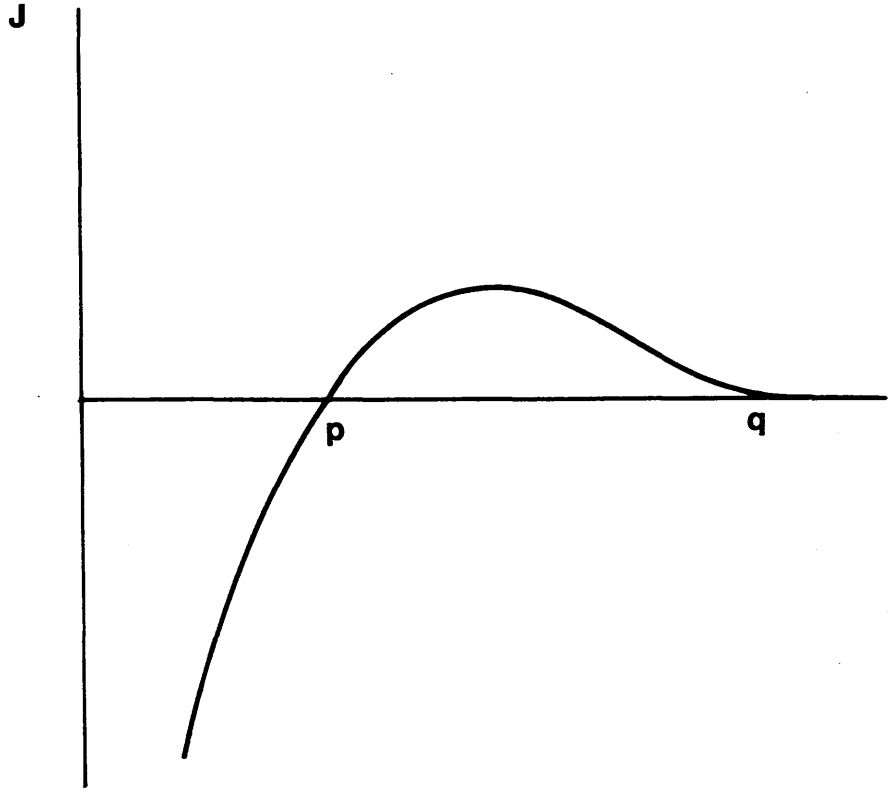

Figure 1.1

The overlap integral J as a function of interatomic seperation r

when the interatomic separation distance is altered the exchange integral for certain materials becomes positive, and as a result of this alteration the ferromagnetic state can now be supported, eg pure Mn is not ferromagnetic but MnAs is. This modification of composition results in a magnetic ion separation distance lying within the range (p,q), where parallel alignment of spins is favoured. The converse is also possible eg ferromagnetic Ni becomes anti-ferromagnetic when the oxide is formed. Obviously each atom within a ferromagnetic solid has more than one nearest neighbour, and consequently the total exchange energy must include a term for each of these neighbours. In fact the exchange interaction within such a solid extends beyond nearest neighbour interactions and must account for all atoms with which it has a non zero overlap integral.

1.4 MAGNETOCRYSTALLINE ANISOTROPY ENERGY

This energy is due to the magnetic vector lying at a finite angle with respect to certain crystallographic axes. The anisotropy energy is minimised when the magnetic vector lies parallel to one of these favoured axes. This energy contribution originates through the indirect coupling of the spin vector of the atom with the symmetry of the host lattice. The localised charge distribution around each magnetic atom is polarised by the permanent magnetic moment it possesses through spin-orbit coupling. This polarisation in turn distorts the electron density of any neighbouring atoms. Through this coupling of the spin system to the lattice symmetry, as a result of

electrostatic repulsion, the nature of the magnetocrystalline anisotropy is strongly influenced by the spatial distribution of atoms within the material. For ferromagnetic materials with a cubic structure the energy term takes the form

$$E_{cubic} = K_1(\alpha_1^2\alpha_2^2 + \alpha_1^2\alpha_3^2 + \alpha_2^2\alpha_3^2) + K_2(\alpha_1^2\alpha_2^2\alpha_3^2) + \ldots$$

where α (i=1,2,3) are the direction cosines of the magnetic vector with respect to the cube edges of the lattice structure, K_1 and K_2 are the anisotropy constants whose values depend on the physical and magnetic characteristics of the material, and which also vary with temperature. For materials with what is termed uniaxial anisotropy, ie one direction of minimum anisotropy energy, the expression has the approximate form

$$E_{uni} = K_1\sin^2(\phi) + K_2\sin^4(\phi) + \ldots$$

where ϕ is the angle between the magnetic vector and the axis of minimum energy. These axes of minimum energy are called 'easy-axes' of magnetisation and are usually those which maximise the inter-atomic separation distance. Therefore, for a body centred cubic crystal structure, eg Fe, the easy-axes are directed along the cube edges. A face centred cubic structure, eg Ni, has easy-axes lying along the body diagonals, while a hexagonal close packed structure, eg Co, has an easy-axis oriented perpendicular to the layers of atomic planes, see figure 1.2. Although we have only described these effects in single crystal specimen, polycrystalline ferromagnetic materials may also

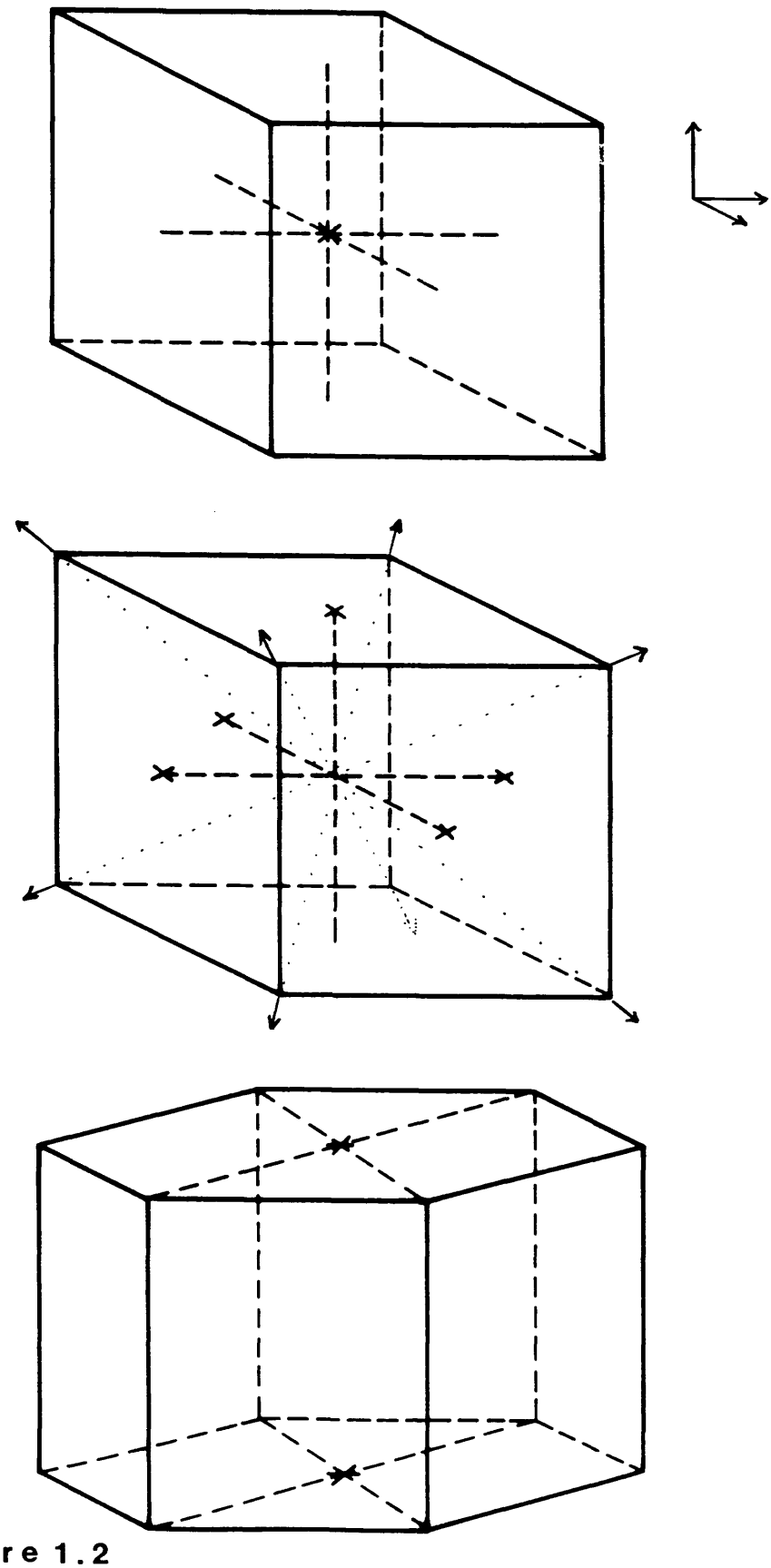

Figure 1.2

Easy axes for BCC FCC and HCP lattice structures

possess substantial magnetocrystalline anisotropy. Fabricating these materials using special crystal growth techniques which can induce a fibre texture, allows the easy-axis of magnetisation to be manipulated to suit particular applications[1].

1.5 MAGNETOSTATIC ENERGY

This energy contribution arises from the interaction of the magnetisation $\underline{M}$, with a magnetic field $\underline{H}$. This magnetic field can be provided by an external source or in fact arise from $\underline{M}$ itself. If the field arises from the magnetisation $\underline{M}$ then the magnetostatic energy associated with this E_{MS} is given by

$$E_{MS} = \frac{\mu}{2} \int_V \underline{H}.\underline{M} dV$$

This magnetic field is known as the demagnetising field and the effect of this interaction is to attempt to redistribute the magnetisation so as to reduce this field, and so lower the energy contribution. If we introduce the magnetic scalar potential V_m, such that $\underline{H} = - \nabla V_m$ then the equation for the magnetostatic energy contribution becomes

$$E_{MS} = \frac{1}{2} \int_V \nabla V_m . \underline{M} dV$$

This integral can be split up into two parts, one part for the energy arising from the induction from magnetic charges within the volume , $\rho = \nabla.\underline{M}$, and another from the surface magnetic charges, $\sigma = \underline{M}.\underline{n}$. The demagnetising field

is produced by these magnetic charges, and these field sources are found where the magnetisation has discontinuities such as at the boundary surfaces of the sample.

1.6 DOMAIN BOUNDARY WALLS

The nature of the transition region between oppositely magnetised domains is of considerable technological importance, as in many magnetic recording applications this region determines the form of the output signal which is measured.

There exist two distinct types of domain wall the Bloch wall[2] and the Néel[3] wall. The nature of the magnetisation variation within these two walls is shown schematically in figures 1.3a and 1.3b. A Bloch wall has the magnetic vector rotating out of the plane of the domain magnetisation, whilst the Néel wall is characterised by a rotation in the same plane as that defined by the domain magnetisation. When there are little or no magnetic charges present, such as within a bulk ferromagnet, the rotation of the magnetisation is controlled by exchange and anisotropy alone and a Bloch wall is formed. A Néel type wall structure is energetically more favourable when the magnetostatic energy contribution becomes significant. A Néel type wall only arises when one of the spatial dimensions of the specimen becomes far smaller than the other two, such as in a thin film. In this situation it is the magnetostatic interaction which modifies the effect of the other energy terms to constrain the rotation of magnetisation within

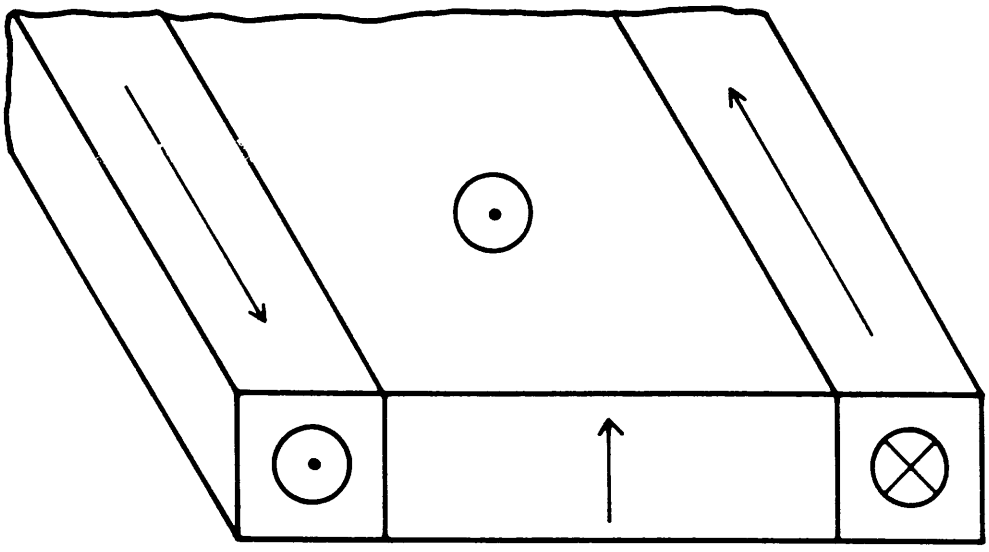

Figure 1.3a

Simplified Bloch domain wall

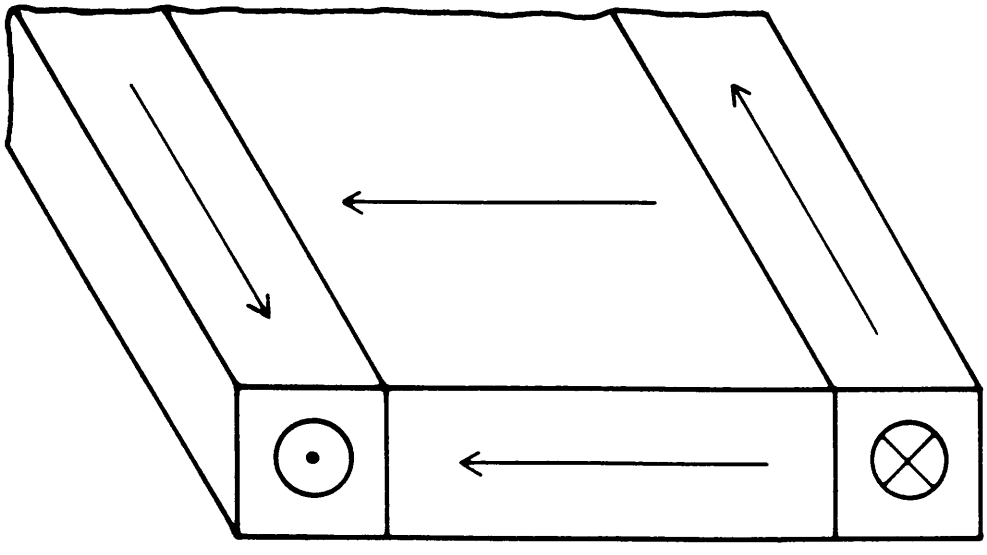

Figure 1.3b

Simplified Néel domain wall

the film plane. Another type of transition structure, the cross-tie wall, is a combination of both Bloch and Néel wall structures. This type of transition is only found in preference to either of these individual forms within a certain range of film thicknesses (20-80nm)[4], which depends on the material considered.

From this brief description of the three principal effects which control the micromagnetic structure of ferromagnetic materials, it should be clear that within a domain wall the exchange energy is in direct conflict with the anisotropy energy. The exchange interaction tries to increase the extent of the transition region by spreading the angular variation out over as many atoms as possible, as this reduces the angle between adjacent spin vectors. This means, however, that an increased number of vectors will lie in directions of increased anisotropy energy so a balance must be achieved. In situations where these are the two principal energy contributions governing the micromagnetics, the final configuration of the magnetisation within the domain wall is one which balances these conflicting effects. The rate of rotation of the spin vectors is therefore more rapid when these make larger angles to the easy-axes of magnetisation, and hence the angle between adjacent spins is smaller when these point close to the minimum anisotropy directions. Only when close to the specimen surfaces will the energy associated with magnetostatic interactions make a significant contribution to the total energy of the system. At the sample surfaces the effect of the magnetostatic interaction is to increase the in plane component of the magnetisation. At domain wall boundaries

magnetostatic effects act to reduce the magnetic charge density by increasing the area over which these are spread, re-orienting the magnetisation at the same time. Therefore in most situations an equilibrium must be reached which balances all of these effects, and any slight variation in any one of these can upset this equilibrium and completely alter the magnetic structure.

References

1. S. Chikazumi, Physics of Magnetism, Wiley, (1964)

2. F. Bloch, Z Physik **74**, 295 (1932)

3. L. Néel, Compt. Rendu. **241**, 533 (1955)

4. E. Huber *et al*, J. Appl. Phys. **29**, 294 (1958)

CHAPTER 2 MAGNETIC RECORDING AND MAGNETIC RECORDING MEDIA

2 INTRODUCTION

This section describes the basic principles of magnetic recording. We describe the various formats commonly used to store information using magnetic recording technology, commenting specifically about the video 8 system, as this was used to perform the vast majority of the recording experiments studied in this thesis. We conclude this chapter with a description of the bulk magnetic characteristics required by all potential high density longitudinal magnetic recording media.

2.1 RECORDING PRINCIPLES

A basic information storage system must fulfill certain criteria. It must be able to store information over a significant period of time without this changing form, and it must also provide a method whereby the original information can be recreated accurately from the structure produced by the recording process.

2.2 THE BASICS OF MAGNETIC RECORDING

Magnetic recording involves the storage of information on a ferromagnetic material through the application of a magnetic field, and today this represents the most widely used method for the recording of information. In contrast to this there exist several different ways in which the input data can be reassembled from the recorded structure.

The different ways used to extract the information from magnetic recording materials rely on two distinct electromagnetic interactions. One technique involves sensing the fringe fields above the recording material, whilst the other measures the change in the polarisation of light scattered by the recorded magnetic structure.

2.2.1 RECORDING INFORMATION ON FERROMAGNETIC MATERIALS

Magnetic recording technology utilises the ability of localised magnetic fields to modify the magnetic state of ferromagnets. Introducing relative motion between these fields and the magnetic materials translates the temporal variations of the magnetic fields into a spatial variation of magnetisation within the medium. To achieve the highest recording density possible requires these magnetic fields to be concentrated into very small volumes of space. Localising a magnetic field into a small region of space is achieved through the indirect magnetisation of a device known as a 'recording head'.

A common type of recording head is the 'ring-head' arrangement, the main components of which are illustrated in figure 2.1. The signal to be recorded is passed along a wire which is wound around the ring shaped iron core. The current carried by this wire generates a magnetic field normal to the plane of the wire turns which magnetises the iron core, and this induced magnetisation propagates throughout the ferromagnetic volume of the ring. To generate the record field the magnetisation within the ring is deliberately disrupted by a small gap. Magnetic charges reside on either side of this gap which produce

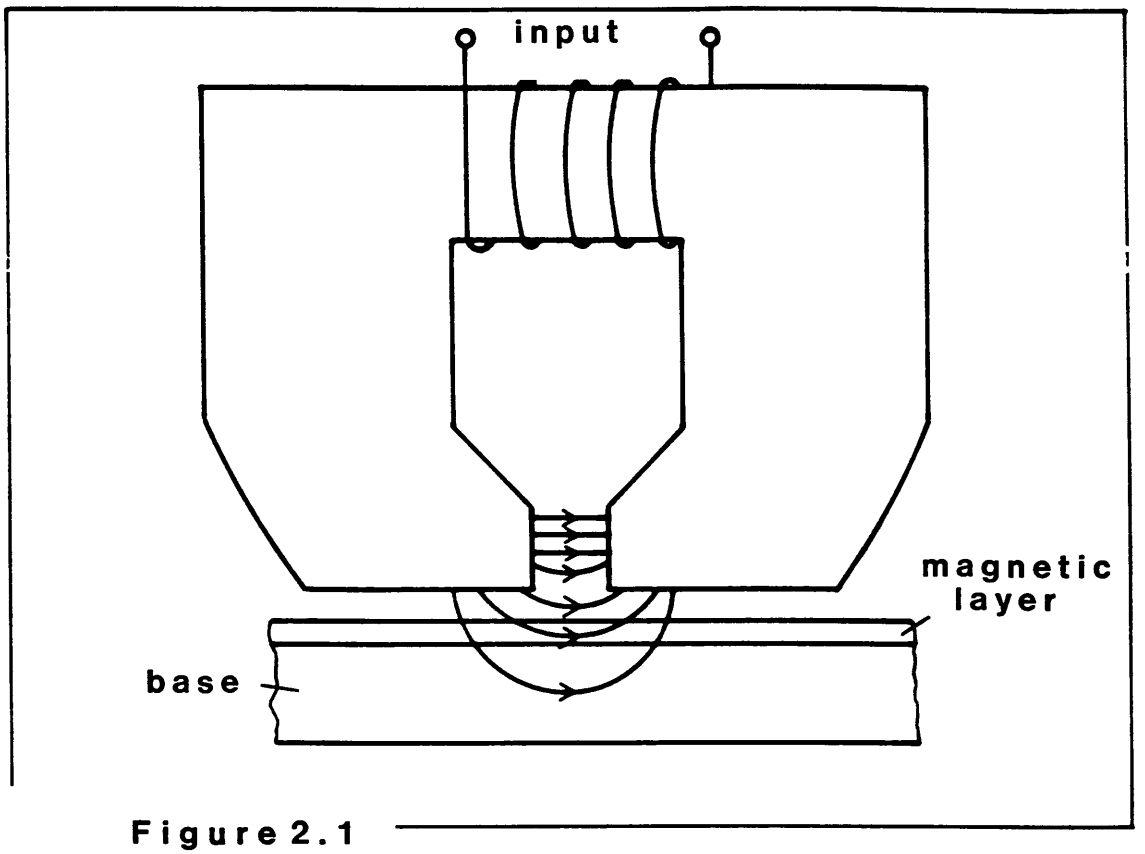

Figure 2.1

Ring type recording head

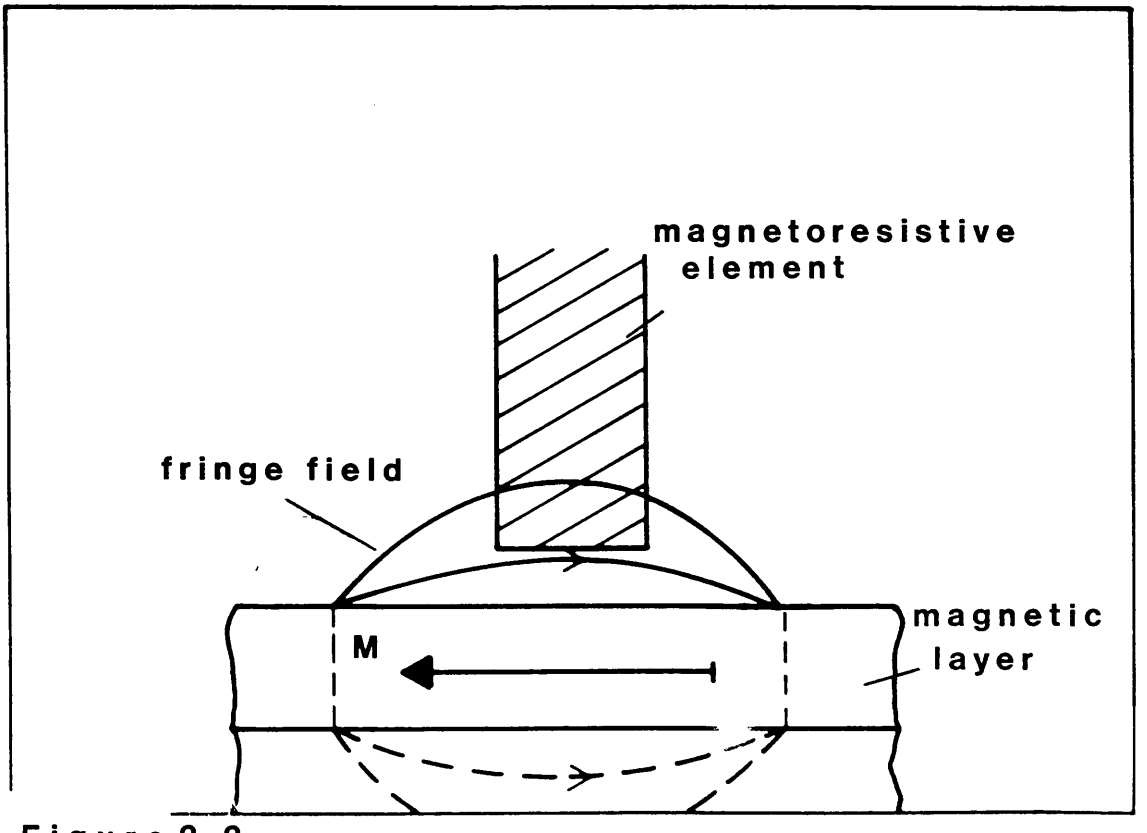

Figure 2.2

Magnetoresistive replay head

the localised magnetic field. This localised field around the gap region performs the same function as that of the current-induced field, only this field magnetises the ferromagnetic recording medium. In this way the input current variations are mapped onto the magnetic recording material.

2.2.2 INTERPRETING THE INFORMATION BY MEASURING THE STRAY FIELDS

Recreating the input by measuring the fringe fields above the recorded structure is in fact the inverse operation to the recording process as outlined above, in which the spatial variation of magnetisation is moved past the same small gap in the ring-head. This ring now provides a flux closure path for the stray fields emanating from the film to follow and it is these stray fields which are now responsible for magnetising the iron core. The variation of the magnetisation within the core produced by these fringing fields induces the output voltage signals which are detected. This process is analogous to that of recording but with the input and output roles reversed. To increase the output signal from these small stray fields on replay the number of wire turns around the core is maximised.

For an inductive head the output signal, ε, from the film is determined by Faraday's Law, which is given by

$$\varepsilon = - \frac{\partial \phi}{\partial t}$$

where 'ϕ' is the magnetic flux and 't' the time. The fixed

speed between the medium and the head means that the maximum voltage must arise from those regions where the flux varies most rapidly, ie $\Delta\phi$ is a maximum. This occurs at the transition region between oppositely magnetised domains, where the flux changes sign.

A different type of stray field sensor used to read the recorded information is the magnetoresistive head. This device relies on the change in resistance of a conductor when it is subjected to a magnetic field. Figure 2.2 is a schematic diagram of a magnetoresistive head. The Lorentz force produced by the stray field above the medium deflects the current carrying electrons and in so doing reduces the effective current flowing through the device. This interaction is observed as an apparent increase in the electrical resistance of the head. The resistance of the device increases from the nominal value as the fringe field above the recorded domains varies. The stray field drops to zero when above a recorded transition and thus, at these positions, the resistance of the head equates with the nominal zero field value. Unlike inductive heads these devices do not depend on the transition zone for maximum effect, and therefore the output from them does not suffer to the same extent from variations within these regions. The output from magnetoresistive heads depends only on the change in resistance and therefore on the magnitude of the magnetic field within which the device is immersed. Unlike inductive heads magnetoresistive devices do not depend on the rate of change of flux and hence do not require large head to medium velocities to increase the output signal.

2.3 FORMATS OF MAGNETIC RECORDING

2.3.1 INTRODUCTION

Today there are three formats used to store recorded information. These are analogue recording, frequency modulated recording and digital recording respectively. Analogue recording attempts to maintain the similarity between the input wave form and the magnetisation distribution which is produced when the signal is recorded. In this system both the phase and amplitude of the recorded magnetisation are important. Frequency Modulation of the input signal before it is recorded is another common method used. The advantage of this method is that higher recording densities can be used and also more than one piece of information can be recorded simultaneously within the same physical track. In this system only the position of the flux crossings are important in determining the form of the output. Lastly there is the system which removes all similarity between the input and recorded form, Digital Recording. The magnetic domain configuration which this system produces is almost exactly the same irrespective of the nature of the information recorded. Everything is represented as a sequence of binary digits, 'BITS', which the system alone can interpret.

2.3.2 ANALOGUE MAGNETIC RECORDING

When recording information in an analogue system it is the frequency of the input signal along with the head to tape

velocity which determines the size of the magnetic domains produced within the recording material. The accurate reproduction of any waveform using analogue magnetic recording requires two things. Firstly a strict linear relationship between the frequency of the input waveform and the linear dimensions of the domain pattern recorded within the material, and secondly that the amplitude of the output signal produced at a particular position of the film be representative of the flux density specific to that area.

Ferromagnetic materials are known to exhibit hysteresis and therefore magnetic recording materials cannot conform to these requirements unaided. However if the recorded signal has a high frequency waveform superimposed on it before recording then a dramatic improvement is made toward reaching these specifications. This additional signal is at a frequency well beyond that of the highest reproducible frequency sought, ie outwith the audible range when recording sound. The effect of this additional high frequency waveform is to improve the linearity between the frequency of the recorded signal and the dimensions of the recorded domains. This process achieves this by producing a recorded film which is composed entirely of very small magnetic domains, considerably smaller than those which produce the highest desirable frequency. The magnetisation resulting from an ensemble of these smaller domains is governed by the more slowly varying information-carrying signal. This procedure is known as AC biasing. In order that the areas of differing flux density should produce on replay comparable output signals, a frequency dependant amplification system

is used. This technique of variable amplification is known as 'compensation', or 'equalisation'.[3]

2.3.3 FREQUENCY MODULATED RECORDING

An increase in the recording density of ferromagnetic recording materials is possible if the stringent restrictions imposed by analogue recording, outlined above, are lifted. Such a recording system has been produced which relies on modulating the frequency of a carrier wave to store the information. In this system the form of the output depends solely on the number of flux crossings per unit length. Therefore an accurate representation of the input, as a sequence of flux crossings, merely requires accurate registration between the positions of the recorded transitions with the input. This can be accomplished providing the response of the write field can match that of the electrical pulses, and also that domains of sufficient extent are recorded when the most rapid system variations are being recorded. Conversion of these pulse count variations into the desired output is controlled entirely from within the electrical circuits of the recording machine and is thereby free from hysteretic effects. This is one of the techniques employed in video recorders allowing very high frequency variations to be recorded.

2.3.4 DIGITAL MAGNETIC RECORDING

Many of the problems associated with frequency dependent recording systems can be solved through digital encoding.

In this mode only two states have to be distinguished. These states are easily resolved and hence there is little chance of misinterpreting the measured signal, however the quality of the output does not depend on this alone. The output also relies on the accuracy with which the input analogue waveform is digitised and also the sampling interval Δt, see figure 2.3 for an explanation of these terms. This quantisation is performed by the microprocessor controlled circuitry of the analogue to digital converter (ADC). The detail with which the continuous wave is chopped is governed by the number of binary digits ('bits') available to the microchip. A sixteen bit system has a possible 65536 (2^{16}) distinguishable levels which is generally adequate for even the most sensitive of applications. To recover the input analogue signal the binary pattern is converted to a pseudo analogue form by the digital to analogue converter (DAC) and output to the amplification unit. In this binary recording system the ease with which the states are distinguished along with the inbuilt error correction techniques ensure excellent reproducibility.

2.4 MAGNETIC RECORDING LIMITATIONS - NOISE

The similarity between the input and the output in magnetic recording can be reduced through various processes. For instance when measuring the fringing fields above a recorded domain pattern it is essential that the head to medium separation remains constant throughout playback. Any variation occurring in this spacing can cause a significant change in the output

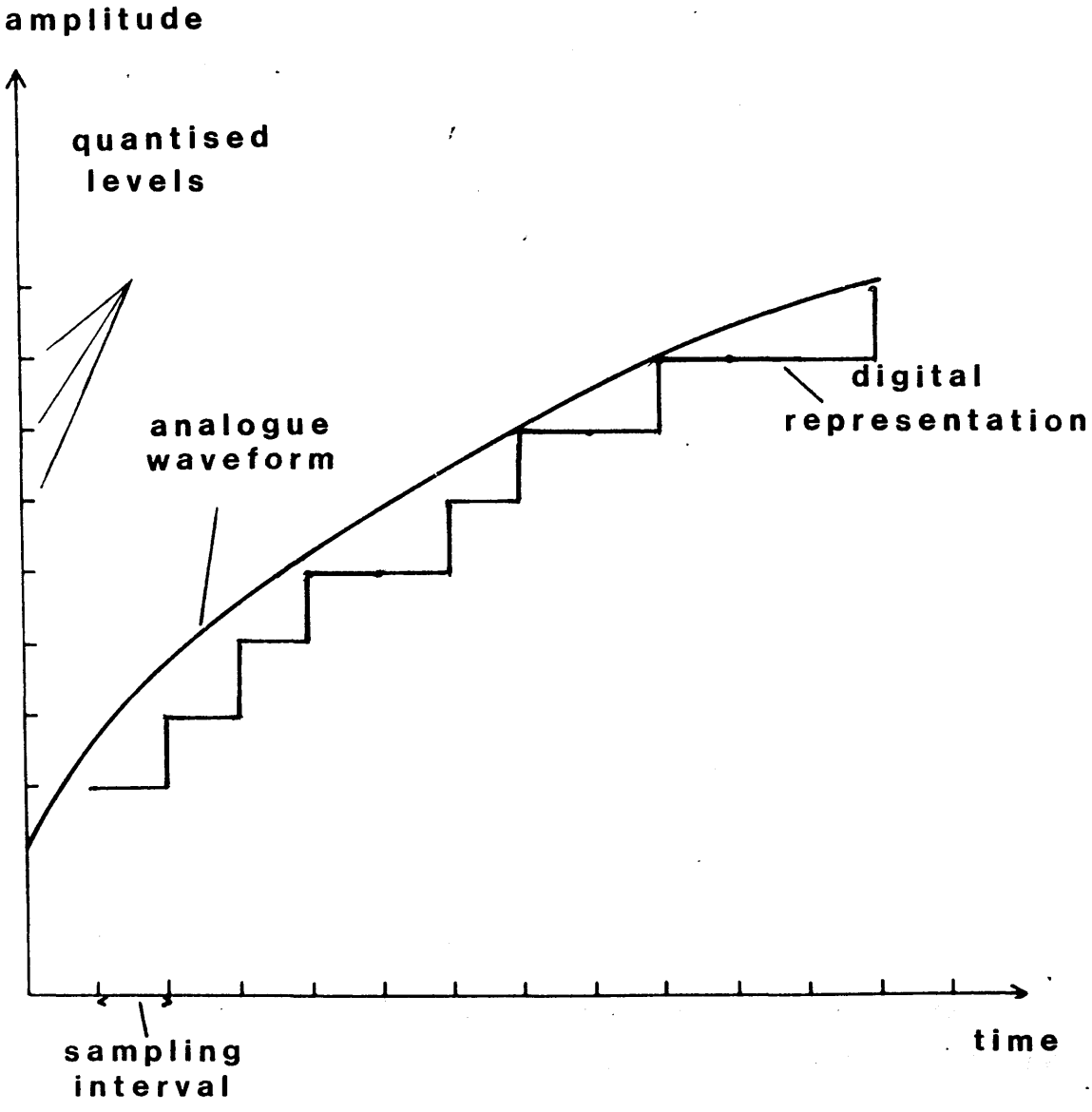

Figure 2.3

Basic principle of analogue to digital conversion

measured from these stray fields which could be mistaken for an actual signal. Increasing this distance during writing also causes problems as it reduces the field strength at the tape surface leading to the incomplete recording of information. Therefore it is essential that the surface of the magnetic recording material be smooth and clean. In systems which use contact recording, surface debris on either the head or the recording film often causes a spurious 'drop-out' in the output, however there are also more fundamental sources of noise which cannot be dealt with quite so straightforwardly as these.

When a varying signal is recorded onto a ferromagnetic material it leaves on it a series of magnetised domains. When using an inductive head the subsequent maximum output measured from these recorded films comes from the region of most rapid flux change, at the domain boundary wall where the flux passes through zero. Clearly, therefore, the form of the domain wall is critical in determining the output signal which is measured. In an ideal system the domain wall would be perfectly straight and lie parallel to the gap within the ring head. This would allow the maximum flux change to occur in the shortest distance possible and therefore yield the maximum output voltage possible. The bulk magnetic characteristics required for potential high density magnetic recording materials however make such a wall form energetically unfavourable. Even for an isolated transition the competing exchange, anisotropy and magnetostatic energy contributions make for a saw-tooth like wall structure across the width of the recorded track[1]. This type of transition structure increases the

length of the domain wall and therefore increases the exchange energy contribution. The anisotropy term is also increased due to the increased angular variation of the magnetic vector in the vicinity of the zig-zag wall. These increases are balanced by the reduction in the magnetostatic energy which accompanies this type of boundary structure. The magnetostatic energy depends on the surface density of magnetic poles and by increasing the area over which these poles are spread the contribution from it is diminished. The effect of this zig-zag wall is to increase the distance over which the flux changes sign and hence, since Δt increases without $\Delta\phi$ changing, it reduces the output. When recording at higher frequencies these zig-zags begin to interfere with one another to produce reversed domains within recorded 'bits'. In this situation the effect of the zig-zag transitions is again responsible for a reduction in the output signal measured. At these densities the individual zig-zags overlap and interfere, modifying the magnetisation distribution within each written 'bit' by producing regions of reversed magnetisation which reduce the net flux change.

At high frequency where the dimensions of the recorded wavelength approach those of the zig-zags other noise mechanisms appear which can alter the form of the output. The detailed form of the adjacent domain walls becomes important as it can lead to either an enhancement or a reduction of the signal measured from the central flux crossing. In addition to reducing the output it is also possible for this type of domain wall structure to remove any periodicity that may have been present in the

input waveform by randomly shifting the position of the output voltage peaks.[5]

Noise can also arise from the previous magnetic state of the film such as that due to the incomplete erasure of a previous recording. There are also side-writing effects, which arise from the write field extending beyond the recorded track, producing effects at the track edge which the reproduce head 'picks up'. Print-through is a problem specific to magnetic recording tapes and arises from contact with another magnetic layer. These numerous sources of noise which degrade the output signal form, in addition to the electronic noise specific to the recording instrument, must all be taken into account when designing a high density magnetic recording system.

2.5 TELEVISION PICTURE BROADCASTING

Television pictures broadcast in the UK are refreshed 50 times every second and are each composed of 625 horizontal lines. To reduce the frequency bandwidth necessary to transmit these 625 lines within this short time interval, each picture is broken down into two separate fields. One field comprises all of the odd numbered lines (1,3,5...) while the other holds all the even numbered lines (2,4,6,...). These fields are interlaced together to produce the observed picture and thus the refresh rate is halved, allowing a lower bandwidth system to be used. A video recorder attempts to replace the source of electromagnetic waves received by the television antenna and consequently this machine must be able to operate at data transmission rates comparable with these.

The programme of research described in this thesis was devoted to examining recorded patterns produced by the video 8 system and hence only this system will be described

2.6 THE VIDEO 8 RECORDING SYSTEM

Substantial technological advances in both magnetic and semiconductor material fabrication processes have made the development of a new miniaturised video recording system possible. This new system employs much of the established video technology, but in a reduced spatial form, and additionally incorporates some new sophisticated features.

The first satisfactory television picture to be produced by a video machine was accomplished using a twin head helical scan recording format in 1969 and this remains the same method employed in the modern video 8 machines produced some 20 years on. This system attains the required data transmission rates through the ability to produce a high relative head to tape velocity. Instead of a high linear tape speed, which can cause severe problems, particularly with magnetic tapes, these systems provide high effective writing speeds by employing a rotating head assembly. This records across the tape, instead of along it, and in this way the linear speed of the tape is dramatically reduced. The limit for the linear tape speed is controlled by the trackwidth and the head rotation speed, since the second head must not interfere with the previous recorded track. One of the error correction procedures, to be detailed later in this section, is considerably more demanding about the linear

tape speed at which these systems operate. The angle across the tape at which the recording track is written, must ensure that the diagonal portion of tape is at least as long as half the head drum circumference. The width of the tape is therefore also important in establishing the correct recording angle. In the 8mm video system the tape is wrapped at an angle around a cylindrical head assembly. The outcome of this helical arrangement of the tape around the head drum is to produce recorded tracks which lie at 5° with respect to the direction of tape travel, each of sufficient extent to store half a picture frame, ie 312.5 lines. This cylindrical drum has two heads, situated diametrically opposite one another, and one flying erase head located midway between these. All three heads are of the inductive type described earlier. The length of these recorded video tracks ensure a stable picture display since the head switching occurs during the vertical blanking period, between successive field transmissions. The 8mm video format produces a recorded pattern of the type indicated in figure 2.4.

The video 8 system can store up to 2 hours of video information onto a cassette which is comparable in size to a standard audio cassette. It achieves this performance by recording without separate head guidance tracks and reducing both the trackwidth and the head gap. This meant that either magnetic films of improved bulk magnetic characteristics, or a recording system of increased sensitivity, needed to be developed for this new format of video recording. Indeed the reduction in component size accentuated the problems associated with maintaining a constant head-medium interface environment and far more

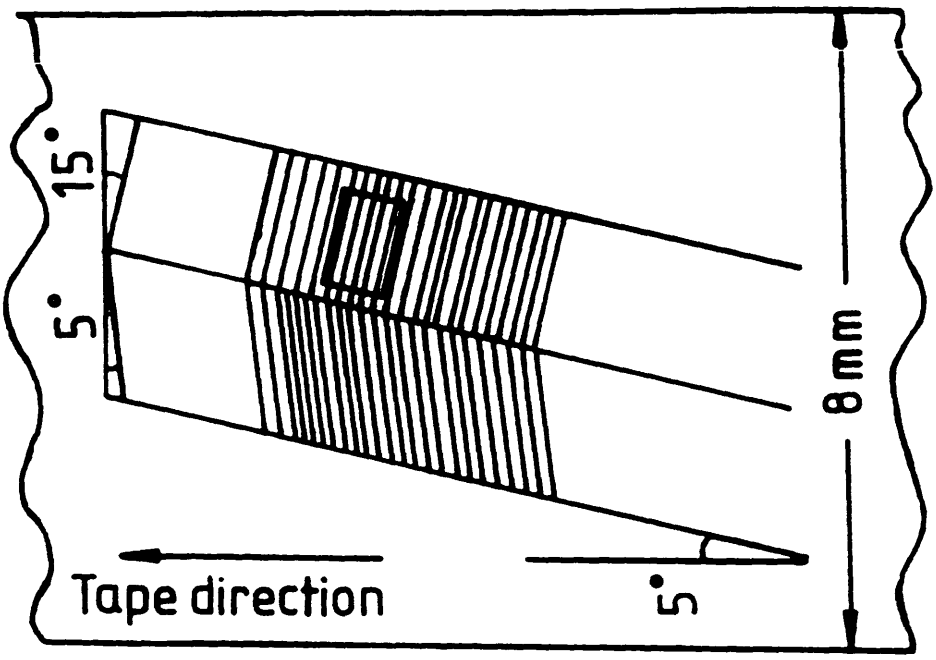

Figure 2.4

8mm video recording format

elaborate error detection and correction schemes had to be incorporated, see appendix 1.

2.7 LONGITUDINAL MAGNETIC RECORDING MEDIA

The quest for ever increasing magnetic storage densities imposes tight restrictions on the bulk magnetic characteristics of any prototype recording media[6]. Unfortunately none of the elemental ferromagnets meet these requirements and alterations to both their physical and magnetic structure have to be made to render them suitable. The bulk magnetic characteristics of a magnetic material are contained within it's hysteresis loop curve. one such curve is illustrated in figure 2.5 along with other important quantities, specific to magnetic recording, derived from the loop. For a ferromagnetic material to be considered for high density magnetic recording applications it must possess at least three suitable bulk magnetic characteristics. Firstly the material should have a high remanent magnetisation M_r. This reflects the ability of the material to maintain the direction of the magnetisation parallel to that of an applied field once this applied field has been removed. Producing a material which supports a high remnant magnetisation can be achieved in two ways. The material can either be magnetically isotropic or exhibit a pronounced magnetic anisotropy, providing of course that this anisotropy is parallel to the direction of the applied field. The advantage offered by a highly anisotropic material is that smaller volumes of the sample are capable of producing detectable signals and hence

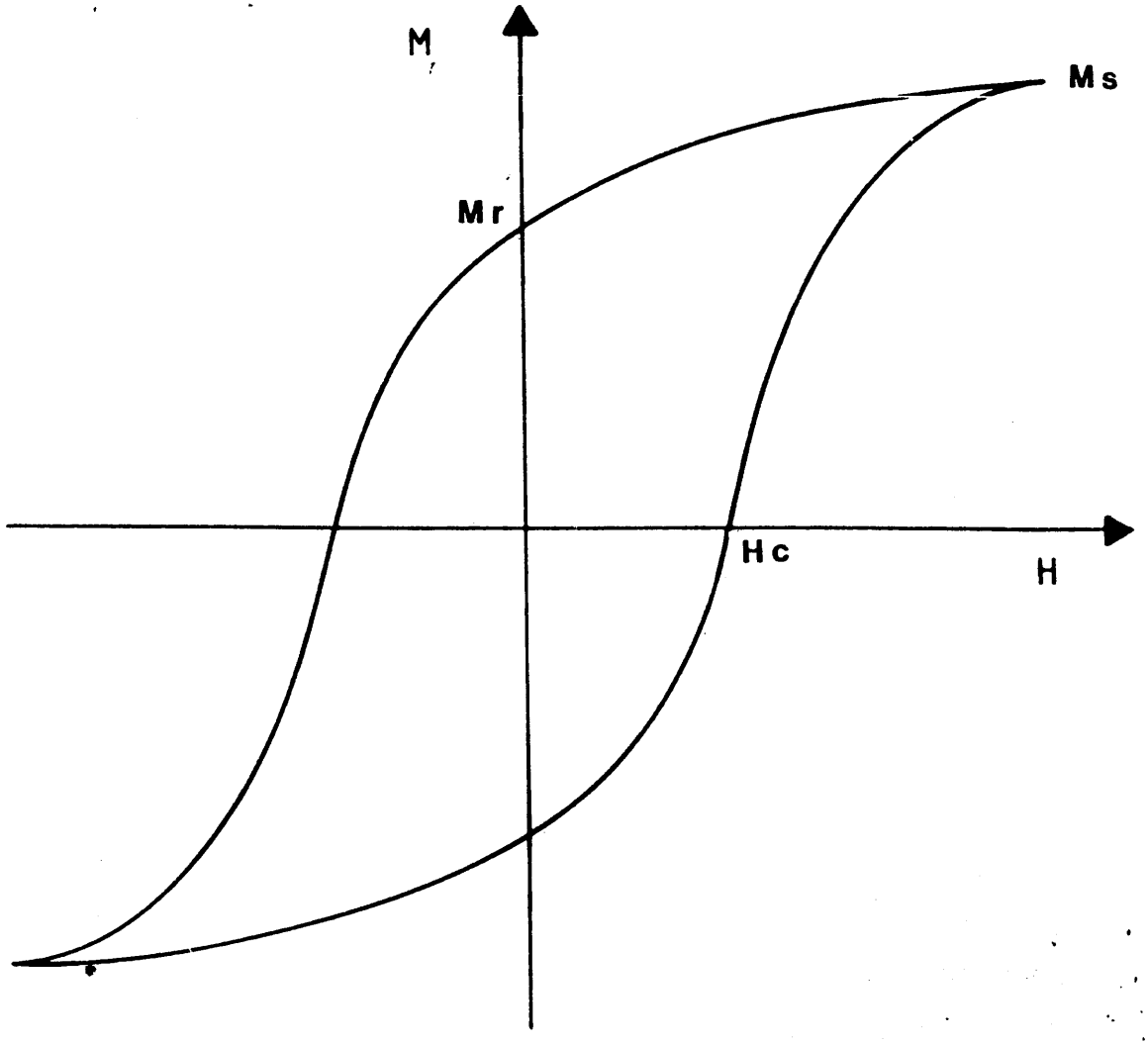

Figure 2.5

Hysteresis loop

offer the possibility of increased recording densities over the isotropic media.

Secondly a high coercivity, H_c, is necessary if high density applications are intended for the material. The coercivity is the magnetic field strength required to reduce the magnetisation from the remanent level to zero. The bulk coercivity of a material indicates the ease with which domain walls may move throughout the sample volume, and is therefore increased by factors which restrict this motion such as non magnetic regions. The magnetostatic interaction between oppositely magnetised domains tries to reorient the written magnetisation once the head field has been removed, and in so doing effects a reduction in the output level. A large coercivity, as well as magnetic anisotropy, helps ensure that these effects are balanced close to the direction of recording. A large coercivity also preserves the integrity of the recorded magnetic structure from reorientation by any stray fields.

Lastly the material must have a steep sided hysteresis loop a measure of which is obtained from two quantities S and S^*. S is the squareness ratio and measures the ratio of M_r to M_s. S^* is the coercivity squareness and indicates the fraction of the film coercivity, H_c, which the applied field must exceed if the film is in fact to return to zero remanence, allowing for the demagnetising effect. This loop squareness reflects the dynamic switching behaviour of the magnetisation within the material. A hysteresis loop with steep sides is indicative of a material with a magnetic anisotropy which is uniform throughout the bulk. It suggests this as only a narrow range of field strengths are required to effect a

change in the bulk magnetisation direction. Thus the magnitude of the forces responsible for maintaining the magnetisation locked in position must be identical throughout the whole material. Following on from this the steeper the slope the narrower the transition zone between oppositely magnetised domains which, in turn, increases the output signal and allows for the possibility of higher recording densities.

A magnetic recording material should therefore possess a rectangular shaped hysteresis loop, and the loop shape is used to assess the applicability of potential candidates from a quick examination of the curve.

SUMMARY

In this section we have described the basic principles of magnetic recording and outlined the three basic formats used to store the information. We detailed the requirements imposed on video machines in order that they are capable of data transmission rates comparable with television broadcasting and commented on the way in which the video 8 system addresses them. We concluded this section with a brief description of the physical and magnetic characteristics which potential high density recording media must possess.

REFERENCES

1. W. Rave *et al*, J. Magn. Magn. Mat., **65**, 7, (1987)

2. J. Dillon Jr, J. Appl. Phys., **29**, 1286, (1958)

3. W. Westmijze, Philips Res. Rep., **8**, 245, (1953)

4. D. Dressler, J. Judy, IEEE Trans. Magn., **MAG 10**, 674, (1974)

5. N. Belk *et al*, IEEE Trans. Magn., **MAG 21**, 1350, (1985)

6. I. Suzuki, IEEE Trans. Magn., **MAG 20**, 675, (1984)

CHAPTER 3 ELECTRON BEAM/SPECIMEN INTERACTIONS

3. INTRODUCTION

As the investigation of the physical and magnetic microstructure of the metal evaporated films was conducted by electron microscopy a brief description of the modes of microscopy used to determine this microstructural information, along with an explanation as to why it provides such information, is given.

3.1 ELECTRON SCATTERING

Scattering from an isolated atom can modify the momentum state of an incident electron; however there is also a finite probability that it may pass the charge assembly undeviated and without loss of energy. Scattering without loss of energy is termed elastic scattering and in the majority of cases this occurs when the incident particles are deflected by the nucleus of the target atoms. Scattering in which there is an associated loss of energy is termed inelastic scattering, and most frequently arises when the incident electrons are involved in interactions with the atomic electrons. The amount of energy lost during an inelastic scattering event by the impinging particles can be used to determine the composition of the target. The transfer of energy from the incident electron normally leaves the target atom in a highly excited state which subsequently relaxes with the emission of characteristic x-ray photons and also Auger electrons.

X-rays may also be generated as the electrons are decelerated by the intense Coulombic field which surrounds the nucleus. This type of radiation is known as 'Bremsstrahlung' and provides little information about the nature of the target atom. However when quantitative x-ray analysis is performed the photons produced by this mechanism must be removed from the x-ray spectrum[1].

When the target is a collection of atoms, such as a solid bulk specimen, these simple processes outlined above can be undergone repeatedly by each incident electron as it travels through the specimen volume. Indeed, besides this multiple scattering complication, the discrete nature of the electronic states change in a solid, becoming mixed with those of adjacent atoms to produce continuous energy bands. The availability of a continuum of energy states enables the incident electron to lose a wide range of energies. Due to these differences and the effect on the secondary scattering processes the output x-ray spectrum from solids contains photons with a wide range of energies. In contrast to scattering from an isolated atom in which the primary electron can effect two distinct processes, ionisation and Bremsstrahlung radiation generation, scattering from a solid provides three additional energy loss mechanisms. Interacting with the electronic band structure results in the production of plasmons and secondary electrons. The secondary electrons are produced when the incoming particle ejects a loosely bound electron, and plasmons result from the incident electron exciting waves within the electron density distribution surrounding the ion cores. The third

additional energy loss event when scattering from a solid target results in the generation of phonons. These phonons are produced when the solid target absorbs a small amount of energy (<0.1eV) from the incident electron which sets up lattice vibrations. The frequency with which each of these five principal scattering processes are undergone depends on the relative probability of each individual mechanism. These probabilities are generally written in the form of 'cross-sections'. The theoretical determination of these 'cross-sections' presents considerable difficulties as the wave-function describing the complete system must be known. Substantial progress has been made in calculation of the cross-sections for inner-shell interactions since the tightly bound electrons are well shielded from the influence of the surrounding atoms and therefore these have little effect on the structure of the core electron states.[2] Although there are numerous energy removal processes, and additional plural scattering complications within a solid, the sharp onset of the inelastic inner-shell scattering cross-sections enables compositional information from such targets to be obtained.

The spatial distribution of the atoms within the sample modulates the elastic scattering events providing additional information. From such diffraction effects it is sometimes possible to determine the separation distance and also the spatial arrangement of the constituent atoms of the film. This effect is described by the familiar Bragg Law:

$$2d_{hkl}\sin(\theta) = n\lambda$$

where d_{hkl} is the interplanar separation distance , λ the electron wavelength ,θ the angle of reflection and n an integer. Thus the crystal structure of the specimen and the wavelength of the illumination govern the form of the electron diffraction pattern.

3.2 MAGNETIC INTERACTION

Classically a particle of charge q with velocity $\underline{v}$ in a region of magnetic induction $\underline{B}$ experiences a force $\underline{F}$, which is given by

$$\underline{F} = q\ \underline{v} \times \underline{B}$$

From this equation it is seen that the force is perpendicular to the plane defined by the particle velocity and the magnetic induction. This is the Lorentz force and this gives rise to the name used to cover the branch of electron microscopy devoted to the study of magnetic structures, namely 'Lorentz Microscopy'. This branch of electron microscopy utilises the modulation of the electron trajectories introduced by the magnetic effect to provide details of the micromagnetism within the irradiated sample. This classical description permits an explanation for the contrast produced within each of the magnetic imaging modes within the electron microscope except holography. If however the fine detail observed in certain instances is to be explained then recourse to the quantum mechanical description of the interaction is necessary.

The wave mechanical description of this effect was first treated by Aharanov & Bohm (1959)[3] who stated that the relative phase change, Δ, between two electron waves originating from the same point is given by

$$\Delta = \frac{2\pi}{\lambda}(l_1 - l_2) + \frac{e\Phi}{\hbar}$$

where Φ is the magnetic flux enclosed by the electron trajectories, e is the electronic charge, λ is the electron wavelength, $\hbar$ is Planck's constant divided by 2π and l_1 and l_2 are the physical lengths of the two electron paths. Therefore if no magnetic induction, or more correctly no vector potential $\underline{A}$ ($\underline{B} = \nabla x \underline{A}$), exists within the region bounded by l_1 and l_2, and furthermore should $l_1 = l_2$, then the initial phase relationship within an electron wave is maintained. The application of this description to the study of thin film magnetic structures within the electron microscope is based on the assumption that any phase excursions introduced by internal components of the microscope are equal for each incident electron, and also that the geometrical path difference, $l_1 - l_2$, between electron waves is negligible. These assumptions reduce the above equation to the following :

$$\Delta = \frac{e\Phi}{\hbar}$$

3.3 THE ELECTRON MICROSCOPE

An electron microscope consists of five basic elements :

1. An electron source.
2. The pre-specimen lenses.
3. The objective lens.
4. The post-specimen lenses.
5. The detection system.

3.3.1 ELECTRON SOURCES

The CTEM and the STEM generally aim to use as small an effective source of electrons as possible as this is beneficial for achieving high contrast, high resolution images and therefore it is essential that all available steps are undertaken to minimise the physical dimensions of the electron source. The electron source is known as the 'Gun' and this is designed to provide maximum emission current density with the energy of the emitted particles confined to the narrowest possible range.

In electron microscopy the figure of merit used to gauge the relative performance of different types of electron source is the 'Brightness'. This is defined as the current density per unit solid angle. The significance of this quantity can be appreciated when consideration is given to the widely different imaging conditions utilised when conducting a complete specimen characterisation by electron microscopy. This figure enables the current densities incident on the specimen to be determined for

the different modes of microscope operation and therefore allows the overall suitability of the gun to be measured. Brightness is conserved throughout the microscope and can only be altered by changing the accelerating voltage.

Two widely used ways of extracting electrons from the 'tip' region of the gun are 'Thermionic Emission' and 'Field Emission' respectively. The names refer to the treatment given to the tip to effect electron production.

Supplying energy to the filament in the form of heat promotes a certain fraction of the bound electrons to energy states above the fermi level. These excited electrons are therefore capable of leaving the host material. The current produced by thermionic emission, J_{TH}, obeys the Richardson equation which is given by

$$J_{TH} = AT^{2} \exp\left(-\frac{\phi}{kT} \right)$$

where A is a constant, T the temperature, k Boltzmann's constant and ϕ the work-function. Increasing the brightness for thermionic emission usually involves heating an electron source material of lower work function, eg LaB_6. These sources normally produce electron beams with an energy spread of ~1.5eV.

Increased brightness electron sources are produced using the field emission extraction procedure. This type of source produces higher current density and reduces the emitted energy spread to <.5eV. These tips achieve better performance as the emission occurs from a very small effective tip area which is subjected to an intense electrostatic field. These fields distort the form of the

potential barrier at the surface of the filament material, lowering this and thereby increasing the probability of electrons tunneling from within the solid. The fine control of the electrostatic field modifying the potential barrier around the filament enable field emission guns (FEG) to produce beams of very narrow energy spread. The current emission for a FEG, J_{FE}, is given by the Fowler-Nordheim equation which is

$$J_{FE} = AE^{2} \exp\left(- \frac{B\phi^{\frac{3}{2}}}{E}\right)$$

where A & B are constants, E is the electric field strength and ϕ the work-function for the tip. The excellent emission characteristics possible with this type of gun are further enhanced by using suitably oriented crystal filaments. The <310> face of a tungsten single crystal can enable production of beams spread in energy by as little as 0.25eV.[4] Electron microscopes which have field emission sources must maintain very high vacuum around the gun. The presence of unwanted particles would severely limit the lifetime of a field emission tip since the intense electrostatic field around this would accelerate the ions and result in damaging collisions.

3.3.2 THE CONVENTIONAL TRANSMISSION ELECTRON MICROSCOPE (CTEM)

There are generally two lenses between the electron source and the specimen in a CTEM. This arrangement allows for

considerable flexibility in illumination which is required for the vast magnification range of these machines (100X - 500kX). The first 'Condenser' lens increases the coherence of the illumination by compressing the electron distribution produced by the source. The maximum workable coherence is dictated by a combination of the lowest current level capable of being measured by the detection system and by the lens aberrations, which will be dealt with in more detail later in chapter 5. Further adjustments to the intensity profile of the illumination are achieved using field limiting circular aperture blades.

The principal lens of a CTEM is the objective lens. This lens produces the first image of the specimen and the subsequent lenses cannot improve this image. Therefore this lens is manufactured to the highest specifications having the lowest coefficient of spherical aberration and fewest defects, since only then will this produce the most easily interpretable image of the specimen. ie that which contains contrast which can be attributed to interactions with the specimen alone. The specimen plane lies within the magnetic field of the objective lens. The top portion of this field can be considered as part of the condenser system since this portion of the field acts to modify the illumination incident on the specimen. The modified electron intensity distribution, arising from the various elastic and inelastic scattering events within the specimen volume, is transferred to the final viewing screen via the post-specimen lenses.

Observation of the electron diffraction pattern is

achieved by adjusting the current within the first post specimen lens situated after the objective, the first intermediate lens. The object plane of this lens is displaced until it coincides with the back focal plane of the objective lens, where the diffraction pattern lies. The other magnetic lenses expand this distribution until the required detail becomes observable, subject to the angular resolution limit of the system.

In the standard imaging mode of electron microscopy it is the unscattered cone of electrons, known as the zero order beam, which is transferred to the magnifying lenses to be displayed. This is referred to as 'Bright-Field' imaging. In addition to those electrons unscattered by the specimen this cone contains electrons which have been inelastically scattered and those only shifted in phase. It is possible to pass other cones from the diffraction pattern to the magnifying lenses to produce images whose contrast arises from areas within the sample of different crystal orientations. This is accomplished by shifting the diffraction pattern within the back focal plane of the objective lens using deflection coils. In this way any of the diffracted spots can be moved onto the optic axis replacing the zero order spot for the purposes of imaging. This is referred to as 'Dark Field' imaging.

In the majority of imaging modes the objective lens is excited. However when we are interested in imaging magnetic structure present within the sample it is normally essential that the objective lens be switched off, otherwise its high magnetic field strength will completely saturate the specimen and erase any magnetic

structure present. This normally limits the performance of the magnetic imaging mode since the first intermediate lens must assume the role of objective lens and the maximum image magnification is seldom >5kX. However at Glasgow a new CTEM with a specially designed objective lens pole piece has been purchased which ensures that the specimen resides in field-free space but still permits magnetic investigations at magnifications of up to 200kX to be carried out. This CTEM will be discussed in more detail in chapter 7.

3.3.3 THE SCANNING TRANSMISSION ELECTRON MICROSCOPE (STEM)

In a STEM a focused probe of electrons is scanned over the specimen in a raster like manner. The convergent illumination in this type of microscope is in direct contrast to that found within a CTEM. Imaging is accomplished by allowing the scattered probe to impinge on an electron detector. At each point within the scan it is the current level striking the detector which dictates the contrast level of the image. In a STEM the overall magnification is controlled by the ratio of the dimensions of the viewing screen to those of the beam scan across the specimen. Therefore altering the magnification does not change the current in the focussing lens and hence once the optimum focus has been established this remains so irrespective of the magnification. This method of magnification also means that equal currents strike the detector at different magnifications which is in stark contrast to the CTEM, in which we reduce the electron

intensity striking the detector as we increase the magnification. In normal bright and dark field operation a STEM does not employ descanning to shift the emergent scattered probe back onto the optic axis. Removing the systematic shift of the probe in normal imaging is unnecessary because the rocking point of the electron beam and the detector plane are conjugate. Imaging modes which require large distances between the specimen exit plane and the detector, ie long camera lengths, such as DPC, are particularly demanding of this criterion and hence in these situations it is necessary to remove the systematic motion of the probe. The significance of removing this will be mentioned later in chapter 4. The camera length and the probe forming angle, α, dictate the size of the detector area intersected by the emergent electron distribution. Together these parameters allow some flexibility in the signal levels produced by the detector.

The bright field detector is centred on the optic axis and surrounded by the dark field detector. The standard mode of operation of the STEM therefore allows both bright and dark field images to be formed simultaneously although the dark field image is somewhat different from that obtained within a CTEM. The dark-field detector in a STEM collects all of those electrons within the annular region of the detector, which have been scattered outwith the zero order beam and therefore these all contribute to the dark field image. It is however possible to shift the scattered electron distribution until the desired diffraction spot replaces the zero order beam on the bright-field detector surface by means of the 'Grigson

Coils'. This enables the same dark field images formed within a CTEM to be produced within the STEM. There is in fact a general rule based on the principle of time reversal, which states that any image formed within a CTEM can also be formed within a STEM providing inelastic scattering effects can be neglected.[5]

3.3.4 FACTORS AFFECTING THE ATTAINABLE RESOLUTION OF AN ELECTRON MICROSCOPE

Even if a point source of monochromatic illumination were used the complete elimination of the effect of lens aberrations would still be impossible. The finite energy spread of the electron beam as it leaves the source leads to an increase in the size of the first crossover, as beams of different energy have different focal lengths. Instabilities in the HT and also the lens currents further complicate the issue. This type of energy dependant aberration is known as 'Chromatic Aberration'. 'Spherical Aberration' results from off axis rays having different focal points to those which originated on the optic axis, the exact difference being a measure of just how far off axis the rays originally were. These off axis rays arise because of the finite angular acceptance range of the microscope lenses. Often lenses are of imperfect construction and the requirements of cylindrical symmetry and field homogeneity are not fulfilled. This manufacturing fault leads to another type of lens aberration known as 'Astigmatism' which is normally rectifiable using additional electrostatic lenses known as

stigmators. Most lenses within an electron microscope are magnetic lenses and therefore subject to hysteresis which provides one other source of concern.

3.4 LORENTZ ELECTRON MICROSCOPY - MAGNETIC CONTRAST GENERATION MECHANISMS

In this section the discussion will be restricted to only those magnetic imaging modes used throughout the course of this work. Two different types of electron microscope were employed to conduct these investigations. Small Angle Diffraction (SAD), the Fresnel mode and the Foucault mode were carried out on a Conventional Transmission Electron Microscope (CTEM), whilst Differential Phase Contrast (DPC) imaging was conducted on a Scanning Transmission Electron Microscope (STEM). A more detailed description of these can be found in reference 6.

3.4.1 GENERATING MAGNETIC CONTRAST WITHIN A CTEM

3.4.1.1 Small Angle Diffraction (SAD)

Consider the hypothetical situation illustrated in figure 3.1 in which a parallel electron beam is incident on a thin ferromagnetic film within which lie two anti-parallel magnetic domains. Those electrons which pass through the domain magnetised into the plane of the page are deflected to the left whilst those on the other side of the domain wall are shifted towards the right. Therefore when these deflected electrons are subsequently brought to a point

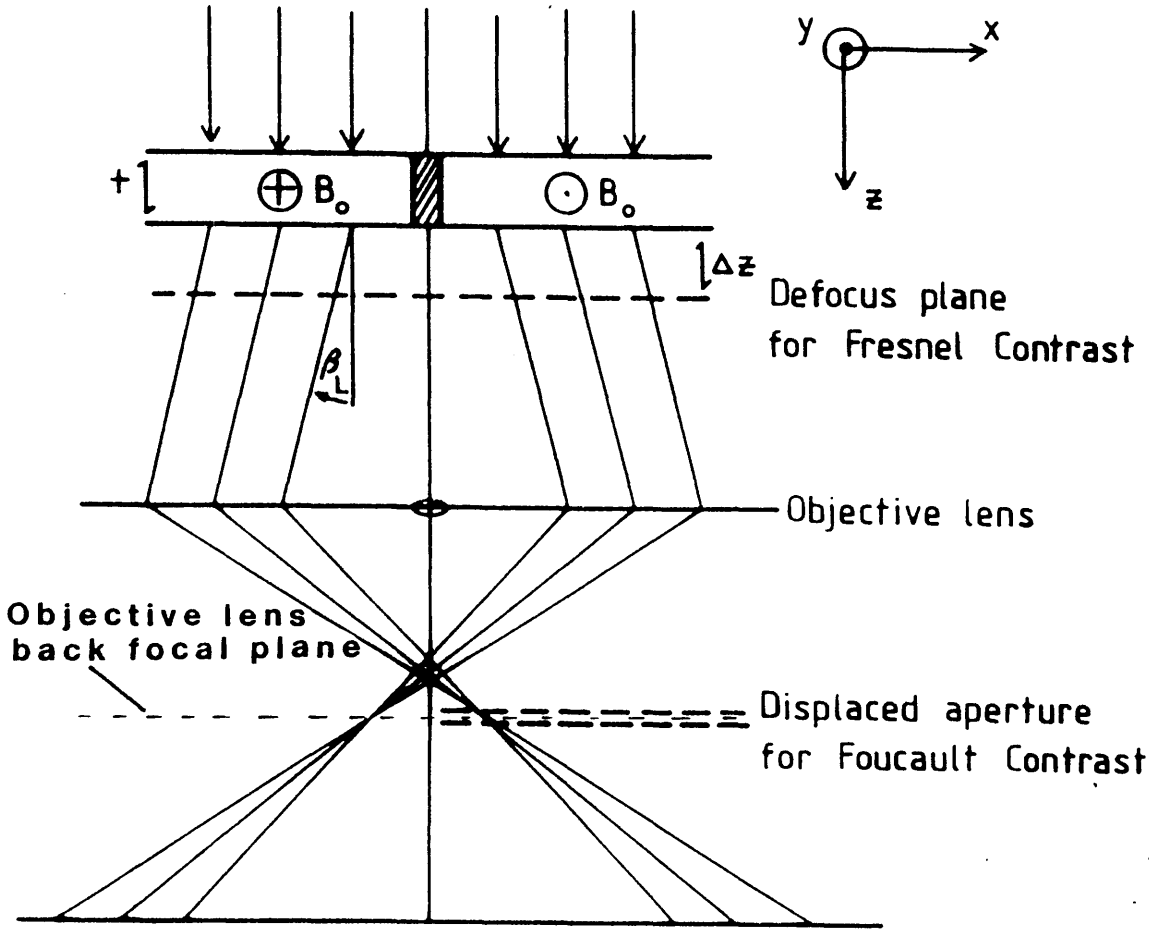

Figure 3.1 The various ways of producing magnetic contrast in a CTEM

focus, such as within the back focal plane of the objective lens, two separate spots will be formed, whereas in the absence of any specimen there was only one. The imaging of these split spots is termed 'Small Angle Diffraction' (SAD) on account of the very small angular deviation introduced by electron transparent ferromagnets, eg for a foil 50nm thick with saturation induction B_s = 1 T and 100keV electrons, β_L = 0.06mrad. To resolve such small angular deviations requires the effective distance between the specimen exit plane and the plane of observation, ie the 'Camera Length', to be ~100 metres. It should be made clear that this magnetic spot splitting is present in all of the diffracted spots, not merely the zero-order spot. From the simple example illustrated it should be clear that it is a straightforward matter to extract micromagnetic information from the distribution of electron intensity to obtain details of the magnetisation within the region of sample analysed. Quantitative analysis is possible using SAD if the undeviated beam can be imaged simultaneously, or recorded onto the same photographic plate, and also providing no other sources of deflection are present.

The next method of magnetic contrast generation to be described is the 'Foucault' method, since the progression from SAD to this mode of magnetic imaging is the most straightforward

3.4.1.2 The Generation of Foucault Contrast

In the 'Foucault' mode the modified zero-order beam is intercepted by an electron opaque object. The careful positioning of this obstruction over certain portions of the modified electron distribution limits the electrons capable of contributing to the final image. The result of this is to 'darken' those areas of the specimen with a particular magnetic vector orientation. In the model example illustrated in figure 3.1 the positioning of the obstruction over one of the two spots would produce an image in which one magnetic domain appeared brighter than the background intensity and the other darker. The presence of a background intensity in the final image is due to electrons having suffered only slight magnetic deflections, such as those passing in and around the domain boundary wall region and those inelastically scattered electrons which also evade the obstruction. Continuous magnetisation distributions, found in real ferromagnetic films, produce a continuous range of Lorentz deflection angles. Correspondingly the SAD pattern is a continuous distribution of electron intensity.

The third CTEM imaging mode used to provide micromagnetic information from the thin films was the 'Fresnel' method. To understand the relationship between the sample magnetisation and the image contrast variations which it generates requires a deeper appreciation for the electron optical arrangement present in normal bright-field imaging.

3.4.1.3 The Generation of Fresnel Contrast

In the standard mode of operation the lens current of objective lens is adjusted so that the specimen plane and the object plane of the objective lens coincide. This is the situation which provides a magnified 'in-focus' image of the specimen. The 'Fresnel' mode reveals the micromagnetic structure of the specimen by adjusting the position of the object plane of the imaging lens away from the 'in focus' condition. The result of this is that it is now the Lorentz modified electron distribution which lies within the object plane, and this modified pattern is magnified and displayed on the phosphor viewing screen. This modified electron distribution is essentially the 'Fresnel' diffraction pattern of the specimen, hence the term given to this imaging mode. Considering figure 3.1 once again, adjustment of the intermediate lens current to move the position of the object plane beneath the specimen would produce regions of reduced electron intensity around the domain wall. If the focal plane is moved above the specimen then these electron rich areas appear electron deficient. Therefore the 'Fresnel' mode reveals the position of domain walls as either a series of 'bright' or 'dark' lines. The terms 'Convergent' and 'Divergent' domain wall are used to describe those which bring electrons together or spread them apart. A convergent domain wall may appear divergent if one moves the object plane of the imaging lens from below the specimen plane to above it, and vice versa.

The image contrast produced by the 'Fresnel' mode

cannot be completely understood on the basis of the classical description of the beam-specimen interaction detailed earlier. Providing the illumination is sufficiently coherent close scrutiny of the convergent domain walls reveals an internal structure comprising a series of peaks the origin of which can only be explained if the wave-mechanical approach is adopted.

3.4.2 GENERATING MAGNETIC CONTRAST WITHIN A STEM

The electron distribution incident on the specimen within the STEM is considerably different from that within the CTEM. In the STEM a focused probe of electrons is scanned in a raster like fashion over the area of specimen under examination. In normal operation the scattered electron distribution leaving the specimen is detected by the bright-field detector. This measures the current within the scattered probe at each point within the scanned region of the specimen. The Differential Phase Contrast (DPC) technique replaces the standard bright-field detector with a position sensitive one.

The magnetic contrast DPC generates is easier to understand if we consider a hypothetical model in which the beam is stationary and the specimen moves from side to side. Consider the situation illustrated in figure 3.2 which shows a stationary electron probe incident on a thin film. If there is no deflection of the beam then the zero-order beam will strike a detector situated on the optic axis symmetrically. Unlike the standard electron detector this magnetic sensor comprises four individual

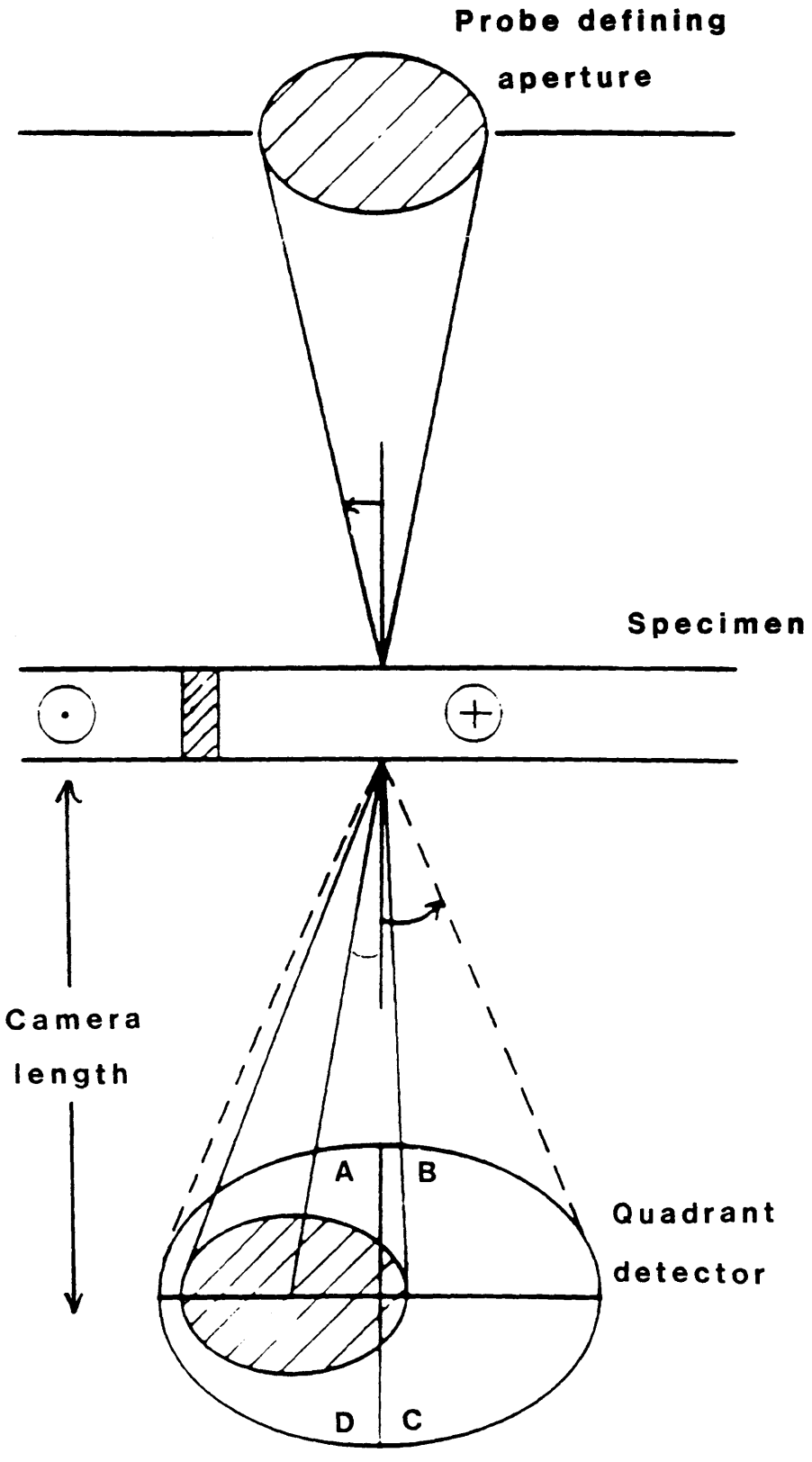

Figure 3.2

Illustration of DPC generation

quadrant segments of p-n type silicon, each of which produces current signals as a result of the electron interaction. With a ferromagnetic sample such as that illustrated in figure 3.2, which contains two anti - parallel domains magnetised into and out of the plane of the page, then the magnetic deflection of the beam passing through these regions shifts the electron distribution striking the detector off centre. In this situation unlike in the undeflected case, the currents from all four quadrants will no longer be equal. The charge distribution on the detector shifts from left to right, passing through the centro - symmetric position, as we move the specimen from left to right. Now if we label the four sectors of the detector A,B,C,D then the current from the (A+D) combination is initially highest with the probe incident on the domain magnetised into the page. This current level remains constant until the domain wall is intersected. With the beam incident on the domain wall the current level from (A+D) gradually diminishes as the specimen is moved further to the left, to the minimum value when the beam passes through the oppositely magnetised domain. At the same time as this the current level from the other combination, (B+C), swings the opposite way, and only when the scattered distribution lies along the perpendicular bisector of (A+D)and (B+C) do these combinations generate equal signals. Therefore if instead of the absolute currents modulating the video display, as is the case in bright field imaging, we use the difference signals we have a method of generating contrast which increases monotonically with the magnitude of the 'Lorentz' shift.

The zero difference signal produces an intensity on the video display units situated in the middle of the grey scale range. Therefore as the difference signal swings back and forth the video display changes from black to white, the precise shade being a measure of the extent of the asymmetry present on the detector surface. In this way the variations in the Lorentz deflection of the probe are translated into changes in image intensity. Essentially this DPC method places the SAD pattern onto the surface of a position sensitive detector, but the great advantage this method has over SAD alone is that it provides the spatial variation of the magnetisation within the area of the specimen scanned, and more importantly that this intensity is in fact directly proportional to the integrated in-plane component of induction.[7] The deflection can therefore arise from any in-plane induction through which the electron passes as it travels the length of the microscope column. The only appreciable difference is normally encountered when in and around the specimen. The relevance of this point in the study of magnetic recording materials is the presence of stray fields, which increase the difficulty when trying to interpret the observed shifts on the basis of the micromagnetism within the sample. The ability to use the difference signal from other sector combinations allows a map of the in - plane induction to be produced at 45° intervals. If the currents from each quadrant are summed and used to control the displays then this situation mimics that found in normal bright-field imaging and therefore enables cross-correlation of the physical microstructure with the

magnetic microstructure. The sequential nature of the STEM enables digital acquisition of the images, and also any other information the machine provides (EDX, EELS etc) which facilitates quantitative analysis of the data. The binary data may be manipulated by image processing packages which, in addition to enhancement features, enable images sensitive to magnetisation at any angle in the plane to be created.

Since the extent of the Lorentz deflection is directly proportional to the product $B_o t$ then, if an area of specimen can be found in which this product is known then the DPC produced by this region provides a 'yard-stick' to which other imaged areas can be compared, assuming of course that these other areas are of the same uniform thickness.

3.4.3 QUANTIFYING THE MAGNETIC CONTRAST

Chapman et al[7] have previously shown that the signal obtained from a quadrant detector is directly proportional to the gradient of the specimen-induced phase shift of the electron wave. In the following section the phase shift introduced to an electron wave as it traverses a thin ferromagnetic sample will be derived in terms of the sample induction and therefore allow the relationship between the DPC signal and the magnetic microstructure of the sample to be established.

Consider the situation illustrated in figure 3.3. If the assumptions outlined earlier remain valid then the phase shift, Δ, between incident electrons, attributable

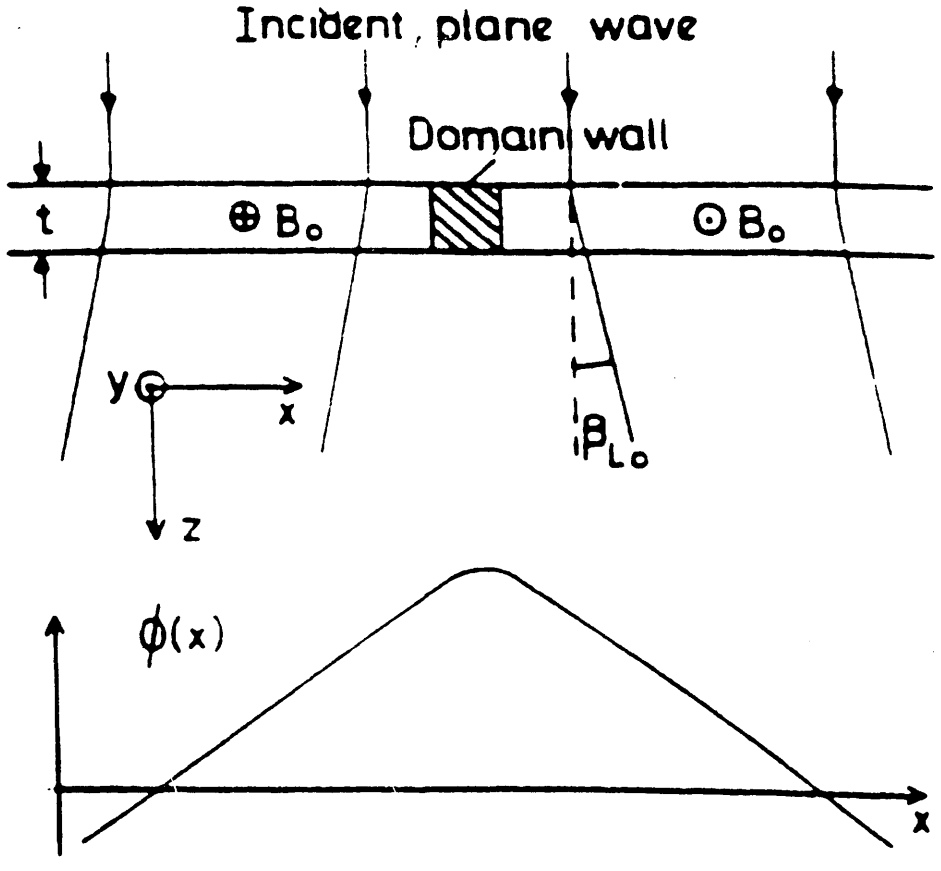

Figure 3.3

Lorentz deflection of an electron beam and the associated phase change of the incident wave

to induction effects alone, is given by

$$\Delta = \frac{e}{\hbar}\Phi$$

$$= \frac{e}{\hbar}\int \underline{B}.\underline{n}\ ds$$

where $\underline{B}$ is the magnetic induction and the integral is over any surface bounded by the trajectories, of which ds is an element and $\underline{n}$ the outward pointing unit vector normal to it. Figure 3.3 shows an electron beam, travelling in the z-direction, incident on a thin ferromagnetic film. The film is considered infinite in both x and y dimensions and further to lie solely within this xy plane. With the coordinate system as indicated we can re-write the above equation as

$$\Delta(x) = \frac{e}{\hbar}\int_{o}^{x} dx \int_{-\infty}^{\infty} dz\ B_y(x,z)$$

where $B_y(x,z)$ is the y component of magnetic induction. If the induction is assumed to lie entirely within the film plane then there are no stray fields present above or below the specimen and the limits of the z integration can be reduced to yield the following expression for the phase shift

$$\Delta(x) = \frac{e}{\hbar}\int_{o}^{t}\int_{o}^{x} B_y(x,z)\ dzdx$$

where t is the specimen thickness. If we also assume that

the induction within the film is independant of z and define the average in-plane induction $B_y(x)$ as follows

$$B_y(x) = \frac{1}{t} \int_{-\infty}^{\infty} B(x,z)\, dz$$

then the phase shift can be expressed as

$$\Delta(x) = \frac{e\,t}{\hbar} \int_{o}^{x} B_y(x)\, dx$$

In this section we have outlined the relationship between the phase shift of the electron wave and the induction in and around a thin ferromagnetic sample. Prior to this it was stated without proof that DPC generates a signal which is, to an excellent approximation, linearly related to the phase gradient introduced to such an electron beam. We can conclude therefore that when studying such ferromagnetic films the DPC technique provides an image in which the contrast relates directly to the average in-plane component of induction. There are however constraints on the range of probe forming angles and Lorentz deflection angles to which this condition applies and more will be said about this in chapter 4. This therefore enables quantitative micromagnetic information concerning the sample to be obtained. If the assumptions on which the derivation of this final expression is based are valid then the spatial variation of this average in-plane component of magnetic induction can be measured, and an unambiguous determination of the magnetic domain wall profiles becomes possible. In general all in-plane

components of induction must be summed over the entire electron trajectory to determine the induced phase shift of the electron beam. This can lead to complications when interpreting DPC images. However more will be said about this in chapter 7.

SUMMARY

In this section we gave a brief description of the interaction between a fast electron and a thin specimen. We described the way in which information concerning the composition and the physical microstructure of the sample can be extracted from these interactions. We described the force experienced by a charged particle as this encounters a region of magnetic field, and illustrated the ways in which an electron microscope can be configured to provide details of this interaction. We concluded this section with a more quantitative description of the magnetic interaction with the aim of obtaining quantitative micromagnetic information about the irradiated specimen.

REFERENCES

1. A. M^{c}Gibbon, Ph. D Thesis, University of Glasgow (1988)
2. Manson, S. T., Phys. Rev. A, Vol. 6, No. 3, 1013, (1972)
3. Y. Aharonov, D. Bohm, Phys. Rev., **115**, 485, (1959)
4. C. Scott, Private communication (1990)
5. J. Cowley, Appl. Letts., **15**, 58, (1969)
6. J. Chapman, J. Appl. Phys., **17**, 623, (1984)
7. J. Chapman et al, Ultramicroscopy, **3**, 203, (1978)

CHAPTER 4 INSTRUMENTATION - OBTAINING QUANTITATIVE MICROMAGNETIC INFORMATION

4. INTRODUCTION

As all the Foucault images of the recorded tracks were obtained from the JEOL 2000 FX CTEM a brief description is given in this section of the advantages offered by this machine. This section also details the requirements which must be met within the DPC mode of Lorentz electron microscopy if quantitative interpretation of the micromagnetic information is to be possible. We describe the incident probes which can be produced by various combinations of the three pre-specimen lenses within the HB5, and assess the relative merits of each of these with regard to obtaining quantitative micromagnetic information. We conclude this section with a description of the steps which must be followed if the systematic motion of the incident beam is to be completely eliminated, and therefore allow the observed contrast variations within each image to be attributed to interactions with the thin specimen alone.

4.1 THE JEOL 2000 FX CTEM

Normally imaging in a CTEM subjects the specimen to an intense magnetic field, the objective lens field. When studying magnetic microstructures in a standard CTEM it is therefore necessary to switch this lens off if the magnetic structure of the sample is to be preserved. As a

consequence of operating without this lens such CTEM investigations are restricted to relatively low magnifications, ie <5kX. The 2000 FX however incorporates a specially designed objective lens pole piece which enables this lens to be excited, even when conducting micromagnetic studies, as the design ensures a field free region around the sample. The design of the pole pieces is such however that a large magnetic field is encountered when the specimen is inserted into the machine and therefore the lens must be switched off during loading and removal of specimen if damage to the magnetic structure is to be avoided.

In addition to providing increased magnifications for magnetic imaging the use of the objective lens provides another distinct advantage for magnetic structure investigations. The diffraction pattern produced using the objective lens now lies within the same plane as the objective aperture and is thus optimum for producing Foucault contrast.

This CTEM has been specially modified to provide quantitative micromagnetic information using the DPC mode of Lorentz microscopy. Indirectly these alterations have further increased the sensitivity with which Foucault contrast can be generated using new additional controls. These deflection controls enable the diffraction pattern to be carefully positioned anywhere within the back focal plane of the objective lens. With these controls Foucault contrast variations can be produced with an increased understanding of the relative position between the aperture blade and the scattered electron distribution and

consequently the information provided by this technique has been greatly enhanced.

4.2 QUANTITATIVE MICROMAGNETICS USING THE HB5 STEM

The resolution within the STEM is increased by reducing the incident electron probe diameter. However, as was outlined in chapter 3, the aberrations of the lenses increase the extent of the source and therefore limit the attainable resolution. The size of the incident aberrated probe may be estimated if the explicit form of each contributory aberration is known. Within the specimen plane the total probe diameter d_{TOT} is determined by summing the various terms in quadrature viz:

$$d_{TOT}^2 = M^2 d_{TIP}^2 + d_S^2 + d_C^2 + d_D^2$$

where d_s stands for the spherically aberrated probe diameter, d_c the chromatically aberrated probe diameter and d_d the diffraction limited probe diameter, d_{TIP} is the diameter of the virtual source at the exit of the electron gun and M is the magnification factor produced by the pre specimen lenses. These quantities may be determined from the following set of equations:

$$d_s^2 = (\tfrac{1}{2} C_s \alpha^3)^2$$
$$d_c^2 = (C_c \frac{\Delta V}{V})^2$$
$$d_d^2 = (1.22 \frac{\lambda}{\alpha})^2$$

in which C_s and C_c are the coefficients of spherical and

chromatic aberration for the probe forming lens, λ is the electron wavelength, α the probe forming semi angle, and V and ΔV refer to the supply voltage and the associated instability in this, or the spread in the electron energy whichever is the greater. In most modern electron microscopes the stability of the supply voltage and lens current contributions is such that this chromatic aberration may be completely neglected. To determine the optimum probe forming angle α_o, ie that which produces the smallest probe, it is necessary to minimise the expression for d_{TOT}^2 with respect to α. This produces the following expression for the optimum probe forming angle α_o :

$$\alpha_o = \left[\frac{4\lambda}{C_s}\right]^{\frac{1}{4}}$$

4.3 THE VACUUM GENERATORS HB5 FIELD EMISSION GUN STEM (FEGSTEM)

The HB5 field emission tip is the <310> face of a single crystal of tungsten. The gun assembly consists of a double electrode system capable of producing electron beams of very narrow energy spread, ~0.25eV. The first anode is held at 3-4kV with respect to the cathode and this potential difference produces the tunnelling emission current. The second anode accelerates the ejected electrons up to a maximum potential of 100kV. These electrodes act as an electrostatic lens and together produce an apparent source some 171mm before the first condenser lens. The size of this virtual source depends on the state of the tip and if in good condition then the

effective source has a diameter of ~6.5nm[1]. A schematic diagram of the HB5 is shown in figure 4.1.

In magnetic structure investigations in which the objective lens is switched off the probe is formed by either C1 or C2 or indeed some combination of both these lenses. In this situation the selected area aperture (SAA) defines the probe angle α. In contrast, in normal STEM operation the condenser lens(es) focus the probe to lie within the plane containing the SAA. In this situation the demagnified image of the source is further compressed by the objective lens field and thus the objective aperture defines the incident probe profile. Morrison determined the aperture sizes which minimised the incident probe size for the HB5 when operated in the magnetic imaging mode, and concluded that with C1 forming the incident probe α_o = $2.5\text{x}10^{-4}$radians and for C2 α_o = $5\text{x}10^{-4}$radians. The choice of which lens/aperture combination to employ is a compromise between the required probe angle, the probe diameter, and the level of probe current. The electron probe best suited for studying the CoNi magnetic recording films was obtained using C1 with a 100μm aperture. Unlike C2 operation, probe formation with C1 produces a magnified image of the electron source within the specimen plane. The advantage of this over the 50μm aperture is the increase in probe current albeit at the expense of a larger incident probe diameter. Higher probe currents are often desirable allowing specimens of greater thickness to be examined. The probe current chosen for a particular application depends on many factors such as specimen thickness, electron detector efficiency and also radiation

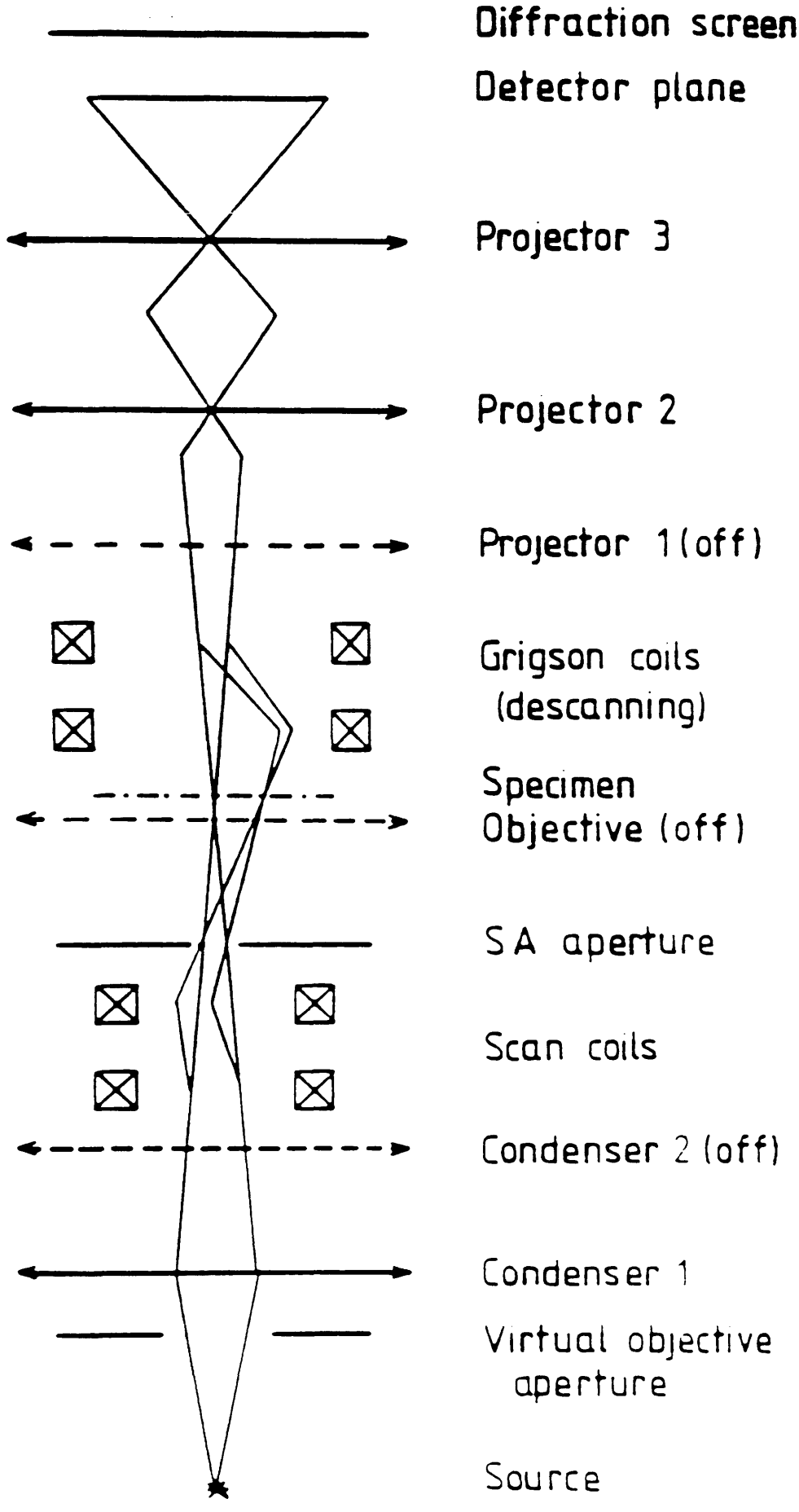

Figure 4.1 The electron optical column of the HB5 STEM

damage considerations. For the specific application in which we are concerned the level of noise associated with the detector is the limiting factor which dictates the acceptable incident probe characteristics. The larger 100μm aperture increases the probe forming angle α and thus the spherical aberration of the incident probe, through the α^3 term, leading to a larger probe diameter. When operating with the 100μm aperture and C1 the total probe size is ~20-30nm. Figure 4.1 illustrates the lens arrangements used in this mode. This compares with 10-15nm when using the 50μm aperture and 10nm when C2 and the 100μm aperture are used. The highest resolution for magnetic imaging is ~3nm and this performance is attained when the specimen is raised from the normal seating position by some 20mm with the aid of a specially designed snout cartridge holder. In this situation the objective lens is now the probe forming lens and need only be weakly excited to form the probe in this displaced plane. Consequently the magnetic field strength produced by the lens within the specimen plane remains small. This is essential if the magnetic structure under scrutiny is to remain completely intact. As will be shown later in this section it is not always possible to utilise this highest resolution imaging mode even though comparable probe currents are obtainable[1].

The HB5 STEM has three post specimen lenses and this offers considerable advantage since the size of the bright field cone can be matched to the physical dimensions of the chosen detector. The DPC detector is a Centronics model QD-100 and consists of a circular p-n type silicon

diode 11mm in diameter. The active layer is partitioned into four equal quadrants by two inactive strips, each approximately 200μm wide. With C1 and a 100μm aperture the optimum match of bright field cone size to detector surface area for the samples studied was effected with a camera length of ~5.4m. The signals from each sector of the detector are routed to four matched pre-amplifiers before entering a mixer unit. The mixer unit allows the various combinations of the individual signals necessary if images sensitive to orthogonal components of integrated induction are to be derived.

In the DPC technique each incident electron from within the emergent probe generates ~10^4 electron-hole pairs within the p-n junction and therefore considerable initial amplification occurs before the signals enter the first electronic stage of amplification. Noise in the system arises from the 'shot-noise' present in the electron beam, due to fluctuations in the emission current, and a dark current from the detector, which is produced through thermal generation of carriers. Crystallite contrast can impede image interpretation when studying micromagnetic phenomena since the origin of this is non-magnetic and therefore when studying magnetic structures this contrast effectively represents another source of noise. The (S/N) ratio is maximised by utilising as much of the detector surface area as possible bearing in mind of course that the magnetic shift must not move any part of the electron distribution from the detector. The reason for this is straightforward and can be understood on the basis of maximising the active surface

area utilised by the electron beam. If the distribtuion is comparable in size with the 200μm wide inactive strips then a substantial portion of the signal will be lost and consequently (S/N) decreases. Care must be taken however to ensure that the electron distribution remains on the detector at all times. Any portion of the electron distribution which overshoots the detector when deflected would be interpreted as a reduction in the magnitude of the difference signal and hence this would lead to incorrect deductions being made about the observed shift of the electron beam. Consider figure 4.2 in which a scattered probe is incident on the detector surface. The radius of the probe is governed by the probe forming angle α and the camera length; the extent of the motion of this distribution over the silicon surface is determined by the Lorentz deflection angle β_L. Now for a thin longitudinal recording medium the Lorentz deflection angle, β_L, is proportional to the product of specimen thickness and magnetic remanence, ie $\beta_L \propto M_R\delta$, which can be determined for example from vibrating sample magnetometry (VSM) measurements. Therefore providing that this quantity remains unaltered by specimen preparation the appropriate probe forming aperture and camera length may be selected prior to microscope examination. The constraints on the ratio of β_L to α, outlined above, can in fact dictate that the probe forming angle employed in DPC studies be other than that which produces the minimum probe size. This was the situation encountered when studying the MET samples and meant that only the lowest resolution magnetic imaging mode was capable of producing DPC data with an adequate

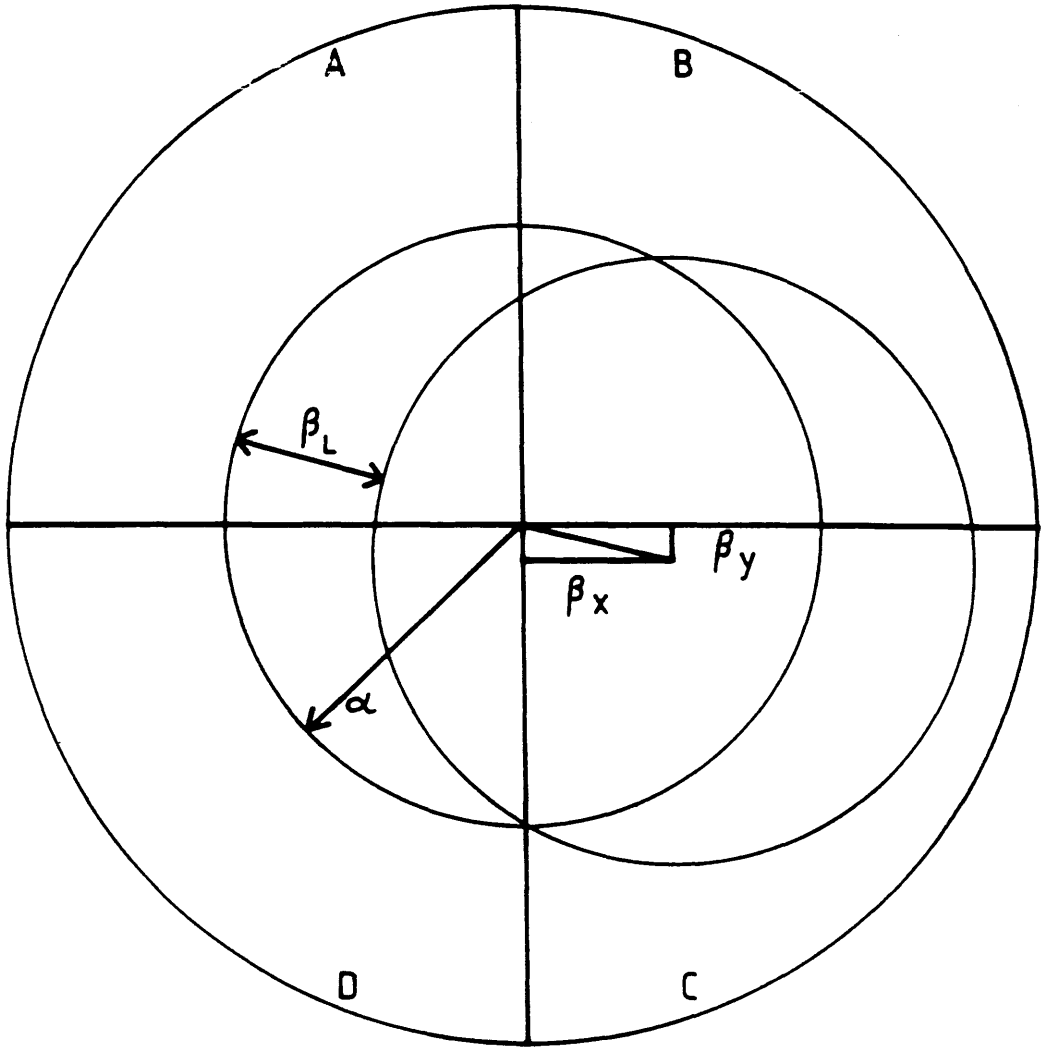

Figure 4.2 The relationship between the electron distribution striking the detector with both the probe angle and the deflection angle

(S/N).

To fulfill the requirement of a stationary electron probe striking the surface of the detector in the absence of any specimen induced shift it is necessary to descan the electron beam. Any residual scan in the beam introduces artifacts to the DPC data; therefore it is vital that this is completely removed if any quantitative analysis is to be possible. The systematic motion of the beam is removed by scan coils situated beyond the specimen plane. To descan the electron beam a region of free space is scanned and the signals from the four individual quadrant sectors monitored on two separate oscilloscopes, one displaying the signals from sectors A and C while the other measures the output from B and D. For both oscilloscopes one signal is inverted before being displayed. This enables the difference signal from each combination to be monitored. The first stage involved in descanning is to adjust the position of the electron beam as it leaves the specimen until each sector produces approximately the same output signal level. This is accomplished using the oscilloscopes in dual display mode and shifting the position of the beam with the Grigson coils until the traces on both displays are symmetric with respect to the zero level. This serves as a means of coarse correction and is followed by a more sensitive method. Changing the oscilloscopes display from dual trace to sum provides a means of fine adjustment. Now that the scattered electron beam has been moved to ensure that each quadrant sector is overlapped by approximately equal areas of the beam, it remains to introduce the correct amount of

signal form the scan generator to complete the descan process. This must be carried out while ensuring that at all times both oscilloscope traces remain symmetric about zero, and is complete when both line and frame components of the scan have been eliminated. The magnitude of the correction signals depends on the extent of excursion of the electron probe over the surface of the specimen, ie the magnification, and therefore must be adjusted for different magnification settings. At magnifications below 5000X the extent of the motion of the electron beam over the surface of the specimen means that it is almost impossible to descan the beam completely. As a result of this we cannot ensure that a stationary probe strikes the quadrant detector and consequently any quantitative DPC analysis must be restricted to magnifications above this, where this requirement can be realised.

SUMMARY

In this section we have described the two electron microscopes used to obtain the micromagnetic information on the MET samples. The various modes in which the HB5 can be configured to provide quantitative micromagnetic data were discussed, and we compared the relative merits of each of these and commented on why it was necessary to study these films using the lowest resolution magnetic imaging mode. Finally we described the actual method employed to ensure that the systematic motion of the beam across the specimen is eliminated before the emergent current strikes the surface of the detector.

REFERENCES

1. G. Morrison, Ph. D Thesis, University of Glasgow (1981)

CHAPTER 5 MET FABRICATION, SPECIMEN PREPARATION, AND THE PHYSICAL AND COMPOSITIONAL CHARACTERISATION OF THE FILMS

5. INTRODUCTION

The purpose of this section is to describe the MET fabrication process and the importance of this in producing a material with the correct bulk magnetic characteristics required for high density magnetic recording applications.

5.1 MET FABRICATION

Metal evaporated tape is produced by oblique incidence evaporation at a continuously varying angle of incidence. This procedure involves evaporating a material onto a moving substrate which is supported on a drum roller. The curved surface of the substrate support varies the distance between the material source and the base film, and therefore the deposition rate changes as well as the angle of incidence during the production of these films. A focused electron beam is used to heat an ingot of the chosen material producing a vapour above the molten reservoir, from which the recording film is produced.

Evaporation onto a continuously moving substrate at oblique incidence produces a polycrystalline film with a curved columnar microstructure[1,2]. The curved columns are found to be narrowest at the substrate interface gradually broadening toward the recording surface; this is in

agreement with the growth model proposed[3], in which initial nucleation occurs at a high incidence angle being succeeded by continuous epitaxial growth[4]. The deposition rate is initially lowest and rises smoothly to reach a maximum when the incidence angle is lowest. The polyester base film support drum acts as a heat sink which reduces the mobility of the impinging particles as they strike the base film. This is necessary to ensure that the impinging particles remain close to the point of impact and allow the desired columnar microstructure, which can be ascribed to a self shadowing effect, to evolve. The atoms from which the film is made are only incident on the base film through a limited range of angles due to an inhibitor shield which surrounds part of the roller drum supporting the substrate, see figure 5.1. Certain characteristics of the film eg the physical morphology, the column inclination angle, and the coercivity[5], depend on the precise angular range of the incident vapour atoms. The fabrication process introduces anisotropic structural imperfections to the film and also elongates the microcrystallites in the direction of the vapour plane, ie along the tape's length.

The recording medium is composed of two elements of different magnetic properties and, although the bulk magnetic characteristics of the film are governed principally by the microstructure[6], subtle modification to the magnetic characteristics of the film are possible by merely changing the relative amounts of each of the components. Manufacturing the film from an alloy does

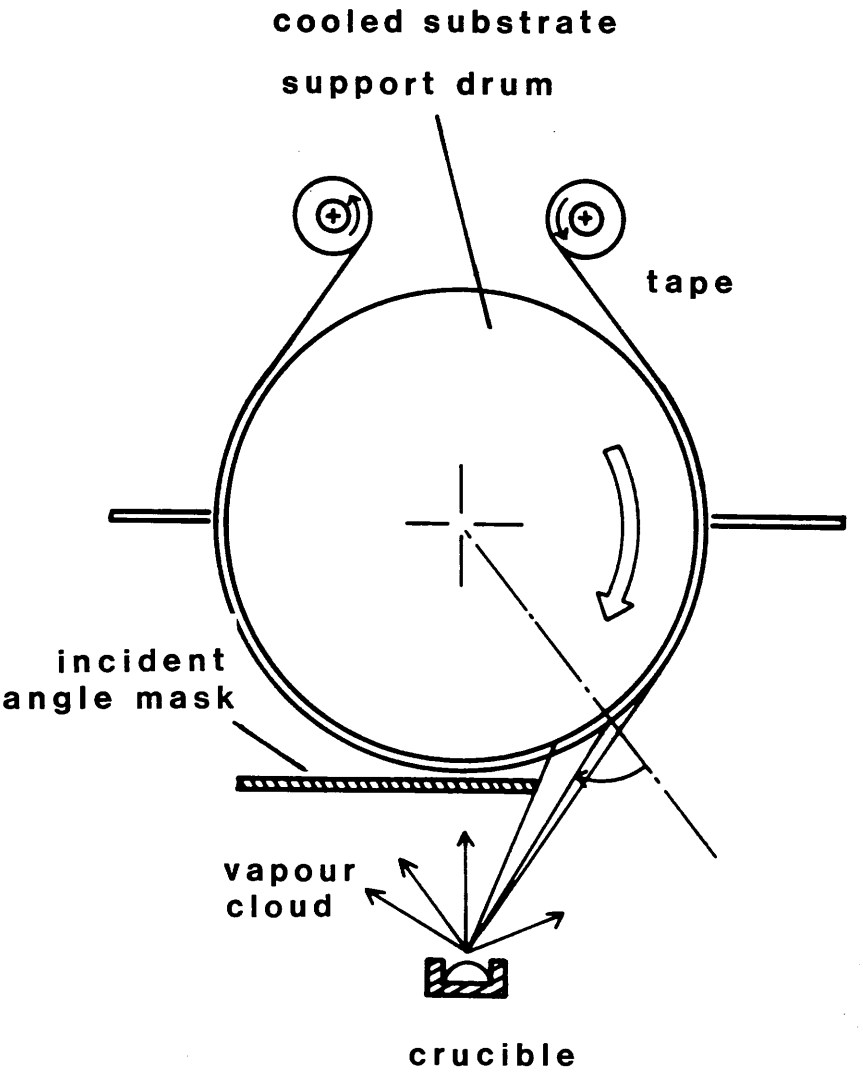

Figure 5.1 Schematic arrangement for depositing obliquely evaporated metal films

introduce certain difficulties during production, associated with the different thermodynamic properties of the individual elements. Maintaining the optimised growth conditions, initially determined in the laboratory, would be very difficult in production as several hundred metres of this medium would ultimately be produced in a single run. Therefore variations in growth conditions during production could be expected and the consequences of this on the structure of the film would need to be considered. The effect of slight evaporation rate changes might result in regions of the final recording film rich in one or other of the components, which could devastate the recording performance of these portions of the film, and therefore lower the overall standard of the tape. Cobalt and nickel were the obvious choice of elements for the MET since the phase diagram for this binary alloy indicates that ferromagnetism is supported over the entire composition range. Thus the recording properties of the evaporated films would survive slight changes in the local composition of the media brought about by variations during full scale production. In this respect the similar vapour pressures of these two elements is also of considerable advantage since this results in a vapour phase with the same composition as that of the bulk material. Using components with dissimilar vapour pressures does not necessarily represent a significant problem, since the extent of preferential diffusion within the vapour could be determined from a knowledge of the vapour pressures of both components, and the bulk

composition of the ingot adjusted to reflect this diffusion effect. However equivalent vapour pressures further reduce the effect of these evaporation rate fluctuations. The only obvious difficulty using Co and Ni concerns the reactivity of each with atmospheric oxygen and measures, which will be discussed later, are taken to counteract this undesirable effect.

As discussed in chapter 2 the output signal from a magnetic recording material is maximised by having as much stray field exude from the material as possible. The amount of stray field that a material produces depends on the strength of the $M_r\delta$ product of the film. Having decided on the constituent atoms for the tape, and therefore fixed the size of the intrinsic magnetic moment, any increase in the magnetisation of the thin film alloy relies on maximising the remanent magnetisation of the tape material. The physical microstructure of the film controls the level of this quantity, and to satisfy the demands of high density recording the packing fraction of the constituent magnetic particles is maximised to ensure measurable output from small volumes of the film. The large macroscopic remanent magnetisation of the MET is established by the highly anisotropic microphysical structure which establishes a square shaped hysteresis loop. The output from a given volume of the MET is increased by producing the magnetic layer in the form of a continuous film, which has a very high density of magnetic entities when compared with other particulate media, eg γ-Fe_2O_3.

The manufacture of a high density recording material aimed specifically for the video recording market means that the candidates chemical stability, flexibility, head wear performance and overall strength must all be considered. The problems of reactivity and wear performance are substantially improved if the magnetic film is coated with a special type of lubricant, a perchloroether[7]. One end of the molecules within the lubricant bond to the metal surface while the other end is free to move, allowing it to cover and protect the recording surface. Obviously the thickness of this layer cannot be too great otherwise it would hinder the recording of information on the film. It is seen therefore that fabricating a material which complies with all of these requirements and additionally meets the demands of high density recording applications takes a great deal of effort, and much work has been done to determine the growth parameters and the film composition which results in a medium optimised for such a high density magnetic recording role.[8]

The dependence of the output signal on the magnetic layer thickness means that it is essential for the evaporated tape to be of uniform thickness throughout. To avoid thickness variations occurring during the production of large volumes of the MET requires continuous monitoring of both the evaporation rate and also the speed of the substrate. The films studied in this thesis were all produced on a prototype evaporation rig at the Central Research Laboratories of Thorn EMI and the method adopted

for varying the thickness of these samples was to alter the speed of the substrate through the evacuated chamber. To produce samples of uniform thickness from this machine the substrate speed was adjusted by measuring the optical density of the film as it passed out of the evacuated chamber. As this changed during production the substrate would either be speeded up or slowed down depending on whether the optical density had increased or decreased. Therefore the microphysical structure would be expected to be different for films of different thickness. The average grain size would be expected to change with film thickness, which obviously would also affect the magnetic characteristics of the films which are related to these changes.

5.2 SPECIMEN PREPARATION

To enable the MET samples to be examined within the electron microscope it is necessary to isolate the magnetic layer from the polyester base film on which it is supported. The excellent adhesion between the polyester base film and the magnetic recording layer is established using an initial layer of aluminium, evaporated onto the substrate before the MET recording layer is deposited. This aluminium underlayer allowed the thin magnetic film to be separated from the PET using a solution of sodium hydroxide, which etched away the aluminium layer. The probability of producing microscope samples containing recorded tracks was increased by first determining the

location of these recordings on the tape using ferrofluid decoration. Having selected the portion of the tape to receive subsequent treatment, the next stage after removal of the lubricant and thorough cleaning, was to cut the tape into small pieces ~1cm on each side. The metal surface of these was scored, with the reverse side of a scalpel blade, into a grid of ~0.2cm spacing. These score lines provided etching channels for the sodium hydroxide solution, enabling this to penetrate the film simultaneously on all four sides. This scored piece of tape was next placed, metal side up, on the surface of a concentrated solution of sodium hydroxide. The solution removed the aluminium underlayer and allowed the recorded layer to float free; this would normally take some 30 minutes to complete. After 30 minutes the solution had removed most of the aluminium underlayer, but the metal layer was still supported by the PET base. The large piece of tape was carefully removed from the sodium hydroxide solution, and dried on filter paper. It was then placed into a beaker of distilled water to complete the separation process and also remove any excess caustic soda. The dried piece of tape was lowered into the distilled water at a large angle to the surface, as this allowed the small pieces of magnetic tape to float away, while the base film was held firmly with tweezers. The pieces of tape which had become separated from the PET base were picked up using microscope support grids and carefully dried on filter paper. Initially normal copper support grids were used; however, it became clear that the

films had a tendency to curl and therefore double sided grids were used from that point onward. These folding grids were folded over completely and then re-opened slightly before attempting to lift the tape pieces from the water. This eased the task of completing the fold once the precious film had been picked up. Finally the small flap, which extends from one side of the double grid, would be folded back over to secure the fold. The specimen was then ready to be examined in the electron microscope.

5.3 CHARACTERISATION OF THE PHYSICAL MICROSTRUCTURE OF THE MET FILMS

Chapter 1 detailed the significance of the physical microstructure of a ferromagnetic material in controlling certain magnetic characteristics. The spatial arrangement of the constituent atoms determines the anisotropy axes and the interatomic separation distance affects the magnitude and sign of the overlap integral, which is involved in the exchange interaction. It is clear, therefore, that the microphysical structure plays a very important role in determining the micromagnetic properties within ferromagnetic materials. We should therefore establish the detailed physical characteristics of each of the MET samples if we are to be able to explain any differences observed in the magnetic structure exhibited by each of these films.

The information on the physical microstructure of the thin ferromagnetic films was obtained from examination

within the CTEM. The techniques used included fairly high resolution imaging, in both the bright field and dark field, and also electron diffraction pattern observation. To enable a three dimensional picture of the samples to be established, cross sectional specimens were also prepared and studied within the microscope.

5.4 THE STRUCTURE OF THE MET FILMS

Imaging microtomed cross sections of each of the three samples, see figures 5.2a and 5.2b, revealed a pronounced curved columnar microstructure for both samples A and B. Sample C does not show anything like the same column definition. The different physical microstructure for sample C is thought to be due to the fact that this film is much thinner than either sample A or B. A similar structural form to this is thought to be present in all of the films, however for the thicker films the presence of this initial layer is more difficult to observe as the curved columnar structure immediately draws the eye. To attempt to and verify that the microtoming process was not the cause of this different physical structure many cross sectional samples were examined in the microscope. From these studies it was clear that both samples A and B were also damaged, however eventually portions of tape with the expected structure were located for these specimen, unlike for sample C. The images of samples A and B also illustrate the distribution of the void regions within the films, which account for the lower density that these MET

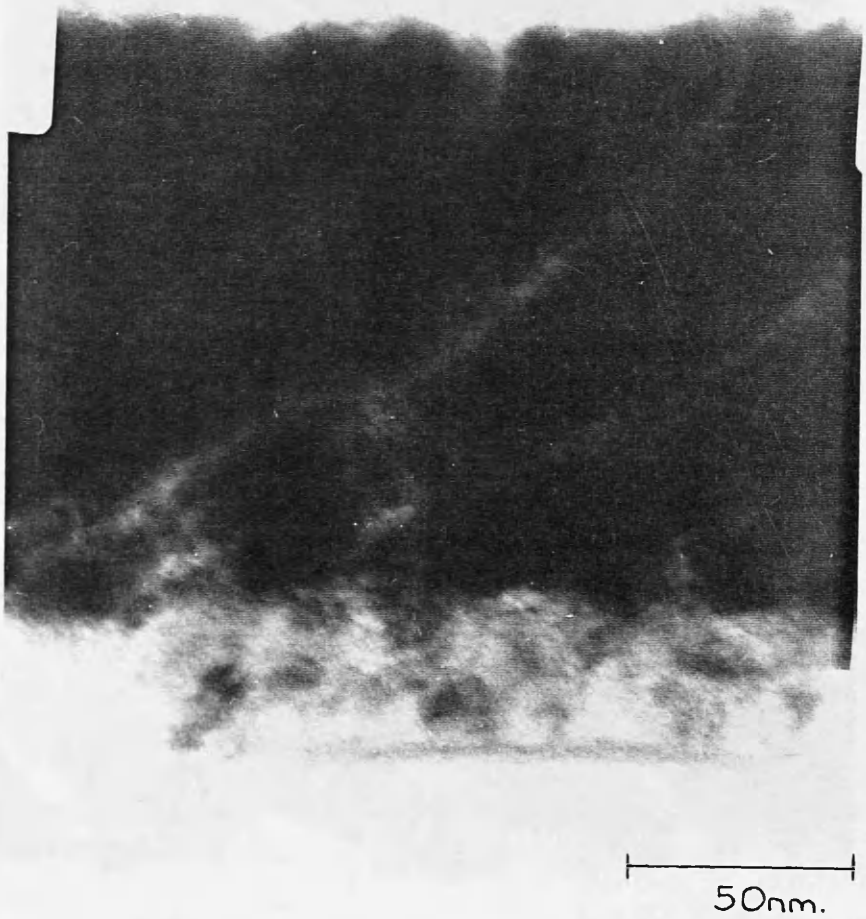

Figure 5.2a Microtomed cross section of sample A revealing the curved columnar physical microstructure. The aluminium adhesion layer is just visible beneath the MET layer.

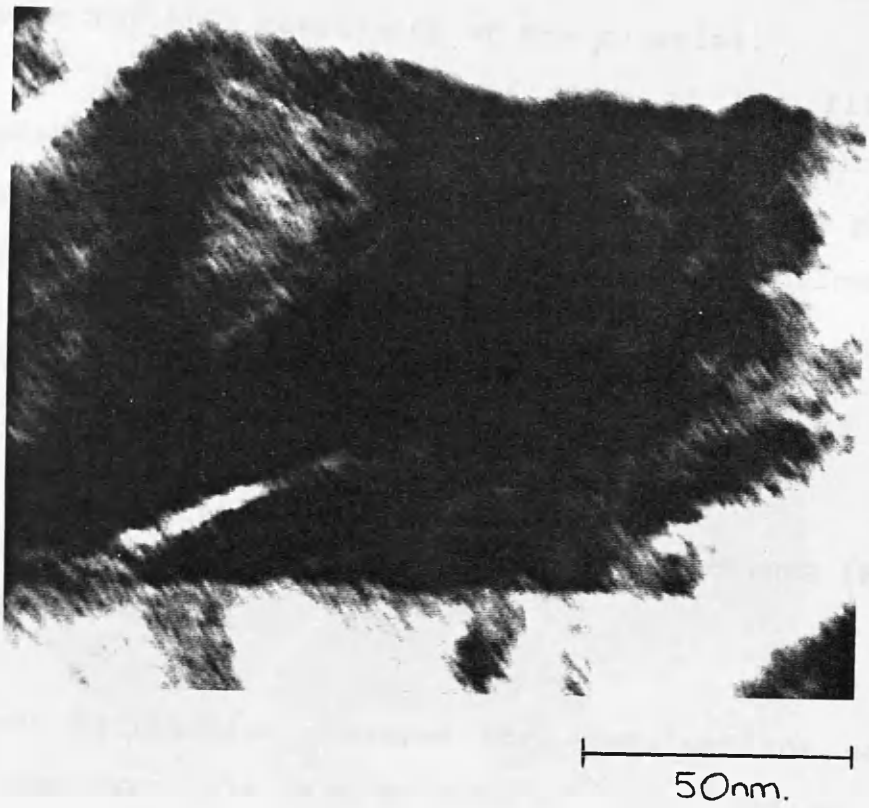

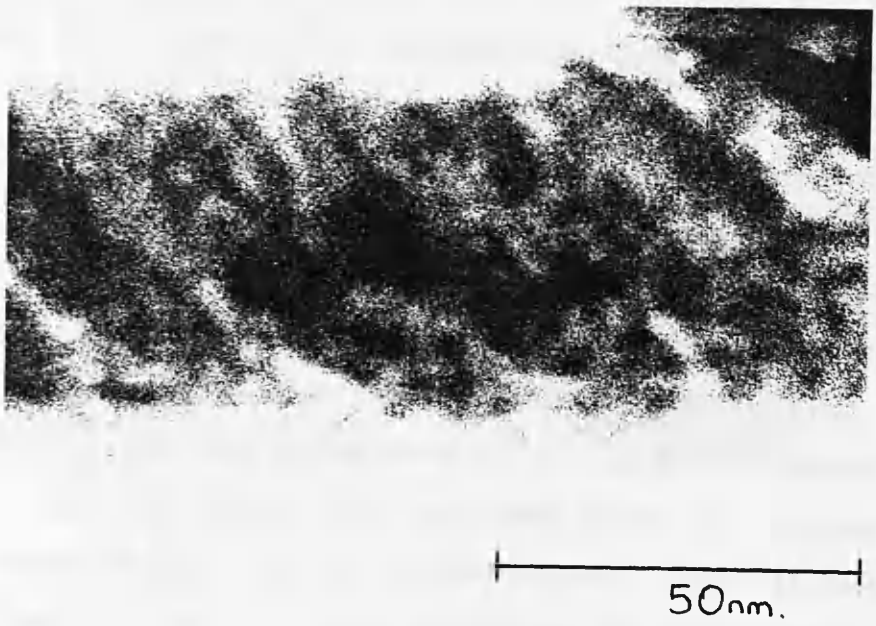

Figure 5.2b Microtomed cross sections of samples B (top) and C (bottom) revealing the curved columnar microphysical structure.

samples have compared with that of the bulk alloy[9]. These regions inhibit the motion of the domain walls and hence increase the bulk coercivity of the material.

The physical thickness of each of the films was established from examination of CTEM images of microtomed cross sections. From these and other images the physical thickness of each sample were found to be as follows :

Sample A = 127±5nm

Sample B = 91±6nm

Sample C = 46±5nm

5.5 DEDUCTIONS FROM ELECTRON DIFFRACTION PATTERNS (EDP) OF THE MET FILMS

Electron diffraction patterns were obtained for each of the three specimens from an area of ~40μm^2 and are shown in figures 5.3(a-c). Each film has a ring diffraction pattern consistent with a polycrystalline sample. The very similar lattice constants of cobalt and nickel mean that the crystal structure of the MET alloy is predominately a hexagonal close packed (hcp) phase of a cobalt-nickel mixture. Evidence has been reported for other phases[2], although isolating these did not prove possible for the films studied. The most significant discovery from these experiments was the appearance of texture. This means that within the polycrystalline specimen there is a degree of alignment between some of the individual crystallites. The evidence for this is the presence of incomplete rings within the diffraction pattern which are symmetric with

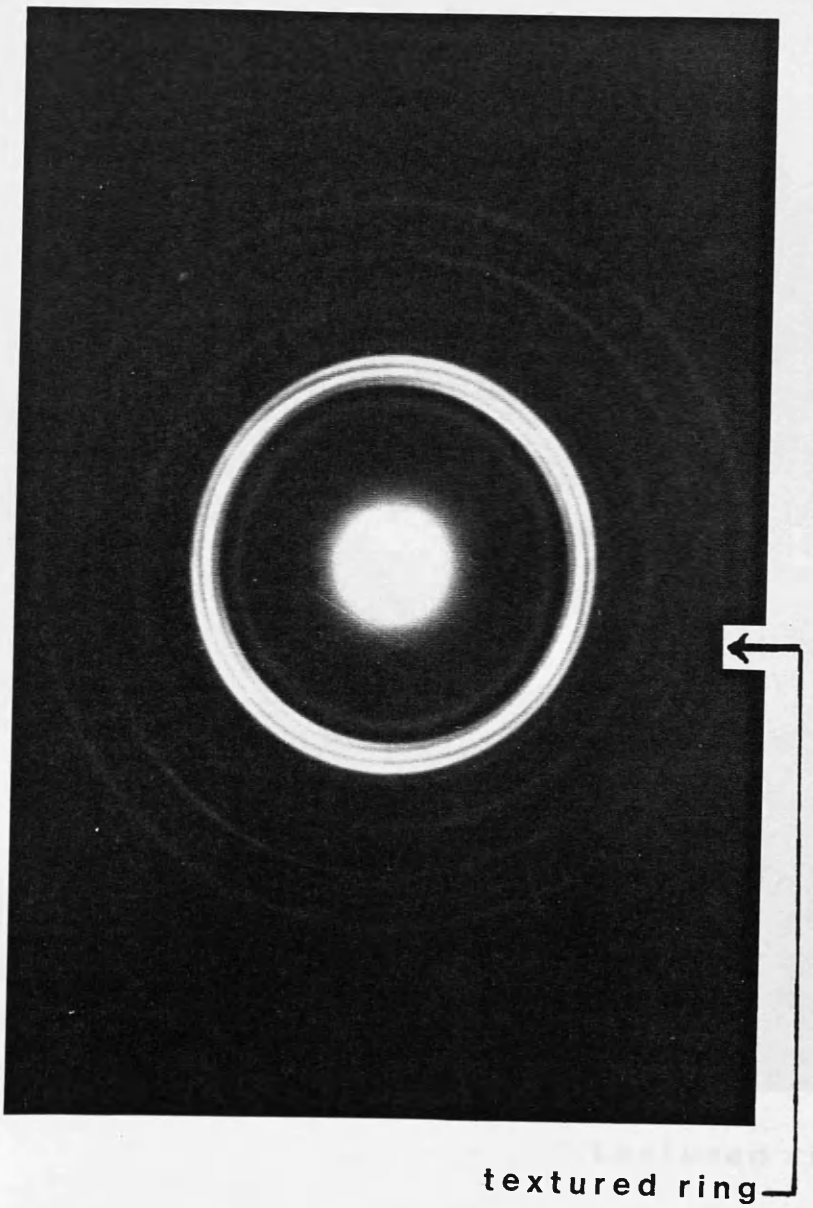

Figure 5.3a Electron diffraction pattern of sample A taken with a camera length of 2.1m.

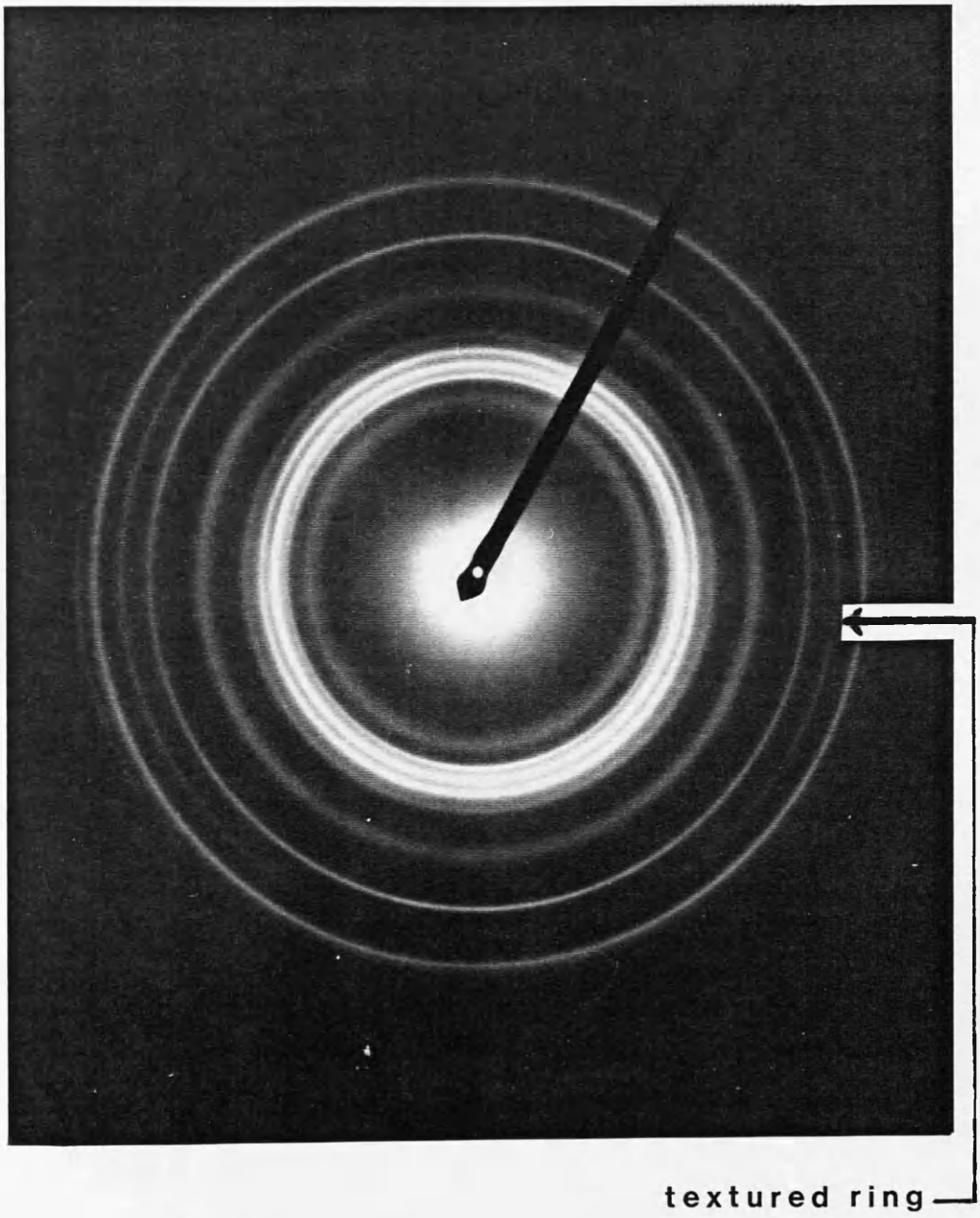

Figure 5.3b Electron diffraction pattern of sample B taken with a camera length of 2.5m.

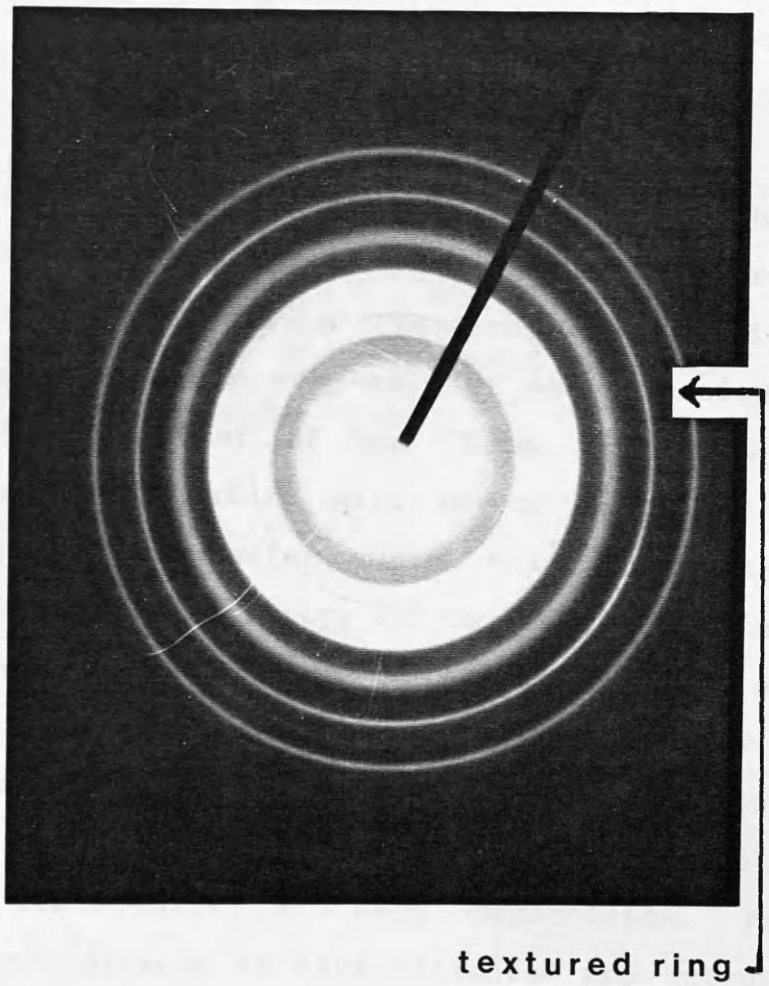

Figure 5.3c Electron diffraction pattern of sample C taken with a camera length of 1.8m.

respect to the centre spot. The radii of the texture rings were carefully measured and used to determine the lattice spacing responsible. The d_{hkl} spacing determined from these measurements were as follows :

Sample	Camera Length	Ring radius	d_{hkl}
A	0.84±.01m	2.44±.02cm	1.16±.02Å
B	1.07±.01	2.33±.02cm	1.15±.02Å
C	1.07±.01	2.40±.02cm	1.12±.02Å

With this information it was possible to index the texture rings. For each film the observed texture ring arises from a reflection with a c-axis dependance which is significant as the c-axis is the easy-axis of magnetisation for the principal constituent of the films, cobalt. Hence the effect of this texture will be to introduce magnetic anisotropy to the system, which will contribute to the overall magnetic anisotropy of the film. From the images it is clear that sample A exhibits the largest amount of texture since the incomplete rings within the EDP for this sample form the least complete circle. The angular extent of these arcs is therefore a measure of the colinearity between the c-axis of each crystallite. From the diffraction patterns we have estimated the extent of the texture within each of the films by measuring the fraction of the texture ring missing. The results are as follows:

Sample A 0.5

Sample B 0.3

Sample C 0.2

The texture ring closest to the straight through beam is

found to be due to a reflection from the (103) plane. The pronounced curvature of each individual column means that even if considerable texture were present the c-axis distribution would be very broad and difficult to detect. The need for a certain 'critical' film thickness before texture can be established is believed to be the factor responsible for the reduced texture in the thinner films. This suggestion is partially supported from the CTEM images of microtomed cross sections, see figures 5.2a, and 5.2b. Unlike samples A and B the physical microstructure of sample C does not appear to support an ordered columnar structure. It is therefore the amount of film deposited in excess of this minimum required which controls the degree of texture present in the film.

5.6 CRYSTALLOGRAPHIC STRUCTURE

The images of the microcrystallites at high magnification in both bright field and dark field allowed the shape and size of the individual grains to be estimated. Dark field imaging provided the more reliable information, as the background intensity present in bright field imaging, where suitably oriented crystals appear dark, is not present in the dark field. A diffraction ring which did not appear to have any texture was used to produce these images. The images must be examined with care because of the effect that the curved columnar microstructure has on the crystallite contrast within the image. In each of the films the narrow column width at the substrate interface

means that small grains would be found in every film. The only way in which any variation in grain size may be estimated is to measure the largest grains within each image of each sample. The maximum grain size in the thickest sample was 118±6nm, for sample B it was 87±15nm and finally 63±6nm for sample C. The easiest way to appreciate the actual difference is in fact to examine the images. These are shown in figures 5.4(a-c). These images also indicate a slight elongation of the individual grains in the direction of the incident vapour, which might add a shape anisotropy along this direction.

5.7 COMPOSITIONAL ANALYSIS OF THE MET SAMPLES USING ENERGY DISPERSIVE X-RAY ANALYSIS (EDX)

Although the magnetic properties of the CoNi metal evaporated tape alloy are not as sensitive to variations in composition as some other binary alloys, which are being considered as potential high density recording media, eg CoCr, it was important to confirm that fabrication and specimen preparation had not affected the composition of the films examined. The relative amounts of cobalt and nickel present within the samples was determined using energy dispersive x-ray (EDX) analysis, which could be practised within the CTEM. Figure 5.5 illustrates typical spectra from samples A, B, and C respectively. The straightforward determination of the ratio of nickel to cobalt K_{α} peaks from the samples was not possible because of the similar energies of the nickel

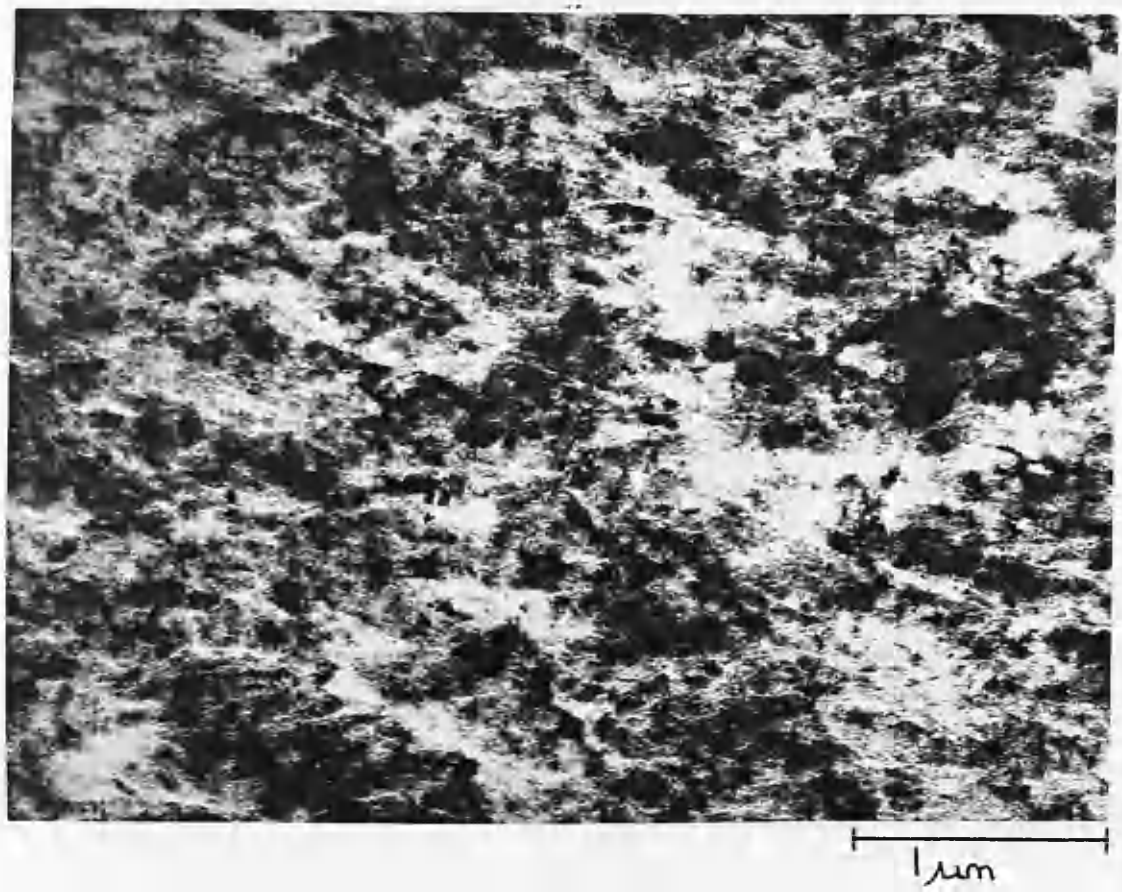

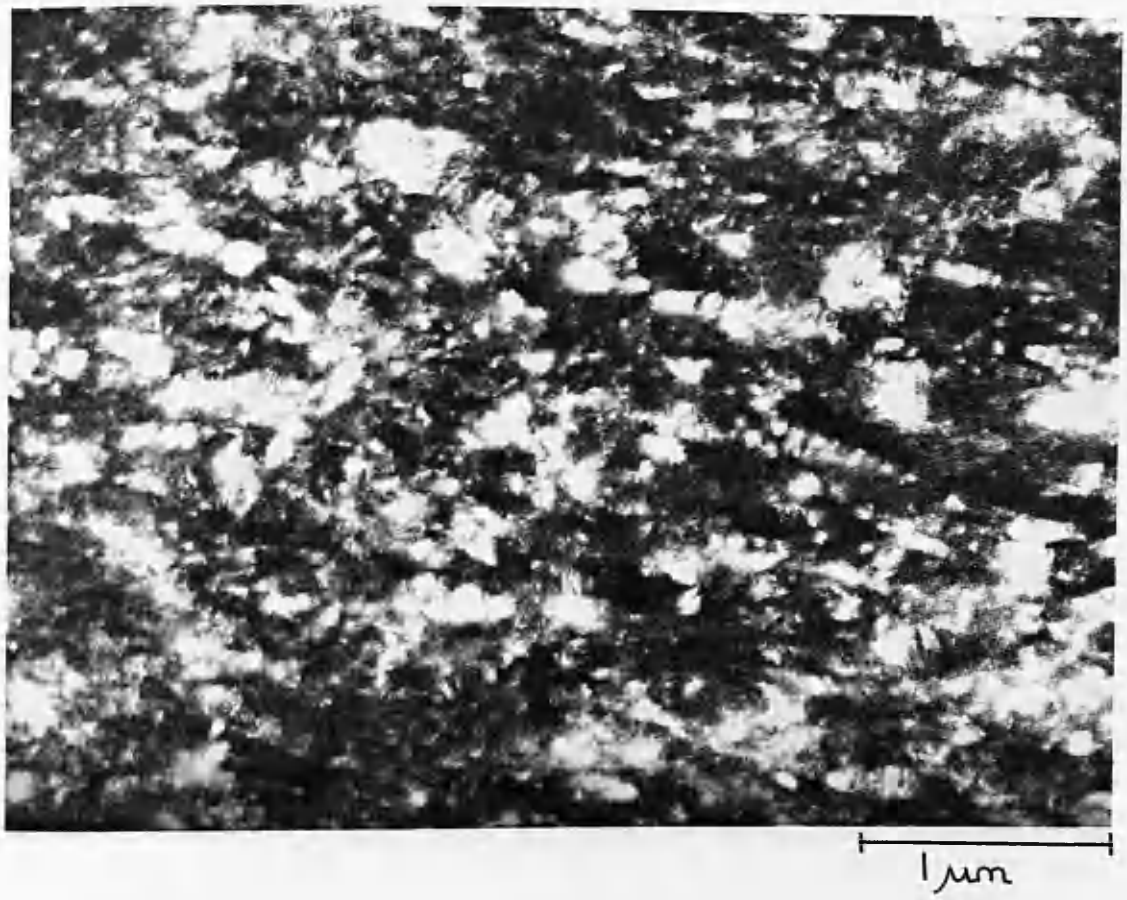

Figure 5.4a Bright field and corresponding Dark field image of sample A

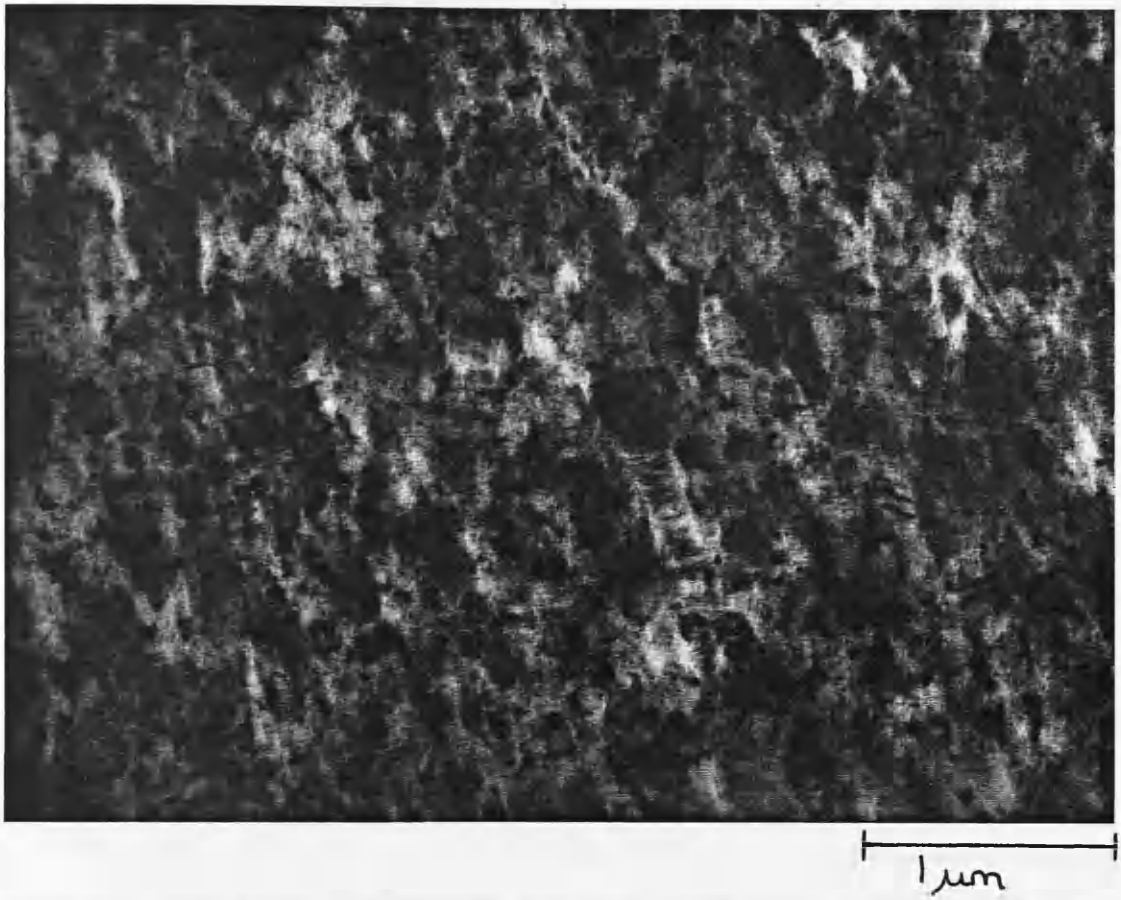

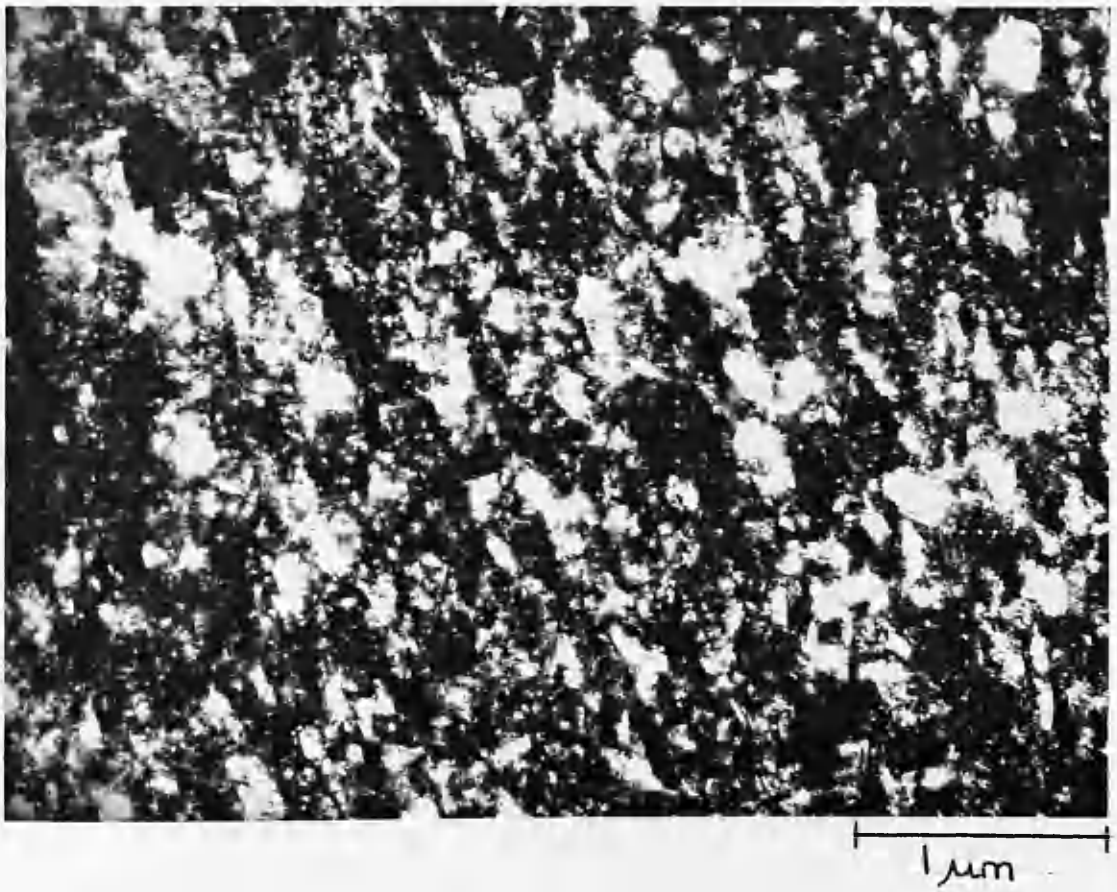

Figure 5.4b Bright field and corresponding Dark field image of sample B

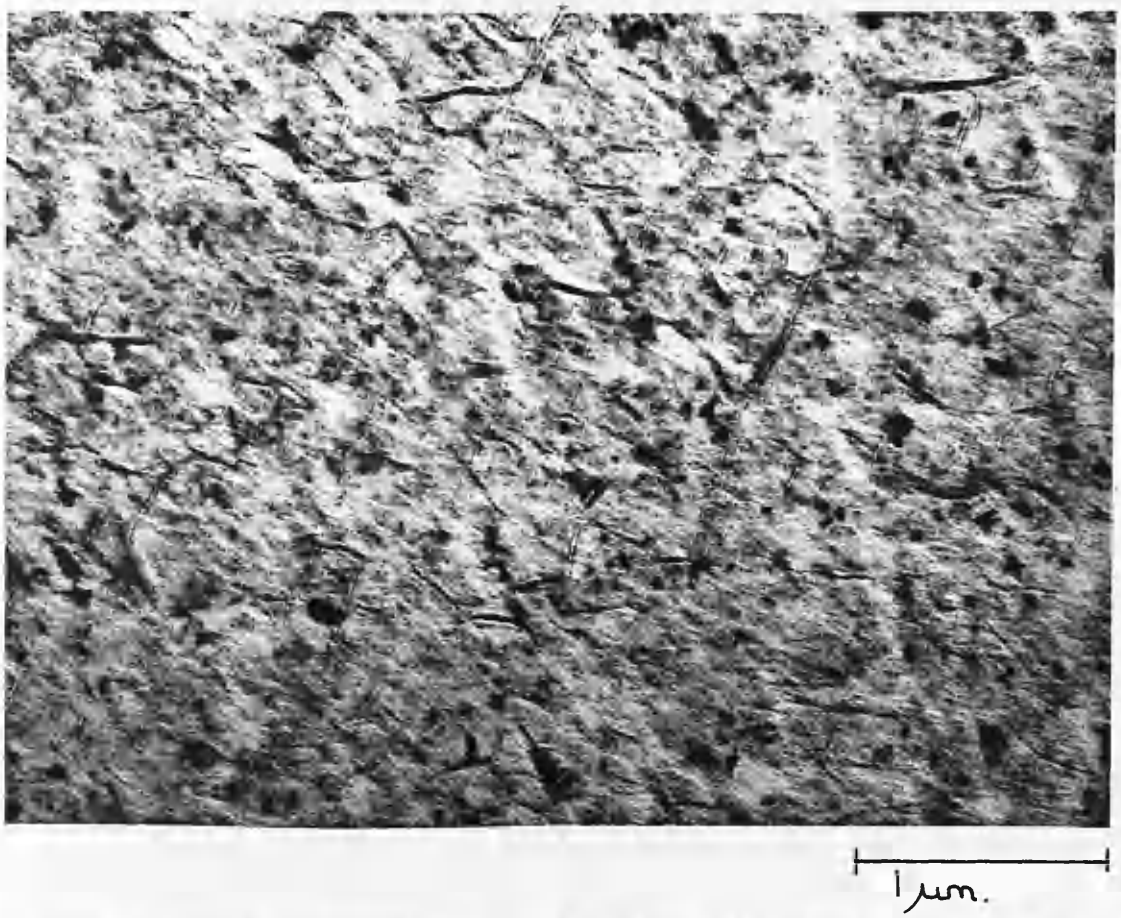

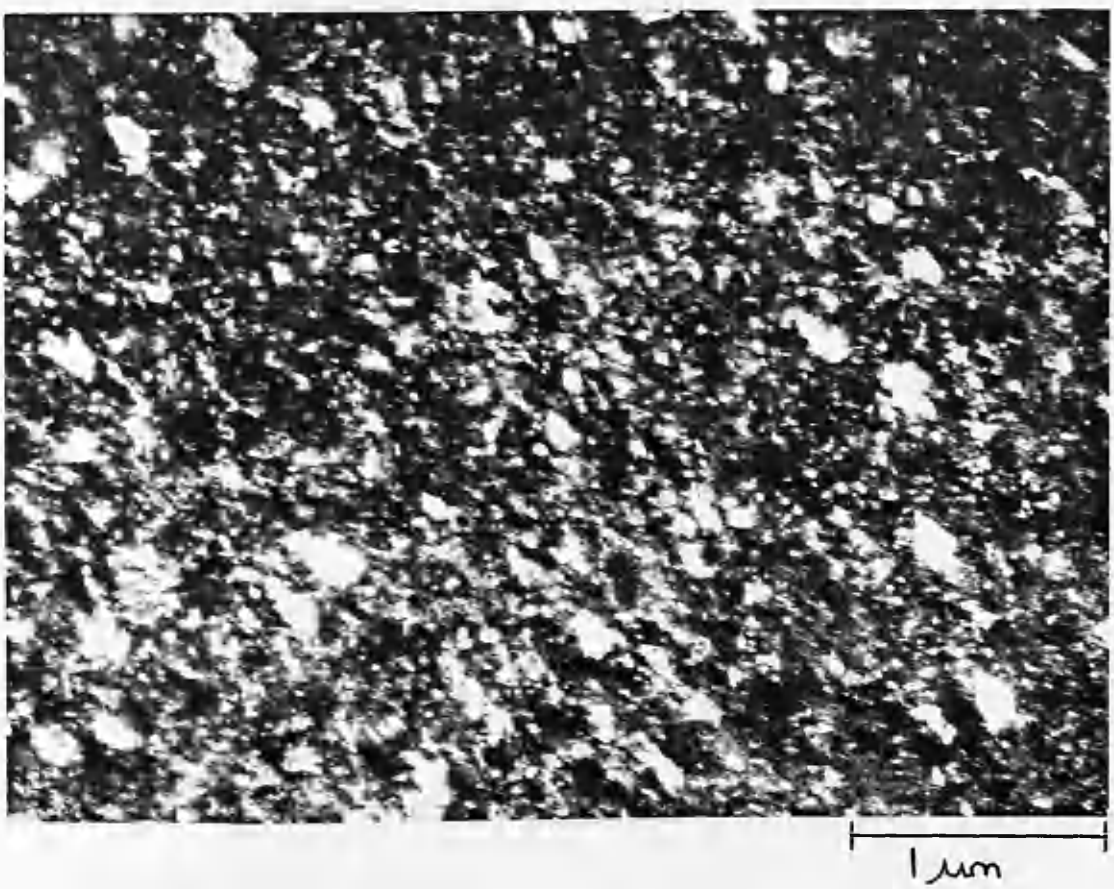

Figure 5.4c Bright field and corresponding Dark field image of sample C

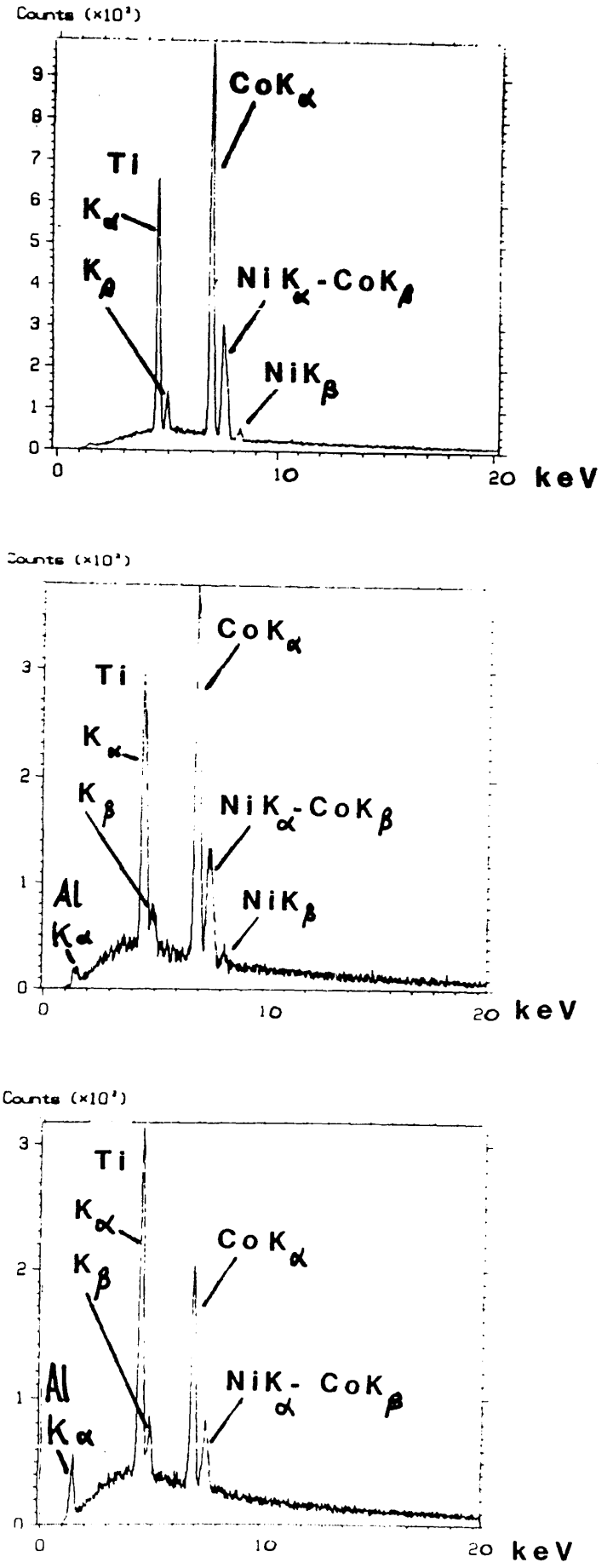

Figure 5.5 Typical X-ray spectra from samples A (top), B (middle) and C (bottom).

K_α and the cobalt K_β peaks. The large overlap between these peaks meant that the only two well resolved peaks were the cobalt K_α and the nickel K_β. To be able to claculate the elemental ratio it was necessary to calculate the Co K_β contribution to the peak centred on the Ni K_α energy using the appropriate partition function. This quantity was then subtracted from the total integral to determine the number of counts which arise from the Ni K_α transition alone. One other x-ray production process which introduces counts to the spectrum, which reveal little about the target composition is Bremstrahlung radiation generation. This is produced when the incident electron is slowed down by the intense Coulombic field, which surrounds the nucleus. The very similar energies of the characteristic peaks for Co and Ni allows the number of photons produced by this additional mechanism to be approximated by a simple linear function of energy. This simplification enabled a straightforward linear stripping procedure to be adopted to determine the actual number of x-ray photons which were produced by the Co K_α and the Ni K_α transitions alone. The results of this analysis are shown below, and show that to within experimental error the composition of the microscope samples is the same as that of the bulk ingots irradiated during fabrication.

	Bulk ratio (Ni/Co)	MET ratio (Ni/Co)
A	0.25	0.28±.02
B	0.25	0.25±.02
C	0.25	0.22±.04

The x-ray spectra needed no further correction as no other

peaks were visible around the energy of the cobalt and nickel peaks used to conduct the compositional analysis.

5.8 THICKNESS DETERMINATION OF THE MET FILMS

The magnetic layer thickness is a very important quantity for thin film magnetic recording media. This quantity influences the form of the domain boundary wall and therefore the recording density. It also affects the size of the output signals measured on replay through the product $M_r\delta$. Clearly, therefore, the magnetic layer thickness of recording materials is of considerable importance in determining the micromagnetics, and hence if an explanation for the observed magnetic microstructure is to be made then this quantity must be known for each sample studied.

5.8.1 PHYSICAL THICKNESS DETERMINATION

In addition to examination of electron microscope images of microtomed samples the physical thickness of sample A was estimated from images of the film edge obtained using a Scanning Electron Microscope (SEM).

5.8.1.1 FILM EDGE EXAMINATIONS USING A SEM

The only treatment necessary to allow edge examination of the specimen within a scanning electron microscope (SEM) was the evaporation of a thin layer of platinum to prevent

the sample charging while under irradiation. A piece of tape, which had been thoroughly cleaned was cut with a pair of scissors. This piece of tape was placed in an angled holder for examination within the microscope. Figure 5.6 is a photograph of sample A taken on a Hitachi S800 SEM. This figure reveals the physical thickness of the tape and additionally illustrates the pronounced curvature of the columnar microstructure induced by the continuously varying angle of incidence (CVI) fabrication procedure. We believe that the rather unexpected success of this method was due to the additional strain present within these films, necessary to prevent the tape 'cupping'. When the film is cut perpendicular to this strain direction, ie along the magnetic easy-axis, the subsequent relief causes groups of columns to 'pop-up' out of the film plane and expose the edge. The measurements were made on tape pieces some distance from the cut edge, to be certain that the images and the measurements made from these were representative of an intact film. The physical thickness of sample A was determined to be 121±7nm.

5.8.2. MASS THICKNESS DETERMINATION OF THE MET FILMS

As the physical thickness of the standard MET film, sample A, had been well established using the methods outlined above, this sample could be used as a reference with which samples of unknown thickness could be compared. This section details experiments which measure the mass

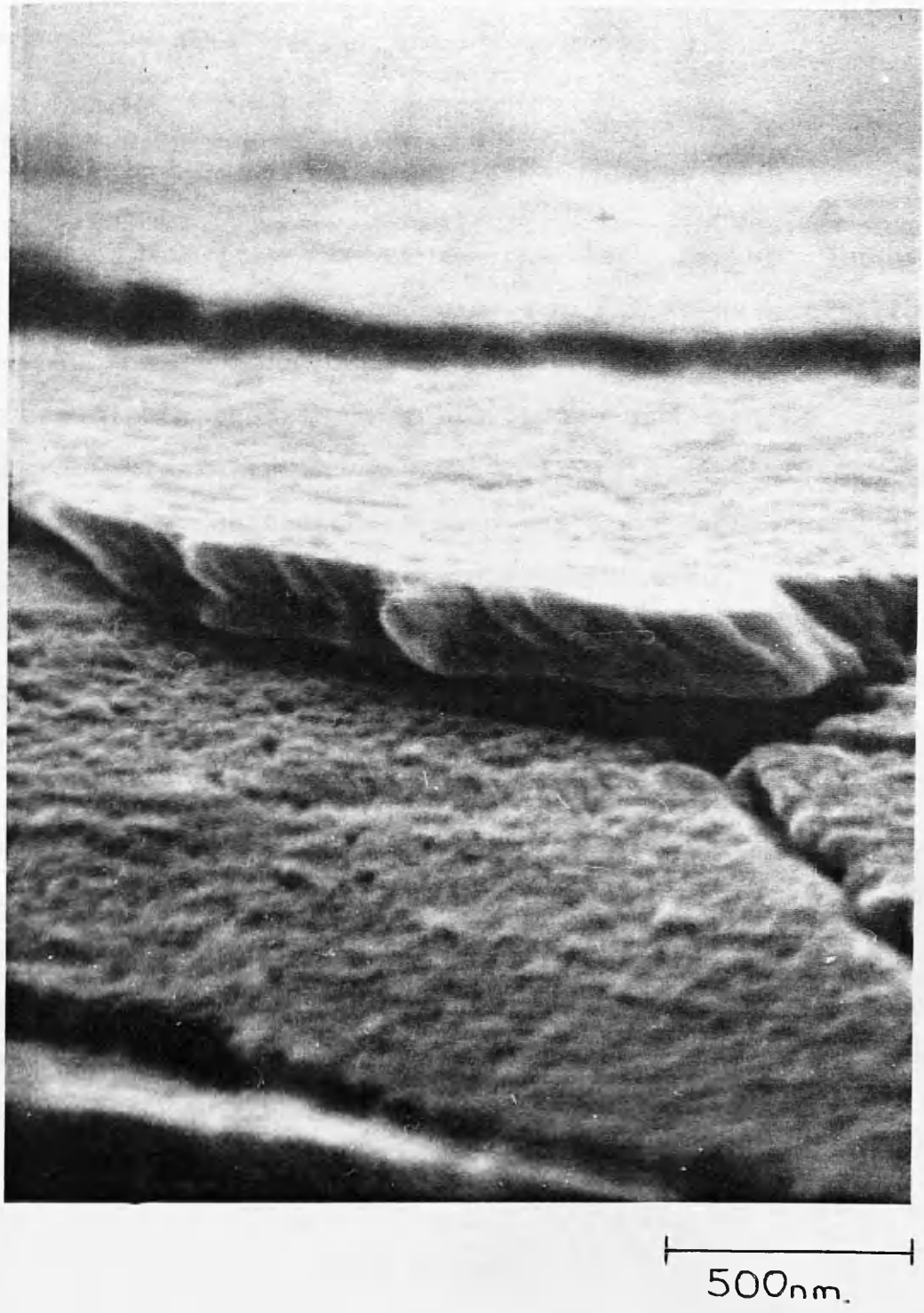

Figure 5.6 SEM image of sample A revealing the curved physical microstructure.

thickness of the samples. This quantity is more important to establish than the physical thickness, since the magnetic interaction within the electron microscope, on which the quantitative micromagnetic analysis relies, is governed by this and not the other quantity.

5.8.2.1 EFFECTIVE ELECTRON ABSORPTION IN THE CTEM

Electron absorption based on the Beer Lambert law was initially used as a rough guide for thickness estimation. In this the electron density which impinged on the viewing screen within the electron microscope was used to compare other samples with the standard. It is essential that the illumination conditions, such as the condenser lens currents and the size of apertures used, are fixed, otherwise the absorption coefficient derived from the standard would vary. Two microscope samples would be loaded into the machine. A quick check on which illumination conditions provided measurable currents for both samples was first conducted. Next a series of measurements of on screen intensity would be made both when illuminating the specimen, I(t), and also when on an empty grid square, I_o. From this an effective electron absorption coefficient could be derived and used, along with the same measurements made for the other sample, to estimate the unknown thickness.

$$I(t) = I_o \exp(-\mu t)$$

The results indicate that sample B has a mass thickness ratio of 0.69±0.1 and sample C 0.36±0.06 relative to sample A compared with 0.72±.06 and 0.31±.04 from the microtomed specimen.

5.8.2.2. ELECTRON ENERGY LOSS SPECTROSCOPY (EELS)

Electron energy loss spectra for each of the samples were obtained to provide another estimate for the mass thickness[10]. From these, and a knowledge of the inelastic mean free path, λ, for the films, the actual mass thickness could be established from the following equation

$$I(t) = I_{o}\exp(-t/\lambda)$$

This would enable an estimate for the density deficit of each film to be made. We are very grateful to Dr C.P.Scott for both helping to obtain these spectra and also for carrying out the subsequent data processing. Figure 5.7 illustrates spectra representative of samples A, B, and C respectively. The results obtained are summarised below:

Sample	(t/λ)
A	1.44±0.03
B	1.25±0.08
C	0.57±0.08

In addition to this information these spectra indicated

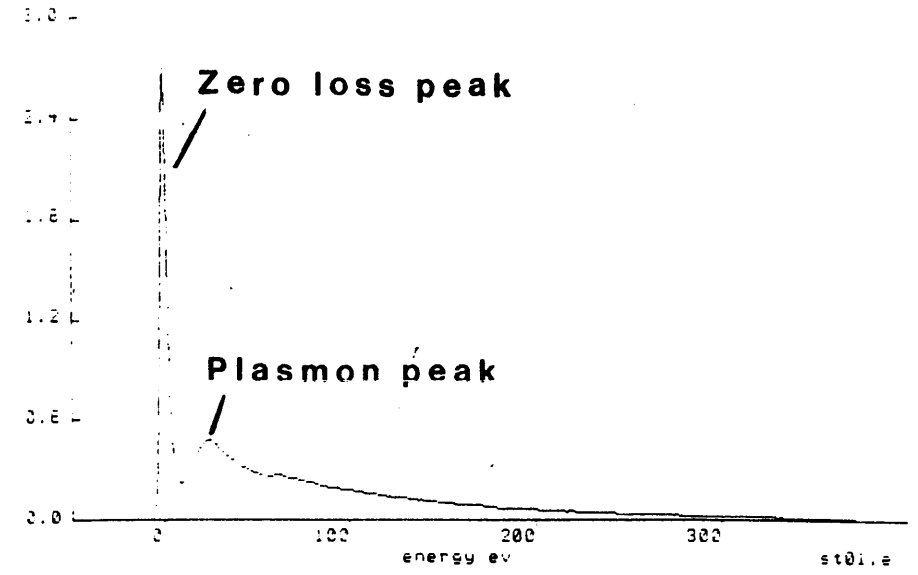

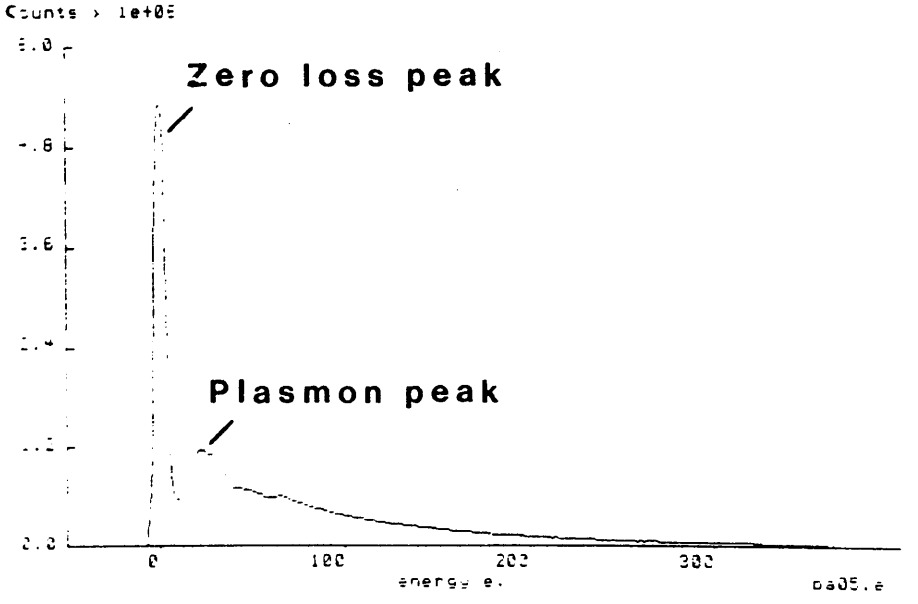

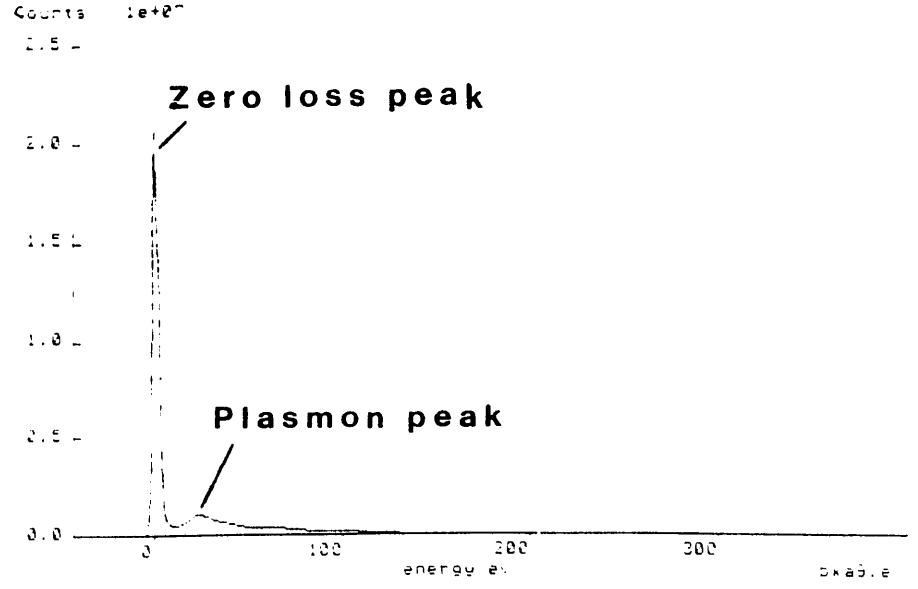

Figure 5.7 Typical EELS spectra from samples A (top), B (middle) and C (bottom).

the presence of oxygen within the films, which, although to be expected, could not have been established using the earlier x-ray analysis outlined. The expanded EELS spectra are shown in figure 5.8, the oxygen edge is most clearly visible in the bottom spectrum, which is the spectrum obtained from sample C.

As no theoretical inelastic mean free path for these particular films could be found an accurate estimate for the mass thickness could not be made. However the value for elemental nickel would serve as a good guide and has the value 50±2nm.[11] Thus assuming that the MET films have the same density as the corresponding bulk materials, then the equivalent thickness of each film is given in table 5.A. The second column of data contains the effective mass thickness of each of the samples having accounted for the reduction in density which the fabrication procedure introduces.[12]

Sample	mass thickness assuming bulk density	mass thickness corrected density	thickness as measured
A	72±3nm	97±4nm	127±5nm
B	63±5nm	85±7nm	91±6nm
C	29±4nm	39±5nm	39±5nm

Table 5.A The mass thickness values as determined from the EELS spectra.

These values cannot be relied on too strongly since the

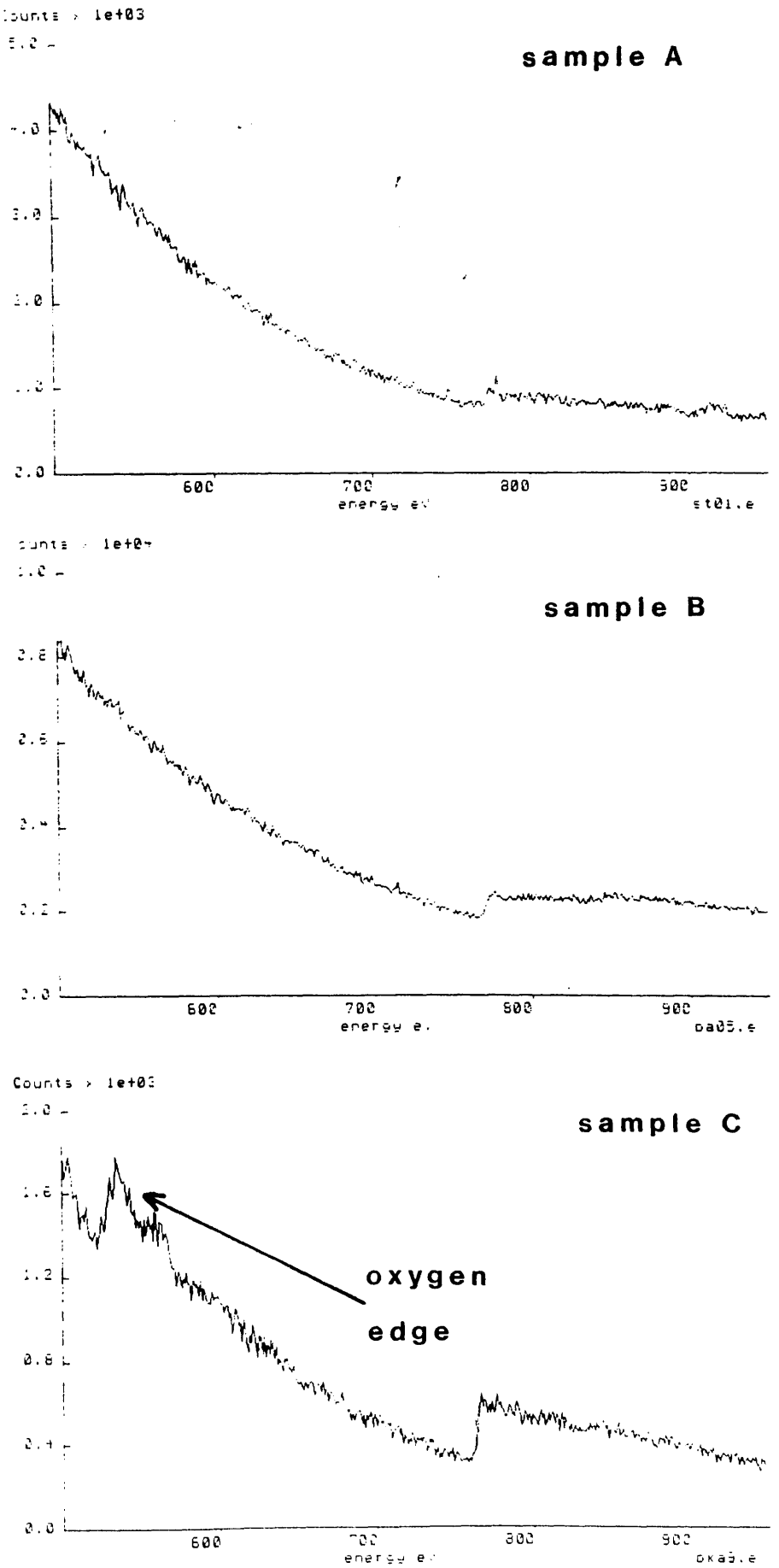

Figure 5.8 EELS spectra expanded to reveal the oxygen edge

actual mean free path values for the MET films are unknown. However these establish a guide with which we may compare our other thickness estimates. The differences between columns 2 and 3 is likely, at least in part, to the different inelastic mean free path which the porous MET will have compared with bulk nickel.

SUMMARY

In this section we have established that the MET films have a curved polycrystalline physical microstructure with a degree of c-axis texture. The composition of the films was seen to be unaltered by the specimen preparation process. However as only planar samples were studied the curved columnar microstructure would obscure any elemental segregation which might exist within these films. The fabrication of the MET alloy using the CVI technique was also seen to produce a porous film which has only 75% of the density of the bulk materials. Combining all of the results the thickness of sample A was established as 124±9nm with (B/A) = 0.76±.08, and (C/A) = 0.37±.02.

References

1. J.S. Gau, W.E. Yetter, J. Appl. Phys., 61, 3807 1987

2. E. Kita *et al*, IEEE Trans. Mag. MAG **17** 6 3193 1981

3. K. Nakamura *et al*, IEEE Trans. Mag. MAG **18**, 6 1077 1982

4. S.L. Zeder, J. Appl. Phys., 61, 3804, 1987

5. Ting-Ho, Dan Lee, IEEE Trans. Mag. MAG **26** 1 171 1990

6. D.E Speliotis *et al*, J. Appl. Phys., 36, 972 (1965)

7. A. Feuerstein, M. Mayr, IEEE Trans Mag MAG **20** 1 51 1984

8. K. Shinohara *et al*, IEEE Trans. Mag. MAG **20** 5 824 1984

9. S. Chikazumi, Physics of Magnetism, Wiley, (1964)

10 Dr A.J. Craven, private communication 1987

11 R.F. Egerton, Electron Energy Loss Spectroscopy in the Electron Microscope, Plenum Press, New York, 1986

12. K. Shinohara *et al*, IEEE Trans. Mag. MAG 24 6 2994 1984

CHAPTER 6 THE BULK MAGNETIC CHARACTERISATION OF THE MET FILMS

6 INTRODUCTION

To be able to understand the micromagnetic form of the recorded tracks that each different MET film adopts, it is essential to have an accurate description of the appropriate bulk magnetic properties. These properties were determined using vibrating sample magnetometry (VSM). Extensive torque magnetometry measurements were only carried out for one of the films.

6.1 BULK MAGNETIC CHARACTERISATION

In a VSM the sample is vibrated at a fixed frequency within a region of homogeneous magnetic field. The uniform magnetic field magnetises the ferromagnetic sample and an estimate of the induction, arising from the magnetisation within the sample, can be made from the AC voltage induced as it moves back and forth through a detection coil. The applied field is cycled through $\mp H_{MAX}$ to produce the familiar B-H loop, ie the hysteresis loop. The bulk magnetic characteristics appropriate for a high density recording material have been detailed in chapter 2. However a straightforward estimate of the suitability of each can be made from the 'squareness' of the loop. This allows a quick overall comparison of each material to be made and should be kept in mind when the graphs included in this section are discussed. For each of the recording

films studied the in-plane hysteresis loops in two perpendicular directions were obtained, one being along the direction parallel to the vapour plane and the other perpendicular to this. In addition the thickest of the MET samples underwent rigorous bulk magnetic characterisation at Philips Research Laboratories in Eindhoven, to whom we are indebted. We are especially grateful to Dr J.P.C. Bernards for the analysis of the data and the conclusions he suggested. The thickest MET film studied happens to be the same thickness as that now sold commercially.

6.2 RESULTS AND DEDUCTIONS FROM THE HYSTERESIS LOOP MEASUREMENTS

The hysteresis loops of samples A, B, and C, taken parallel and perpendicular to the 'easy-axis', are shown in figures 6.1a, 6.1b and 6.1c respectively. These graphs were obtained from a VSM machine at IBM Research Laboratories in San Jose. In every case the loop squareness is higher with the applied field direction parallel to the vapour plane, indicating that this direction has the more suitable bulk magnetic characteristics for magnetic recording applications. The loops from sample C most clearly illustrate an apparent diamagnetic effect, which only close examination of the other graphs confirms. The field dependence of this effect meant that only the remanence values obtained from these graphs would in fact be representative, all other derived quantities would require suitable adjustments to account for this effect. The magnitude of the observed effect,

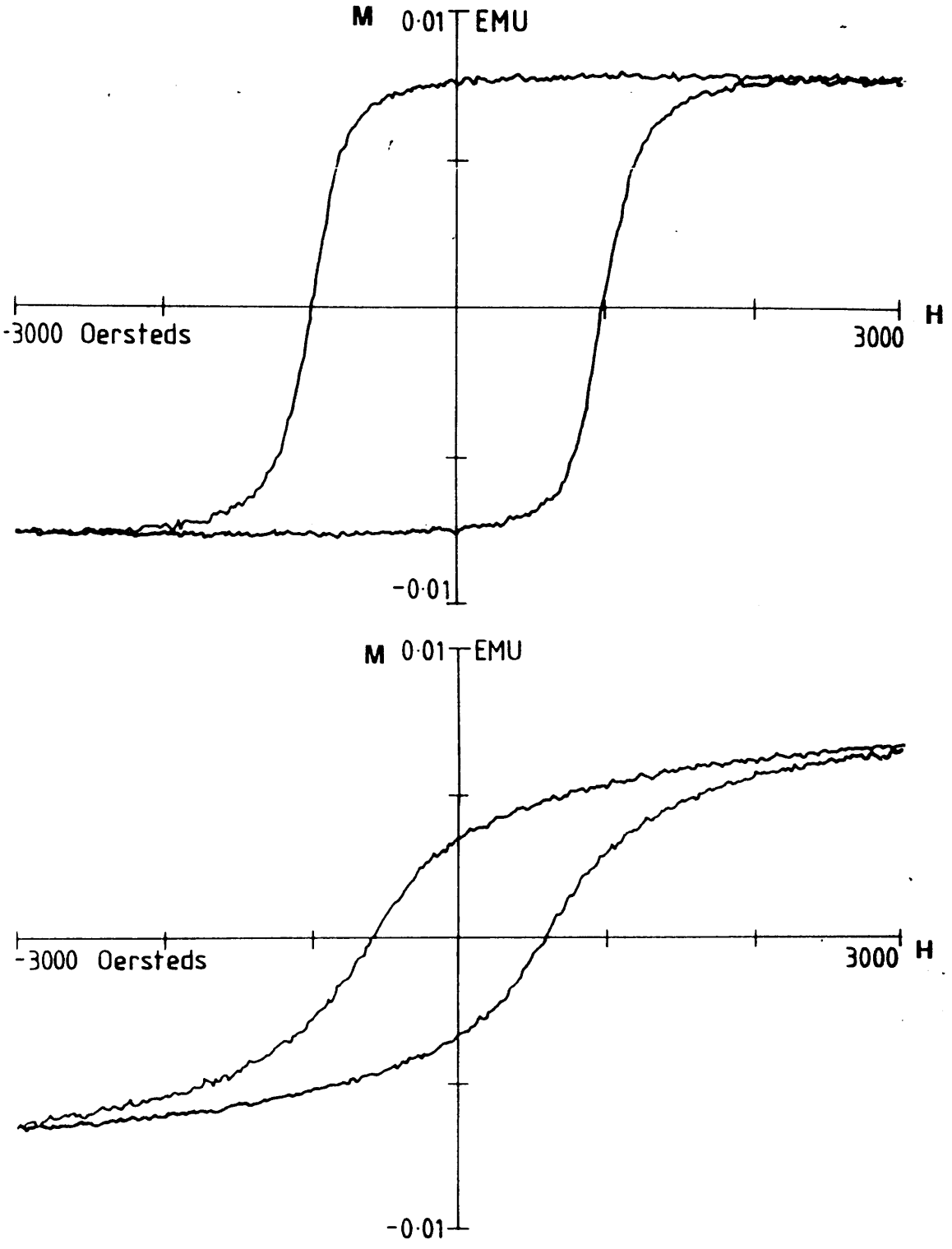

Figure 6.1a Sample A hysteresis curves taken parallel (top) and perpendicular (bottom) to easy axis

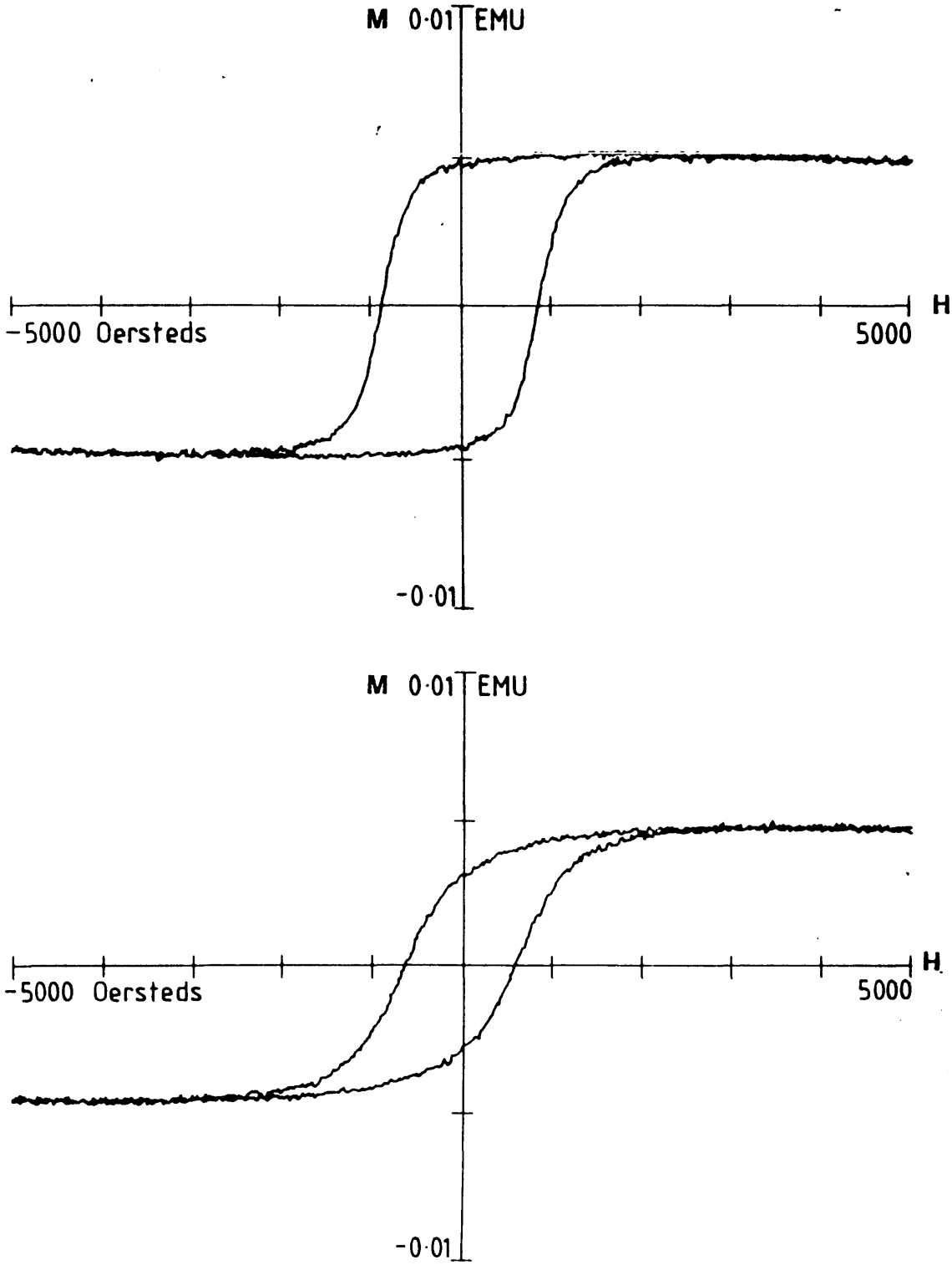

Figure 6.1b Sample B hysteresis curves taken parallel (top) and perpendicular (bottom) to easy axis

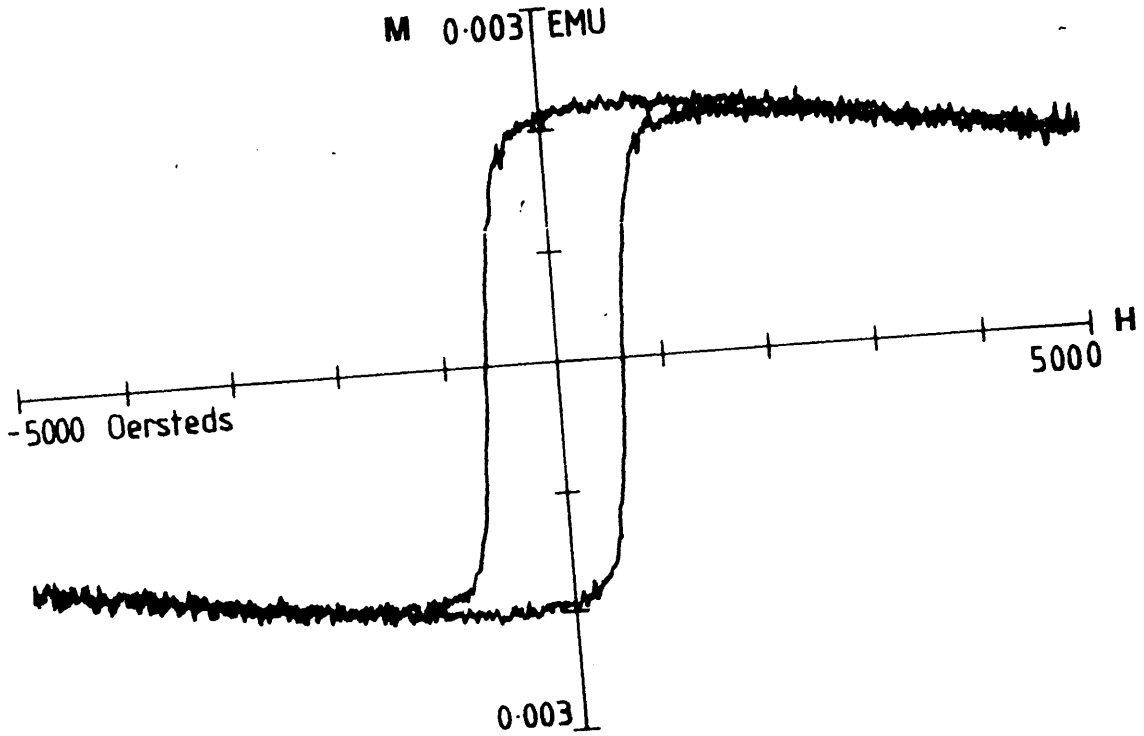

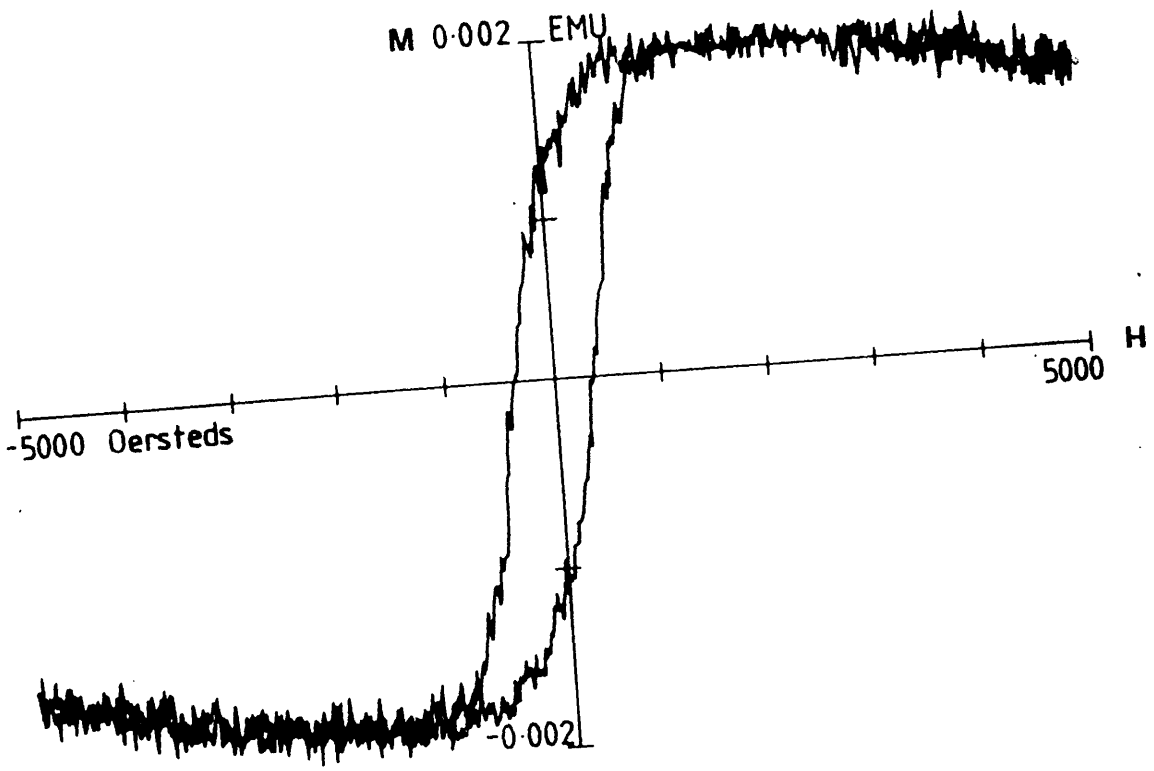

Figure 6.1c Sample C hysteresis curves taken parallel (top) and perpendicular (bottom) to easy axis

which introduced a diamagnetic contribution to the sample, is far too large to be true diamagnetism. We believe that the phase detection system, which these machines employ to extract the signal arising from the magnetisation of the sample, was experiencing some form of 'pick-up' during these measurements.

Fortunately the bulk magnetic properties of sample A had been characterised on another VSM machine in Philips Research Laboratories in Eindhoven, which did not show this effect. An estimate of the diamagnetic contribution could be made by comparing the data obtained for sample A from this VSM with the data from the VSM in San Jose. This was necessary as neither sample B nor sample C were measured in Eindhoven, and with this information the modified hysteresis loops for samples B and C could be correctecd. This was achieved as follows. The problematic hysteresis loops were able to provide accurate estimates for the remanent magnetisation, since these were measured at zero applied field. The hysteresis curve obtained using the VSM in Eindhoven provided an accurate estimate for the ratio of the remanent magnetisation to the saturation magnetisation, ie (M_R/M_S). With this information we could estimate the diamagnetic contribution by subtracting the calculated M_S from that measured graphically. In each case we had two estimates of the diamagnetic effect, one at each of the two different directions of applied field. Having established the contribution made by this unwanted effect, the magnetisation for each of the samples could be determined. We must exercise caution however since we cannot be

certain that the effect responsible for the apparent diamagnetism exhibits a similar field dependence. The effect of this on the saturation magnetisation was calculated at ~±4400 Oersteds, and found to be ~7E-4 emu and only ~2E-4 emu around the film coercivities. Table 6.A contains the results determined from these MH loops corrected for this effect.

	$M_{r_{\parallel}}\delta*10^{-3}$	$SR_{\parallel}$	$H_{c_{\parallel}}$	$M_{r_{\perp}}\delta*10^{-3}$	$SR_{\perp}$	$H_{c_{\perp}}$
	$emu.cm^{-2}$		Oe	$emu.cm^{-2}$		Oe
A	14.8±.3	0.85±.04	968±12	6.9±.3	0.40±.03	591±13
B	9.4±.3	0.70±.05	880±25	6.1±.3	0.47±.08	616±25
C	4.1±.1	0.58±.04	628±25	2.5±.2	0.37±.09	364±50

TABLE 6.A Bulk magnetic properties of samples A, B, and C.

The most significant result from the VSM analysis is the reduction in magnetic anisotropy found as the thickness of the recording layer is reduced. Sample C is seen to be the most isotropic since SR(90°)/SR(0°) = 0.64, although moderate anisotropy is still indicated from the loops. The variations observed in the remanence values, unaffected by any diamagnetism, cannot strictly be used to confirm this reduced anisotropy, since these contain contributions from both changes in film thickness as well as any changes in film remanence. To isolate these two effects we used the information about the thickness of sample A, detailed earlier in chapter 5, to normalise these results to this thickness, each VSM sample having the same area. The thickness corrected values are contained in table 6.B.

	$M_{R\parallel}$	$M_{R\perp}$	$M_{S\parallel}$	$M_{S\perp}$
	$emu.cm^{-2}$	$emu.cm^{-2}$	$emu.cm^{-2}$	$emu.cm^{-2}$
A	(14.8±0.3)E-3	(6.9±0.3)E-3	(17.5±0.7)E-3	(17.3±0.9)E-3
B	(12.5±1.6)E-3	(8.2±1.2)E-3	(17.7±2.5)E-3	(16.9±2.4)E-3
C	(11.7±1.1)E-3	(6.0±0.6)E-3	(18.9±2.2)E-3	(18.1±2.1)E-3

TABLE 6.B Remanence and Saturation Magnetisation values normalised to thickness of sample A.

The results contained in the first column indicate that the remanence does not scale with specimen thickness, indicating that it is in fact the strength of the anisotropy which varies between samples. One factor which might explain this variation is the reduction in the amount of c-axis texture present within the individual columns as the film thickness is reduced. The only factor which we have neglected with this assumption is the sheet demagnetising effect, which will be most pronounced for the thinnest sample, sample C. Although this effect does not favour any particular in-plane direction it will attempt to increase the magnitude of the in-plane component of magnetisation. Therefore the significance of this effect will have to be considered in addition to any variations in magnetic anisotropy when we discuss the quantitative micromagnetic results in chapter 7.

From the squareness ratios we can conclude that the perpendicular saturation magnetisation, $M_{S\perp}$, is in every case lower than the corresponding parallel saturation magnetisation, $M_{S\parallel}$. This can be explained from the fact

that this direction is the hard-axis and therefore the field strength must be substantially larger in order to saturate the magnetisation in this direction, and perhaps the maximum field strengths used with these VSM machines (5KOe) have been insufficient to effect this.

Explanation of the coercive force variations observed requires appreciation of the distribution of the magnetic domain wall pinning sites throughout the microstructure of these films. The variation in parallel coercivity for the films can be understood in terms of the changing surface area of the individual columns and also the lateral extent of the internal voids. As the film thickness is increased the volume restricting domain wall motion is also increased, since larger grains cast longer shadows, and the coercivity rises accordingly. The fabrication process introduces on average a fixed number of these barriers per unit length along the film and therefore when we magnetise the film in the orthogonal direction, a direction in which the magnetic material is more continuous, we encounter fewer obstructions and consequently this direction has a lower coercivity.

The presence of these voids is clear from the hysteresis loop measurements since these films must have a lower density than the bulk alloys to explain the rather low saturation magnetisation levels cf tabulated data, even from the Philips VSM data. The effect of the oblique incidence evaporation is to lower the MET film density by ~25%[1]. In addition to posing physical barriers these voids allow atmospheric oxygen to penetrate the microstructure and form oxides with the ferromagnetic elements. In the

production of these films at no time were other impurity elements deliberately introduced to modify the coercivity, however the reaction of the constituents with atmospheric oxygen is also important in determining the complete mechanism responsible for the coercivity of these materials[2]. The reaction of the components of the film with oxygen increases the coercivity of the films as the oxides of cobalt and nickel restrict the movement of domain walls and therefore introduce additional domain wall pinning sites. Although the films are exposed to the atmosphere which produces significant oxidation, subsequent lubrication of the films reduces the rate of further oxide formation. One other factor which may influence the anisotropy of the MET films is the tangential strain to which the films are subject to prevent the foils from cupping. The effect of this is to introduce what appear as cracks, when examined in the electron microscope, and these would act to increase the anisotropy of the films along the easy-axis, although we cannot be certain that these structures have the same form prior to specimen preparation.

From the extensive bulk magnetic characterisation of sample A the coercivity of this was shown to vary as $(\cos\alpha)^{-1}$ in the vicinity of the 'easy-axis', where α is the angle between the applied field and the tape direction, see figure 6.2; this is indicative of coherent rotation of the magnetisation[3,4].

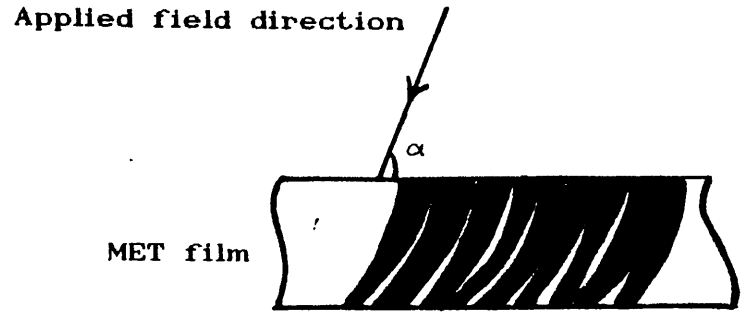

Variation of remanence and coercivity measured with respect to film plane

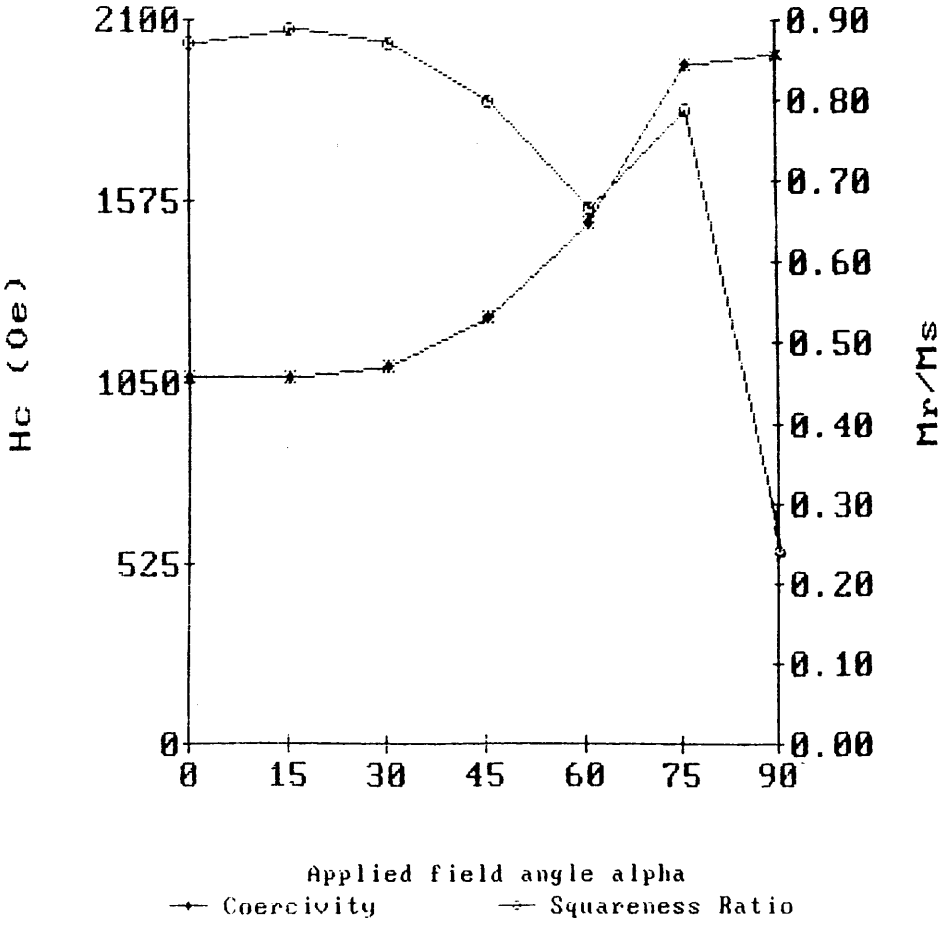

Figure 6.2 Diagram at the top of the page is a schematic illustrating the direction of the applied field. The lower diagram illustrates the variation of the squareness ratio, (Mr/Ms), and coercivity, Hc, as a function of angle between applied fieid and filmplane.

6.3 DETERMINING THE FILM THICKNESS USING VIBRATING SAMPLE MAGNETOMETRY

The last experimental method from which we were able to determine the mass thickness of the samples came from these bulk magnetic measurements. The magnetic volume of each sample could be estimated from the saturation magnetisation level of each, and since the area was the same for each sample any difference could be attributed to different thicknesses. The magnetic volume ratios for both loop directions are given in table 6.C.

	Field Strength	Parallel Loop	Perpendicular Loop
(B/A)	5027 Oe	0.76±0.03	0.75±0.03
(C/A)	5027 Oe	0.39±0.03	0.39±0.03

Table **6.C** The magnetic volume ratios for samples A, B and C.

We were also able to determine the amount by which the effective density of the MET films differed from the bulk values using the Philips VSM data. The high field saturation magnetisation values were consistent with a reduction of some 26% when compared with the bulk alloy data[5], weighted according to the relative amounts of cobalt and nickel present, which agrees with values quoted in the literature.[6]

6.4 REMANENCE CURVES

To complete the bulk characterisation of the three MET samples the angular variation of the magnetic remanence was measured. In each case the sample is initially saturated at the chosen field-specimen orientation, and then allowed to relax in zero field. The remanent magnetisation at angles ranging from 0-90 degrees from the easy-axis, at 10° intervals, was then measured using the standard VSM phase sensitive detection methods. Figures 6.3a, 6.3b and 6.3c are the remanence curves for samples A, B, and C respectively. From each of these three graphs it is evident that some rotation of the specimen had occurred when attempting to load these within the pole pieces of the electro-magnet. The maximum remanence occurs after saturating the material along the magnetic easy-axis ie along the tape's length. When these samples were initially positioned inside the VSM we attempted to orient the magnetic easy-axis parallel to the applied field and the angle between these should therefore have been 0°. The fact that the maximum remanence dose not occur at 0° we attribute to unintentional misalignment introduced by the operator and not to the easy direction changing.

The important information contained within these graphs is the way in which the remanent magnetisation falls as we increase the angle between the applied field and the easy-direction. The curves are almost flat when the magnetic field lies at small angles from the easy-axis, indicating the increased possibility of local potential energy minima. The gradient of the curve

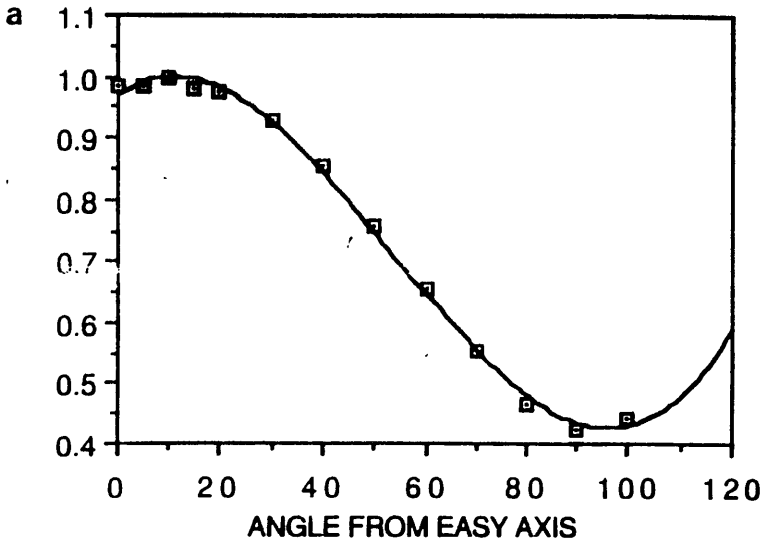

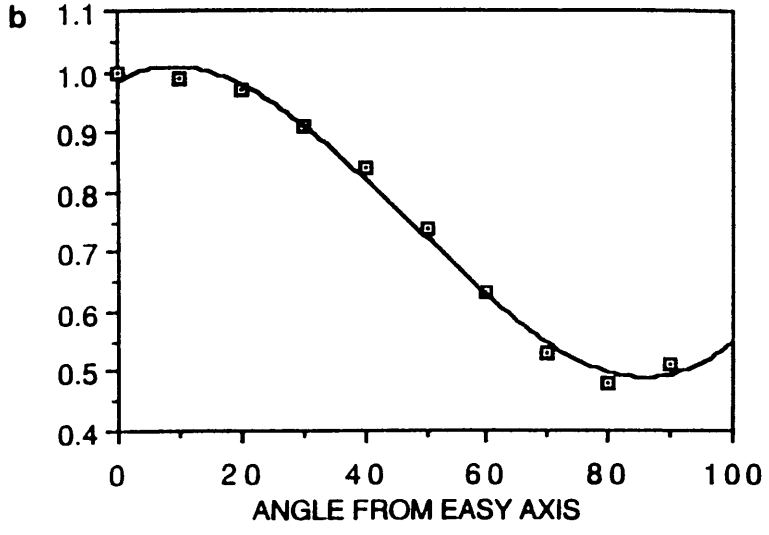

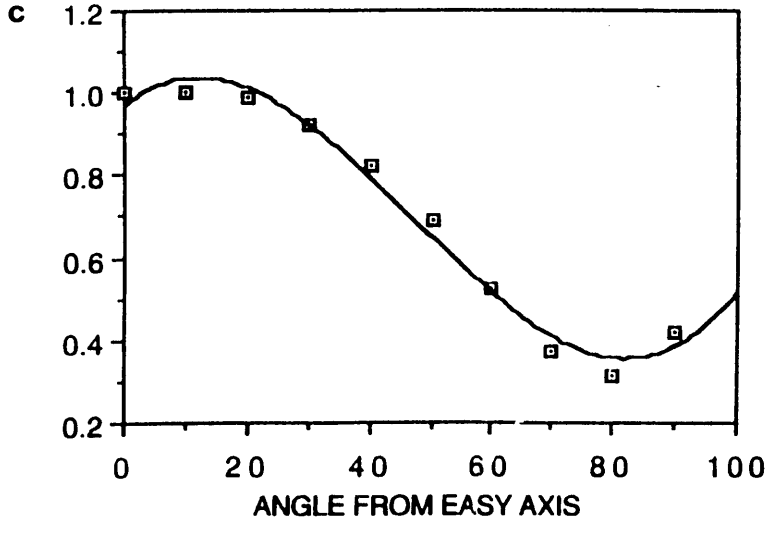

Figures 6.3(a-c) **The remanence curves of samples A (top), B (middle) and C (bottom)**

increases as we introduce larger and larger angles between the field and this easy-direction. This information has a bearing on the magnetic structure of the video tracks, dealt with in detail in chapter 7. At present we only wish to stress that the level of residual magnetisation will be greater when we saturate close to the easy-axis for each of these films, and falls as we increase the angle between the applied field and this direction.

6.5 TORQUE CURVE MEASUREMENTS

The angle of inclination of the easy-axis has been established using torque magnetometry[7] for each of the three thicknesses of films studied in this thesis. The results are contained in table 6.D. We were only able to obtain the actual torque curve for sample A, which is shown in figure 6.4.

Sample	Angle (Degrees)
A	17
B	12
C	6

TABLE 6.D Inclination angle of magnetic easy-axis for the three samples.

The effect of these different angles of inclination would be to modify the size of the demagnetising field experienced by the magnetisation within recorded tracks. The relative size of the in-plane component of

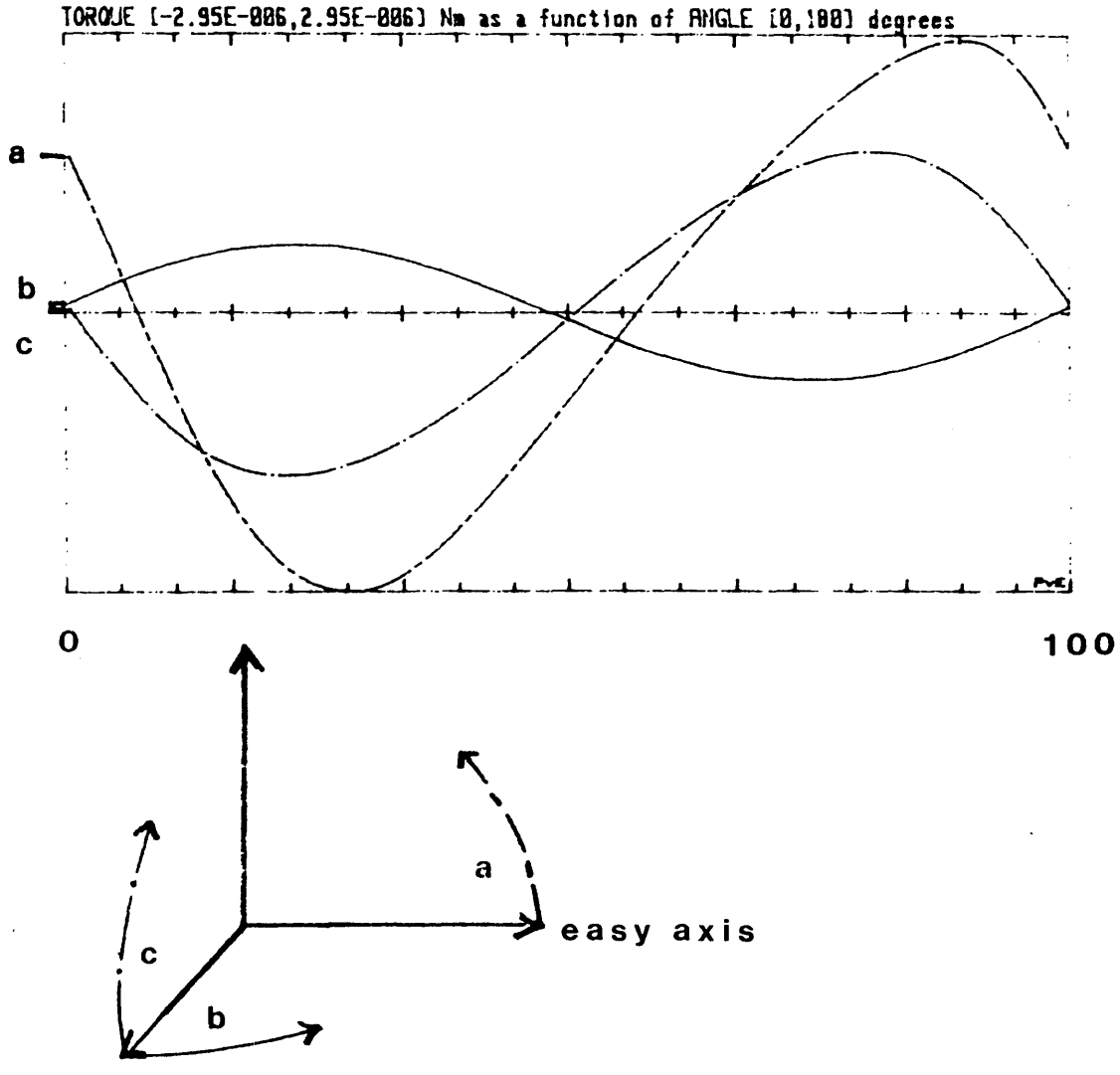

Figure 6.4 The three in plane torque curves obtained from sample A courtesy of Dr J Bernards

magnetisation would be greatest for sample C as a result of the reduced angle of inclination of the magnetic easy-axis, and therefore the magnetisation within the recorded domains written on this specimen would experience the largest demagnetising field effects. Although the differences between the in-plane components would be slight, ~4%, the effect of this may be considerable particularly as the thinner film has a reduced magnetic anisotropy. The effect of both of these effects on the equilibrium magnetic structure of the written tracks must therefore be considered when similar structures observed in the thicker films are compared.

We believe that the magnetic anisotropy of CoNi MET is due to a combination of several effects. The curved columns try to induce an easy-axis which is canted out of the film plane, which is presumably enhanced by c-axis texture, while the elongation of the microcrystallites and the thin film sheet demagnetising effect, try to restrain the magnetisation to lie within the film plane. The net effect of these conflicting forces makes for an overall easy-axis pointing along the tape direction but not lying entirely within the film plane.

SUMMARY

This section described the experiments conducted to determine the bulk properties of the films and commented on the observed variations. We were able to estimate the relative mass thicknesses of the samples which were seen to provide close agreement with the estimates made using

electron microscope methods. We also discussed the significance of the inclination of the easy-axis out of the film plane on the micromagnetic structure of recorded transitions, which we attributed to a curved columnar microphysical structure perhaps modified with some c-axis texture.

References

1. K. Shinohara *et al*, IEEE Trans. Maq. MAG 24 6 2994 1984
2. J.S Gau *et al*, IEEE Trans. Maq. MAG 22 5 582 1986
3. J.S. Gau *et al*, IEEE Trans. Maq. MAG 24 6 2994 1988
4. K. Shinohara *et al*, IEEE Trans. Maq. MAG 20 824 1984
5. S. Chikazumi, Physics of Maqnetism, Wiley (1964)
6. K. Shinohara *et al*, IEEE Trans. Maq. MAG 24 6 2994 1984
7. S. Swaving *et al*, J. Maq. Maq. Mat. 67 155 1987

CHAPTER 7 MICROMAGNETIC RESULTS FROM BOTH QUALITATIVE AND QUANTITATIVE STUDIES OF THE WTITTEN TRACKS

7. INTRODUCTION

This section describes qualitative observations of the magnetic structure of the recording tracks using the Fresnel and Foucault modes of Lorentz electron microscopy[1], and attempts to explain the images obtained using these techniques based on our knowledge of the recording experiments carried out by THORN EMI. All of these examinations were performed on two CTEM machines, a JEOL 1200EX, and a JEOL 2000FX.

7.1 MAGNETIC CHARACTERISATION OF THE WRITTEN TRACKS USING A CTEM

Initial electron optical observations of the magnetic structure of the recorded samples was carried out using two well established methods of Lorentz electron microscopy, the Fresnel and Foucault methods, both of which were detailed in chapter 3. Using these the geometry of the recorded domains could be determined, as could an indication of the form that the domain boundary wall adopted within these films.

The video recorder used has two heads which have opposite gap azimuths (±10°), to reduce crosstalk between tracks, as detailed in appendix 1. As the tracks lie at 5° with respect to the 'easy-axis' this means that the

direction in which the recorded magnetisation is oriented by the head field during writing is different for each head. For one head this direction is only -5° from the 'easy-axis' but for the other a more considerable 15°, see figure 7.1. The track written at 15° to the easy-axis will be referred to as track A, and the track which is written at -5° to this same direction will be known as track B.

Contrary to the picture of the recorded magnetic structures that ferrofluid decoration of the samples had established, see figure 7.2, these transmission electron microscopy techniques revealed a marked difference between the tracks recorded at +15° to the easy axis of magnetisation and those written at -5°. It was clear from the images that a substantially larger Lorentz deflection was experienced by electrons which passed through the track written at +15°. Figures 7.3(a-d) and 7.4(a-e) are Foucault images of samples A, B, and C recorded with wavelengths of 1μm and 10μm respectively and illustrate these differences between the recorded tracks.

The differences observed between tracks A and B, can be explained by the angular variation of the bulk magnetic remanence curves, detailed in chapter 6, which are illustrated in figure 7.5. Assuming that the write field is sufficient to saturate the magnetisation in the applied field direction then when recording at 15° to the easy-axis, the level of residual magnetisation along the track will be lower than that within the track written closer to the easy-axis. As a result of this the final

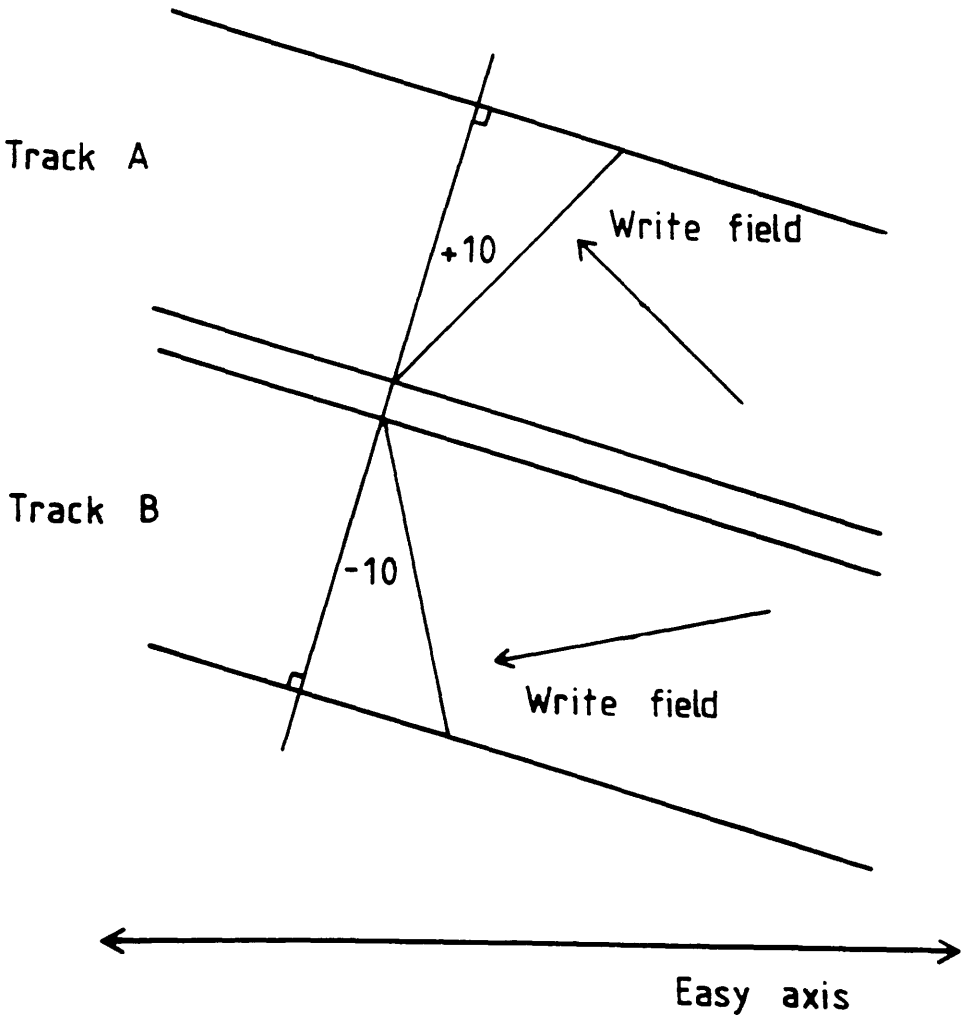

Figure 7.1 Illustration of the different directions in which the two video heads orient the recorded magnetisation during writing.

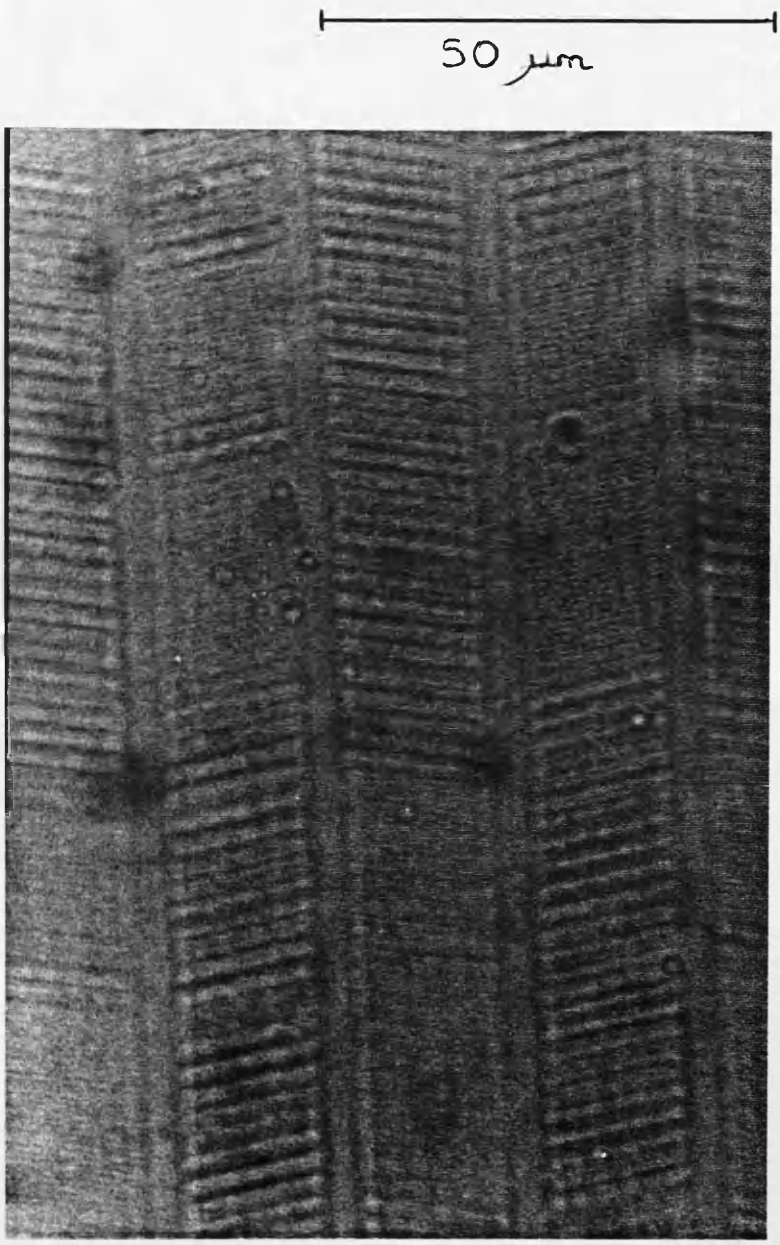

Figure 7.2 Ferrofluid image showing both types of video recording tracks, written at +15° and -5° with respect to the easy-axis. The smallest spacings within each track correspond to a recorded wavelength of 0.8μm.

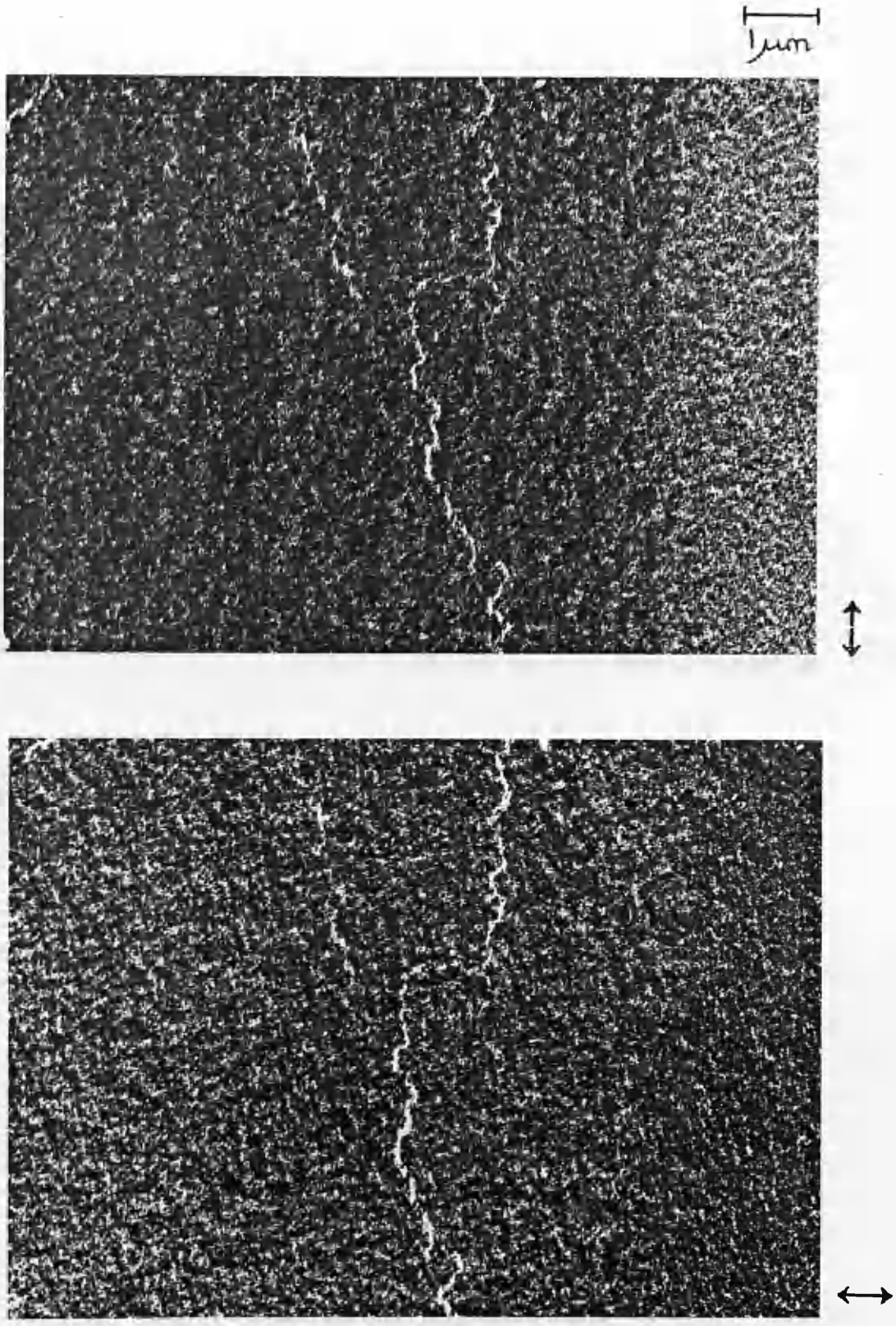

Figure 7.3a Foucault images of the video track written on sample A with a recorded wavelength 0.8μm at -5° to the easy-axis. These images map induction parallel (top) and perpendicular (bottom) to the track direction, as indicated by the arrows.

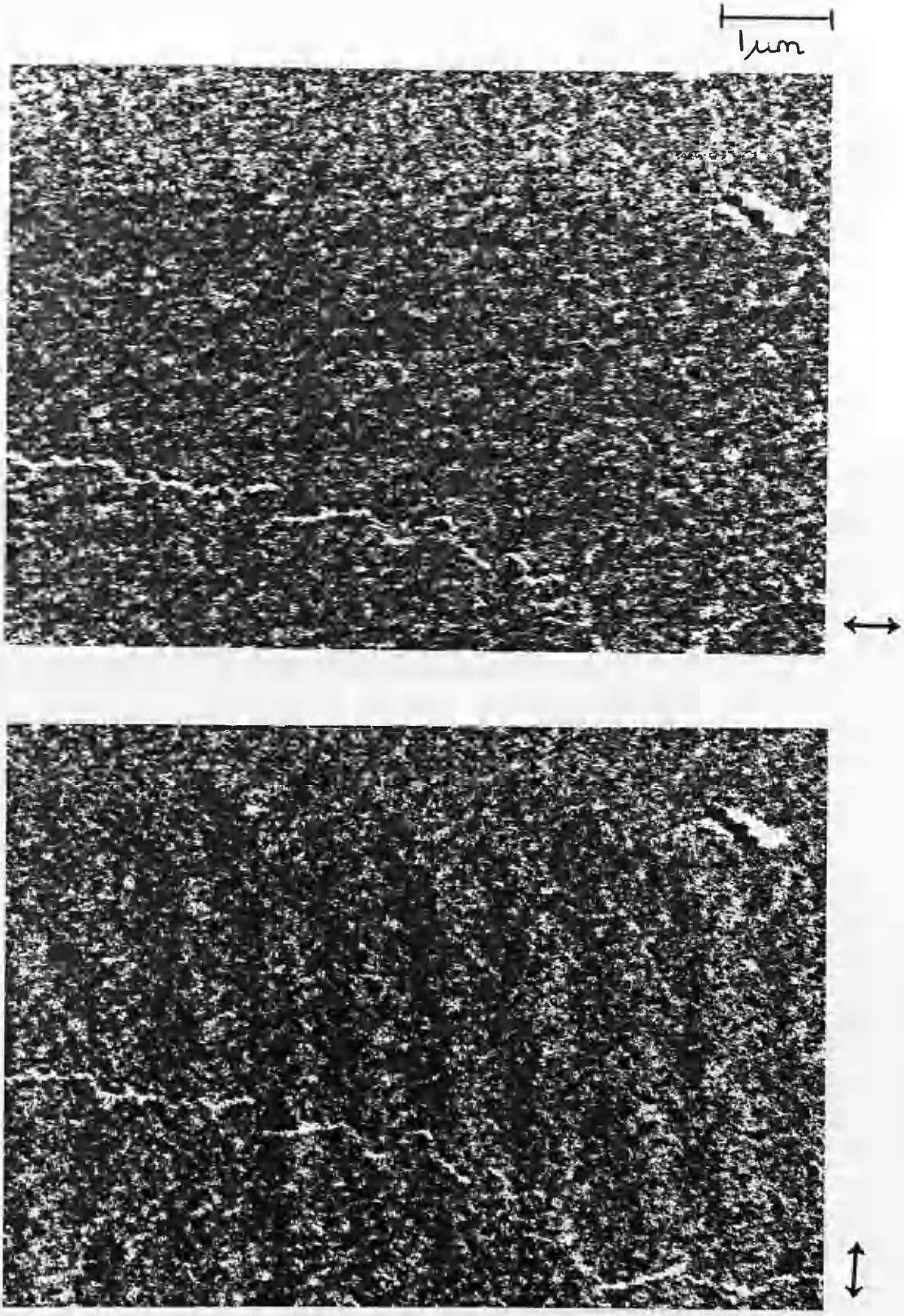

Figure 7.3b Foucault images of the video track written on sample A with a recorded wavelength 0.8μm at 15° to the easy-axis. These images map induction parallel (top) and perpendicular (bottom) to the track direction, as indicated by the arrows.

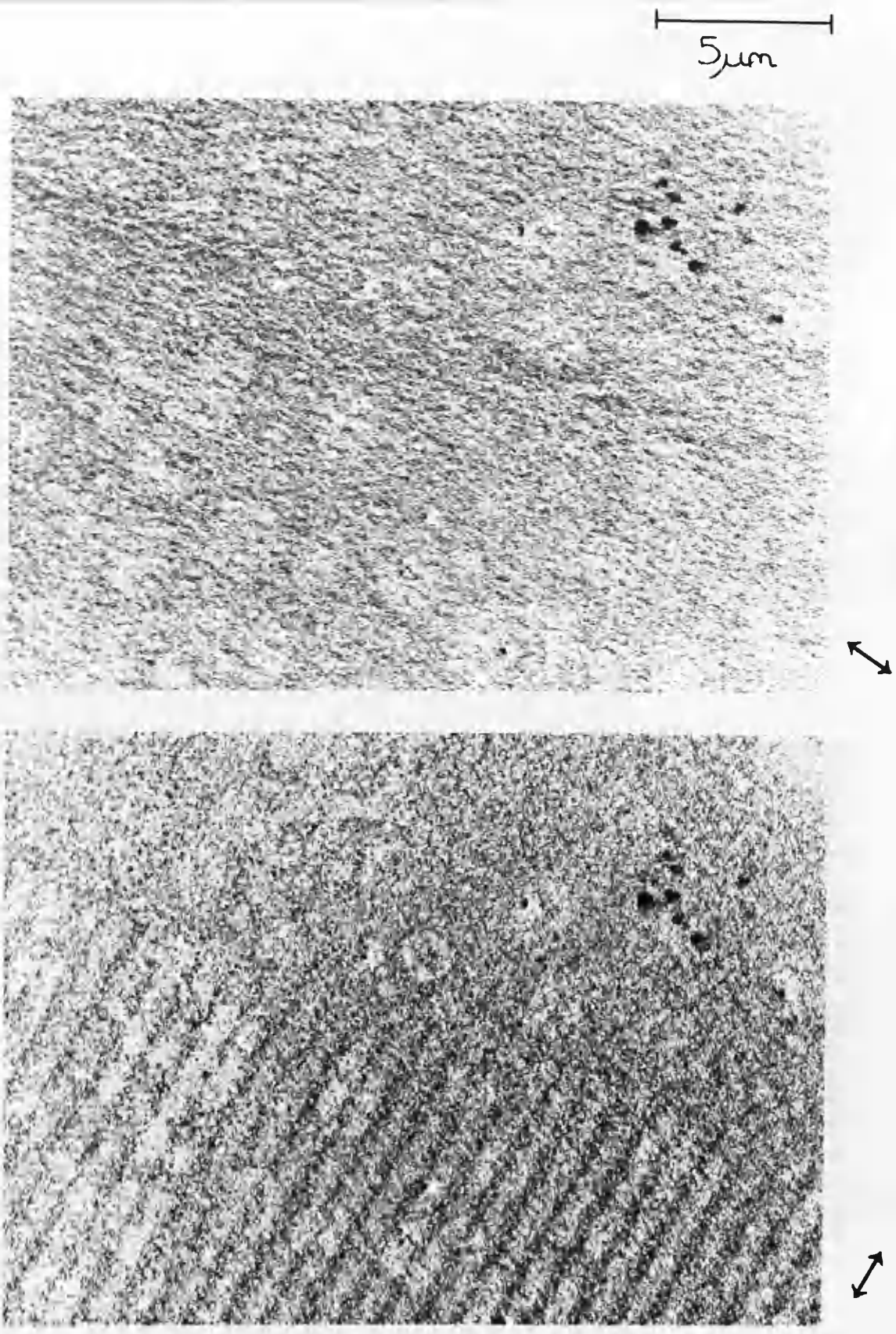

Figure 7.3c Foucault images of both video tracks written with a recorded wavelength 1.0μm on sample B. Only the track written at 15° is clearly visible, however the other track is actually within the upper right diagonal of these images, which map induction parallel (top) and perpendicular (bottom) to the track direction, as indicated by the arrows.

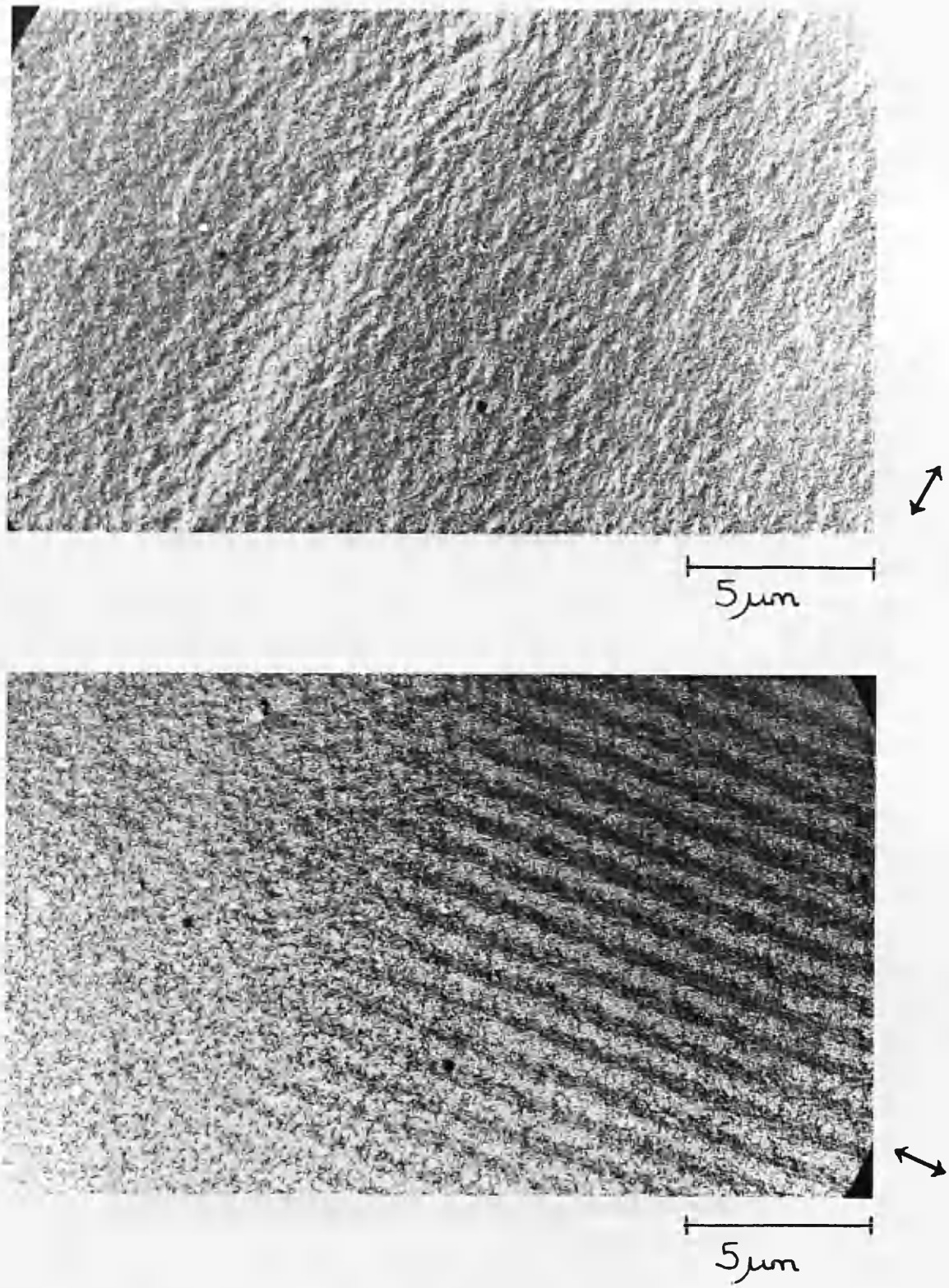

Figure 7.3d Foucault images of both video tracks written with a recorded wavelength 1.0μm on sample C. Only the track written at 15° is clearly visible, however the other track is actually within the upper left diagonal of these images, which map induction parallel (top) and perpendicular (bottom) to the track direction, as indicated by the arrows.

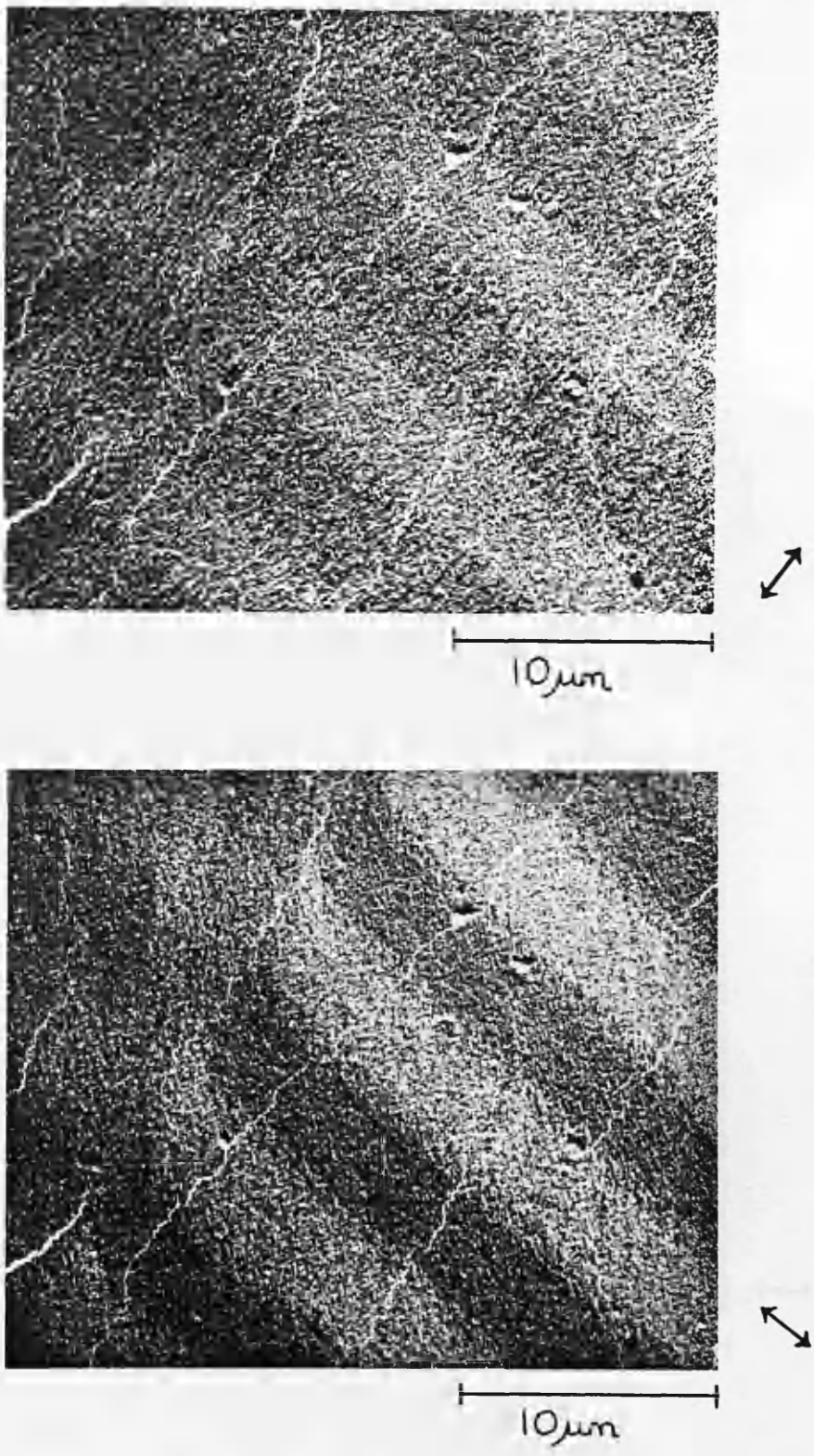

Figure 7.4a Foucault images of both video tracks written with a recorded wavelength 8μm on sample A. Only the track written at 15° is clearly visible, however the other track is actually within the upper left corner of these images, which map induction parallel (top) and perpendicular (bottom) to the track direction, as indicated by the arrows.

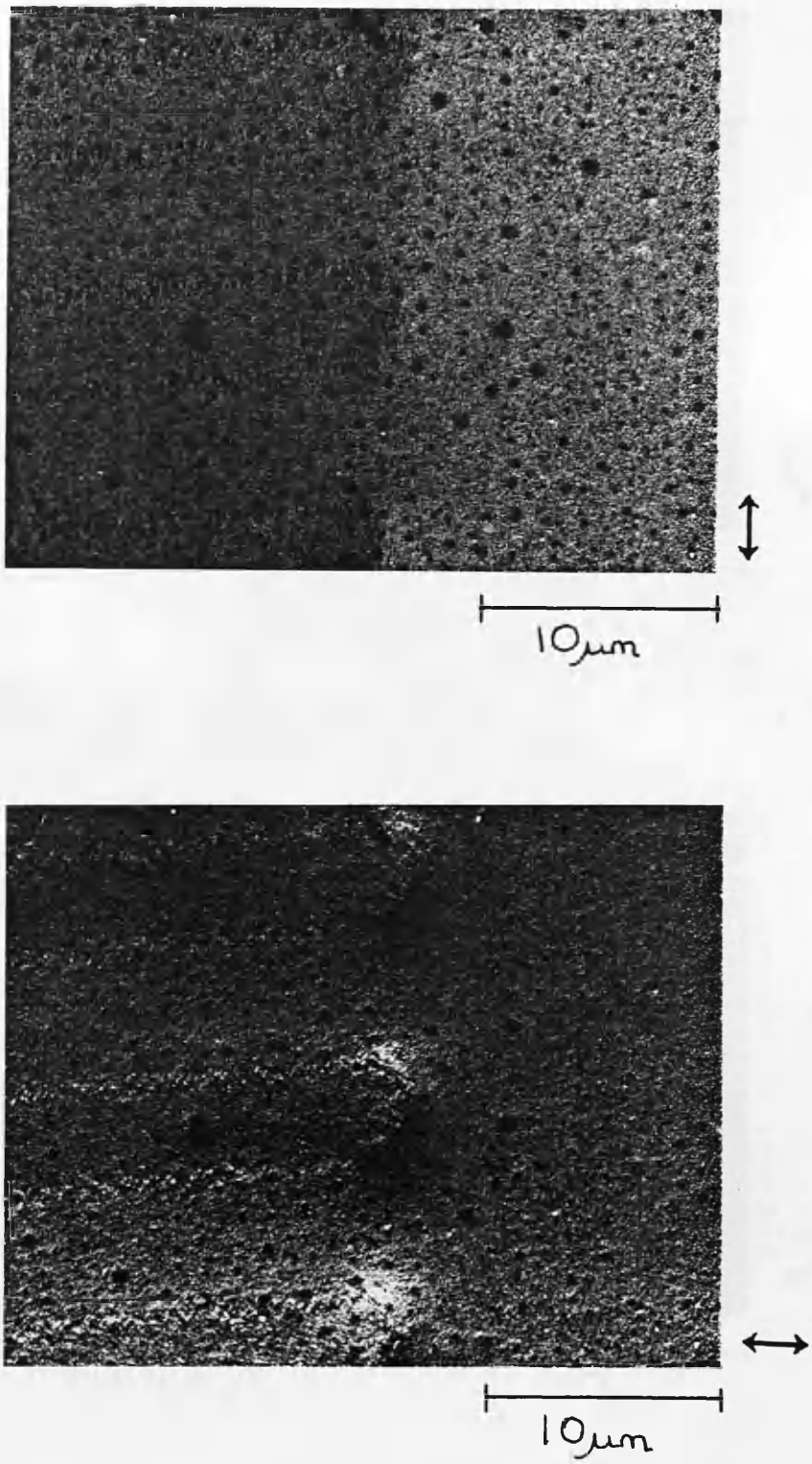

Figure 7.4b Foucault images of the video track written on sample B with a wavelength 10μm at -5° to the easy-axis. These images map induction parallel (top) and perpendicular (bottom) to the track direction, as indicated by the arrows. The track is on the left half of the images.

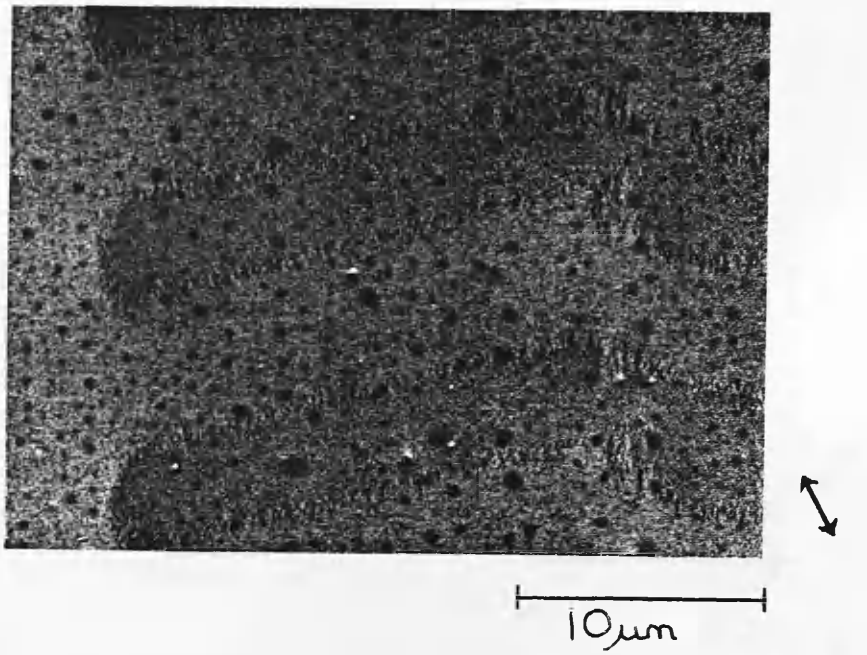

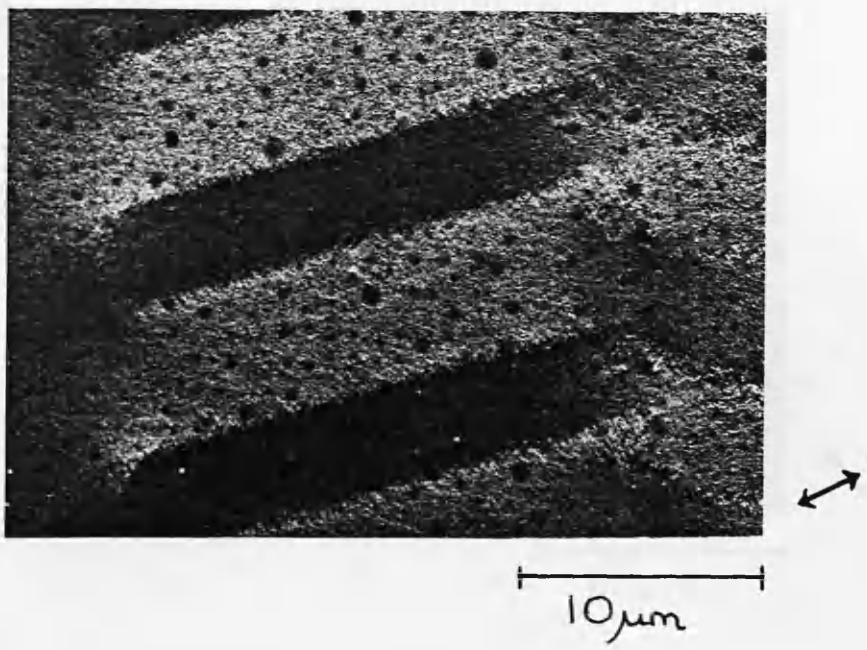

Figure 7.4c Foucault images of the video track written on sample B with a wavelength 10μm at 15° to the easy-axis. These images map induction parallel (top) and perpendicular (bottom) as indicated by the arrows.

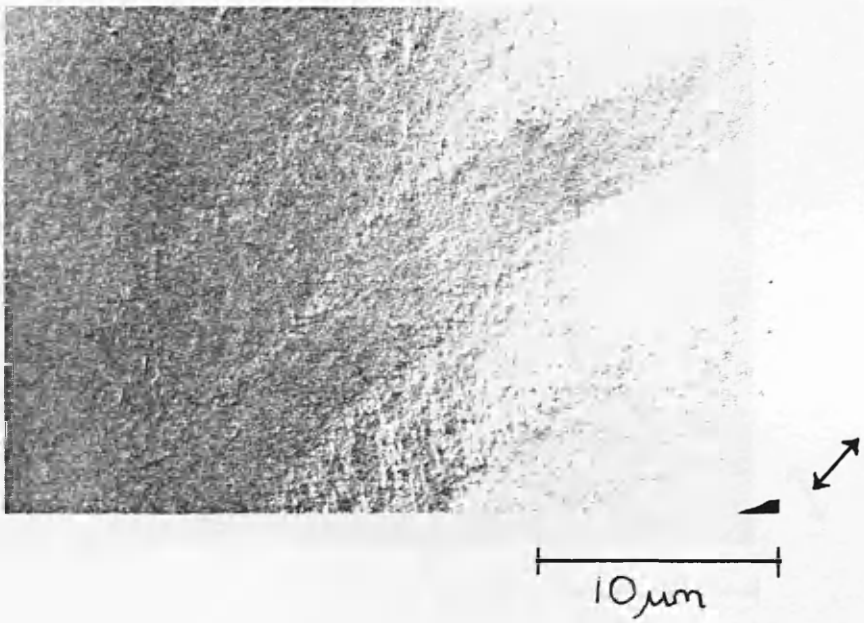

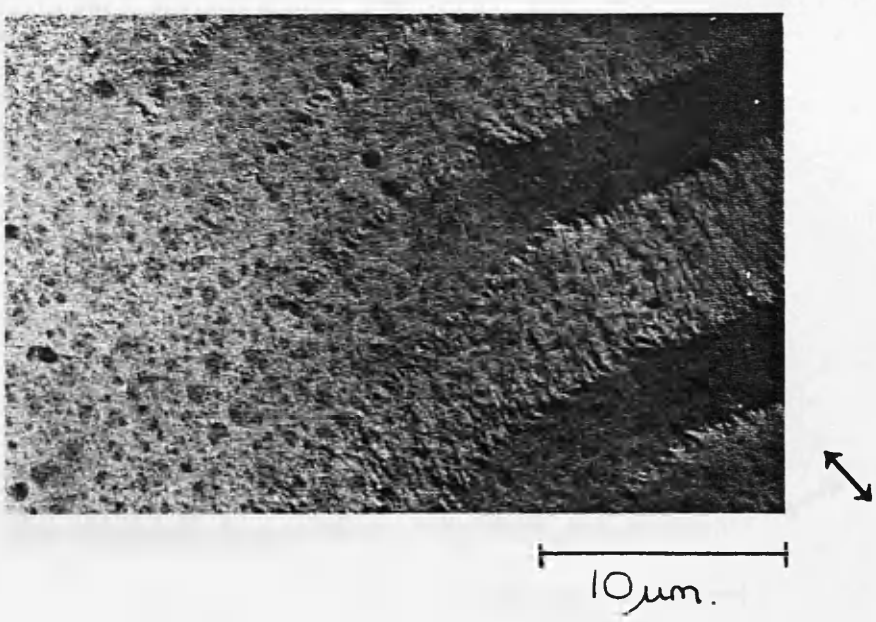

Figure 7.4d Foucault images of the video track written on sample C with a recorded wavelength of 10mm at -5^{o} to the easy-axis. These images map induction parallel (bottom) and perpendicular (top) to the track direction, as indicated by the arrows. The other video track is just visible at the right hand edge.

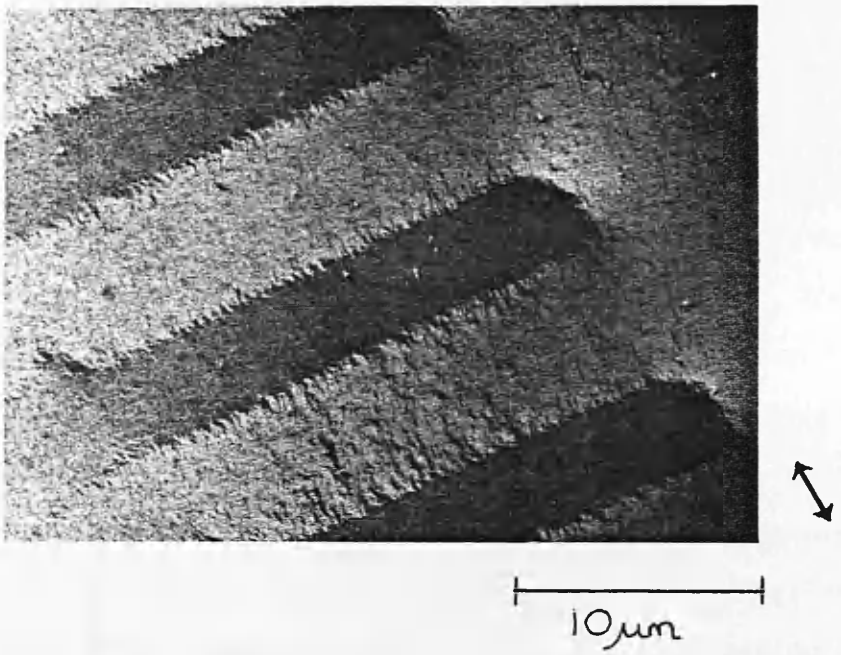

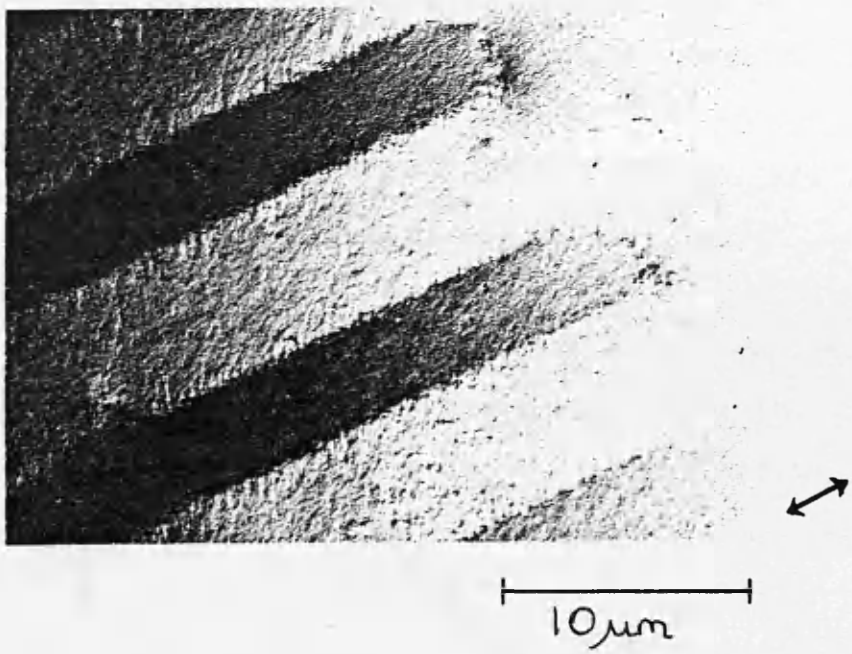

Figure 7.4e Foucault images of the video track written on sample C with a wavelength 10μm at 15° to the easy-axis. These images map induction parallel (top) and perpendicular (bottom) as indicated by the arrows.

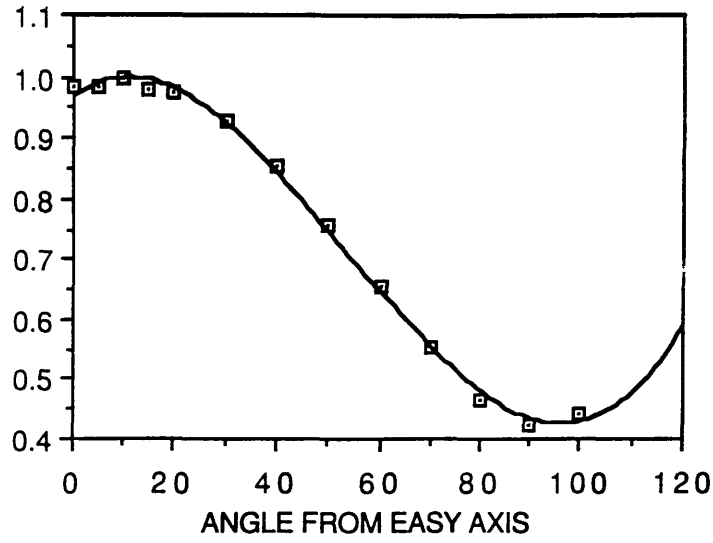

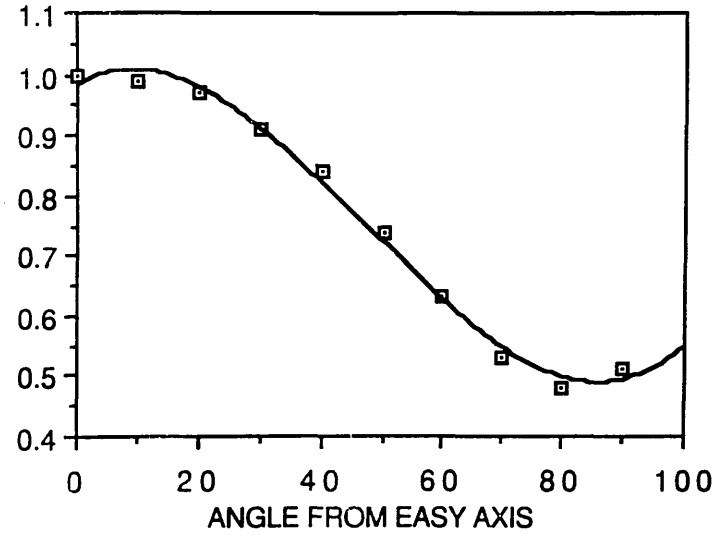

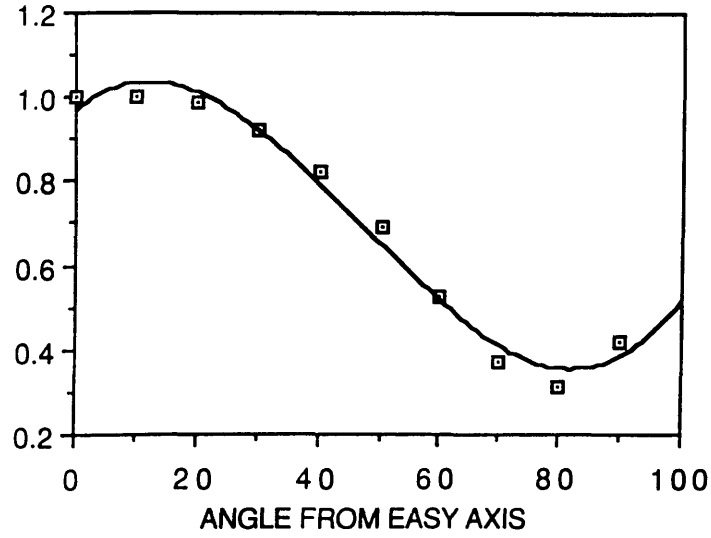

Figure 7.5 The variation of the magnetic remanence as the angle between the applied field and the easy-axis is varied for samples A (top), B (middle), and C (bottom).

orientation of the written magnetisation will be different for the two video tracks. Track A will have a smaller component of magnetisation along the recorded track direction compared to track B, and consequently track A will possess the larger component normal to the track. As the remanence curve is almost flat close to the easy direction, the probability that the magnetisation written in track B might remain at -5° to the easy-axis is increased. The significance of this would be to render track B almost invisible to electron optical observation since M and H would be very nearly anti-parallel and, to first order, any deflection produced by the magnetisation is cancelled by that effected by the stray field. If the magnetisation does relax the full 5° then the perpendicular component in track B would only be ~1/3 of that in track A and, as the image contrast depends on the net deflection of the incident electrons, track A will be the more clearly visible, which agrees with our observations.

It follows from the above discussion that the amount of magnetic flux which passes through the replay head should be lower for track A and consequently the output voltage step should also be reduced. Therefore we would expect that track B should produce larger output signals than track A. As yet no difference in the output levels from tracks A and B has been established. The similarity in output from track A and B might seem surprising given our description of the micromagnetics needed to account for the electron optical observations of these tracks.

However, we believe that other factors might offer a possible explanation. Any redistribution of the magnetisation which may occur as a result of the modification to the demagnetising fields, produced when the replay head is introduced to the system, remains unknown. Unlike the situation with recording heads which fly above the recording surface[2,3], for a contact recording system there is the possibility that the magnetic distribution responsible for the measured output signal is in fact the same within both video tracks when the effect of the high permeability replay head is considered. It is also possible that the difference in output is so small that it is completely masked by the background noise. With the magnetisation lying at 15° to the head gap the signal has only dropped by 3%.

We also considered that the observed difference in track visibility might arise from the specimen preparation procedure. It was postulated that the stress relief which followed the removal of the magnetic layer from the base film might be responsible for this change, as this would alter the internal stress pattern within the film and possibly the magnetic anisotropy. A change in the magnetocrystalline anisotropy might alter the position of equilibrium and the micromagnetic structure adopted within tracks A and B, at the new minimum energy position, might be substantially different. However, if this were responsible then strain variations present within each sample, would produce variations in the observed magnetic microstucture within both the written tracks and the DC

regions. No evidence was found to support this which we believe effectively eliminates specimen preparation as a major contributory factor for the observed differences between the recorded tracks.

7.2 RECORDING ON THE MET FILMS

7.2.1 INTRODUCTION

Each MET film was DC erased along the easy-axis prior to all of the recording experiments detailed in this section. In this section we attempt to explain why different 'bit' patterns would be expected from recordings made on DC erased media using a sine wave. The significance of recording on films with different coercivities is also explained. We also describe the effect that writing onto DC erased media has on the position of the recorded transitions at both high and low recording densities, with the specific aim to explain all of our observations.

We begin by explaining the simplest situation that of recording a transition in the same direction as the background magnetisation, and also when anti-parallel to this direction. Next we address the significance that different coercivities have on the magnetisation distribution expected. Finally we describe the situation at higher recording densities when the transitions are no longer isolated and the consequences of this. Having set the scene we will attempt to account for the results taken from electron microscope images of samples B and C at

wavelengths of 1μm and 10μm respectively. Sample A was not recorded directly onto DC erased media and hence the domain sizes observed required no explanation. For this sample the DC field was produced by the head at -5° to the easy-axis.

7.2.2 RECORDING ON MEDIA PREVIOUSLY SATURATED WITH A DC FIELD

When recording a transition on DC erased media the direction in which the magnetisation is written influences the final position of the domain wall[3]. When recording a transition against the DC magnetisation the field lines exceeding the coercivity produce two distinct transitions, one at the leading edge and another at the trailing edge, see figure 7.6. It is the demagnetising field which arises from the leading edge transition which modifies the position of the final transition written by the trailing edge. In this situation the trailing edge transition is written within this demagnetising field and consequently its position is shifted and the transition broadened. In contrast to this situation when recording in the same direction as the DC magnetisation no leading edge transition is present and therefore the trailing edge transition is unaffected and written in the position dictated by the write field alone.

This situation dominates at low recording frequency where the transitions are sufficiently far apart that the effect of the demagnetising field from neighbouring

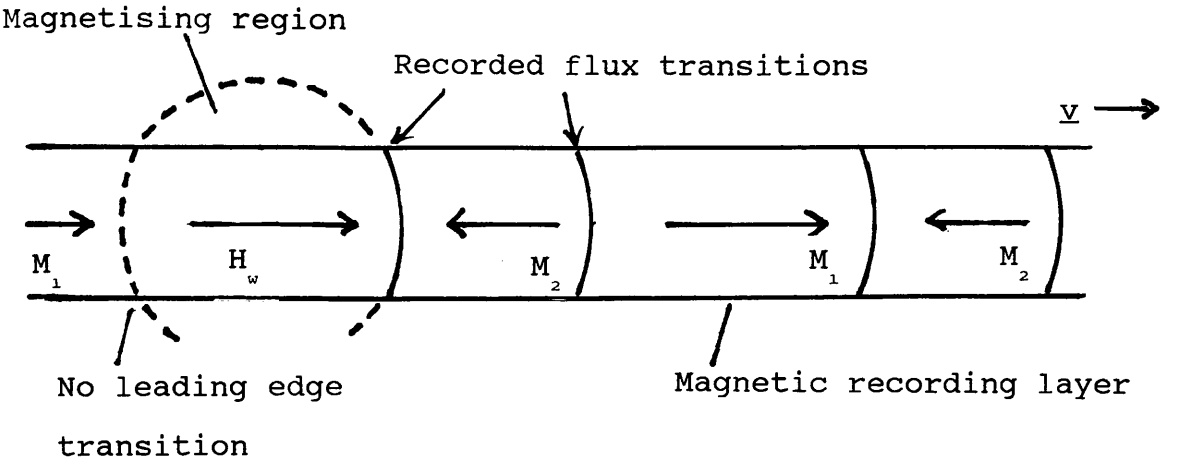

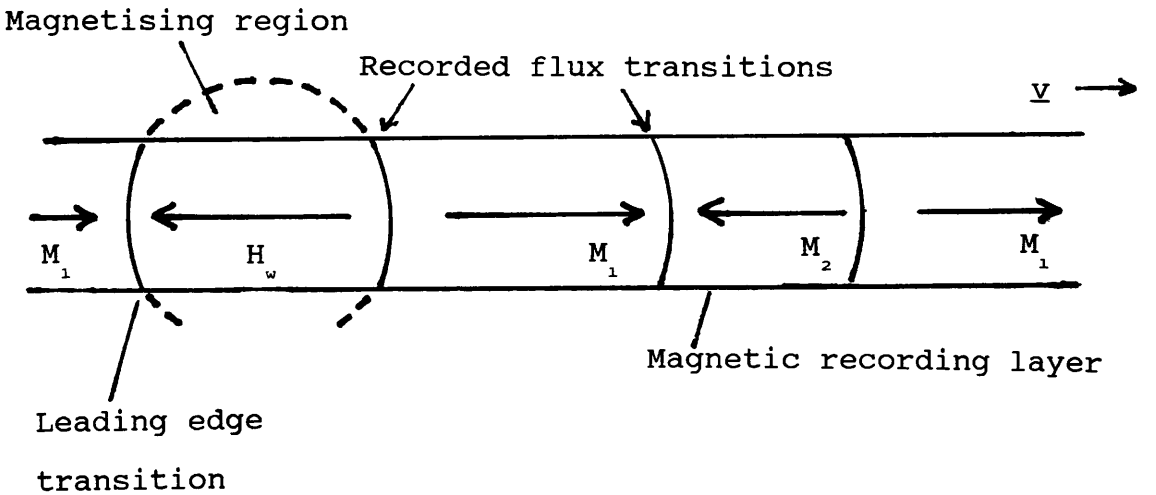

Figure 7.6 Diagram to illustrate the different magnetic field distributions present when recording parallel (top) and anti-parallel (bottom)to the DC magnetisation.

transitions can be neglected, as the distance between these is substantially greater than that between the leading and trailing edge transitions within the head field distribution.

The extent of position shift and transition broadening is determined by the strength of the demagnetising field[4] and therefore quantities which directly affect the size of this field will produce different amounts of transition shift and output reduction. The $M_r\delta$ product is involved as is the proximity of the leading edge transition to the trailing edge transition. Thus a knowledge of the $M_r\delta$ product for the samples will enable the relative contribution made by this to be established. With a constant write current and head to tape separation, an increase in coercivity also leads to an increase in the demagnetising field strength within which the trailing edge transition is written, due to the reduced distance between the leading and trailing transitions.

Irrespective of the previous magnetic state of the sample when recording at increased 'bit' densities the distance between the recorded transitions is much less, and the demagnetising field from the previous transition also contributes to the write field[5]. The effect of this demagnetising field is analogous to that produced by the leading edge transition during DC overwrite already mentioned; however, there is one subtle difference. At high recording densities, when recording within the demagnetising field of the previous transition, the head field is augmented and together these attempt to erase the

previous transition. Due to this we would therefore expect the output signals from both transitions to be reduced in addition to any shift in position.

When recording onto previously DC erased media at high 'bit' densities, we can expect that the shifts in transition position and also the reductions in output, mentioned above, will be different for each of the two directions of recording. When we record parallel to the DC erased state the situation will only involve the demagnetising field of the previous transition and be the same as that when recording on AC erased media already outlined. When the write field attempts to magnetise the film antiparallel to the magnetisation already present within the film, an additional factor comes into play. In this situation we will encounter a demagnetising field which contains two contributions, one from the previous transition and the other from the leading edge transition. The demagnetising field from the leading edge transition reduces the applied field strength while the field arising from the adjacent recorded transition acts to increase this. Therefore we can expect a demagnetising field strength somewhere in between the two extremes and these transitions will as a result be shifted by slightly different amounts from the other types. The output measured from the previous flux crossing would also be expected to be slightly larger than that from a transition written at the same frequency within the demagnetising field of a previous flux crossing, on account of the reduced erasing ability of this modified write field.

These effects would therefore change the recorded periodic pulse pattern into a series of spikes each reduced in size, from which the output would occur shifted from the positions predicted by the write field. In this situation the output signal from the two distinct types of flux crossing discussed would be reduced by different amounts, with the transition written against the DC magnetisation being affected least.

7.2.3 RESULTS FROM OBSERVATIONS OF FOUCAULT IMAGES OF THE RECORDED TRACKS

Observations made on Lorentz images of the low frequency recordings (λ=10μm) revealed a difference in the bit sizes, see figures 7.4d and 7.4e. Table 7.A contains the bit size ratio for samples B and C at both high and low recording frequency. Initially this was surprising as these recordings should have been made onto AC erased media using a symmetric sine wave signal. It was later established that the recordings had not been carried out as requested and the tracks were actually written directly onto previously DC erased media. Having ascertained this, an explanation could be put forward to account for the different domain sizes observed.

Sample	λ(μm)	Track A domain width ratio
B	1	0.75±.05
C	1	0.99±.06
B	10	0.61±.03
C	10	0.69±.04

Table 7.A Width ratio of domains written against background magnetisation to those written in the same direction as this.

Prior to recording, both of the thinner samples had been DC erased along the tape transport direction using a NdFeB magnet. With a sinusoidal write field the domain width can vary depending on the distance between the points at which the head field just exceeds the coercivity of the medium, see figure 7.7. When the record current has been optimised for a particular media, ie chosen to maximise the output signal by producing the sharpest transitions possible, these crossing points are positioned as close as possible to the position at which the head field gradient is a maximum. For a sine wave the maximum gradient occurs at the zero crossing points, and therefore when recording solely with this type of waveform the transitions can never be placed at these positions as the material would need to have a coercivity of zero. An indication of the strength of the write field was provided by the domain pattern which resulted from the recording of a 3.0MHz sine wave signal onto sample C. This produced a series of approximately equal sized domains and therefore, as the amplitude of the recording signal remained constant

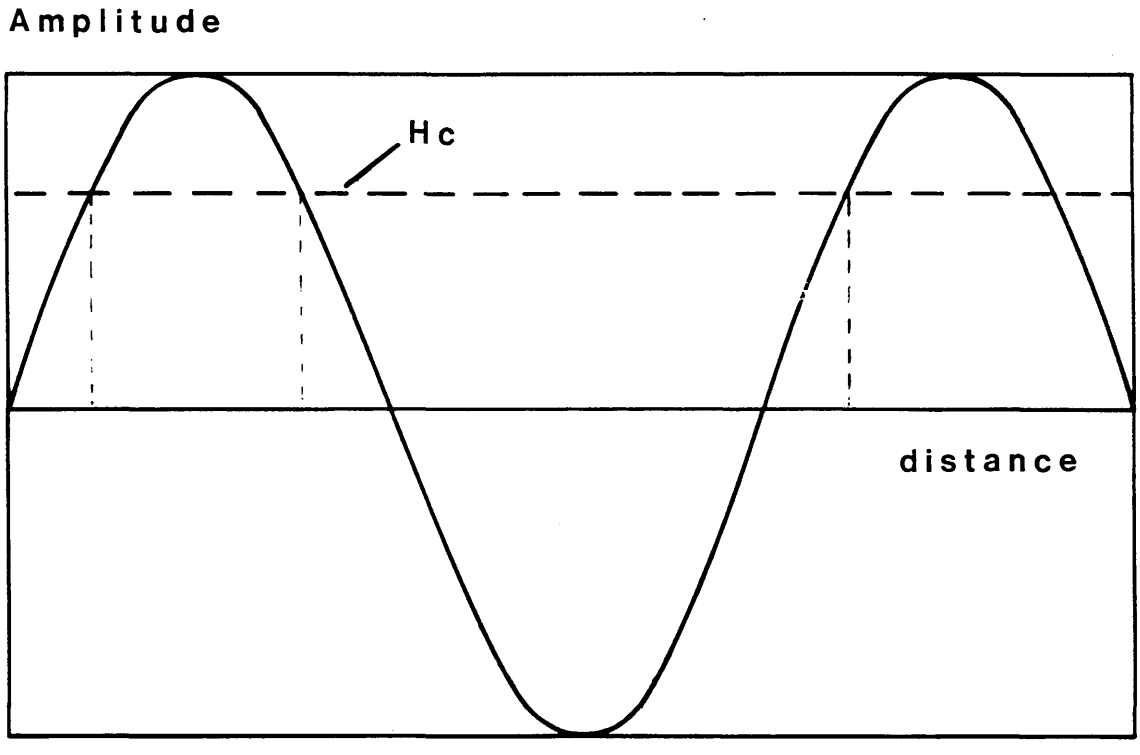

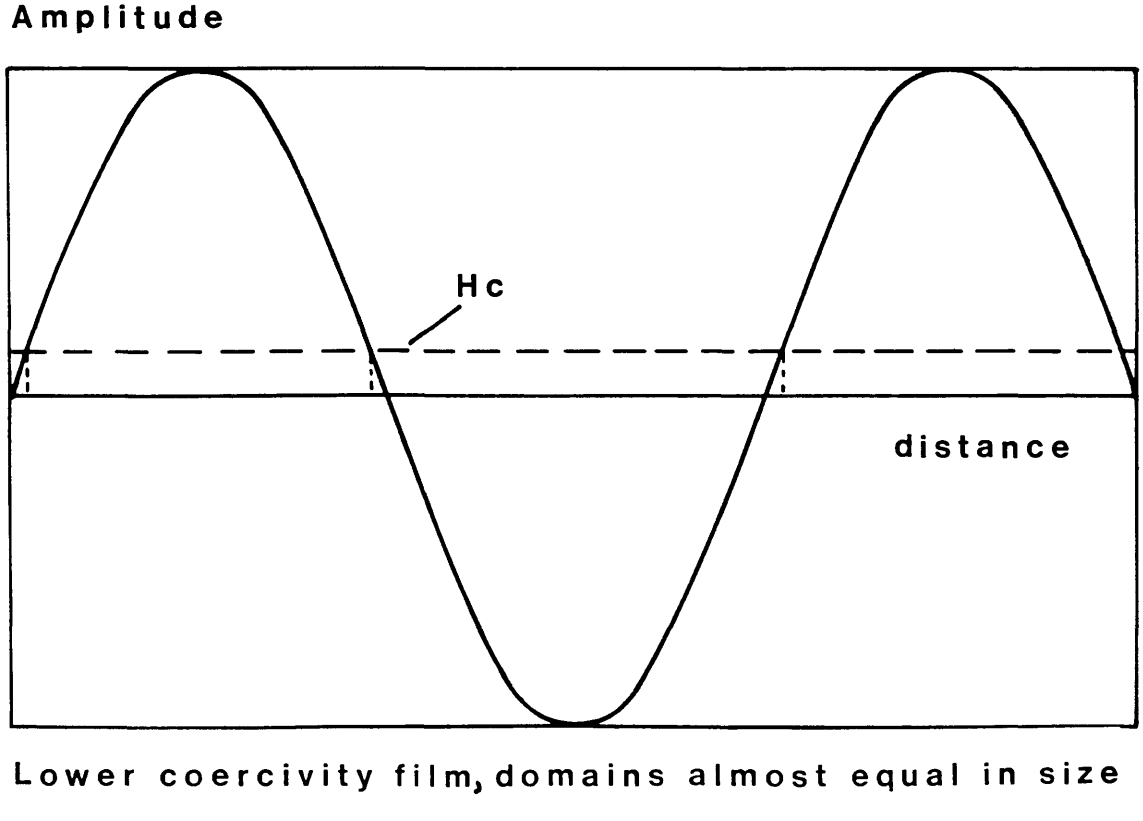

Figure 7.7 Illustration of the different domain sizes predicted when recording using a sine wave, and the difference expected when the film coercivity is changed.

throughout all of these experiments, the write field used was, quite by chance, close to optimum for this particular sample. With this information about the strength of the write field and also the bulk coercivity of sample B, we expected that the domains resulting from the same recording conditions as those for sample C, would not be equal in size. The exact amount of asymmetry in bit size depends on the coercivity of sample B and also on the amplitude of the sine wave, see figure 7.7. If both of these quantities were known then we could determine the positions at which the head field just exceeds the coercivity of sample B, and by dropping perpendiculars to these points the expected difference in bit sizes could be estimated.

As already mentioned in this section when we record at high densities onto DC erased media we can expect the position of both recorded transitions to be displaced. The significance of a larger coercivity for sample B leads to a lower record field gradient, which introduces an additional complication when trying to determine the extent of domain asymmetry. The fact that both recorded transitions are displaced means that we cannot make a straightforward comparison with the asymmetry as measured directly, with the differences in the bulk coercivities. The unknown amplitude of the record field renders this task impossible. As we expected due to the higher coercivity sample B has increased asymmetry present within the 'bit' pattern compared to sample C, a ratio of 0.75 ± 0.05 was determined from direct image measurements.

When recording at the reduced frequency of 0.3MHz, we would expect that the further reduction in write field gradient would produce transition shifts larger than those found at 3.0MHz. This is confirmed from our observations, the domain width ratios for sample B falling from 0.75±.05 to 0.61±.03, while those for sample C changed from 0.99±.06 to 0.69±.04.

7.2.4 ADDITIONAL INFORMATION PROVIDED BY THE LOW FREQUENCY RECORDINGS

At high frequency within track B, the overlapping zig-zags and lack of an observable transverse component, meant that we could not use the images of the 3.0MHz track to compare with the equivalent recordings made at 15° to the easy-axis. At the lower recording frequency however the domain boundary walls were clearly discernable and the comparison could be made at this lower recording density using the Fresnel technique, see figures 7.8a and 7.8b. Certain significant differences are present when writing at only -5° to the easy direction which we could utilise to allow us to predict the 'bit' pattern differences in advance. Lying closer to the easy-axis of magnetisation the film coercivity is greater in this direction and therefore the position at which the sinusoidal write field exceeds this is also different. Consequently a different degree of asymmetry would be expected from that within track A. Another consequence of an increase in coercivity is a reduction in the distance between the leading and

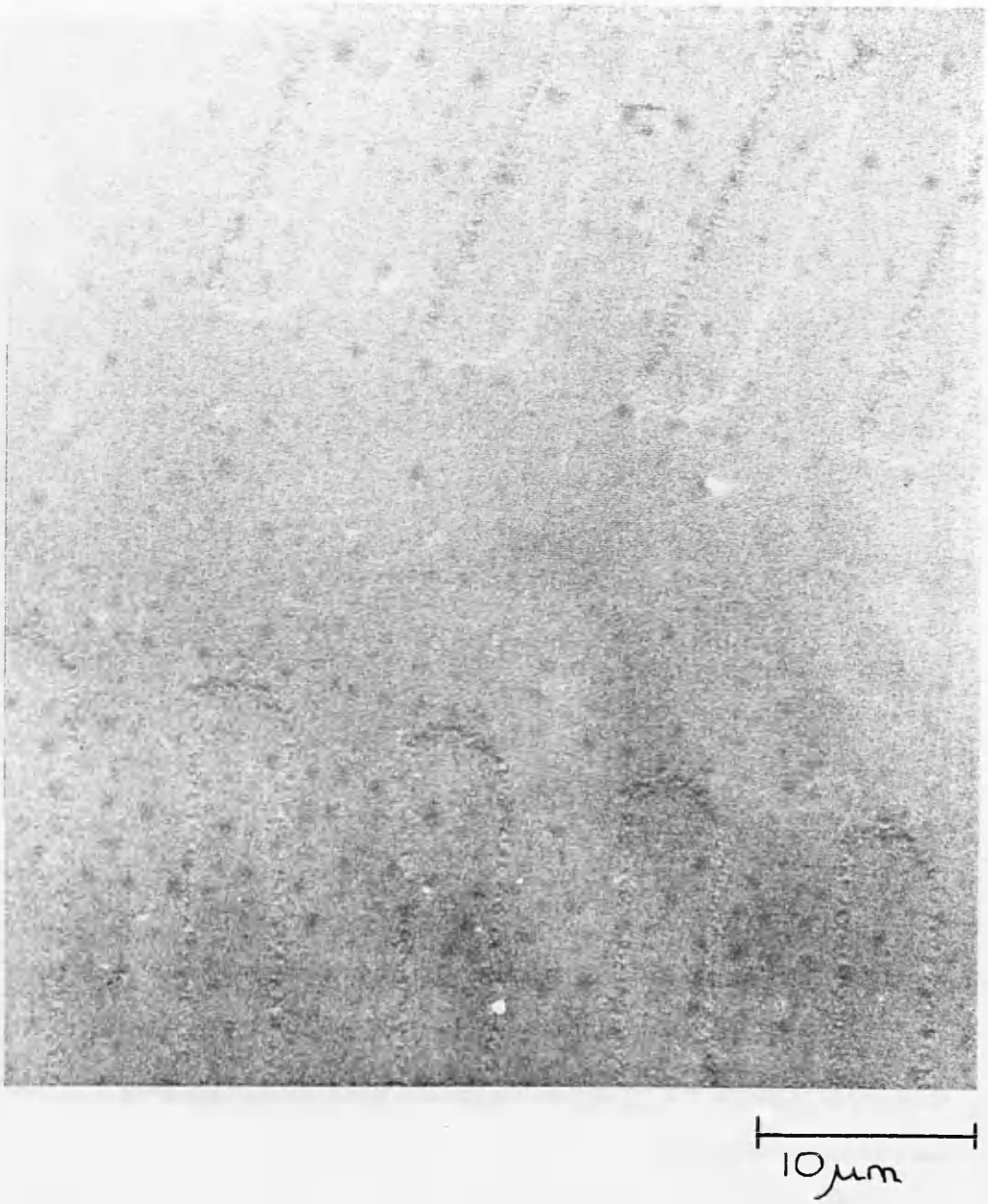

Figure 7.8a Fresnel image of both tracks A (upper track) and B (lower track) written with a wavelength of 10μm on sample B.

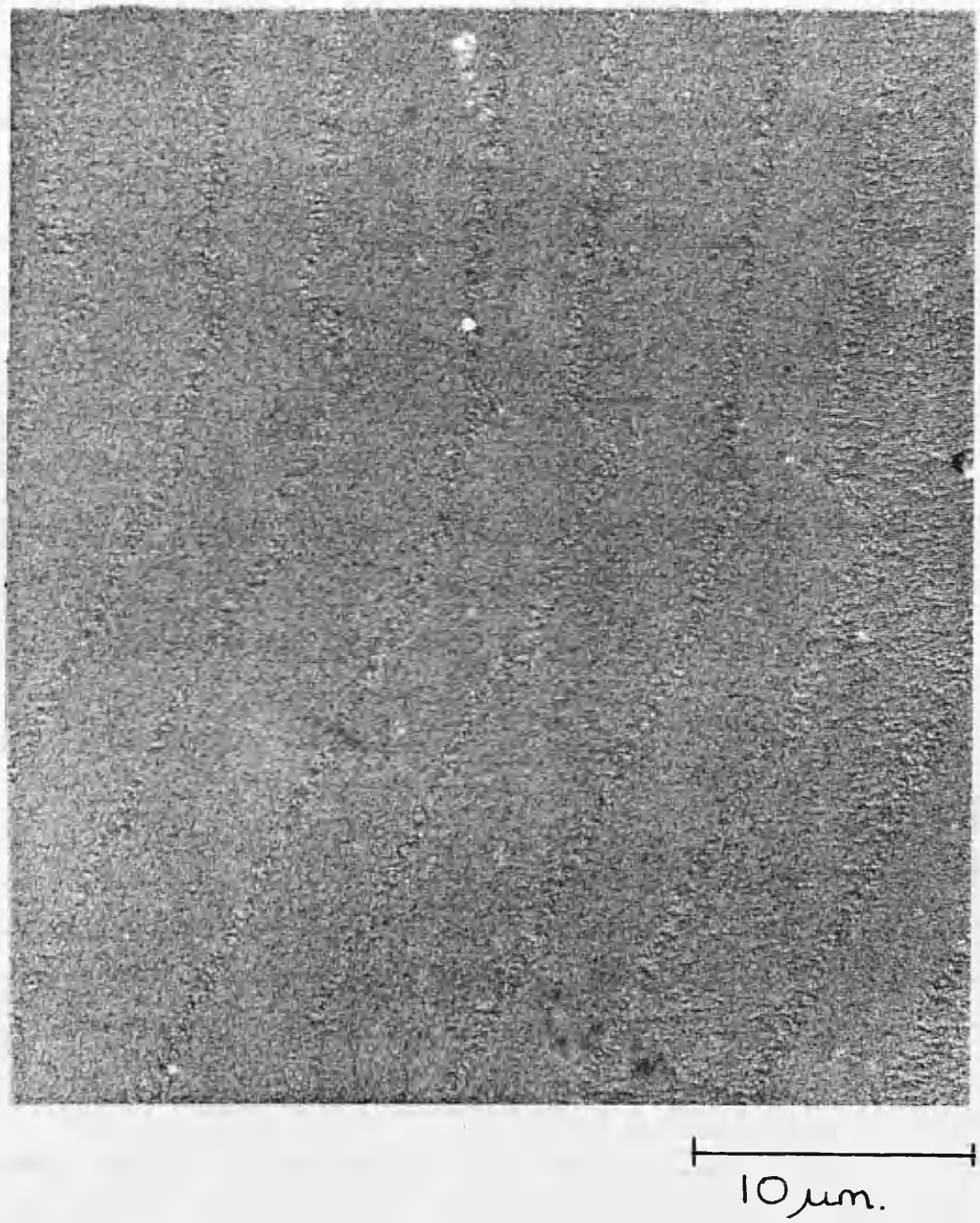

Figure 7.8b Fresnel image of both tracks A (upper track) and B (lower track) written with a wavelength of 10μm on sample C.

trailing edge transitions, produced when writing against the DC magnetisation. Therefore the transitions written against the DC magnetisation within these low angle tracks will be recorded within an increased demagnetising field compared to those written at the same frequency in track A. The remanence level is also greater for these tracks which increases the strength of the demagnetising field even further. For both samples B and C therefore when recording the tracks at -5° to the easy-axis any asymmetry present would be further increased by both of these effects to a greater extent than that in track A.

The results from measurements of track B from images such as 7.8a and 7.8b, see table 7.B, for both sample B and sample C indicate a recorded pattern with increased symmetry, which completely contradicts our expectations. This has lead us to question whether or not the record field used to record track B was in fact the same as that used for track A.

Sample	Wavelength	Track A	Track B
B	10μm	0.61±.03	0.76±.01
C	10μm	0.69±.04	0.88±.03

Table 7.B Domain widths for tracks A and B.

It would have been extremely useful if we could have compared the observed structures at the higher frequency as well in order to verify this, but this was not possible. One thing which we do know is that some head height inaccuracy was present during the recording of

these tracks. If the height of each head is correct then there should be an equal sized gap on either side of each recorded track. From the observations of the written tracks we were able to determine that the gaps were not the same width on either side of the tracks see figures 7.3c and 7.3d. The diagram in figure 7.9 illustrates why differences in the head height leads to recording tracks which have different sized gaps on either side. To understand why such a difference should be present requires information on the error detection and correction procedures employed in the video 8 recorders used to make these recordings. Normally when these machines are used to record video information tracking information is also encoded within each of the recorded tracks, see appendix 1. As additional tracking frequencies would have complicated the micromagnetism considerably the recordings made for the purpose of our investigations were made without such correction signals. As a consequence of this the position of the recording heads would not be corrected during our experiments and indeed the exact position of these would have been established from an earlier recording or replay session. With this knowledge an explanation for the differences observed at the lower recording frequency between tracks A and B can be made. We believe that these differences are in fact due to a different head to tape distance for tracks A and B, as a result of this head height inaccuracy. The results lead us to believe that the head recording the A tracks is slightly farther from the tape than that writing the other

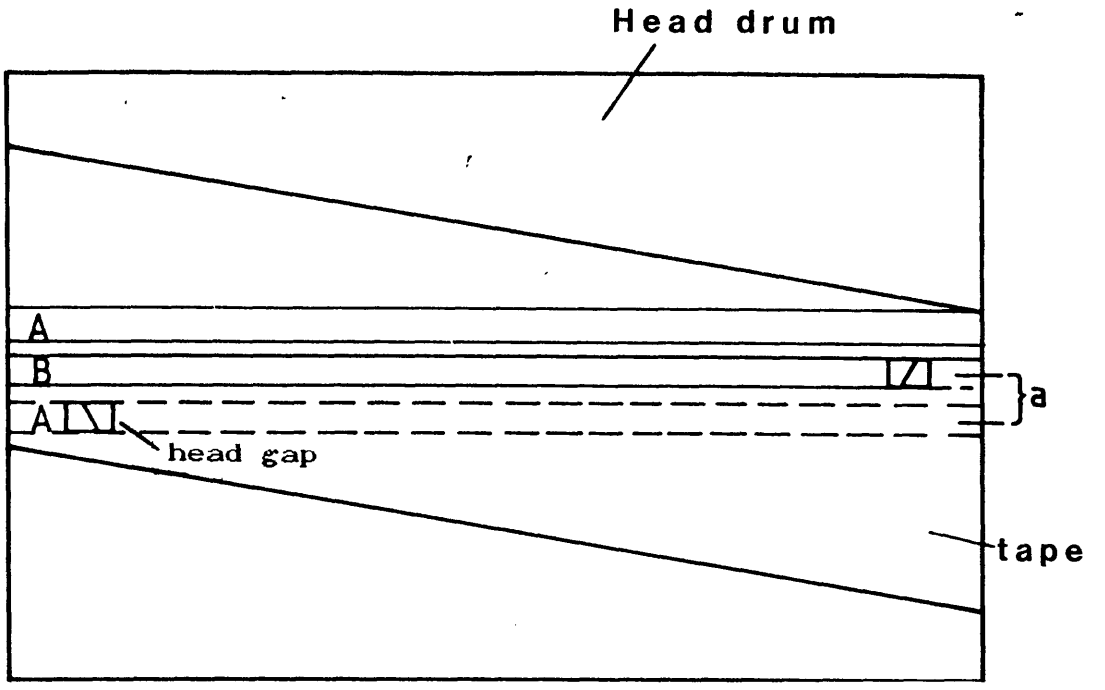

Correct head height equal track spacing a

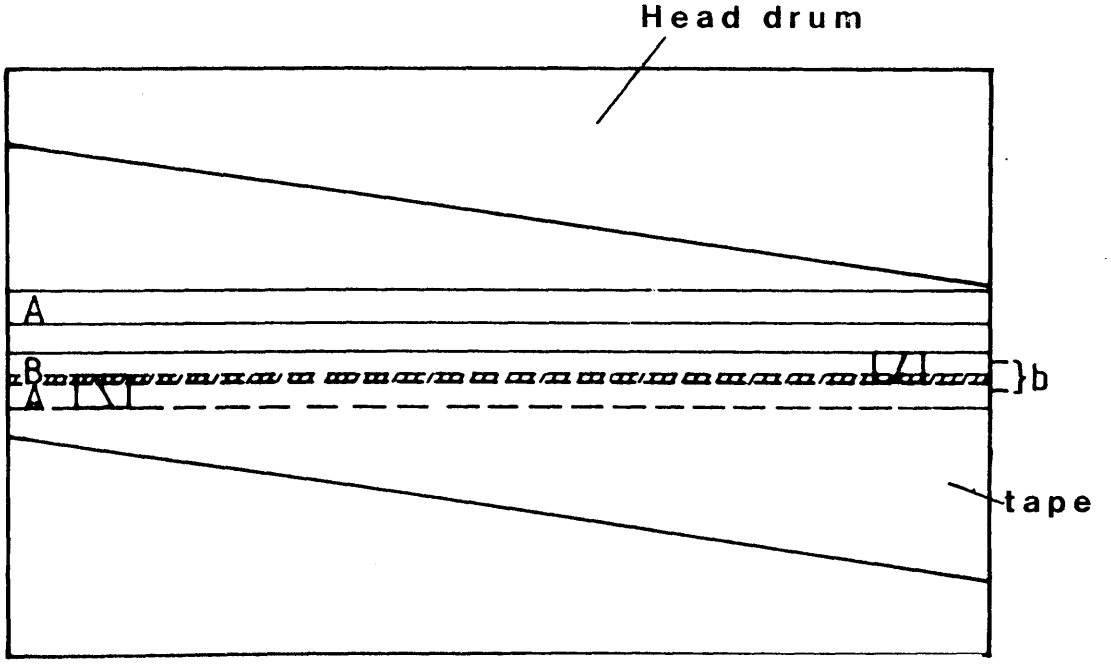

Incorrect head height spacings b and 2a-b

Figure 7.9 Diagram to illustrate the effect of head height inaccuracy on the pattern of recorded tracks.

track. This means therefore that the effective record field strength is greater for track B. Consequently only the comparisons made for each individual track, on the basis of equivalent write fields, remain valid. If this is an accurate description of the actual situation then the results concerning the 'bit' sizes in track A at the two frequencies are consistent. The results for track B at 0.3MHz are also consistent.

7.3 QUANTITATIVE MICROMAGNETIC CHARACTERISATION OF THE VIDEO TRACKS

7.3.1 INTRODUCTION

This section outlines a method whereby quantitative micromagnetic information on the orientation of the magnetic vector within each recorded track is obtained, and attempts to correlate these results with the bulk magnetic properties specific to each film. We also attempt to confirm these quantitative results using another related technique.

7.3.2 DIFFERENTIAL PHASE CONTRAST ON AN ABSOLUTE BASIS

To be able to conduct quantitative micromagnetic analyses from digitally acquired DPC images it is useful to have a reference contrast level from a region of known magnetisation. If this can be achieved then the net induction experienced by an electron traversing the

specimen at any point, can be gauged directly by comparing the contrast levels. For the samples studied in this thesis such a reference level was produced by saturating the films along the magnetic 'easy-axis' prior to recording. This produced a region of known magnetisation, outside the recorded tracks, with which the micromagnetism of the written information could be compared. In DPC, the image intensity is to a good approximation linear with respect to the magnitude of the in plane component of magnetic induction integrated along the electron trajectory[6]. Thus once a reference is established it is a relatively straightforward procedure to construct micromagnetic models for the magnetisation within the recorded tracks.

When quantitative analysis of DPC image data is desired it is essential to be able to determine accurately the signal level which corresponds to an undeflected beam striking the detector surface symmetrically. Knowing the direction of the magnetisation within the DC erased regions enabled this quantity to be estimated. With the direction of detector sensitivity orthogonal to the direction of magnetisation ie the easy-axis, the DPC signal produced within these reference regions provided an estimate for the undeflected signal. Knowing the signal origin in each image enabled the magnitude and direction of the vectors defining the magnetic scattering within the entire image to be determined from either of two pairs of images. One set produced by the quadrant differences, ie (A-C), and (B-D), and the other pair from the split

differences, ie (A+D)-(B+C) and (A+B)-(C+D). The difference between these pairs of images is a 45° rotation of the axes of differentiation. The exact direction of induction established using DPC can be out by 180°, however the relative directions within each vector map should be correct.

The aim of the quantitative DPC analysis of the magnetic recording tracks was to establish the final orientation of the written magnetisation. Unfortunately the Lorentz deflection due to the stray field is opposite to that effected by the magnetisation, and this prevents the micromagnetic configuration being established directly from either orthogonal pair of DPC images. To be able to evaluate the component of magnetisation parallel to the track and obscured by the fringe field required the reference DC signal and the conservation of magnetisation. The component of magnetisation lying parallel to the track, M_y, could be estimated from the intensity values due to the transverse component, M_x, and the reference level, M_R, on the basis that the magnetisation is conserved ie

$$M_R^2 = M_x^2 + M_y^2$$

and therefore $$\langle M_y \rangle = \sqrt{\langle M_R \rangle^2 - \langle M_X \rangle^2}$$

Since we believe that the amount of stray field above these extensive DC erased areas is negligible we can attribute the deflections directly with M_R. Further if we assume that flux closure, for the x component of

magnetisation, occurs entirely within the film plane at the track edge, then the deflections due to this transverse component arise from M_x alone. We can therefore determine M_y and hence the direction of the written magnetisation ε within the film can be determined from the following equation

$$\varepsilon = \tan^{-1}\left(\frac{<M_x>}{<M_y>}\right)$$

This angle ε describes the amount of rotation that the written magnetisation undergoes upon relaxation. The DPC images contained within figures 7.10a, 7.10b and 7.10c were used to produce the results which are summarised in table 7.C.

Sample	Wavelength	Rotation Angle
A	0.8μm	22±2
B	1.0μm	32±3
C	1.0μm	38±10

Table 7.C The quantitative micromagnetic results obtained from analysis of the DPC images in figures 7.10a, 7.10b and 7.10c.

It can be seen that as the recording layer thickness is reduced the extent of rotation away from the direction parallel to the write field increases. The final configuration of the magnetisation is one in which the sum of these two energy terms is minimised.

An explanation for these trends can be made on the basis of the different anisotropy present within each

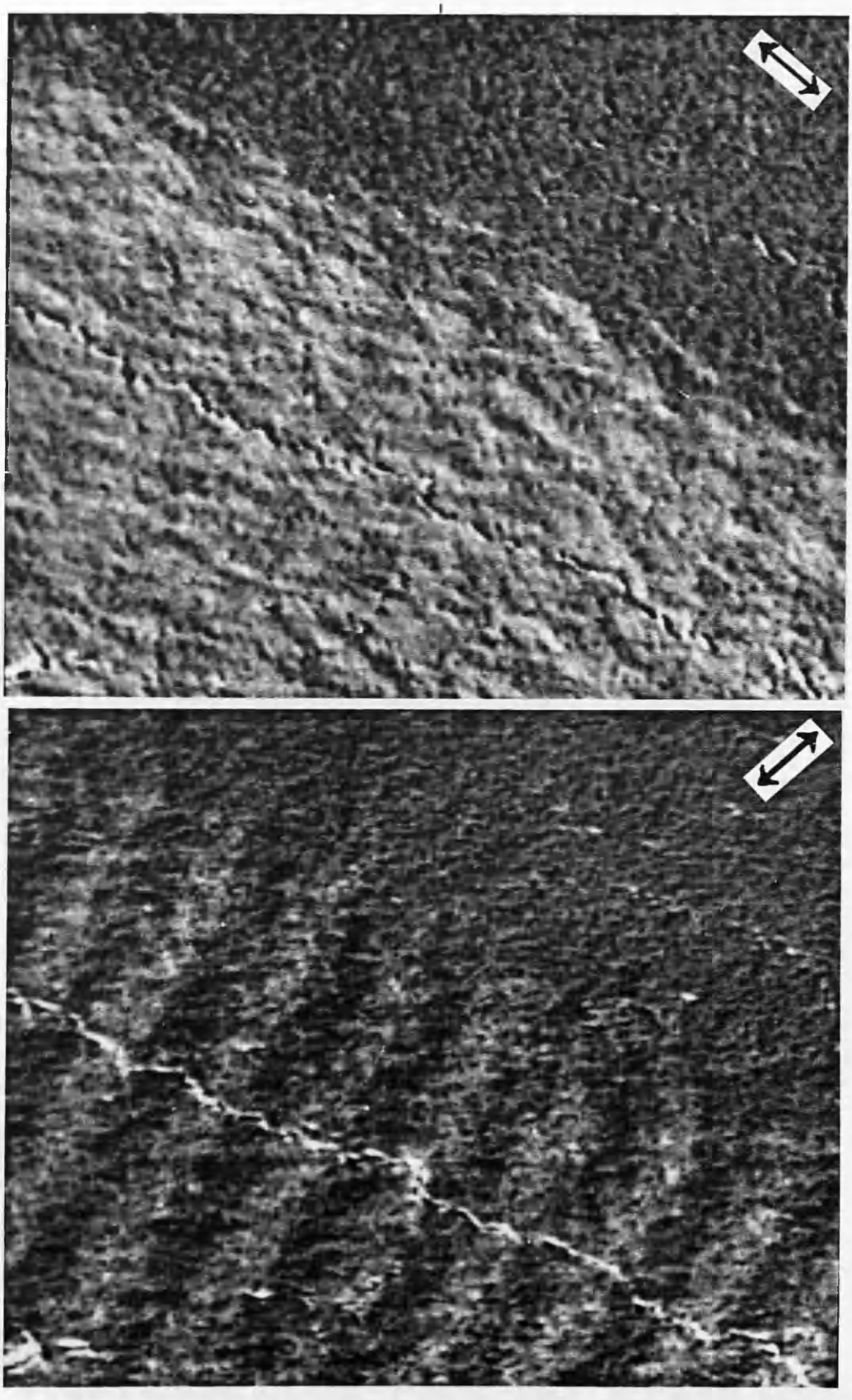

Figure 7.10a DPC images of sample A recorded with a wavelength of 0.8μm. The contrast within these images is sensitive to induction in the directions indicated by the arrows.

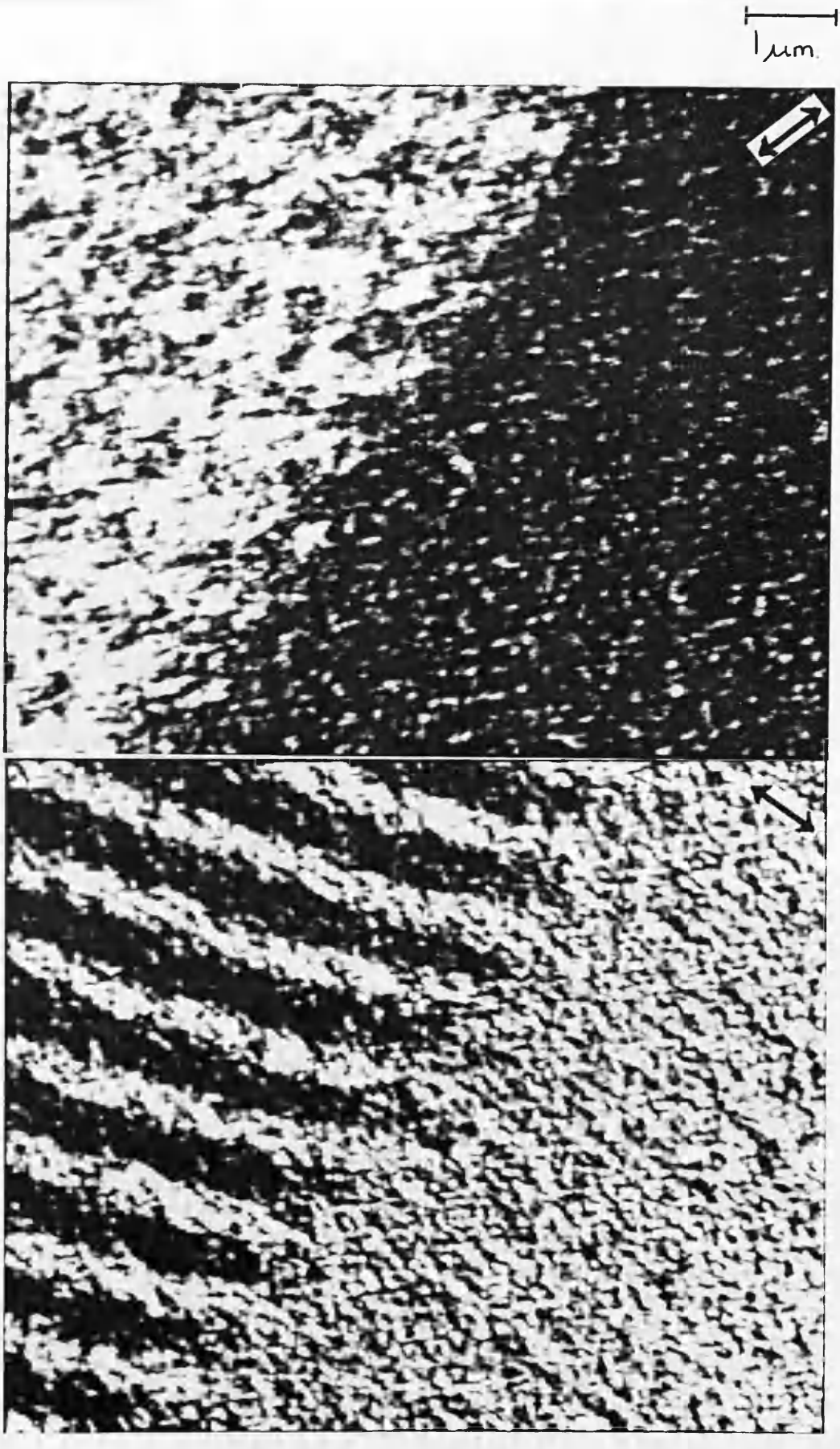

Figure 7.10b DPC images of sample B recorded with a wavelength of 1.0μm. The contrast within these images is sensitive to induction in the directions indicated by the arrows.

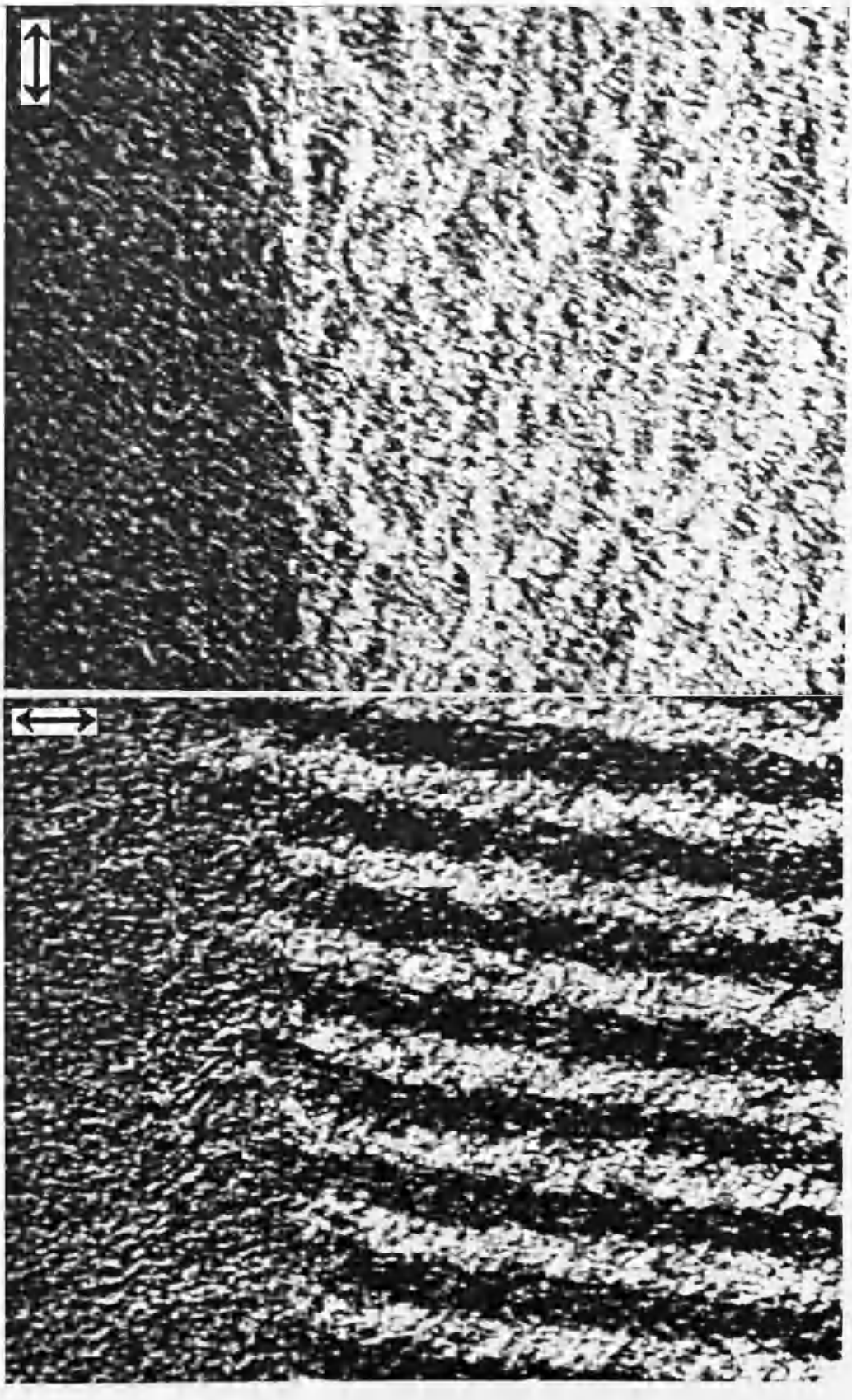

Figure 7.10c DPC images of sample C recorded with a wavelength of 1.0μm. The contrast within these images is sensitive to induction in the directions indicated by the arrows.

individual film. Immediately after recording a transition, the magnetic vector within the domains on either side are in a head-on arrangement. The magnetic charges produced by the head-on components of magnetisation within adjacent domains set up a large demagnetising field which tries to modify this micromagnetic distribution. The demagnetising field tries to rotate the magnetisation away from the head on situation until the magnetic vectors within neighbouring domains are anti-parallel[7]. However, as the magnetisation has a tendency to rotate into the easy-direction these conflicting forces exert a torque on the magnetisation within each recorded domain. The anisotropy falls with sample thickness and therefore the resistance this provides to the demagnetising effect is diminished. Consequently the degree of magnetisation rotation which this effect causes will increase as the anisotropy falls and as sample C was seen to exhibit the lowest anisotropy we would expect the written magnetisation within this sample to undergo the largest amount of rotation. Our results agree with this model for the relaxation of the written magnetisation. It is interesting to note that even when the magnetisation lies farthest from the recorded track direction, which we have established to be some 37° for the thinnest film, the flux passing through the replay head is still 81% of that obtained in the parallel case, although this takes no account of any influence that the high permeability reproduce head has on the magnetisation within the film.

The image analysis carried out to determine the orientation of the magnetic vector within the high frequency recording tracks was also performed for lower recording densities; the DPC images are contained within figures 7.11a, 7.11b and 7.11c respectively. The results for the three different thicknesses of MET recorded with a wavelength λ = 10μm are summarised in table 7.D. In each case it is seen that, for a given film thickness, the vector within the larger domains lies closer to the 'easy-axis'. This can be understood in terms of the new equilibrium position established due to the reduced strength of the demagnetising field, present within these larger magnetic domains. The increase in 'bit' size reduces the demagnetising field strength and therefore the magnitude of the force moving the magnetic vectors away from the head on situation, imposed by the write field. Hence at low frequency we would expect the anisotropy to be more significant in determining the position of equilibrium and lower angles of relaxation would be expected when compared to the high frequency situation.

Sample	Wavelength	Rotation Angle
A	8μm	17±1
B	10μm	30±1
C	10μm	33±7

Table 7.D Angle of recorded magnetisation vector with respect to track direction.

From this table of results it is seen that for each film

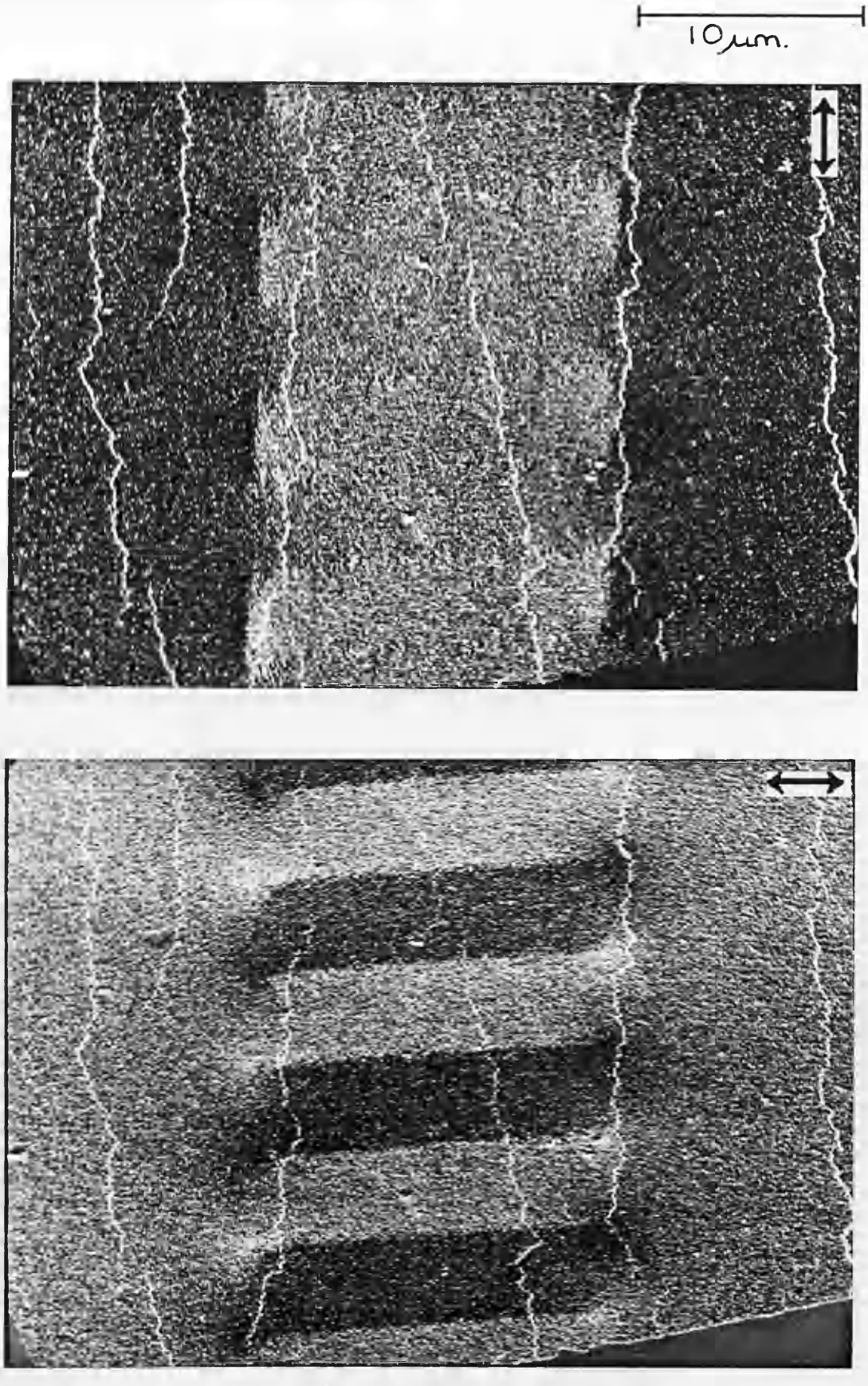

Figure 7.11a DPC images of sample A recorded with a wavelength of 8μm. The contrast within these images is sensitive to induction in the directions indicated by the arrows.

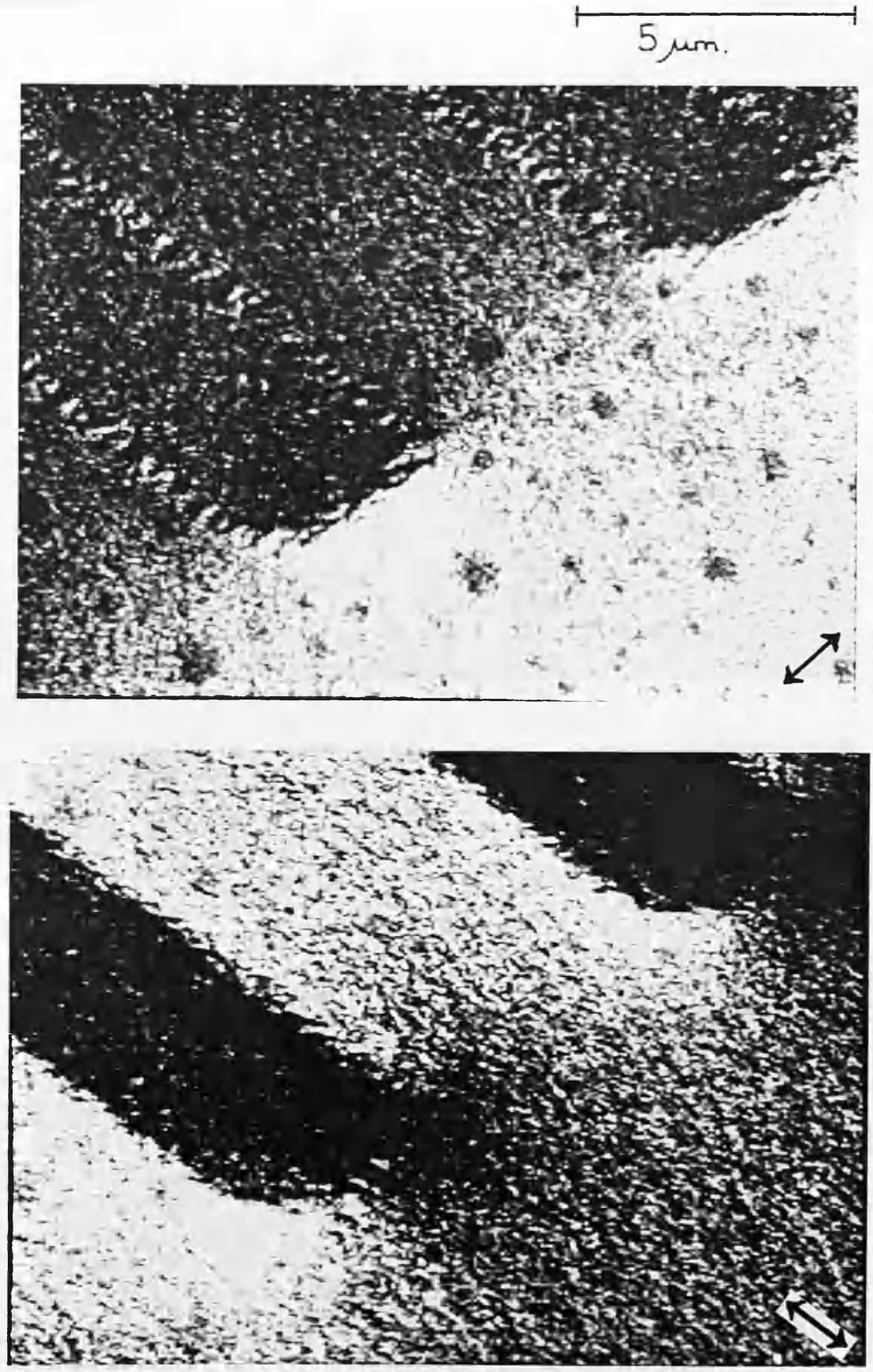

Figure 7.11b DPC images of sample B recorded with a wavelength of 10μm. The contrast within these images is sensitive to induction in the directions indicated by the arrows.

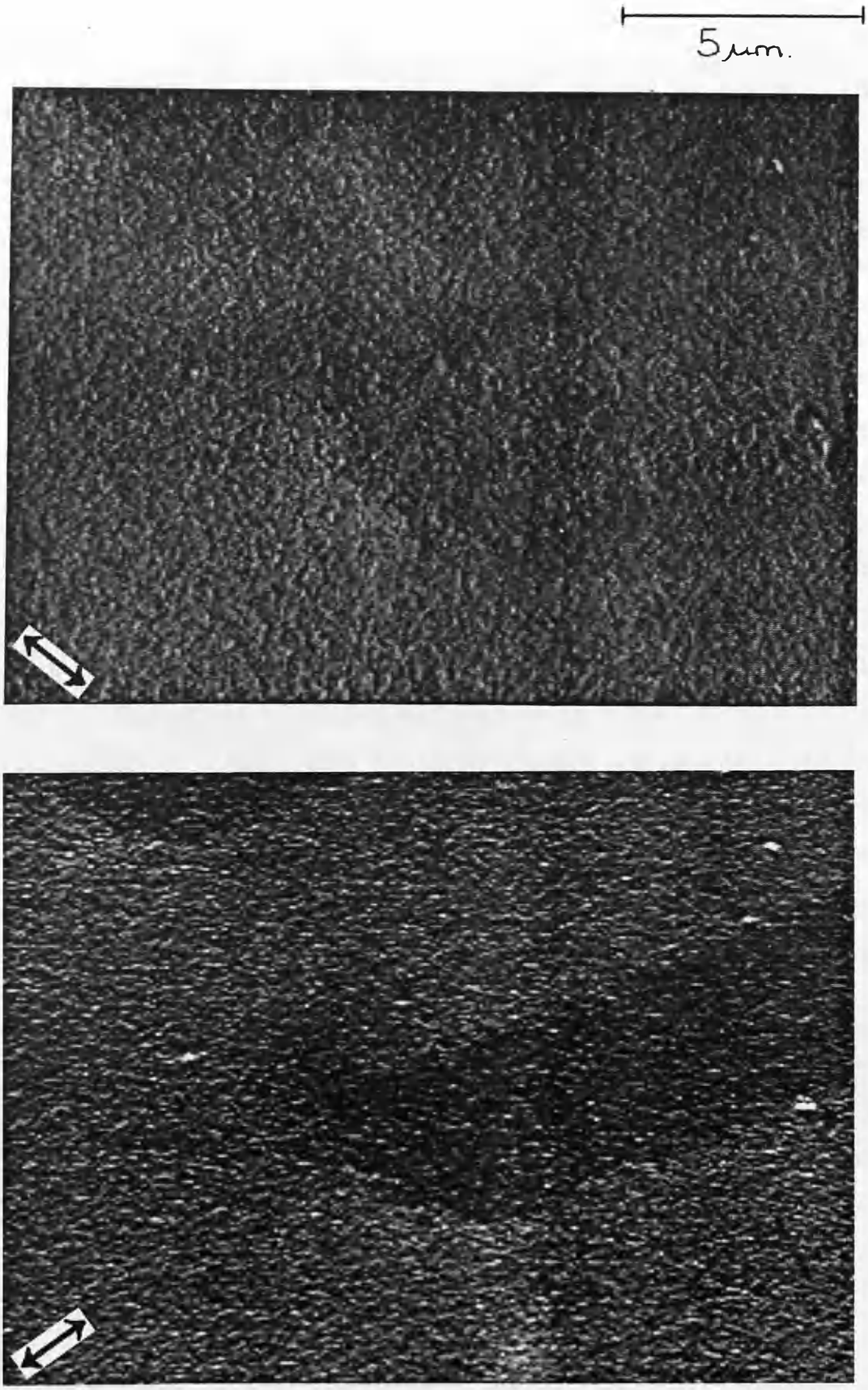

Figure 7.11c DPC images of sample C recorded with a wavelength of 10μm. The contrast within these images is sensitive to induction in the directions indicated by the arrows.

the magnetic vectors relax closer to the easy-axis than those within the high frequency tracks, see table 7.C. These results also exhibit the same trend as those in table 7.C, the angle of relaxtion increasing as the anisotropy falls from sample to sample.

As a means of checking the quantitative results the analysis was also carried out using data from images produced by the other combination of detector geometry. The results from this analysis are contained in table 7.E. Figures 7.12(a-c) and 7.13(a-b) are the DPC images obtained from the same areas of specimen as those in figures 7.10(a-c) and 7.11(a-c) with a different direction of differentiation, as indicated by the arrows. The majority of these are in very close agreement with the results derived from the first pairs of DPC images. The only discrepancy arises from the low frequency recording on sample C, which we believe is due to the fact that this sample produces the smallest Lorentz deflection and consequently the S/N is poorer.

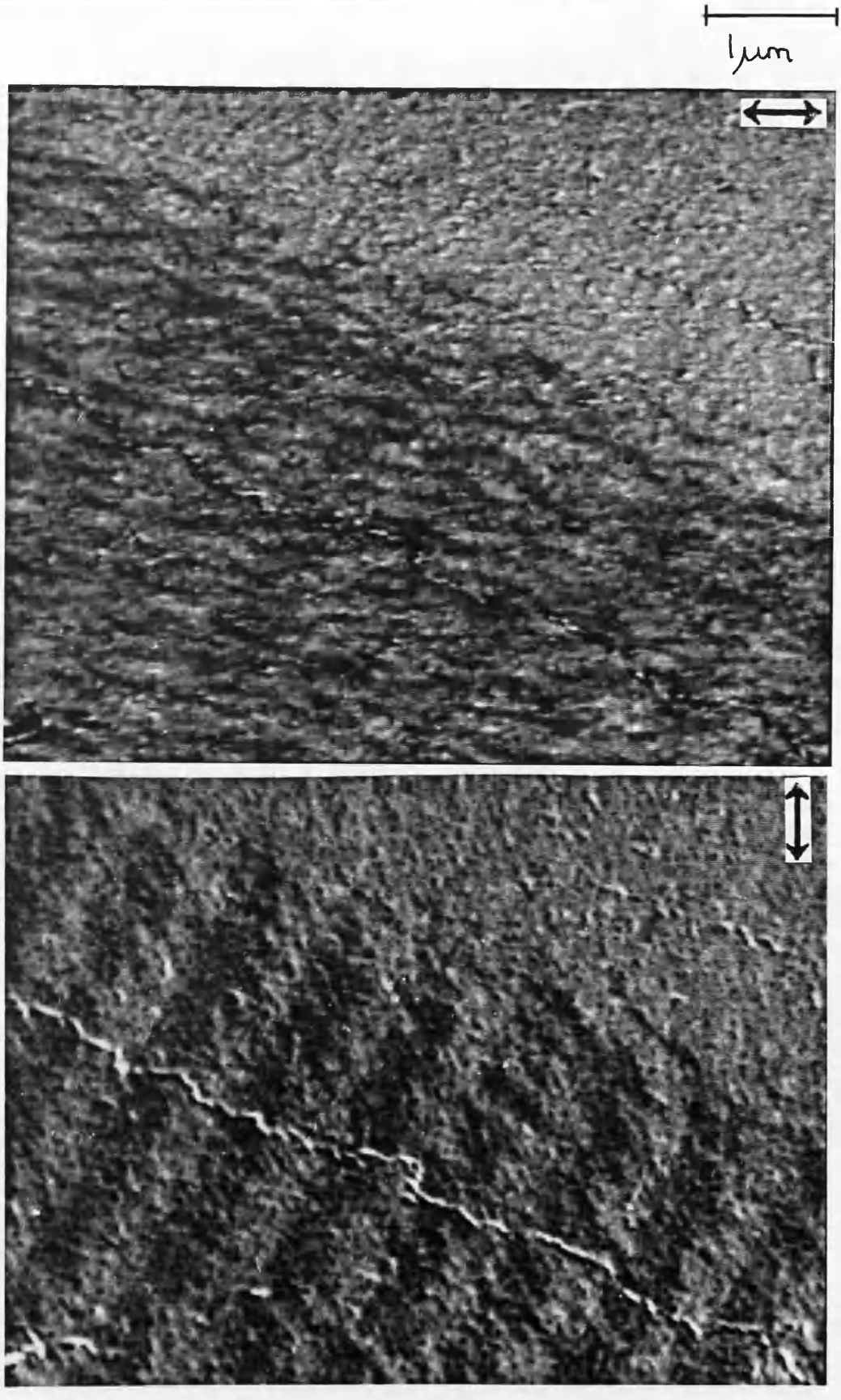

Figure 7.12a DPC images of the same track area of sample A as mapped in figure 7.10a, however the directions of differentiation have been rotated through 45°. These images map induction in the directions indicated by the arrows; the recorded wavelength is 0.8μm.

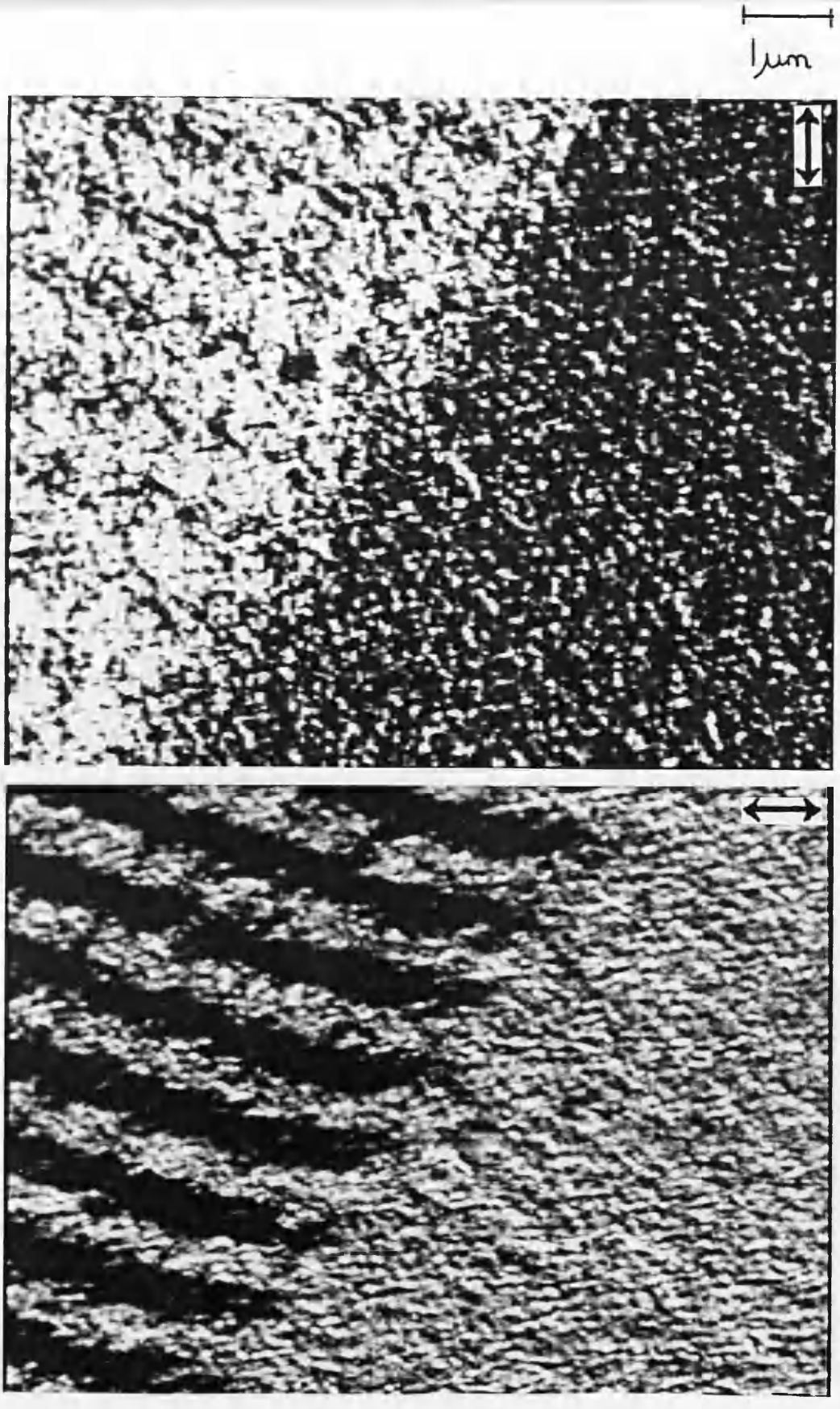

Figure 7.12b DPC images of the same track area of sample B as mapped in figure 7.10b, however the directions of differentiation have been rotated through 45°. These images map induction in the directions indicated by the arrows; the recorded wavelength is 1μm.

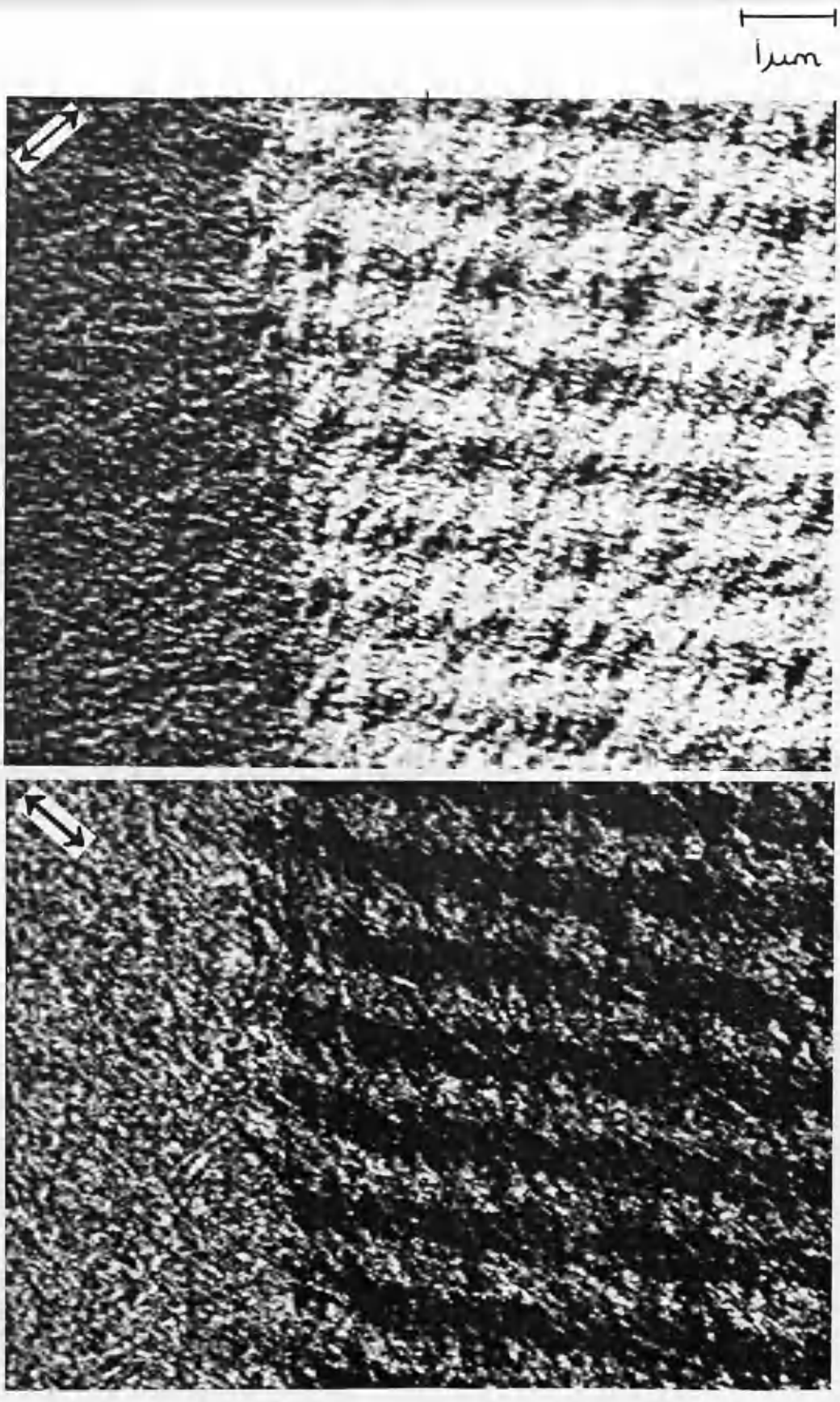

Figure 7.12c DPC images of the same track area of sample C as mapped in figure 7.10c, however the directions of differentiation have been rotated through 45°. These images map induction in the directions indicated by the arrows; the recorded wavelength is 1μm.

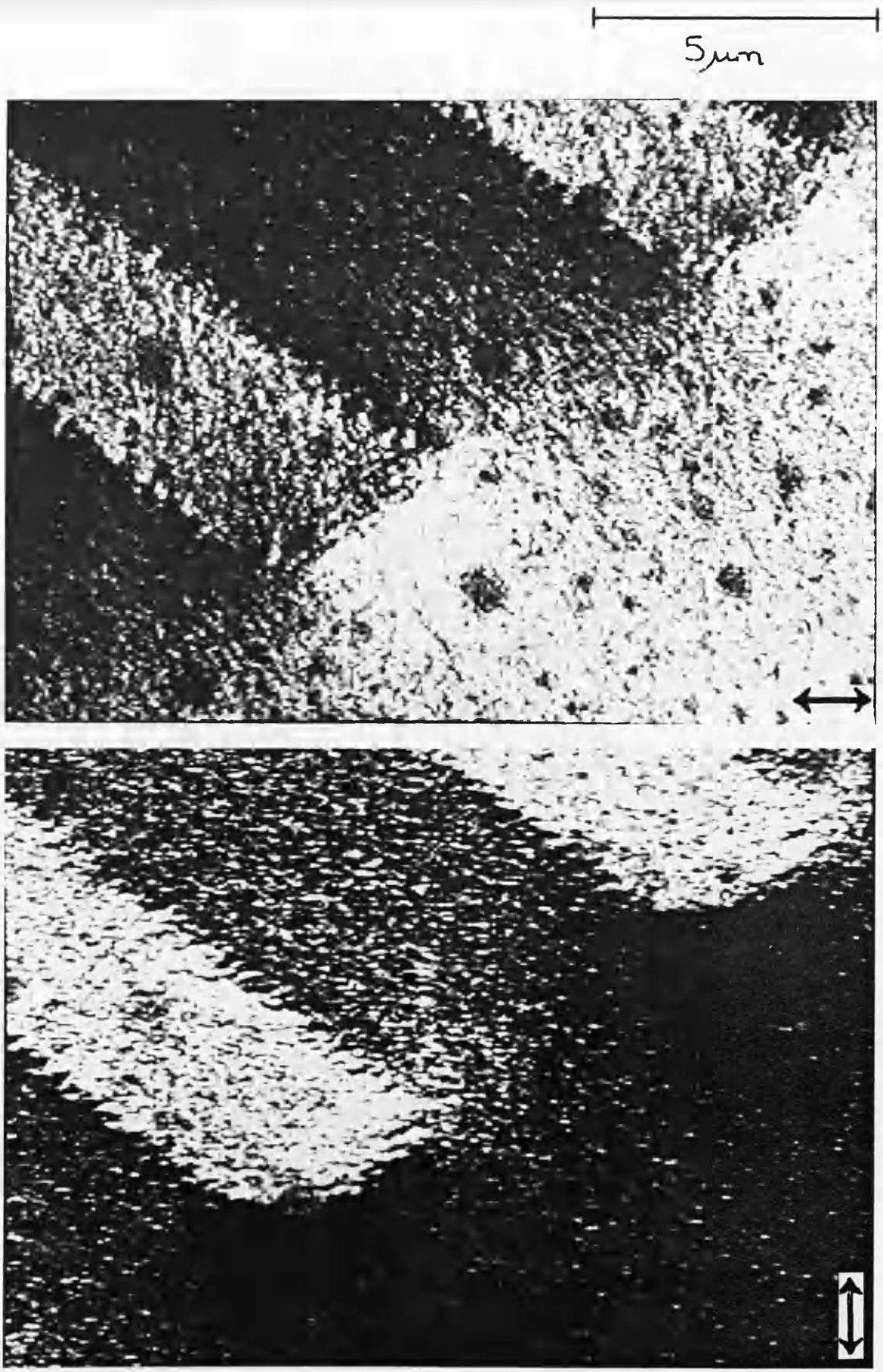

Figure 7.13a DPC images of same areas of sample B as mapped in figure 7.11b, however the directions of differentiation have been rotated through 45°. These images map induction in the directions indicated by the arrows; the recorded wavelength is 10μm.

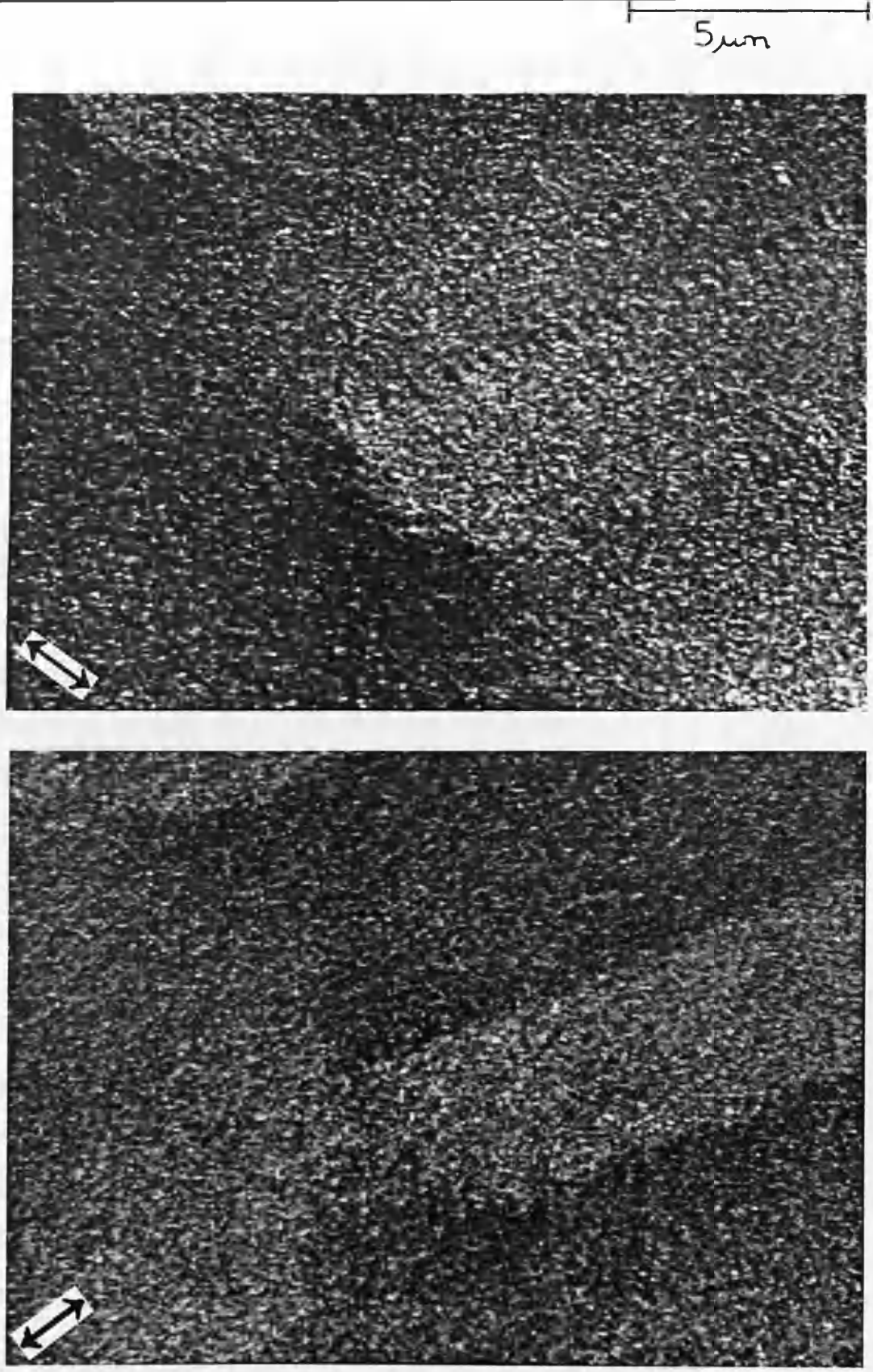

Figure 7.13b DPC images of same areas of sample C as mapped in figure 7.11c, however the directions of differentiation have been rotated through 45°. These images map induction in the directions indicated by the arrows; the recorded wavelength is 10μm.

Sample	Wavelength	Rotation Angle
A	0.8μm	22±2.0
A	8μm	N/A
B	1μm	32±5
B	10μm	33±2
C	1μm	36±10
C	10μm	27±1*

Table 7.E Results obtained from other DPC set of images.

Figures 7.14(a-c) contain DPC images from the same portion of track A for each of the three samples A, B and C, and are provided to facilitate a straightforward comparison of the micromagnetic details provided by the different directions of differentiation.

The results from the torque curves obtained during the bulk magnetic characterisation of the three films, and discussed in chapter 6, indicated that the magnitude of the inplane component of magnetisation was seen to vary from sample to sample. The easy axis was found to lie ~17° out of the plane for sample A, ~12° for sample B and ~6° for sample C. If the magnetisation within the recorded tracks adopts the same orientation as that in the bulk, then the demagnetising field strength within equal sized domains will vary. This is important since this was ignored in the above theory to account for the different orientations adopted by the written magnetisation. Hence for each sample at a particular frequency we cannot attribute the changes in vector orientation, observed as

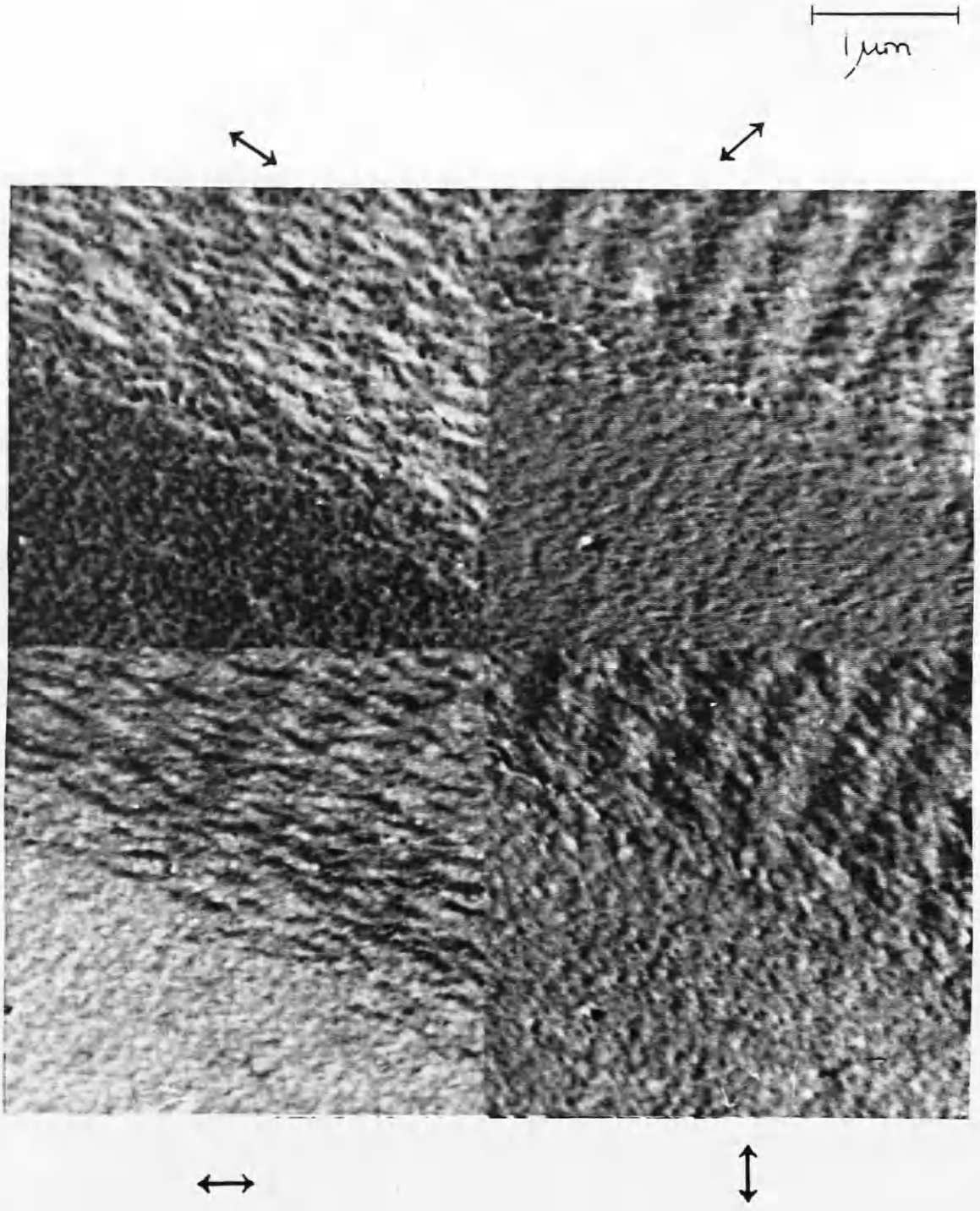

Figure 7.14a To facilitate direct comparisons of the images produced by the four different detector geometries, this image illustrates the four DPC images of sample A recorded with a wavelength of 0.8μm. These images were obtained from a different portion of sample A from that shown in figures 7.10a and 7.12a.

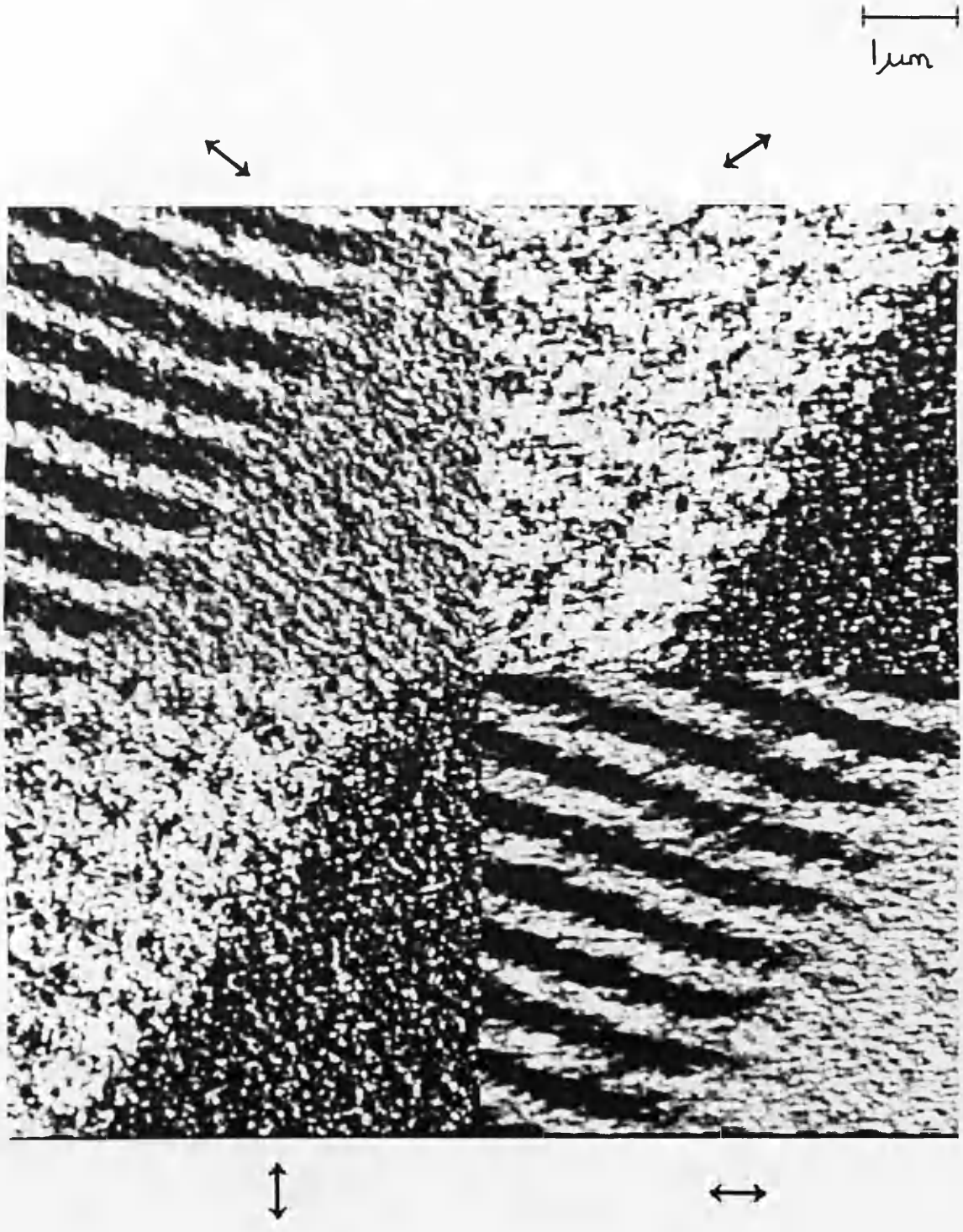

Figure 7.14b To facilitate direct comparisons of the images produced by the four different detector geometries, this image illustrates the four DPC images of sample B recorded with a wavelength of 1μm. These images were obtained from a different portion of sample B from that shown in figures 7.10b and 7.12b.

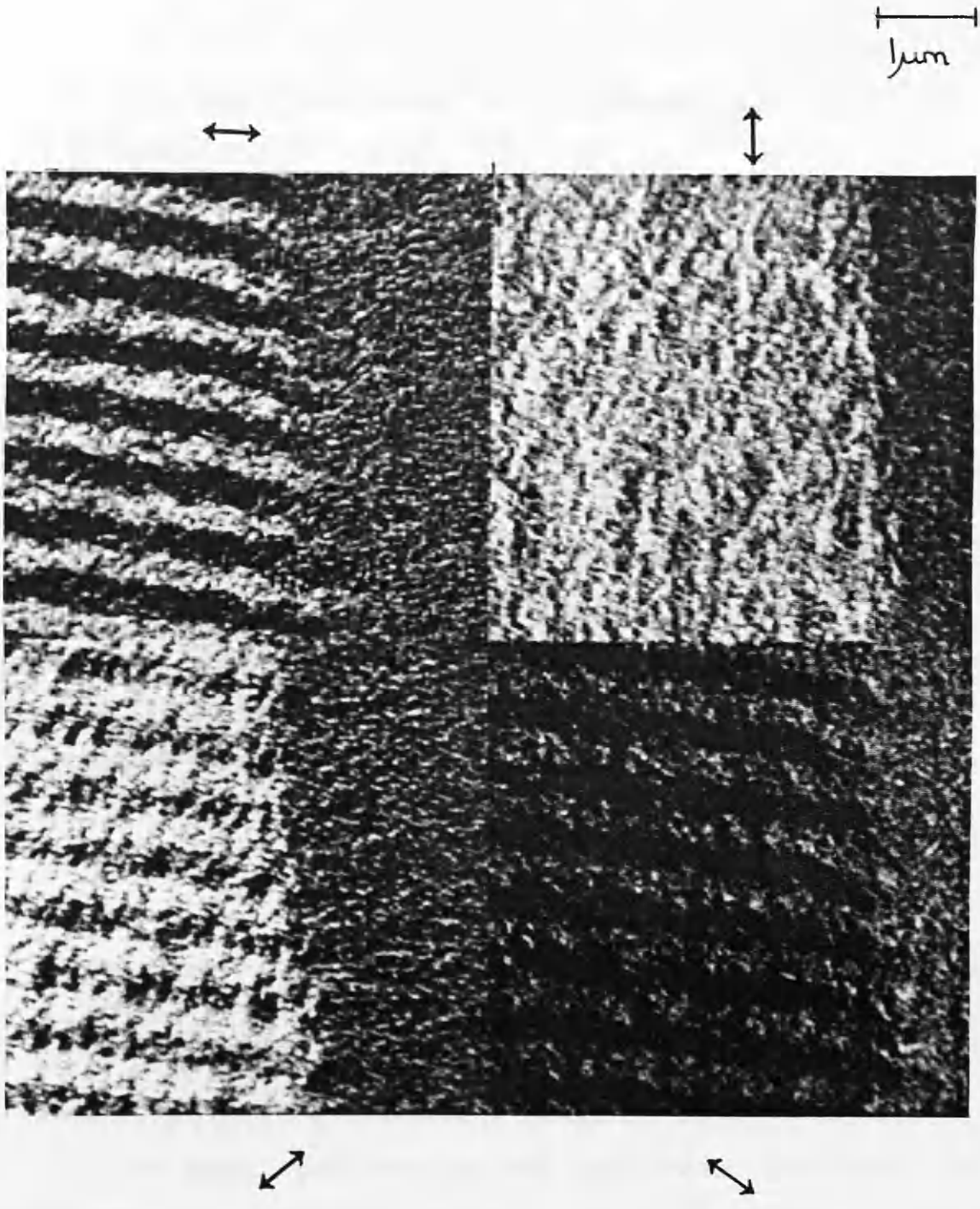

Figure 7.14c To facilitate direct comparisons of the images produced by the four different detector geometries, this image illustrates the four DPC images of sample C recorded with a wavelength of 1μm. These images were obtained from a different portion of sample C from that shown in figures 7.10c and 7.12c.

the film thickness is reduced, to variations in the film anisotropy alone.

7.4 SMALL ANGLE SCATTERING (SAS) EXPERIMENTS

Although the results of the DPC analysis on the recorded tracks were consistent given the bulk magnetic characteristics of the films, it was important to confirm these findings using another technique. Of the other methods detailed in chapter 3 which provide information relating to the magnetisation within the specimen, only small angle diffraction would provide results which in principle would allow straightforward quantitative interpretation.[9] The thickness of samples A and B resulted in a high degree of inelastic scattering which meant that the small angle diffraction pattern (SADP) produced from these films could not be interpreted. As a result of this it was only possible to obtain SADP from sample C and attempt to verify the results of the DPC analysis for this at each of the two recording frequencies.

In order to extract quantitative information concerning the sample from small angle scattering it is necessary to know the exact position of the undeviated electron beam, just as we had stipulated the need for knowing the 'intensity origin' for DPC images. In an attempt to obtain this, double exposure photographs were taken, one when illuminating the magnetic structure of interest, the other when no specimen was in the field of

view. From observations of spot patterns, produced from equivalent areas of recorded track, it was clear that the position of the entire electron distribution shifted as the electron beam was moved onto the thin metallic film. Therefore an absolute measurement of the Lorentz deflection due to the magnetisation within the recorded tracks and also from the DC reference regions could not be obtained. The relative induction directions within the recorded tracks and that within the DC regions could however be established from these SAD patterns.

To extract more information from the small angle diffraction patterns we devised a technique which enabled us to obtain the angle between the recorded track direction, and therefore the easy-axis, and the induction responsible for each spot within the diffraction pattern. To be able to carry this out we needed to be able to image both the specimen and the small angle diffraction pattern produced from the magnetic induction within this area. To increase the information provided by this SAD mode we used a standard line grating specimen to enable us to determine the rotation introduced by the electron optics as we varied the focus control. We would alter the lens current by a specific amount and photograph the Fresnel image, which clearly revealed the direction of the gratings. The excursion from orthonormality between the direction of the gratings and the line of spots in the diffraction pattern would be due to the rotation introduced by the rotation of the electron trajectories produced by the magnetic lenses, see figure 7.15. Next we would move the specimen rod and

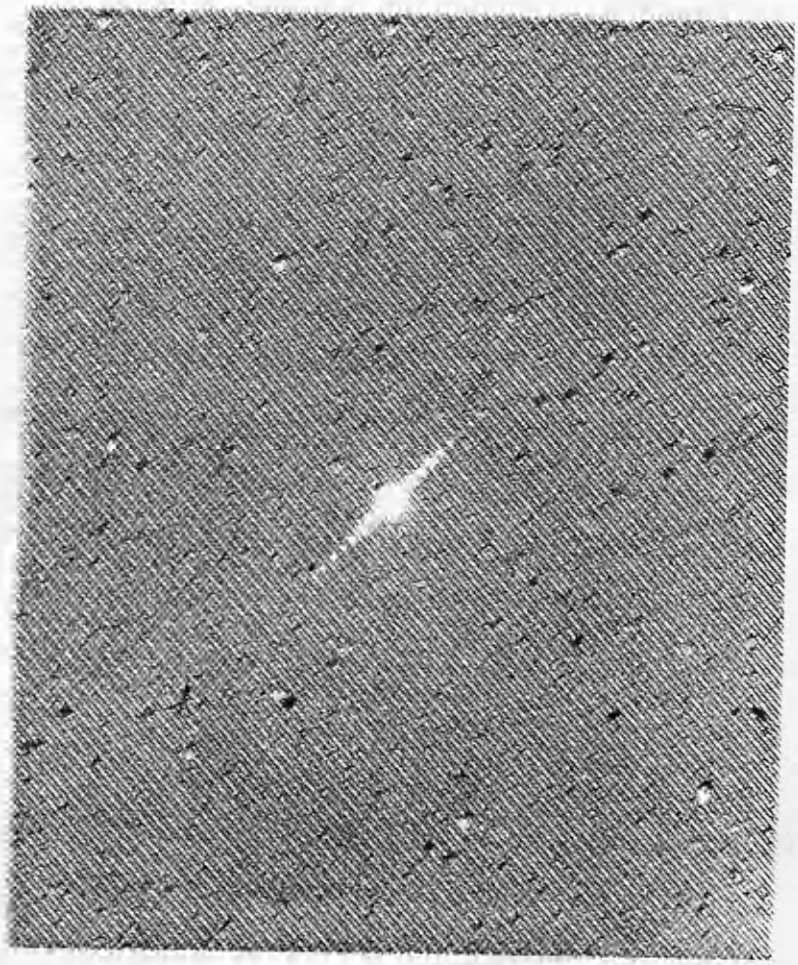

Figure 7.15 Double exposure photograph of a 2160 lines/mm line gratting which allowed the amount of rotation introduced by the electron optics to be determined.

introduce into the beam path the MET film of interest, and then follow the same procedure.

Using this technique we were able to confirm that the spots which resulted when electrons passed through track A, arose from magnetic induction which was parallel to the recorded domain boundary walls. We were also able to establish the orientation of the induction within the DC erased reference regions. Measured with respect to the transverse component the induction within these areas was found to lie at an angle of 84±3° for the high frequency recording, and 82±3°, for the low frequency recording. From the known geometry the angle expected is some 75°.

The spot patterns obtained are shown in figures 7.16a, 7.16b and 7.16c. In each case an expanded schematic diagram of the arrangement of the spots is also shown for clarity. The spots indicated by the letter R, arise from deflections within the reference DC erased areas and those which are produced by the transverse component are marked with the letter T. The undeflected beam is marked O.

7.4.1 FINE STRUCTURE WITHIN THE SMALL ANGLE DIFFRACTION PATTERNS (SADP)

The SADP from the high frequency recordings made on sample C clearly contained fine structure which was not obvious from the DPC images. The spot pattern indicated the presence of an additional splitting subdividing each of the spots produced by the transverse components of

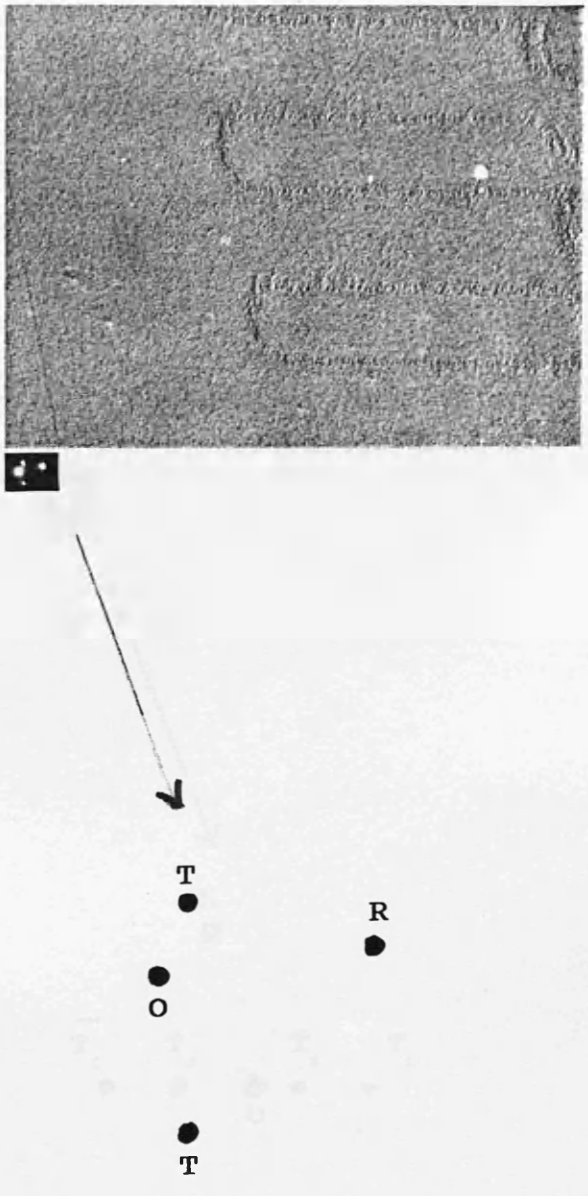

Figure 7.16a Small angle diffraction pattern obtained from the track written on sample C at 15° to the easy-axis, and a Fresnel image of the portion of track which produced this spot pattern. The recorded wavelength was 10μm and the camera length ~260m.

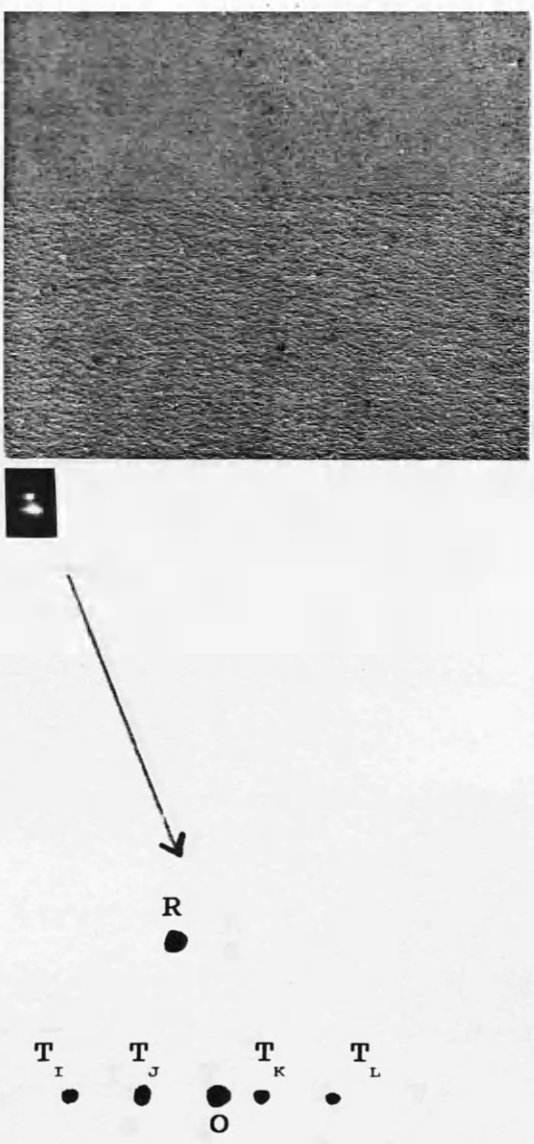

Figure 7.16b Small angle diffraction pattern obtained from the track written on sample C at 15° to the easy-axis, and a Fresnel image of the portion of track which produced this spot pattern. The recorded wavelength was 1.0μm and the camera length ~260m.

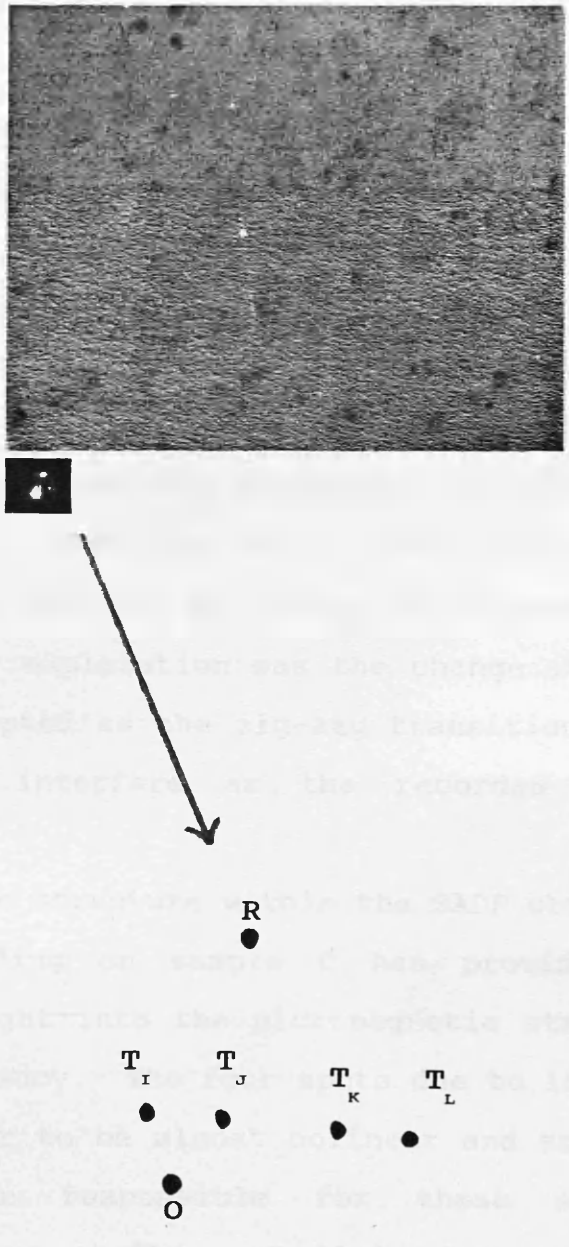

Figure 7.16c Small angle diffraction pattern obtained from another track written on sample C at 15° to the easy-axis, and the Fresnel image of the portion of track which produced this spot pattern. The recorded wavelength was 1.0μm and the camera length ~260m.

induction. Initially this was thought to arise from the other track, track B due to difficulties associated with establishing the region of specimen responsible for the SADP. The finite distance between the specimen and the objective aperture plane means that the visible region is not strictly the area which produces the diffraction pattern. The area which contributes to the SADP is in fact somewhat larger, although in comparison to the distance between the specimen exit plane and the final viewing screen, ie the camera length, these are very nearly the same. The ability to move the specimen when conducting small angle scattering experiments enabled us to rule out any effect of track B as a possible explanation for these observations. The fact that these patterns were only obtained from the high frequency recordings suggested that a more likely explanation was the change in micromagnetic structure adopted as the zig-zag transitions beginning to overlap and interfere as the recorded wavelength is reduced.

The fine structure within the SADP obtained from the 3.0MHz recording on sample C has provided us with a detailed insight into the micromagnetic structure present at this frequency. The four spots due to induction within track A appear to be almost colinear and the direction of the induction responsible for these splittings was established as being parallel to the 'transition boundaries'. The explanation for the additional deflection, not observed at the lower recording frequency where only two transverse spots are present, lies with the

substructure within each 'bit', see the middle image in figure 7.17. From Foucault images such as these it became clear that each 'bit' contains small regions within which the orientation of the induction is different from that which predominates. It is the different micromagnetic structure found within what appear to be reversed domains which we believe produces the additional deflection observed within these higher frequency recordings.

To account for the observed SADP we propose that the micromagnetism these recordings produce is similar to that illustrated in figure 7.18 This diagram illustrates four distinct micromagnetic configurations which account for the general form of the diffraction pattern. These are designated I, J, K, and L. If we assume that the magnetisation which predominates within any written bit lies along the easy-axis, although not an essential requirement, and then resolve the induction into components parallel and perpendicular to this, we can calculate the Lorentz deflection from within the 4 zones. Omitting constant factors the deflections from each of these areas would arise from a force given by an equation of the form:

$$\underline{F} = \underline{v} \times (\underline{H}+\underline{M})$$

As mentioned the magnetisation which predominates in these written 'bits' need not lie parallel to the easy-axis, the significance of this would only be to alter the size of deflection due to the components of induction perpendicular to the recorded track direction. To be able

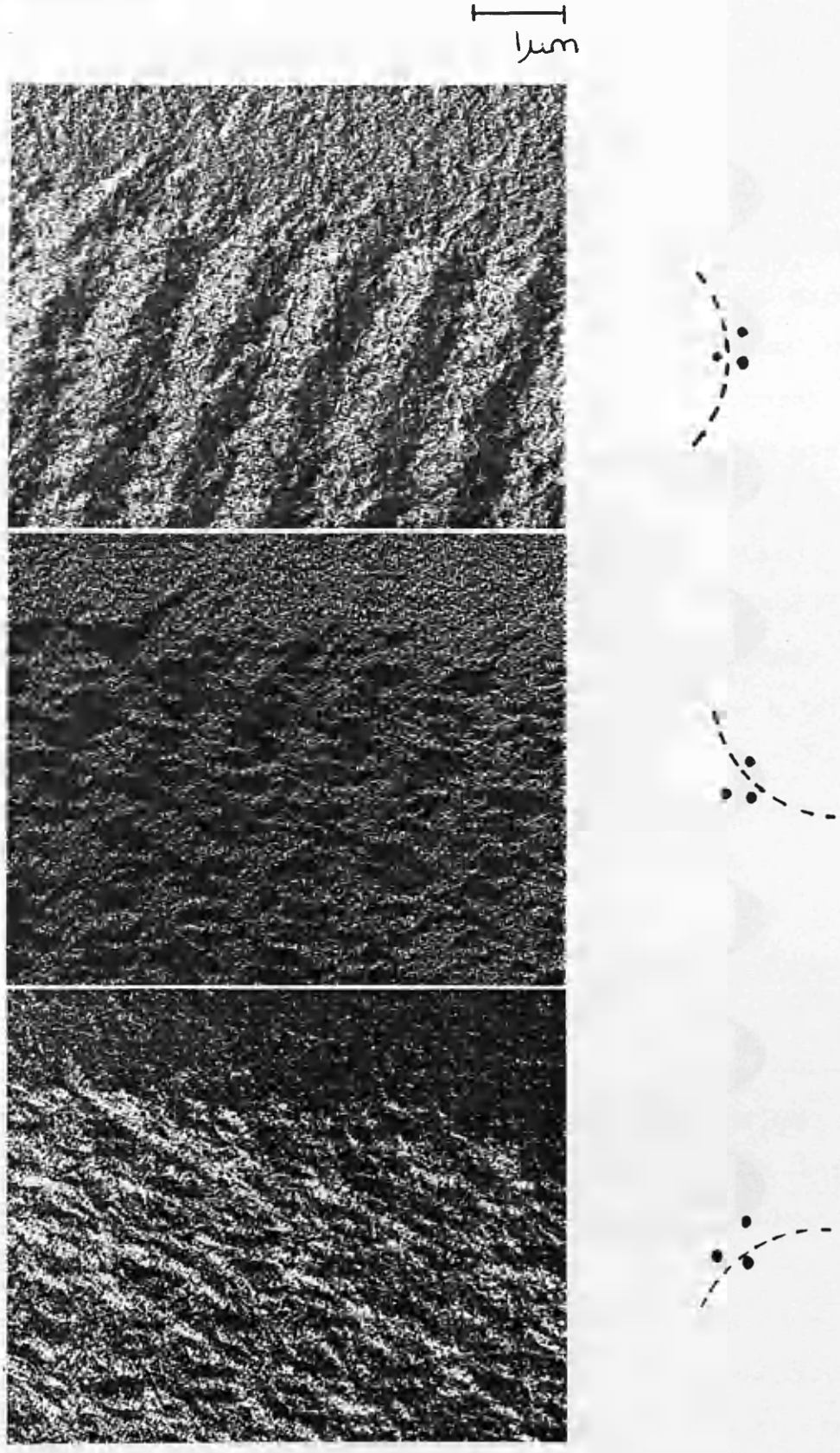

Figure 7.17 These three Foucault images were produced by attempting to remove each of the three distinct spots, only observed at much longer camera lengths, with the objective aperture in turn. The recorded wavelength was 1μm.

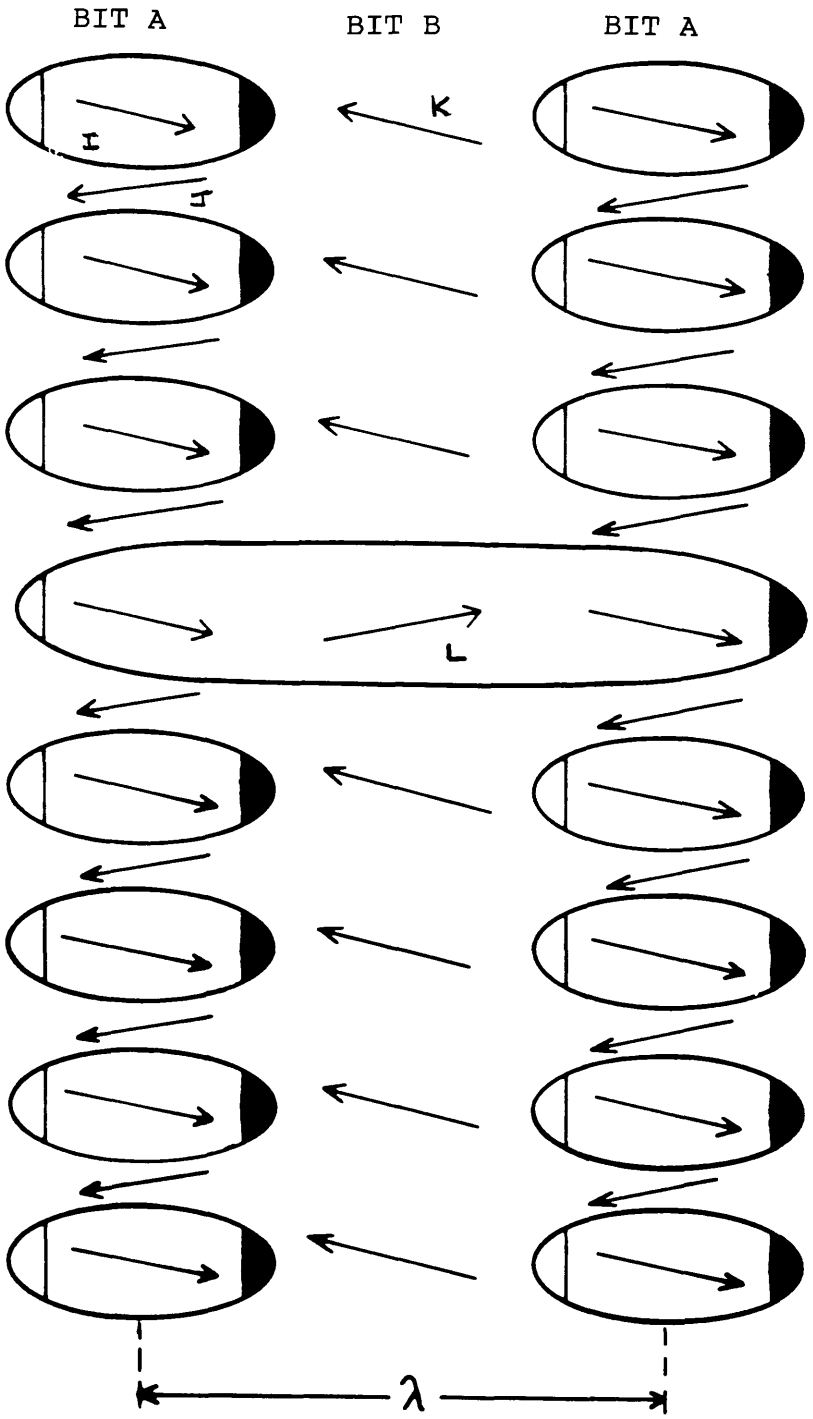

Figure 7.18 Possible micromagnetic structure of the written bits to account for the fine structure observed in the small angle diffraction pattern from track A high frequency recordings made on sample C. The measured signals are produced by the stray field which is produced by the magnetic charge concentrated at either end of the domains written against the DC erased state.

to determine the magnitude of the deflections produced within these four areas requires the accurate determination of the position of the undeflected beam. The specimen charging effect discussed earlier ruled out the location of this spot obtained from double exposure photographs. The direction of the magnetisation within these small regions we believe adopts the configuration as illustrated in figure 7.19 in order to reduce the exchange energy. With this arrangement the components of magnetisation perpendicular to the track direction within both the reversed domains and also the written 'bits', are parallel within any given 'bit'. Therefore the magnetisation across each written 'bit' forms a zig-zag like structure as indicated in the diagram.

Close examination of the SADP indicates that the subspots have slightly different intensities. Those indictated by T_I, T_J both appear slightly more intense than the other pair, T_K, T_L. From this we conclude that both of the spots, T_K and T_L, arise from the minority distribution within the written 'bits'. In one case this is the lozenge shaped domains within the predominantly DC magnetised region, and in the other the small thin DC magnetised areas between the lozenge shaped domains which dominate within the other 'bits'.

The very long camera lengths needed to resolve these individual spots is produced by switching the objective lens off and using one of the condenser lenses to control the illumination, and thus the back focal plane of this lens no longer coincides with the objective aperture

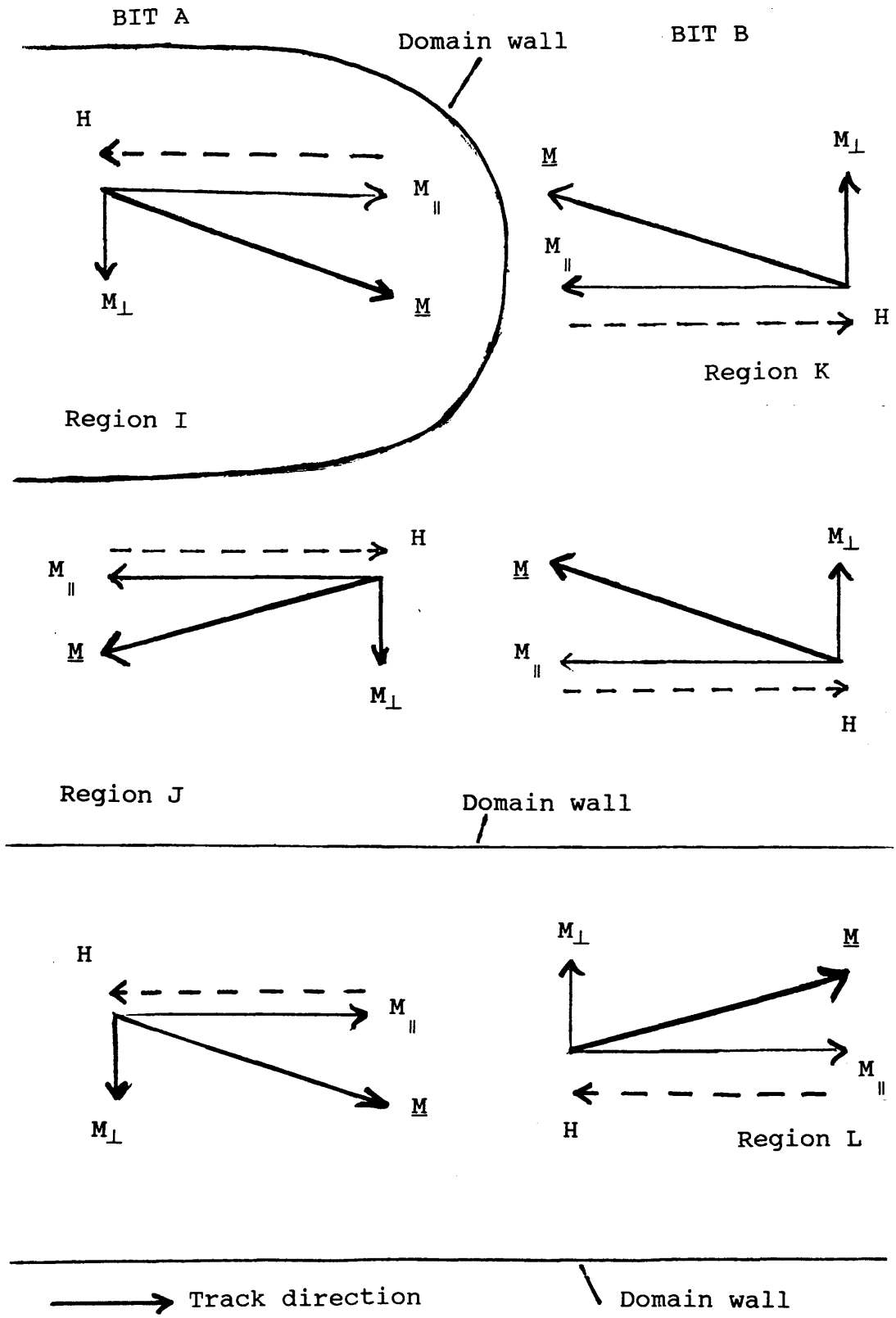

Figure 7.19 Expanded diagram of the proposed micromagnetics within the written bits to illustrate the components of induction which produce the observed Lorentz deflections.

plane. The lens combinations which provide these long camera lengths are therefore incompatible with the generation of Foucault contrast which would have enabled us to selectively remove each individual spot and observe the consequences which might have verified whether or not the reversed domains were in fact the cause of the additional splittings.

A camera length of ~1.0m can routinely be realised on the 2000FX CTEM with the objective lens strongly excited, and this short camera length limits the information contained within the Foucault images generated. A camera length of ~1.0m could not resolve the fine substructure observed from sample C at the much longer camera lengths, nor could any indication of the regions of increased intensity within the SADP be produced at this distance, which might have provided additional information to answer this question.

Successful attempts were made to increase the camera length by adjusting the magnification produced by the post specimen lenses. In an attempt to increase the camera length the post specimen lens currents were adjusted as follows :

Lens	Normal mode	Modified mode
I1	Focus	Not altered
I2	6.90	Focus
I3	2.59	0.00
PROJ	7.88	8.01

Thus because we had not adjusted the objective lens

current, performing these adjustments in Free Lens Control mode, the back focal plane would still coincide with the aperture plane and facilitate the production of Foucault contrast. From observations the electron distribution at the new PSL settings appeared to contain structure not seen by either the operator nor the photographic film at 1.0m, and therefore an increase in camera length had been achieved. When the appropriate spot was allowed to pass through the aperture blade the extremely low level of intensity striking the phosphor screen prevented direct observations of the Foucault images. Even long exposures on fast x-ray film could not produce a Foucault image with clearly discernable features. We were convinced that electron intensity was in fact striking the viewing screen because identifiable images were possible with only very subtle adjustments to the relative position of the electron distribution to the aperture, using a low light level video camera unit. Figure 7.17 illustrates the Foucault images obtained using this new post specimen lens arrangement.

In conclusion therefore we were unable to verify the cause of the sub-splitting or the suggestion that the spots of lower intensity arise from the minority magnetic distribution within each of the written 'bits'. We are also unable to explain why the spots within the SADP appear distinct since from our model we would expect a more continuous change in the electron intensity. We did however manage to increase the camera length at which the generation of Foucault contrast remains possible.

7.5 ADDITIONAL EXPERIMENTS TO VERIFY THE RELAXATION MECHANISM OF THE MAGNETISATION WRITTEN AWAY FROM THE EASY AXIS

The transverse component of magnetisation was believed to originate as a consequence of recording at 15° to the 'easy-axis' of magnetisation. The consequence of recording at an angle to the easy-axis was further studied by examining tracks produced on a system which enabled circumferential tracks to be recorded which varied the angle between the record direction and the easy-axis over a large range. In this way we were able to examine the range of angles over which the transverse component was found.

To perform these experiments it was necessary to use complete webs of MET some 4" in width. Only sample A was available in this size and therefore these experiments were restricted to this thickness. The recording measurements were carried out on an experimental recording set up at Philips Research Laboratories in Eindhoven[10] to whom we express our sincere thanks.

The results of these experiments indicated the presence of a transverse component of magnetisation at all of the recording angles studied. Determining the precise angle of recording was not possible as considerable skewing of the tape occurred during loading of the tape web into the ring shaped holder, which was further complicated as the head used had a gap skewed at 10° with respect to the track direction. This effect meant that all

of the angles at which we thought we were recording were incorrect. Very strange domain patterns were also observed in certain images, see image 7.20. It appeared that maintaining a constant head to tape distance during recording had proved impossible, and therefore peculiar domain geometries resulted. This distance was varying because the tape did not have a lubricating layer and thus head sticking occurred, causing severe problems. As a result of these problems the value of the results obtained from these experiments is substantially less than at first hoped. However as the relative angle between the recording directions are known a comparison could be made between the relative magnitude of the transverse components at the various angles, and compared with the data already obtained for recordings made at 15° and -5° to the easy-axis.

Microscope samples of recordings thought to be along the tape direction, perpendicular to the tape direction and at angles intermediate between these two extremes were prepared. DPC images of these are illustrated in figures 7.21(a-e) and 7.22(a-c). Unfortunately no reference contrast level was available to us for these samples, since no saturated regions of the tape had been recorded. However as the amplifier gains employed throughout these experiments were all equal and if we assume that the position of the undeflected beam lies midway between the two transverse components of induction it is possible to gauge the relative magnitude of this component at each of the different recorded directions. The results of the DPC

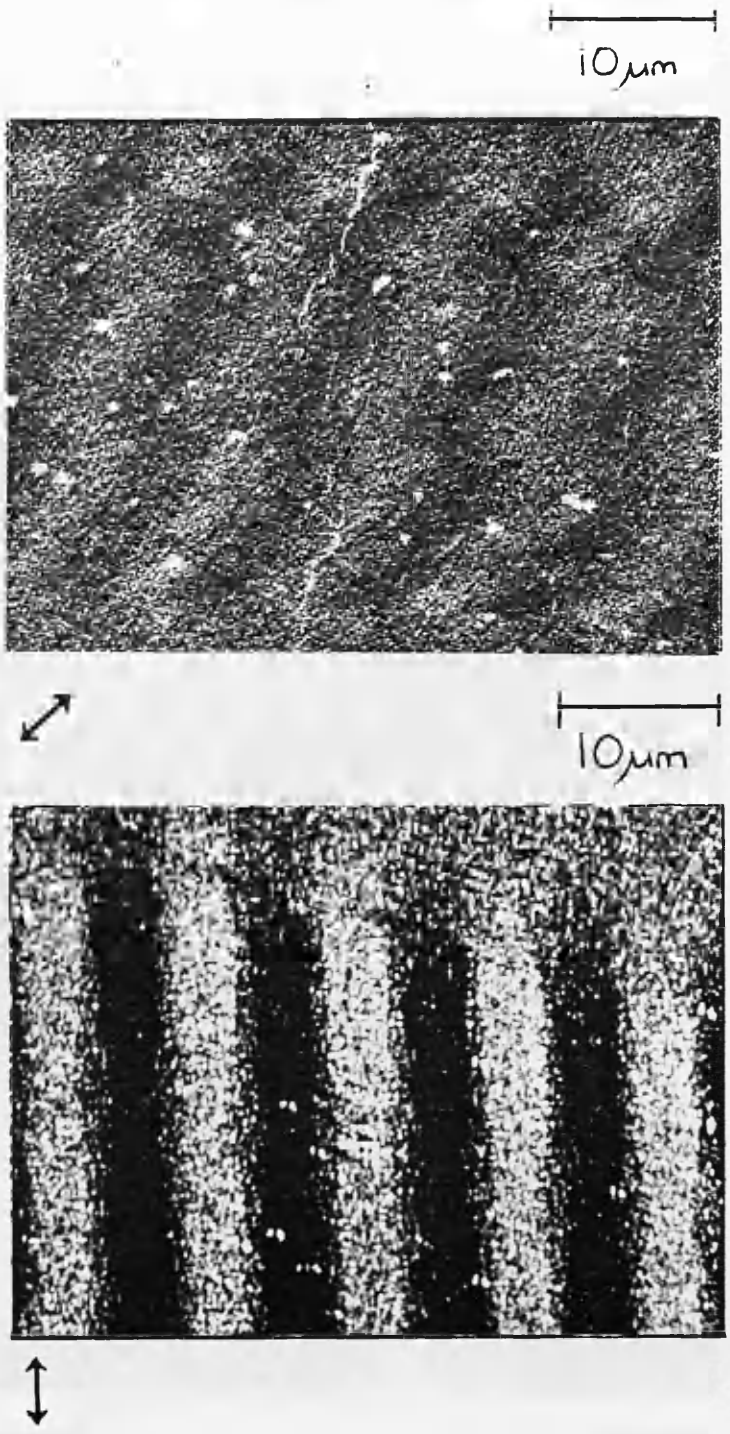

Figure 7.20 The top DPC image is of a low frequency recorded track produced with the same head drum assembly as that used to produce the tracks shown in the figure below and also the figures 7.21(a-e) and 7.22 (a-c). The images map induction as indicated by the arrows (bottom left). The irregular structure across the track in the top image, indicated that head sticking was occurring during part of these recordings.

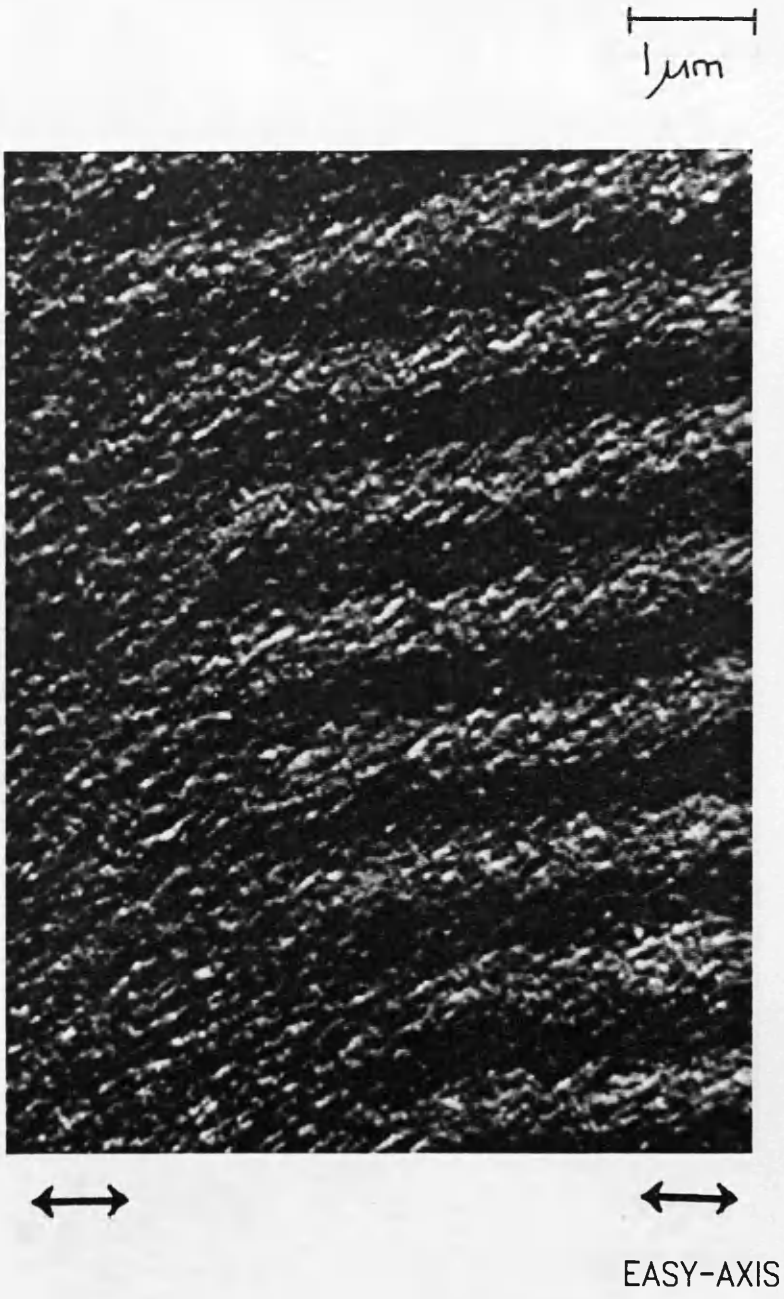

Figure 7.21a DPC image of sample A written at ~90° to the easy-axis of magnetisation. As indicated by the arrow (bottom left) the contrast within the image is sensitive to induction perpendicular to the track direction; the recorded wavelength was 1μm.

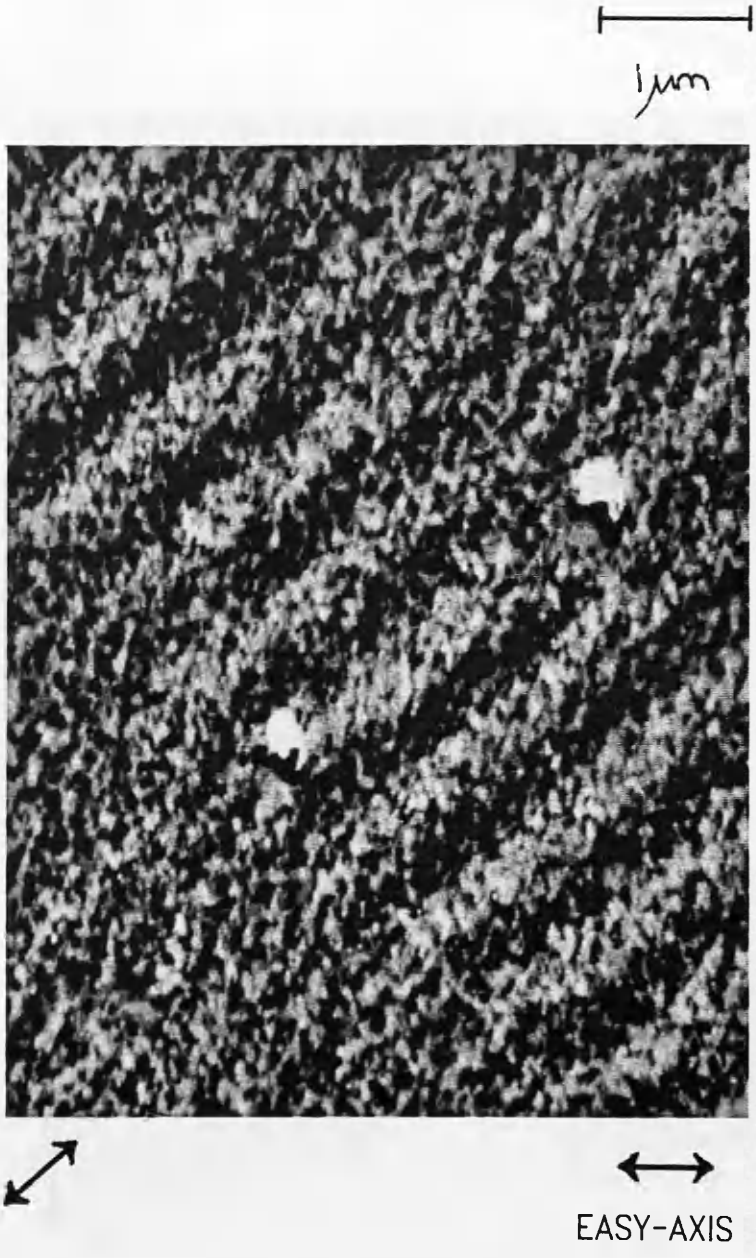

Figure 7.21b DPC image of sample A written at ~45° to the easy-axis of magnetisation. As indicated by the arrow (bottom left) the contrast within the image is sensitive to induction perpendicular to the track direction; the recorded wavelength was 1μm.

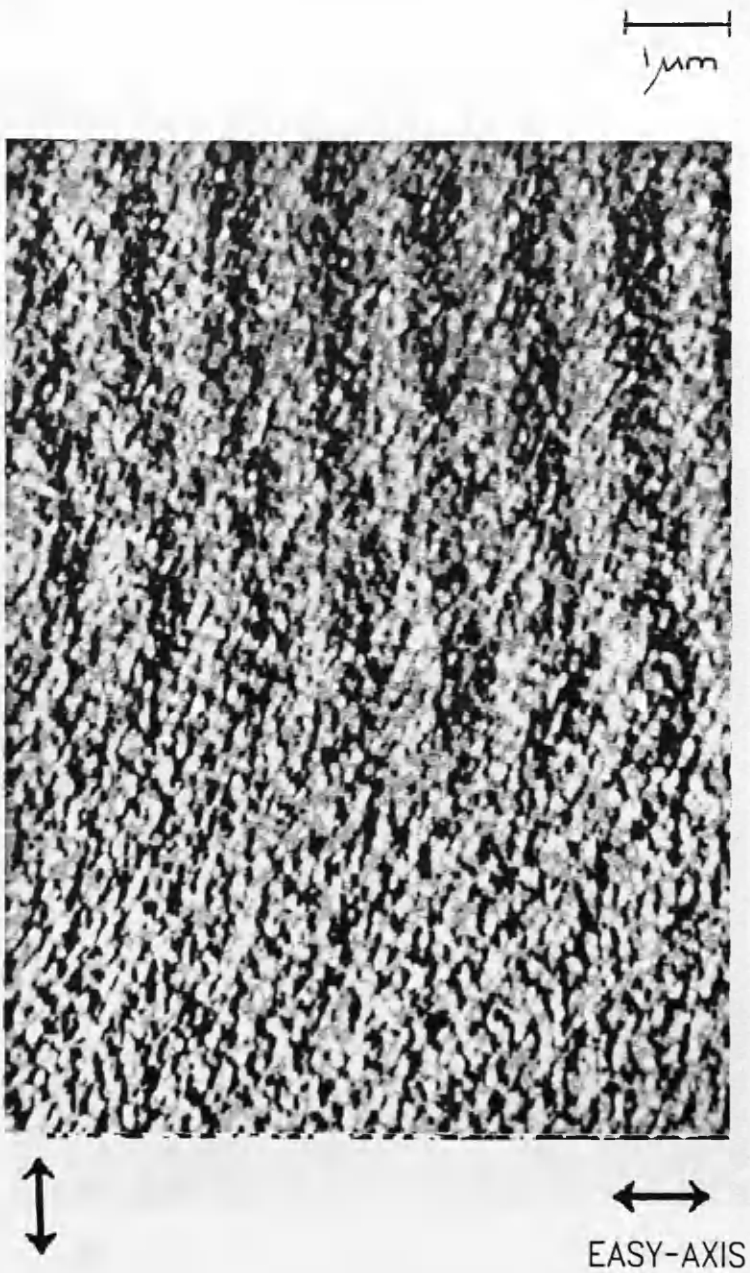

Figure 7.21c DPC image of sample A written ~parallel to the easy-axis of magnetisation. As indicated by the arrow (bottom left) the contrast within the image is sensitive to induction perpendicular to the track direction; the recorded wavelength was 1μm.

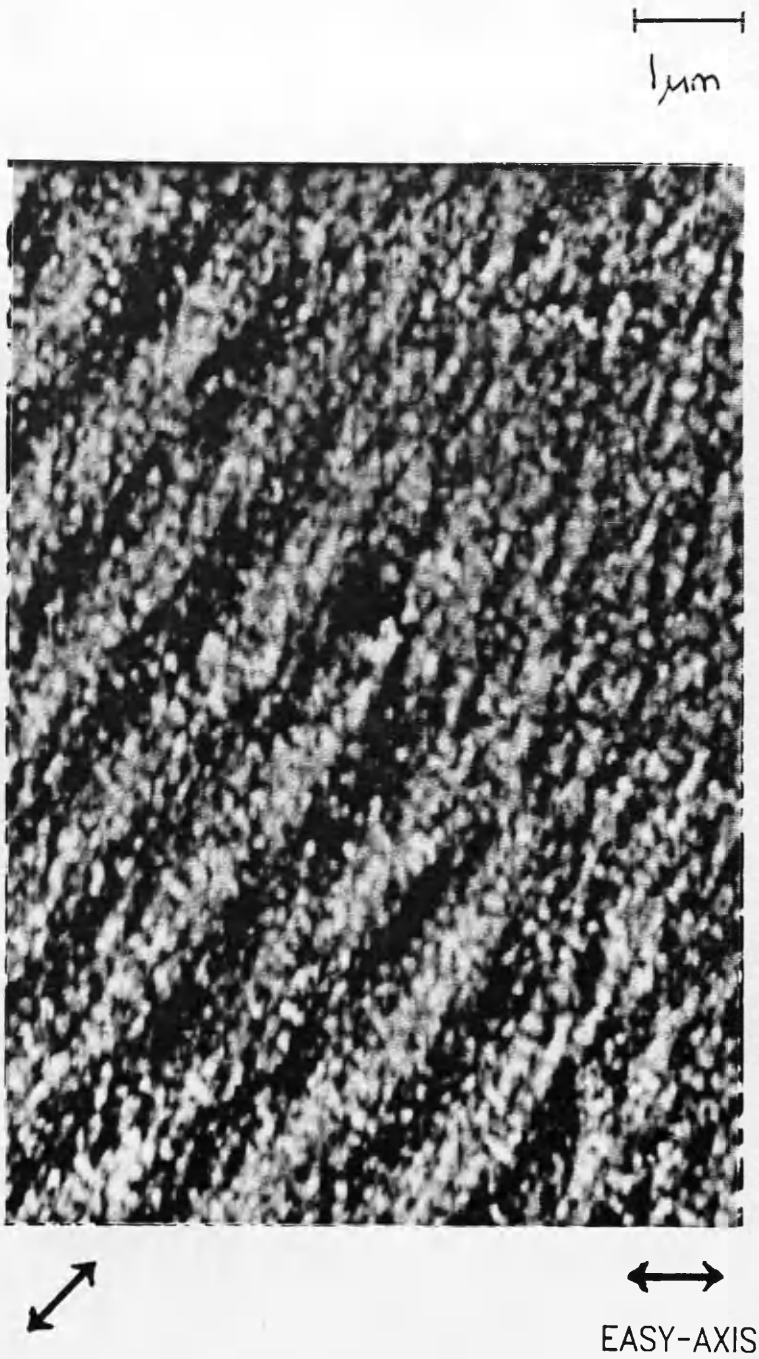

Figure 7.21d DPC image of sample A written at ~-45°to the easy-axis of magnetisation. As indicated by the arrow (bottom left) the contrast within the image is sensitive to induction perpendicular to the track direction; the recorded wavelength was 1μm.

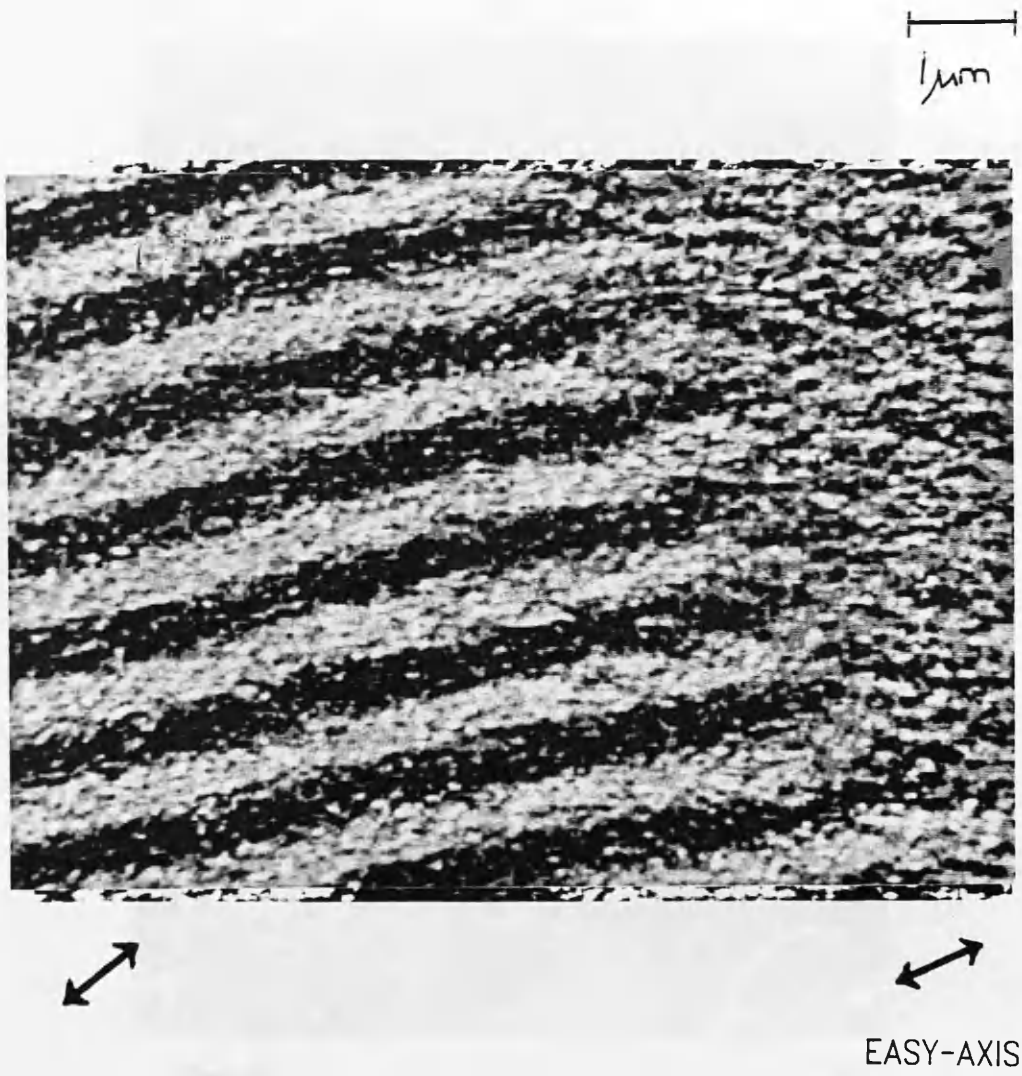

Figure 7.21e DPC image of sample A written at ~-90°to the easy-axis of magnetisation. As indicated by the arrow (bottom left) the contrast within the image is sensitive to induction perpendicular to the track direction; the recorded wavelength was 1μm.

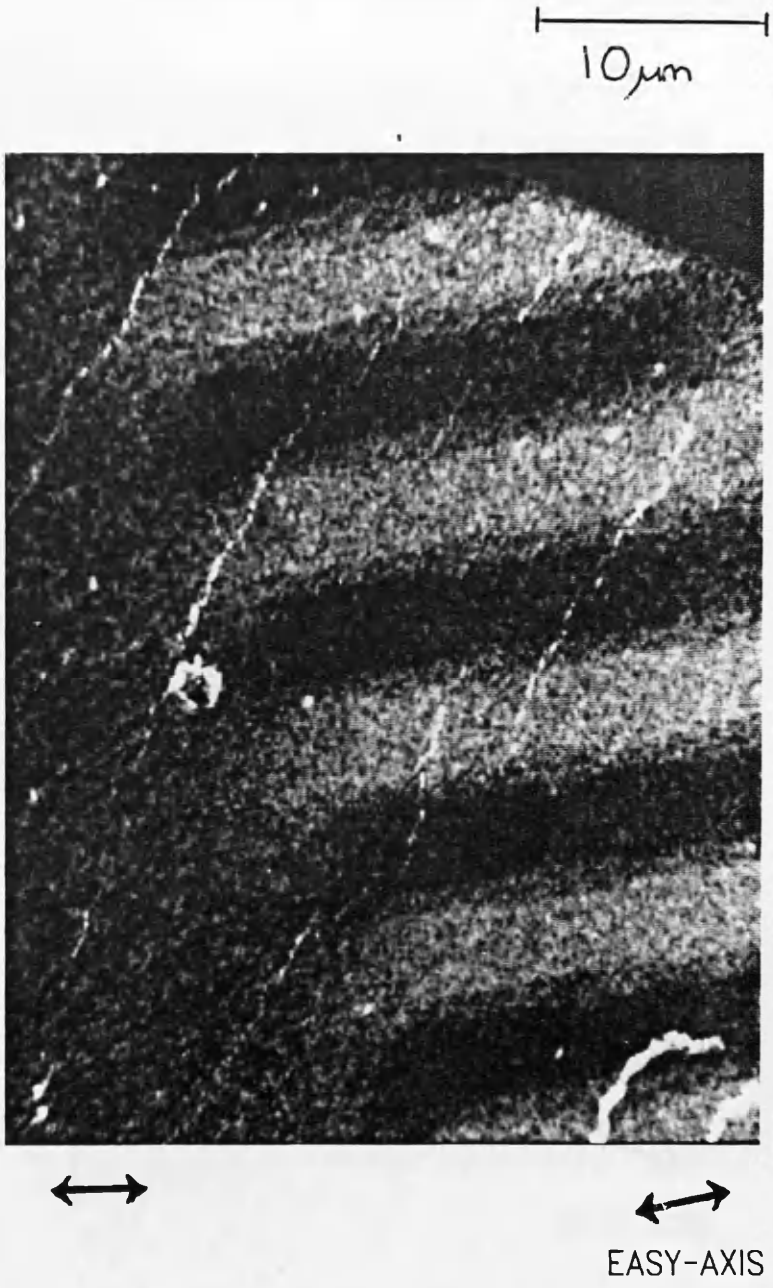

Figure 7.22a DPC image of sample A written at ~+90°to the easy-axis of magnetisation. As indicated by the arrow (bottom left) the contrast within the image is sensitive to induction perpendicular to the track direction; the recorded wavelength was 10μm.

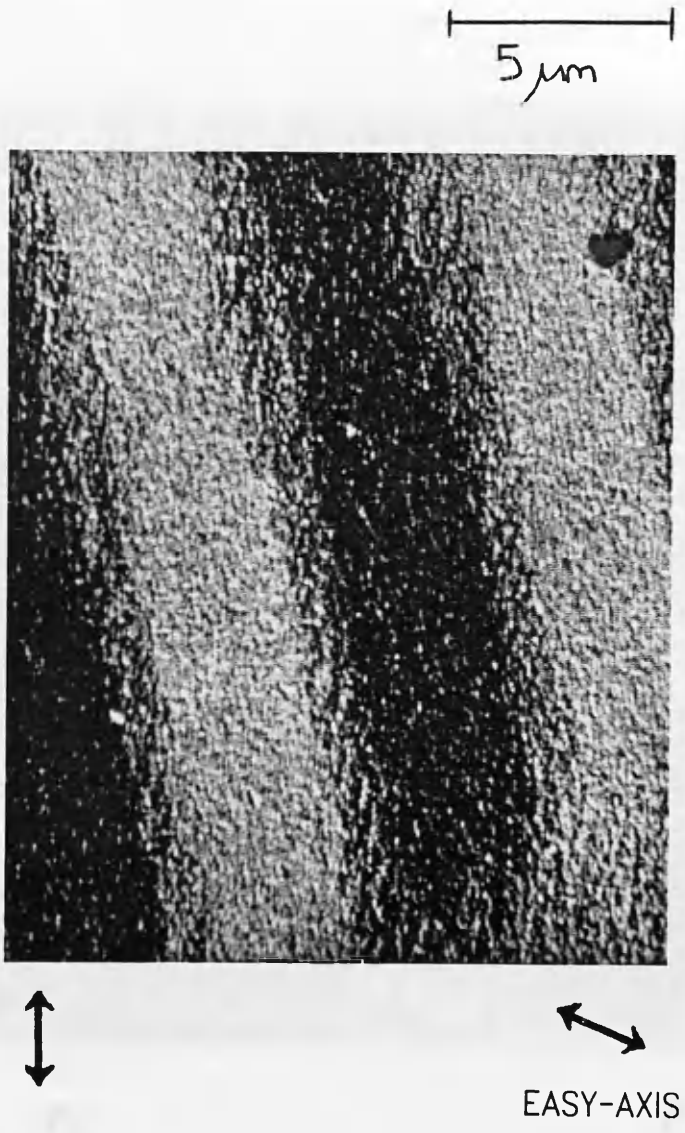

Figure 7.22b DPC image of sample A written at ~+45°to the easy-axis of magnetisation. As indicated by the arrow (bottom left) the contrast within the image is sensitive to induction perpendicular to the track direction; the recorded wavelength was 10μm.

Figure 7.22c DPC image of sample A written at ~-45°to the easy-axis of magnetisation. As indicated by the arrow (bottom left) the contrast within the image is sensitive to induction perpendicular to the track direction; the recorded wavelength was 10μm.

analysis of these samples are contained in table 7.F

Angle to easy-axis	Wavelength	Approximate size of Transverse component
+90±7°	1.0μm	68
+45±7°	1.0μm	33
0±7°	1.0μm	18
-45±7°	1.0μm	37
-90±7°	1.0μm	36
+90±7°	10μm	50
+45±7°	10μm	34
-45±7°	10μm	56

Table 7.F Magnitude of transverse component of induction from recordings made at various angles to the easy-axis.

These results do exhibit the trends already established from the DPC results from the video tracks. The magnitude of the transverse component is seen to increase as the recorded magnetisation is required to rotate through larger and larger angles in order to orient itself as close to the easy-axis as the demagnetising field will permit.

7.6 INTERPRETATION OF THE ELECTRON OPTIC IMAGING OF THE WRITTEN TRACKS

To complete the micromagnetic characterisation of the recorded structures found in these films requires the introduction of an additional stray field effect. We illustrate the interaction by considering the recording of a transition, written at 15^{o} with respect to the easy-axis onto a highly anisotropic media, so anisotropic in fact that the magnetisation always relaxes parallel to this direction irrespective of the record direction. Immediately after recording the magnetisation and the stray field are parallel with each other irrespective of the angle to the magnetic easy-axis. The magnetisation next begins to rotate into alignment with the easy-axis; however, the direction of the stray field remains unaltered. Since the orientation of the fringe field is governed by the position of the domain walls, which are unaffected by any rotation of the magnetisation, the direction of the stray field remains parallel to the recorded track[11]. The effect of the magnetisation relaxing into the easy direction serves only to reduce the amount of stray field passing above the recorded pattern. Therefore the final equilibrium configuration for our hypothetical recording material, written at an angle to the easy-axis, consists of a magnetic vector which is parallel to the easy-axis and at 15^{o} to the stray field, see figure 7.23. Now consider the DPC image produced from such a magnetic microstructure when sensitive to

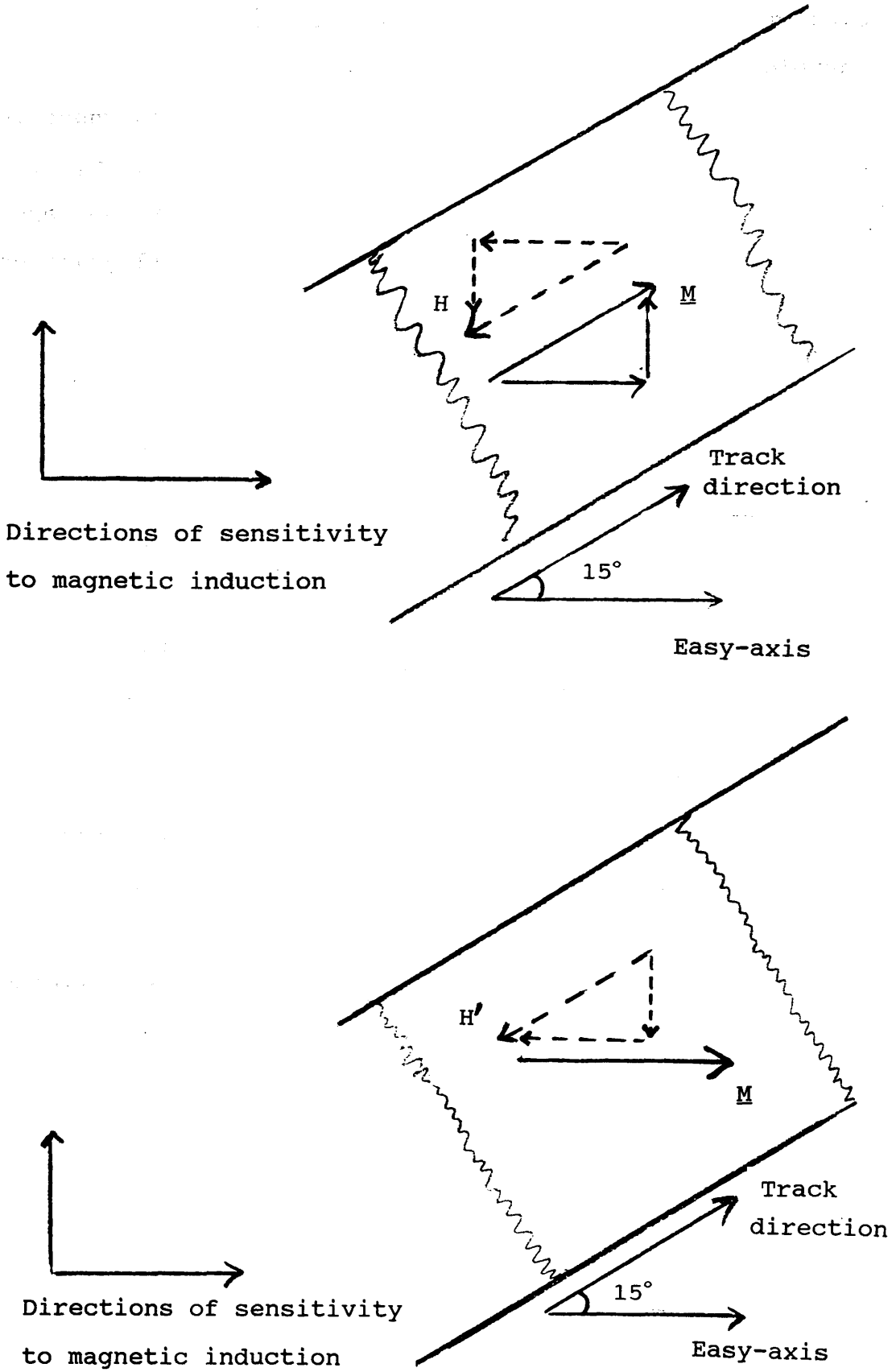

Figure 7.23 Illustration of the situation present within a recorded domain a) as it is written, and b) after relaxing along the easy-axis. The two directions of DPC sensitivity are also shown to enable the components of induction parallel and perpendicular to these axes to be resolved.

magnetisation perpendicular to the easy-axis. In this direction the phase shift arises solely from the relevant component of the stray field, since the magnetisation has no component in this direction. Therefore the resultant image contrast would be governed by the functional form of the stray field, which is quite different from that of the magnetisation within the sample. The size of the Lorentz deflection that this effect induces depends on the angle between the direction of the recorded track and the magnetic easy-axis, since it is only the component of magnetisation perpendicular to the domain walls which gives rise to this stray field. In this particular direction the magnetisation, which normally produces a shift opposite to that effected by the associated stray field, plays no part and consequently what appear to be abnormally large phase shifts can arise. The variation in integrated induction as we move along the recorded track from the centre of the domain toward the transition region is a slowly varying function, and only when in close proximity of the recorded transition does significant variation occur[12]. Therefore with this description of the situation found in and around the recorded tracks we can account for the appearance of extremely sharp transitions at high frequency. This micromagnetic description, which we have proposed, is consistent with observations of recorded tracks on a highly anisotropic ferromagnetic material, FeCoCr, at similar recording densities, recorded at an angle to the easy-axis.[13]

The significance for a material which does not have

an infinite anisotropy, such as the MET films studied, coupled with differentiation along non optimum directions, ie not perpendicular to the easy-axis, mean that the results which we originally ascribed solely to a transverse component of magnetisation, contain substantial contributions from this stray field effect. If we assume that the magnetisation within each written 'bit' does lie parallel to the easy-axis then we can resolve the stray field and the magnetisation, into components parallel and perpendicular to the direction of differentiation. With this information we are now in a position to compare the observed shifts from the component of induction orthogonal to the direction of differentiation with that expected if the magnetisation does lie parallel to the easy-axis. The effect of the stray field could now be taken into account. The theoretical values in table 7.G are obtained by assuming that the magnetisation lies parallel to the easy-axis whereas the experimental values are determined directly from the rotation angles calculated using DPC.

Sample	λ	Theoretical	Experimental
A	0.8	1.4	1.6±0.5
B	1.0	1.3	3.4±1.9
C	1.0	1.1	6.3±6.7

Table 7.G Ratio of transverse components of magnetisation within track to reference. The theoretically predicted values assume that the magnetisation lies along the easy-axis. The experimental values are measured directly from the DPC images.

The differences between these two sets of figures arises

from the fact that these MET films do not have a sufficiently large anisotropy to enable us to be absolutely certain that upon relaxation the magnetisation within each written 'bit' lies parallel to the easy-axis. The effect of this modifies the above table of results, but not in such a way that can be resolved easily. Determining the exact orientation of the magnetisation cannot readily be achieved using a technique which is sensitive to both the influence of the stray field and the magnetisation. If a material with extreme uniaxial anisotropy were used then by rotating the direction of differentiation with respect to the recorded tracks these effects could perhaps be separated. Only once this experiment had been carried out would it be possible to address the problem encountered with the MET films studied.

The closest agreement, between theory and experiment, is seen to be found for sample A which we attribute to these samples having the largest uniaxial anisotropy, and therefore the magnetisation within these recorded patterns lies closer to the easy-axis than it does in the either sample B or sample C.

In theory the smallest Lorentz deflection observable to the DPC system could be made if a similar analysis addressed the situation present when recording track B, since no transverse induction could be detected for this track. As above, the analysis would require the magnetisation to relax along the easy-axis. We believe that the absence of magnetic contrast from a transverse

component of induction within track B does not rely on the small angle between the magnetisation and the stray field alone. At only -5° to the easy-axis it is entirely possible that the magnetisation does not reorient itself along the easy-axis and therefore might remain parallel to the stray field, which would explain why these tracks do not exhibit the same micromagnetic structure as track A.

7.7 FREQUENCY MODULATED RECORDINGS

As a result of recordings carried out incorrectly video tracks containing more than one recorded frequency were discovered using the DPC mode of Lorentz electron microscopy. This has important implications on the use of this technique to examine the magnetic microstructure of magnetic recording tracks. Figures 7.24a and 7.24b illustrate modulated recordings where the base signal was recorded at 3.8 and 0.38MHz respectively. As discussed previously, in an electron microscope the deflection of the incident beam not only depends on the magnetisation within the irradiated sample but also on the stray fields which are present outwith the sample volume. This limits the applicability of Lorentz electron microscopy to the study of magnetic recording tracks since the nature of both the medium magnetisation and also the stray fields govern the observed contrast, which makes separating the contributions made by each of these more difficult.

Unfortunately we cannot be certain of the origin of the additional low frequency signals present in these

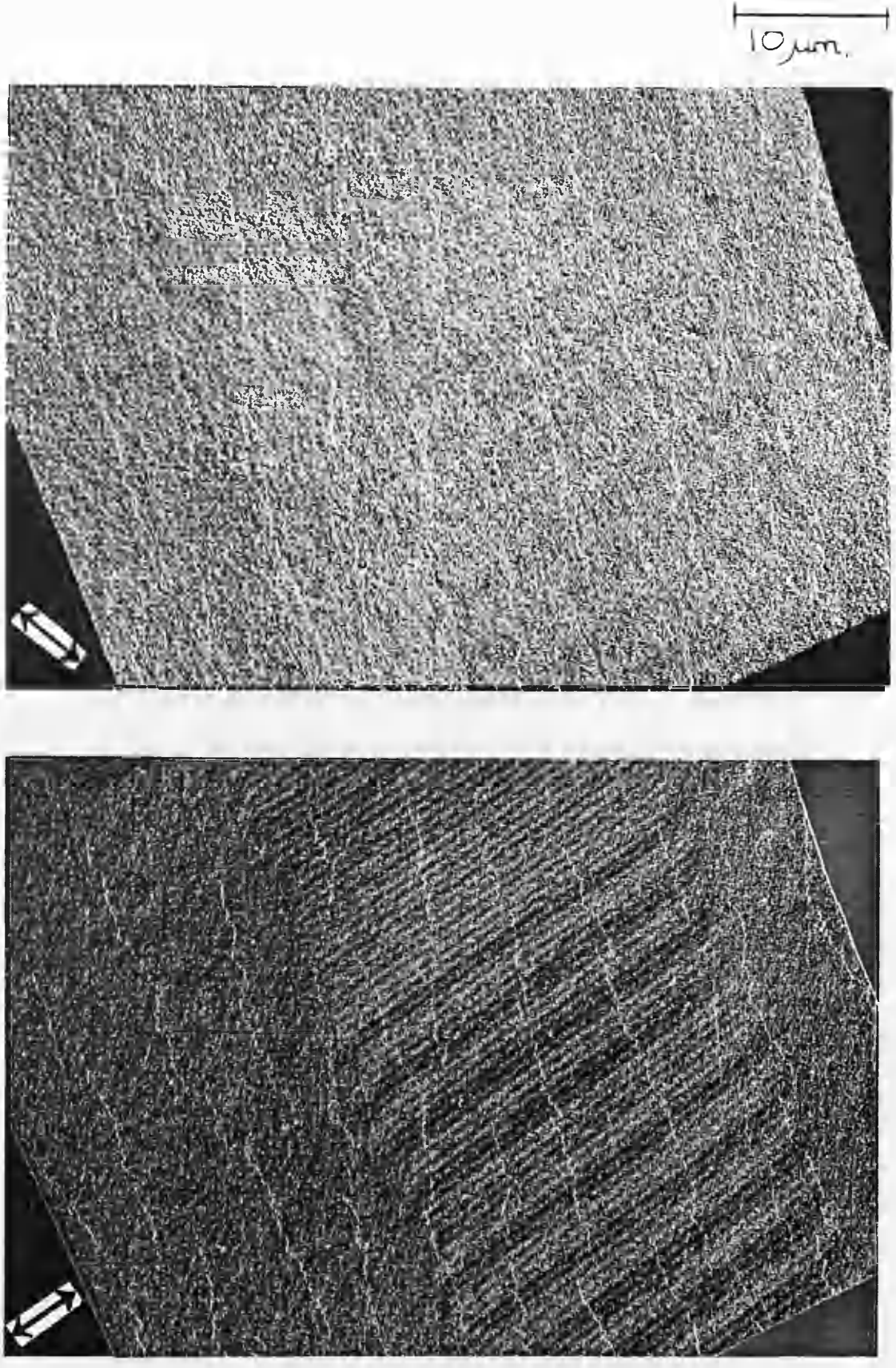

Figure 7.24a DPC images of both tracks written on AC erased media, the track recorded at 15° to the easy-axis is on the right hand side. These images were produced with a base frequency of 3.8MHz, which produced a wavelength of 0.8μm, and illustrate the modulation effect. The induction directions mapped are indicated by the arrows.

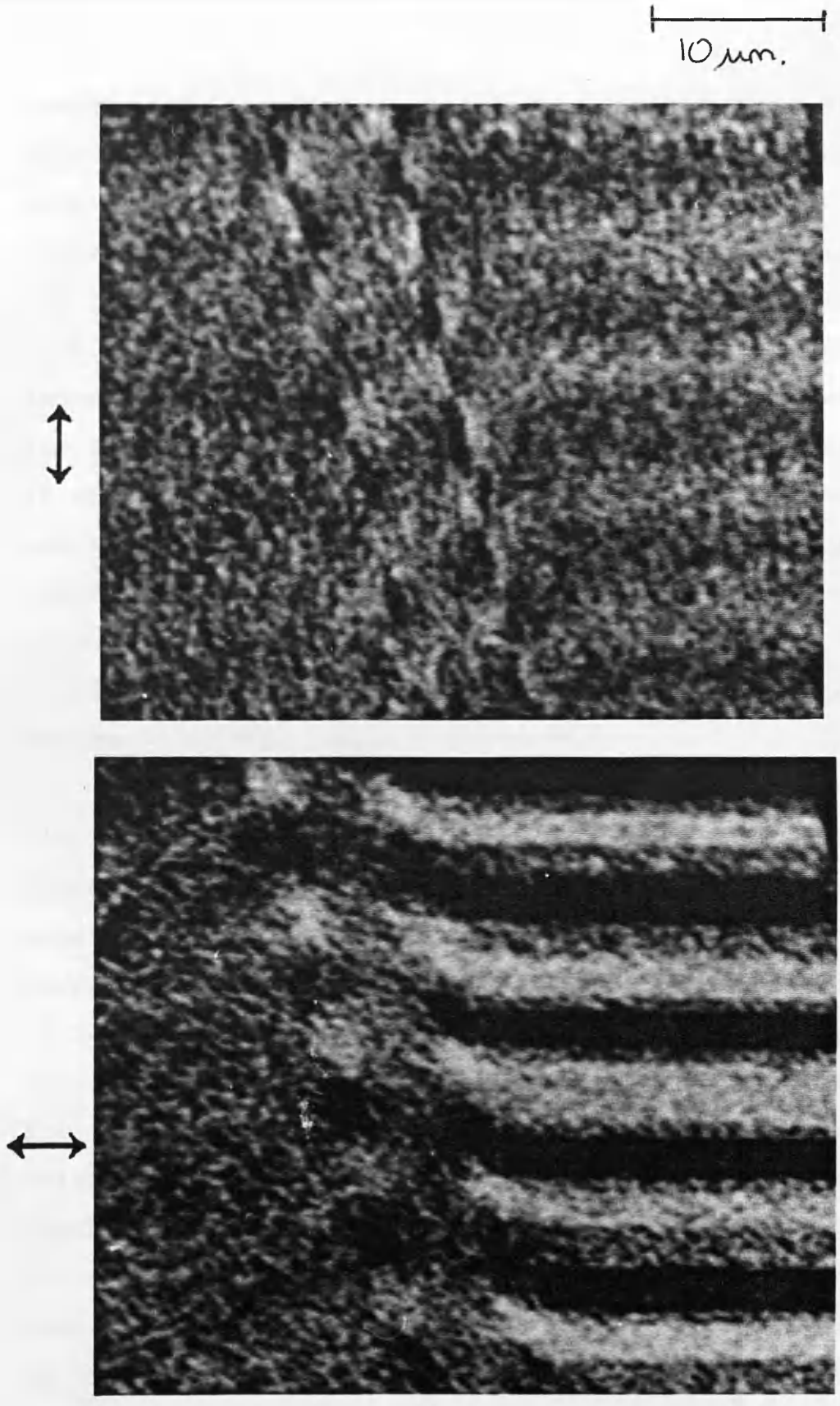

Figure 7.24b DPC images of both tracks written on AC erased media, the track recorded at 15° to the easy-axis is on the right hand side. These images were produced with a base frequency of 0.38MHz, which produced a wavelength of 8μm, and illustrate the modulation effect. The induction directions mapped are indicated by the arrows.

images, and therefore we do not know whether these signals were recorded simultaneously or separately, which further complicates the issue when trying to interpret the image contrast variations. We do know that in order to maintain the position of the heads with respect to the centre of each recorded track, low frequency guidance signals are recorded in addition to the video picture information. The frequency spectrum of the video 8 system, illustrated in chapter 2, does at least inform us that if these are the tracking frequencies, then these are recorded with a lower amplitude than any other signal present; this allows us to propose a simplified explanation which at least accounts qualitatively for the variations in intensity observed in these images.

In order to explain these images we consider the simplified situation illustrated in figure 7.25. In our hypothetical experiment each signal is recorded separately, in phase, and at frequencies of ν and 2ν respectively. If we record the larger amplitude signal, at 2ν, first and then record the long wavelength signal on top of this, then we assume the reduced write current used for the second recording prevents the head field from writing the low frequency signal throughout the entire depth of the film. If the head was in fact writing well through the thickness of the film then the low frequency recording would completely erase the previous recording. As the amplitude of this signal is insufficient to accomplish this a residue of the high frequency recording remains within the bottom layer of the film after this

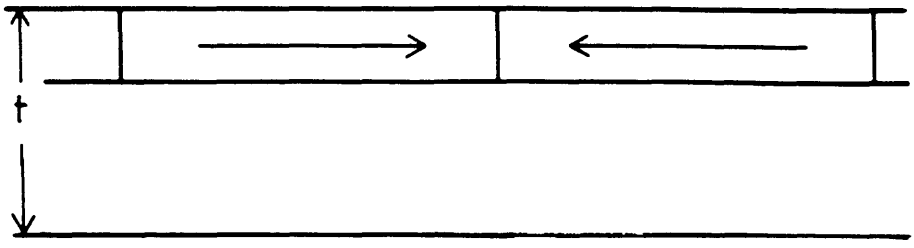

Low frequency and low amplitude recording

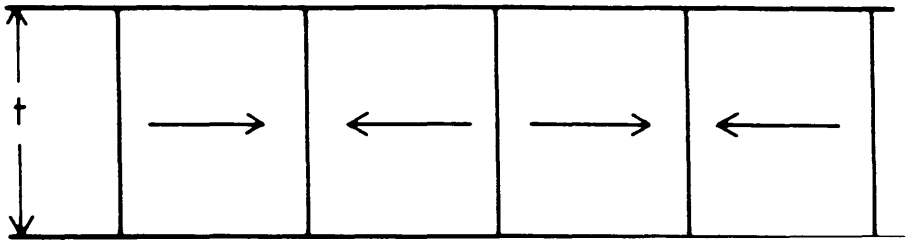

High frequency and large amplitude recording

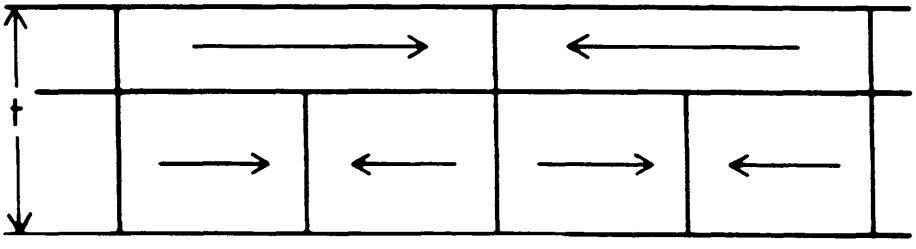

Composite recording

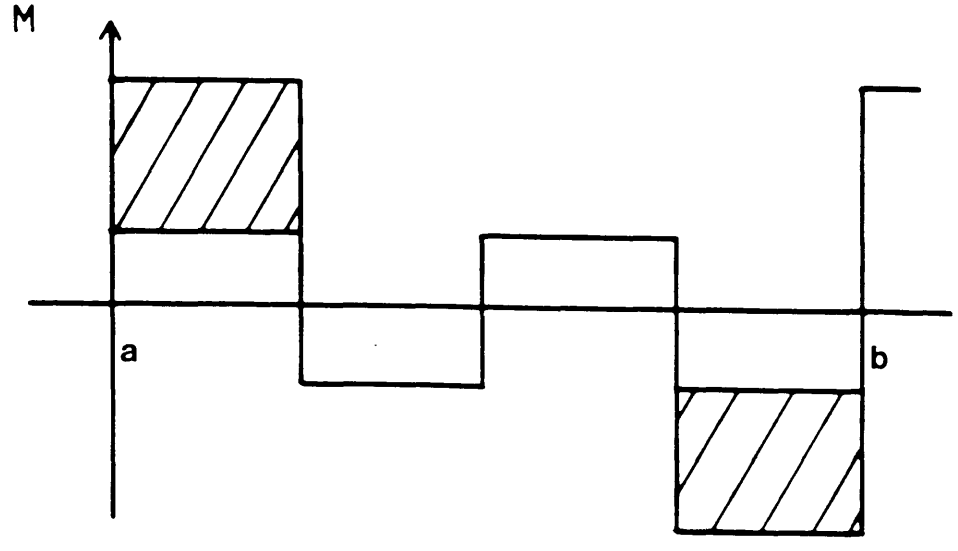

Figure 7.25 Possible magnetic configuration of the frequency modulated tracks. The increased magnetic charge density at positions a and b account for the observation of the low frequency signal.

recording. The top two illustrations in figure 7.25 show the expected magnetisation patterns if the the two recordings were performed in isolation onto AC erased media. As the lower amplitude low frequency recording has only written the upper portion of the film the number of magnetic charges which this produces, around the position of the magnetisation transitions, is less than those which result from writing the higher frequency signal. We believe that it is the modulation of the number of charges present at the domain boundary walls which explains why more than one frequency is apparant using Lorentz electron microscopy. This is illustrated in the bottom diagram of figure 7.25 where those charges, which arise from the greater level of magnetisation within the hatched regions, contribute to the longer wavelength signal.

Lack of information concerning the level of the write current used for these recordings, and also about the nature of the head field distribution which these would set up, prevents us from being able to make any quantitative deductions from these DPC images. If, however, care is taken to establish these quantities and if additionally a reference contrast level can be provided, by for instance DC erasure, then we believe that Lorentz electron microscopy has the potential to study the micromagnetics which are present when both amplitude and frequency modulation are present within the same written track.

SUMMARY

In summary we have observed that one of the two video tracks appears to have a substantial component of magnetic induction perpendicular to the written track direction. We also established the factors which control the position of recorded transitions, and the differences encountered when at high and low frequencies. The results presented for track A are consistent with this model, while the low frequency recordings made on track B are not. The explanation for this inconsistency we have attributed to differences in the distance between the recording head and the medium. The quantitative results describing the magnetisation distributions present within recorded tracks on three MET films with different bulk magnetic characteristics, provided data which suggests that the final equilibrium magnetisation configuration is reached by establishing a balance between the demagnetising field and the film anisotropy. The position of equilibrium was seen to shift to larger angles as the films became less anisotropic. The results from small angle diffraction patterns illustrated a significant charging effect which prevented quantitative interpretation on an absolute basis. The direction between the DC magnetisation and the transverse component of induction was however determined from these spot patterns and found to agree closely with the transverse component theory. Finally we discussed the possible micromagnetic forms which could account for the observation of frequency modulated tracks in terms of the

reduced writing capability of the lower amplitude signals.

REFERENCES

1. J. Jakubovics, in 3rd Course of the International School of Electron Microscopy, Part IV, p1303, (1975)

2. R. Potter, R. Schmulian, IEEE Trans. Magn, **MAG 7**, 873, (1971)

3. D. Bloomberg *et al*, IEEE Trans. Magn., MAG **15**, 1450, (1979)

4. P. Arnett *et al*, IBM Research Report, RJ6265, (61662), (1988)

5. R. Fayling *et al*, IEEE Trans. Magn., MAG **20**, 718, (1984)

6. J. Chapman *et al*, Ultramicroscopy, **3**, 203, (1978)

7. I. McFadyen, Ph. D Thesis, University of Glasgow, (1986)

8. D. Mee, E. Daniel, in "Magnetic Recording Vol. 1: Technology", ed's D. Mee, E. Daniel (McGraw-Hill) (1987)

9. R. Ferrier, Advs. Optic. and Elect. Microsc. 155

10. S. Luitjens *et al*, IEEE Trans. Magn., MAG **21**, 1438, (1985)

11. T. Arnoldussen, Private communication (1990)

12. R. Ferrier, Private communication (1990)

13. F.J. Martin, Private communication (1990)

CHAPTER 8 FUTURE WORK

The work contained in this thesis demonstrated that the DPC mode of Lorentz electron microscopy is capable of providing quantitative micromagnetic information from within high density magnetic recording tracks. We were able to show that the written magnetisation relaxes into a position at which the forces controlled by anisotropy and demagnetisation are balanced. Having established this for three magnetically distinct ferromagnetic thin films recorded at 15° to the easy-axis, we next attempted to study the role of these forces in more detail by examining recordings made over a wide range of angles to the easy-axis. Unfortunately this could not be completed in the remaining time available; however, we feel that more effort should be concentrated on such experiments if the resultant image contrast which an angle between the stray field and the magnetisation produces is to be more fully understood. The contribution made by the demagnetising field to the equilibrium configuration of the written magnetisation could be studied in a systematic way if several different frequencies were recorded at a fixed angle with respect to the easy-axis. We also feel that computer modelling has much to offer in this same respect and some progress has already been made in this area[1].

Changing the film composition or the microstructure can alter the film anisotropy and indeed DPC images of a sample which had a composition of $Co_{70}Ni_{30}$ clearly demonstrate the significance composition has on the resultant micromagnetic structure of the written tracks,

see figure 8.1.

An important aspect of the work, the quantification of the micromagnetic distribution present within the recorded tracks, can now be refined due to recent developments which have improved the DPC system used to obtain the data[2]. The undesirable crystallite contrast which hampers quantitative interpretation of the information is present in each of the DPC images contained within this thesis. A significant proportion of this non-magnetic contrast can now be removed from the images by using an annular quadrant detector inplace of the quadrant detector used to obtain these images. Chapman et al developed this detection system which utilises the outermost portions of the bright field cone to generate the magnetic contrast, and since these regions are less affected by crystallite contrast, images more representative of the micromagnetic structure alone result. A future project would benefit considerably from the use of this system. Another development of the DPC system which would enhance the project is the ability to acquire all four individual quadrant signals simultaneously. The various linear combinations of these signals, necessary to produce DPC, can be performed using the image processing facilities of the computer used to acquire these. The advantage of this system over that which digitises the analogue difference signals is the ability to determine the absolute beam shifts. The system also minimises the effects of any temporal fluctuations present during acquisition of the images. If this facility were available on the annular quadrant detector

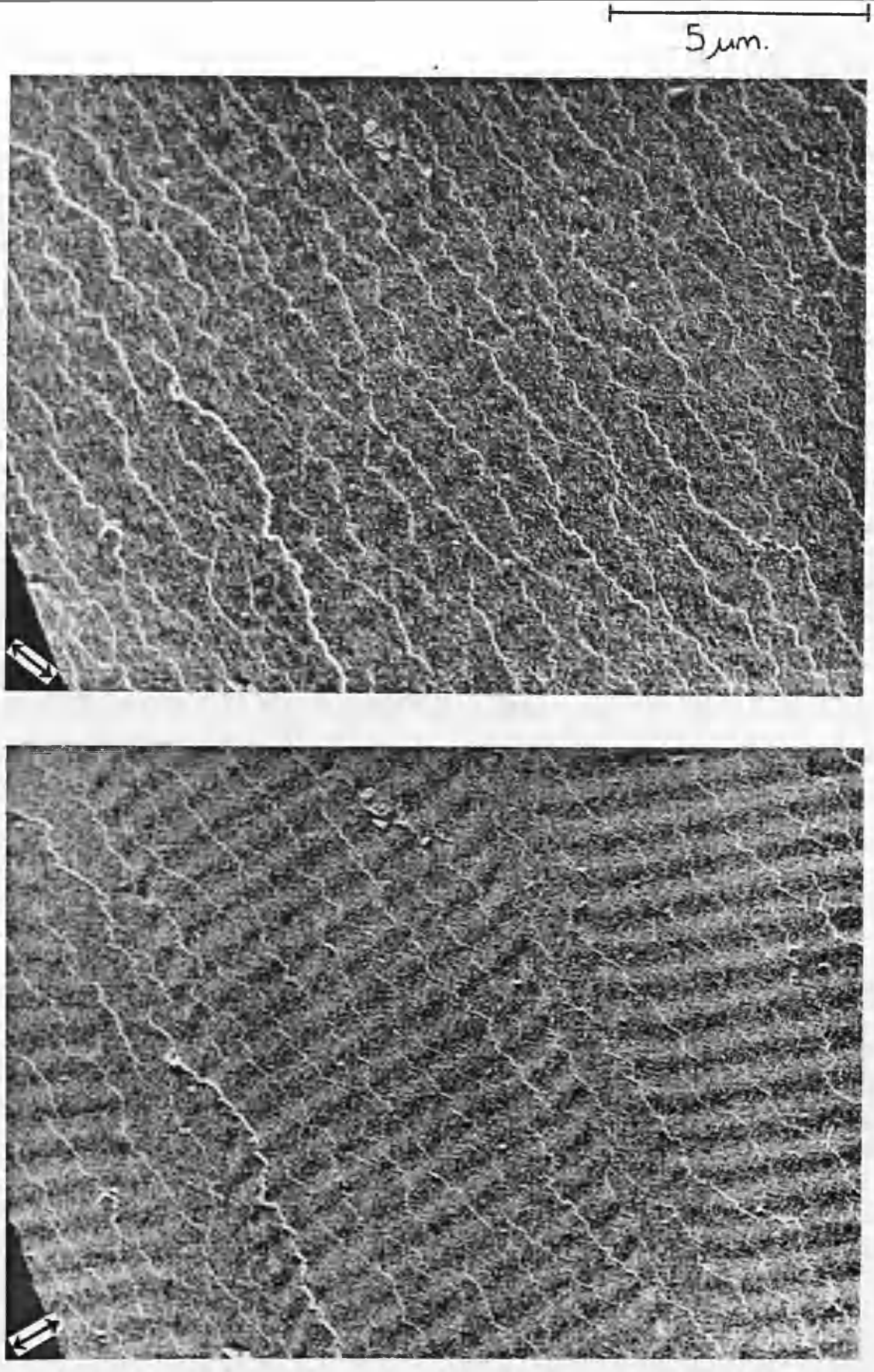

Figure 8.1 DPC images of both video tracks recorded on a MET film with a composition of 70:30 $Co_{80}:Ni_{20}$. The striking difference between these images and those obtained from the 80:20 films, also recorded with a wavelength of 0.8μm, is the appearance of a transverse component of induction for the track written at -5° to the easy-axis. The induction directions mapped are indicated by the arrows.

already discussed then significant improvements would be possible and some of the difficulties which we encountered might no longer present a problem.

Any data obtained from experiments conducted on samples which have been subjected to some form of preparation must always be discussed with this fact in mind. It is important that the magnetic structure present should be studied before specimen preparation is carried out to try and establish whether any changes occur as a direct result of this treatment. Unfortunately none of the micromagnetic investigation methods used in this thesis is capable of carrying out such examinations and other techniques would be required to perform these measurements. Of those available we feel that spin polarisation[3] and magnetic force microscopy[4] represent the most likely to provide the necessary information, and should be performed to establish the consequences of removing the base support film on the magnetic microstructure of the written tracks.

With these suggestions we believe that appropriate additional information could be obtained and the task of interpreting the micromagnetics present within high density magnetic recording materials would be made considerably easier.

REFERENCES

1. T. Arnouldussen Private communication (1990)

2. J. Chapman, Proceedings Intermag 1990, Brighton, session BB01.

3. J. Unguris *et al*, Journal of Microscopy, Vol. 139, RP1, (1985)

4. Grutter *et al*, J. Vac. Sci. Tech., **A6**, 279, (1988)

APPENDIX 1 VIDEO 8 - ERROR DETECTION AND CORRECTION

The recreation of a colour television image requires two separate signals at every picture point, one for the colour and one for the intensity of that colour. These signals are known as the chrominance and luminance respectively. The complete intensity range from absolute darkness to maximum brightness lies within the spectral limits of 4.2MHz and 5.4MHz. These extremes are referred to as the 'sync-tip' and the 'top-white' respectively. In video 8 these two signals are separated in the frequency domain, as shown in figure A.1. The different frequencies of these signals mean that distinct error detection and correction procedures are needed for each. Also present in figure A.1 are the audio and tracking signals used in the video 8 scheme. The sound is frequency modulated onto a carrier at 1.5MHz, and the tracking signals occupy the low end of the spectrum. From the diagram of the frequency spectrum the range of carrier frequencies used for the luminance signal are seen to be substantially higher than those used for the chroma signal. Recording these together on the same track enables the luminance signal to act as an AC Bias for the lower frequency chroma signal and this therefore improves the recording of this signal.

Error correction of the luminance signal is performed using video heads which have gaps skewed in opposing directions. This ensures that should one head try to read a track written by the other then little or no signal will be measured. The lowest frequency within the luminance spectrum, along with the trackwidth and writing speed,

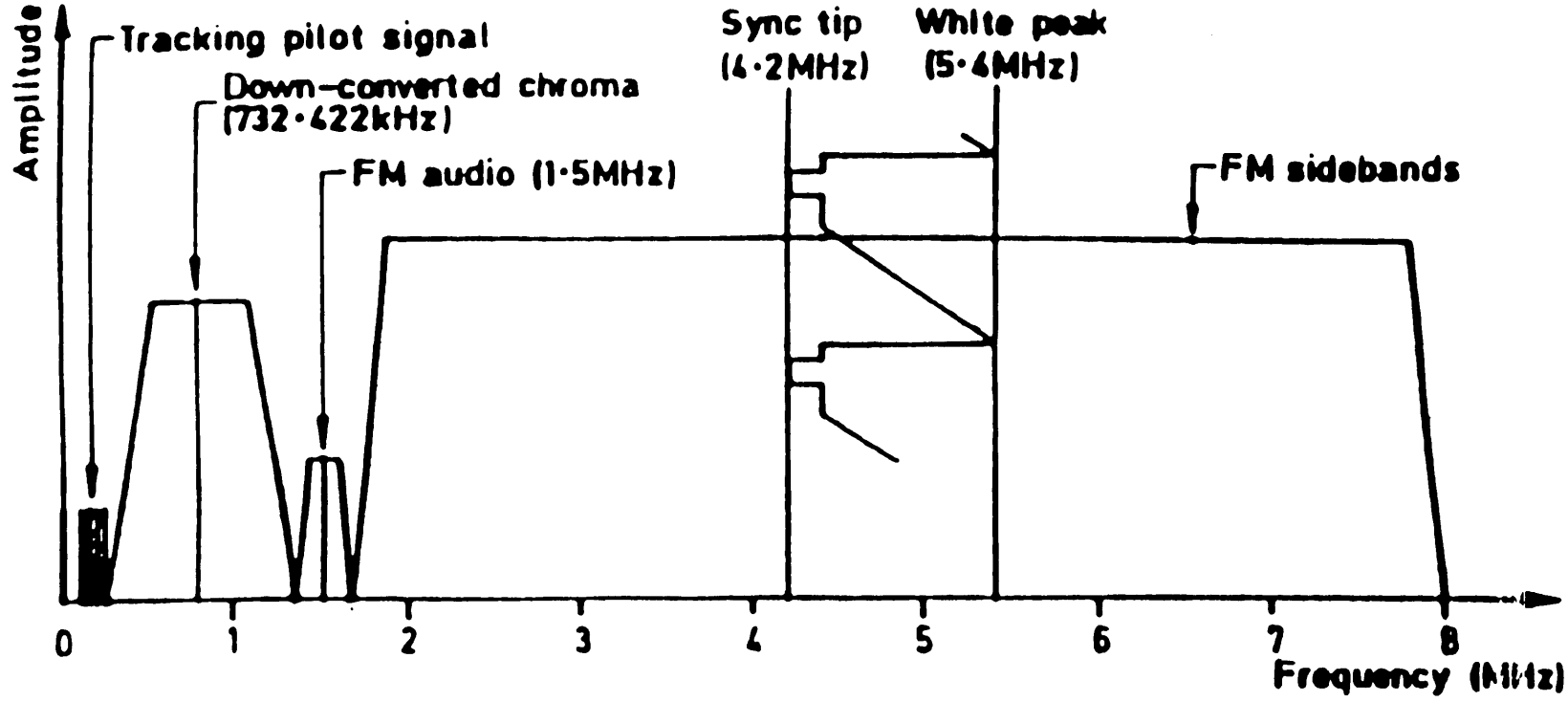

Figure A.1

Video 8 system signal frequency spectrum

dictate the precise degree of skewing necessary for this to prove acceptable. In the video 8 system the 34μm trackwidth, the luminance frequency spectrum, shown over, and the 2.005 cms^{-1} linear tape speed mean that azimuths of ±10° are employed for this purpose.

Since the video 8 system does not employ guardband recording the integrity of the low frequency chrominance signal is maintained by introducing a systematic 90° phase shift to the chroma signal for one of the recorded tracks. This phase shift is in addition to the ±135° used in PAL systems. When the chroma level is being measured during replay the output signal from the track in which the chroma phase is not delayed during recording, comprises the sum of a 128μs delayed signal and the level dynamically measured. When the output is being measured from the phase shifted track, track B in figure A.2, the as measured signal is advanced by 90° before the signals are combined. The sum of these chroma signals is used for the output because any crossatlk from the adjacent track is completely removed. This method is employed even although the registration between the luminance signal and the chroma information suffers directly from this averaging process. Complete chroma crosstalk removal is accomplished as a result of this process because when the measured chroma is added to that from the line but one previous (128μs), the chroma signals within the adjacent track, which produce the crosstalk, happen to be exactly out of phase. It might seem at first that using the chroma from the line immediately previous would reduce the significance of the averaging process; however, the 135°

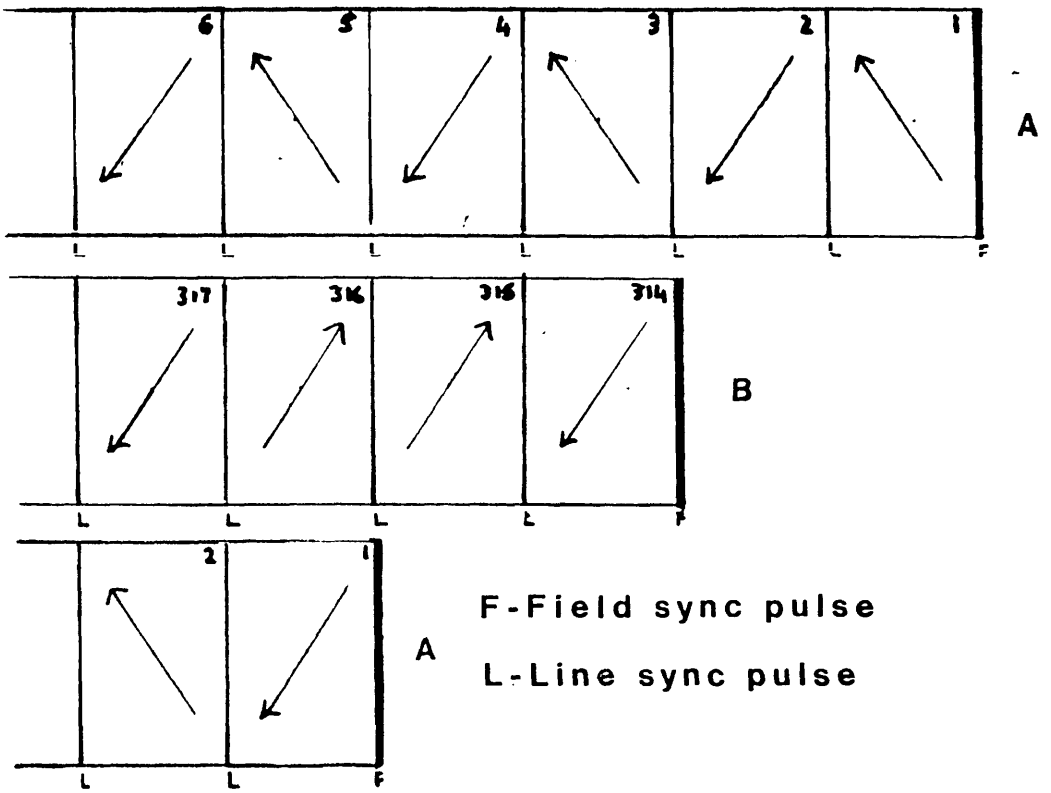

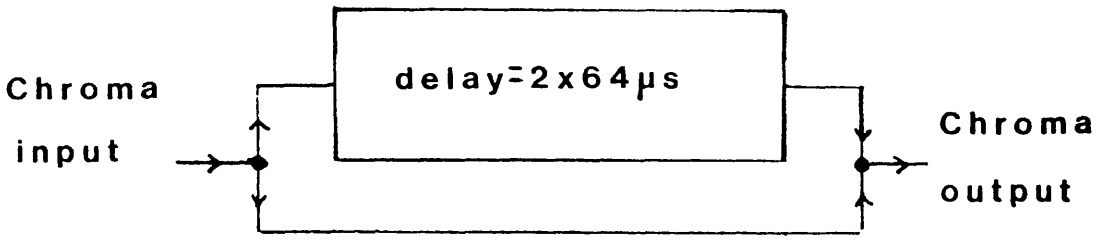

Reading track A					
	3+5	4+6	5+7	6+8	signal
	314+316	315+317	316+318	317+319	crosstalk

Figure A.2 Chroma output is produced by adding the level measured to the signal delayed by 128μs

line by line shift introduced when using the PAL system would mean that these two signals would have opposite phase, (+135^{o} and -135°), and explains why the chroma from the line 128μs previous must be used.

The other feature necessary if this procedure is to have minimum effect on the picture quality is the correct choice of linear tape speed. This is to ensure that the vertical sync pulse, indicated by the letter F in figure A.2, of track two lies exactly midway between the line syncs, which are indicated by the letter L in the same diagram. This procedure ensures registration between the two tracks and means that the line syncs of one track coincide with those of the other track. The origin of this crosstalk is the side writing effect mentioned earlier. It is clear that the ultimate success of this process is strongly dependent on the phase of the written magnetisation being maintained throughout recording. This is substantially improved through the ac biasing effect that the luminance signal provides for this chroma signal.

Accurate positioning of the video heads along the centre of the recorded tracks is achieved using pilot tracking signals and position adjustable heads. To enable the recording of these additional pilot frequencies the tape has to be wound some 221° around the head drum, which is more than that necessary for recording the video information. While one head is scanning the video track the other measures these guidance signals. The tracking signals were written by the other head when this was in contact with the tape some half rotation earlier, onto this additional portion of the tape, and are of

sufficiently long wavelength to be measured using the head with the opposing gap. From this measurement an error signal is derived and fed to the head positioning circuit. This circuit controls the piezo-ceramic element on which the heads sit and maintains the accurate alignment of these heads with respect to the centre of the recorded video tracks. In record mode only one head is adjusted while during playback both receive correction signals.